

TECHNISCHE UNIVERSITÄT MÜNCHEN

Department Chemie

Lehrstuhl für Biotechnologie

Regulation of human small heat shock proteins

Mareike Riedl

Vollständiger Abdruck der von der Fakultät für Chemie der Technischen Universität München zur Erlangung des akademischen Grades eines Doktors der Naturwissenschaften (Dr. rer. nat.) genehmigten Dissertation.

Vorsitzender: Prof. Dr. Matthias Feige
Prüfer der Dissertation: 1. Prof. Dr. Johannes Buchner
2. Prof. Dr. Bernd Reif

Die Dissertation wurde am 09.01.2020 bei der Technischen Universität München eingereicht und durch die Fakultät für Chemie am 27.02.2020 angenommen.

ABSTRACT

Small heat shock proteins (sHsps) are ATP-independent members of the molecular chaperone family. They represent key players during the stress response as they bind to a large variety of non-native protein substrates and prevent them from irreversible aggregation. In contrast to ATP-dependent chaperones, sHsps do not refold substrates actively, but they can modulate and improve the disaggregation process after stress conditions. sHsps form characteristic large oligomer ensembles, that are crucial for their holdase activity. In order to transfer sHsps in an active conformation, mainly a shift of oligomer size towards smaller species needs to be induced. There are several commonly known factors to modulate a size shift like the increase of temperature, a change in pH value, the presence of hydrophobic surfaces or phosphorylation. In the present thesis three further effectors were investigated in more detail: the formation of hetero-oligomer complexes between different sHsp family members, the influence of the N-terminal region in α B-crystallin and the interaction with the co-chaperone Bag3.

The effect of hetero-oligomer formation may depend on the composition of the sHsp ensemble present in a cell. Therefore, the expression pattern and level of class I sHsps (HspB1, HspB5 and HspB6) were investigated in different cancer-derived cell lines. It became apparent that HspB1 is widely expressed in the cell lines, whereas HspB5 and HspB6 are barely expressed and exclusively in addition to HspB1. The expression levels vary drastically between the different cell lines and sHsp members. HspB1 and HspB6 expression was enhanced upon heat stress, but HspB5 did not show increased levels. Thus, the modulation of hetero-oligomer formation under stress conditions is feasible. Size distribution analysis of sHsps in cell lysates after standard and heat shock conditions did not show significant changes. HspB1 was present in large and small oligomer ensembles, while HspB5 co-eluted as a large oligomer only and HspB6 was exclusively found as a small oligomer. CoIP experiments give evidence for the existence of all possible hetero-oligomers in cells expressing more than one sHsp member. Using the hetero-oligomer ratios determined from the lysate experiments, *in vitro* assays were performed to further characterize the influence of hetero-oligomer formation on sHsp size and activity excluding other factors like substrates or phosphorylation. In general, the HspB1-HspB5 hetero-oligomer was increased in size and mainly reduced in activity. In contrary, the addition of HspB6 decreased the oligomer size of HspB1 and HspB5. However, the effect of the incorporation of HspB6 was surprisingly different for the two sHsps. In the case of HspB5, the hetero-oligomer complex showed a general increase in activity while HspB1-HspB6 hetero-oligomer activity was modulated in a substrate-dependent fashion. Strikingly, a difference in hetero-oligomer structure was observed as HspB1-HspB6 form hetero-dimers, but HspB5-HspB6 do not.

The function of the N-terminal region of sHsps is largely unknown because of its challenging flexible and unstructured characteristics. By generation of different truncation mutants of α B-crystallin, it became obvious that the first 20 amino acids are involved in 24mer formation and the region between position 20-28 is required for hexamer formation. The loop region between position 28 and 51 turned out to be proteolysis-prone and highly flexible, but nevertheless

important for the chaperone activity whereas the deletion of the first 28 amino acids did not affect the chaperone function. Furthermore, the function of the accumulated aromatic residues in the N-terminal region was investigated by exchanging tyrosines, tryptophanes and phenylalanines to alanines. Especially, the depletion of phenylalanines resulted in destabilization of the α B-crystallin and in a reduction of chaperone activity in a substrate-dependent manner. Furthermore, the replacement of the tryptophan residues impaired the 24mer formation most likely because of their location within the first 20 amino acids that were shown to be important for 24mer formation before. Replacement of phenylalanines and tyrosines resulted in inhibition of hexamer formation. In addition, FRET experiments to characterize the subunit exchange abilities of the different mutants confirmed the predicted three-step oligomer assembly mechanism for α B-crystallin. Moreover, the exchange rates correlated with the chaperone activity, independent of the oligomer size. The overall accessibility, determined by hydrogen-deuterium exchange experiments, correlated with the oligomer size. Furthermore, increasing temperatures during aggregation assays reduced the holdase capabilities of the tested proteins. In order to determine preferred substrate interaction sites within the N-terminal region of α B-crystallin crosslink experiments were conducted using different N-terminal lysine mutants and an amine-specific crosslinker. Surprisingly, even though the lysine residues were evenly distributed over the α B-crystallin sequence, crosslinks accumulated within the ACD and not within the N-terminal sequence except position 51. For this loop, that has been described before as highly flexible and proteolytic prone, a clear increase of crosslink events was detected. Two different substrates were used to define a binding motif from the primary sequence of the substrates. The results gave strong evidence for positively charged amino acids to be important for interactions whereas negative charged amino acids were identified as non-binders.

The effect of the multi-domain protein Bag3 on sHsp behavior was investigated to determine if this protein functions as a co-chaperone. Recombinant protein expression and purification was optimized for the full length Bag3 protein as well as for a mutant including only the two IPV motifs and the sequence in between (Bag3 IPV). A basic characterization confirmed a large amount of random coil with relative low α -helix (20 %) and even lower β -sheet (10 %) content. The Bag3 IPV mutant was even decreased in its secondary structure content, as the structured WW domain, PXXP domain and BAG domain are deleted. Quaternary structure analysis revealed a monomeric structure of Bag3 whereas Bag3 IPV was found to form a monomer/dimer mixture in an approximately 1:1 ratio. In the presence of Bag3 or Bag3 IPV, HspB1 showed a slight oligomer size decrease. The influence of Bag3 on the HspB1 holdase activity was substrate-dependent as Bag3 induced an activity increase for some model substrates tested, but not in general.

Taken together, sHsps can be activated by hetero-oligomer formation but different hetero-oligomers have unique behaviors. sHsp quantifications in cell lines showed that an altered hetero-oligomer composition under heat shock conditions is likely. The experiments with N-terminal mutants of α B-crystallin confirmed a large impact of the region on oligomerization and substrate interaction. Aromatic residues have a certain impact on substrate interplay and in crosslink experiments positively charged amino acids were found to play a major role in this context. Bag3 is a sHsp co-chaperone and influences sHsp behavior.

CONTENTS

ABSTRACT	I
1 INTRODUCTION	1
1.1 Life is all about proteins - the proteostasis network	1
1.2 The guards of the proteome - molecular chaperones	4
1.3 The human small heat shock protein family	5
1.3.1 Structure of small heat shock proteins	6
1.3.2 Functions of small heat shock proteins	9
1.3.3 Substrate recognition by sHsps	10
1.3.4 The role of sHsps in diseases	11
1.4 The role of the scaffolding protein Bag3	13
1.5 Regulation of small heat shock proteins	16
2 OBJECTIVE	19
3 MATERIAL AND METHODS	20
3.1 Material	20
3.1.1 Chemicals	20
3.1.2 Consumables	21
3.1.3 Primers and Plasmids	22
3.1.4 Substrate proteins	23
3.1.5 Antibodies	23
3.1.6 Cell strains	23
3.1.7 Media, buffer and stock solutions	25
3.1.8 Reagents, kits and enzymes	26
3.1.9 Software	27
3.1.10 Online Tools and databases	27
3.1.11 Devices	27
3.1.12 Cuvettes	29
3.1.13 Columns	29

3.2 Methods.....	30
3.2.1 Molecular biology	30
3.2.2 Protein expression	31
3.2.3 Protein purification.....	33
3.2.4 Protein biochemistry.....	34
3.2.5 Spectroscopic analysis.....	37
3.2.6 Functional assays.....	39
3.2.7 Transmission electron microscopy	41
3.2.8 Mass spectrometry.....	41
3.2.9 Analytical ultracentrifugation.....	43
4 RESULTS	44
4.1 Regulation of small heat shock proteins by hetero-oligomer formation.....	44
4.1.1 Expression of sHsps in human cell lines	44
4.1.2 Size distribution of sHsps in cancer cells	47
4.1.3 Size distribution of hetero-oligomers <i>in vitro</i>	50
4.1.4 Prevention of aggregation of cellular proteins by sHsps.....	53
4.1.5 Chaperone activity of human sHsp hetero-oligomers on model substrates	55
4.1.6 Comparison of chaperone activities	57
4.1.7 Disaggregase activity of sHsp hetero-oligomers.....	58
4.2 Regulation of sHsps by their N-terminal region	60
4.2.1 The influence of N-terminal truncated mutants	60
4.2.2 The influence of aromatic substituted mutants.....	67
4.2.3 Substrate-sHsp interaction analyzed by cross linking experiments	70
4.3 Regulation of sHsps by the postulated co-chaperone Bag3	75
4.3.1 Production of recombinant Bag3 protein from <i>E. coli</i>	75
4.3.2 Basic characterization of Bag3 and Bag3 IPV	78
4.3.3 Bag3 influence on sHsp chaperone activity	79
4.3.4 Bag3 influence on sHsp size distribution	81
5 SUMMARY AND DISCUSSION.....	83
5.1 Regulation of sHsps by hetero-oligomer formation.....	83
5.2 Regulation of sHsps by their N-terminal region	87
5.3 Regulation of sHsps by the possible co-chaperone Bag3	92

6 REFERENCES	95
7 APPENDIX.....	111
Abbreviations.....	124
Publications.....	126
Danksagung	127
Eidesstattliche Erklärung	128

1 INTRODUCTION

1.1 Life is all about proteins - the proteostasis network

The term ‘proteostasis’ is a portmanteau of the words protein and homeostasis and describes the balance of the proteome within a cell. This includes the control of protein synthesis, folding, conformational maintenance, trafficking and degradation of proteins (Figure 1) (1). Furthermore, proteostasis is influenced by cell development, aging, alterations in physiology and exposure to environmental stress (2). In the human cell, there are more than ~10,000 proteins expressed at the same time (3). Around 2,000 of them participate in regulation of proteostasis (4). Thus, 20 % of the human proteome is involved in maintaining the proteome. This remarkable amount reveals the fundamental importance of the proteostasis maintenance.

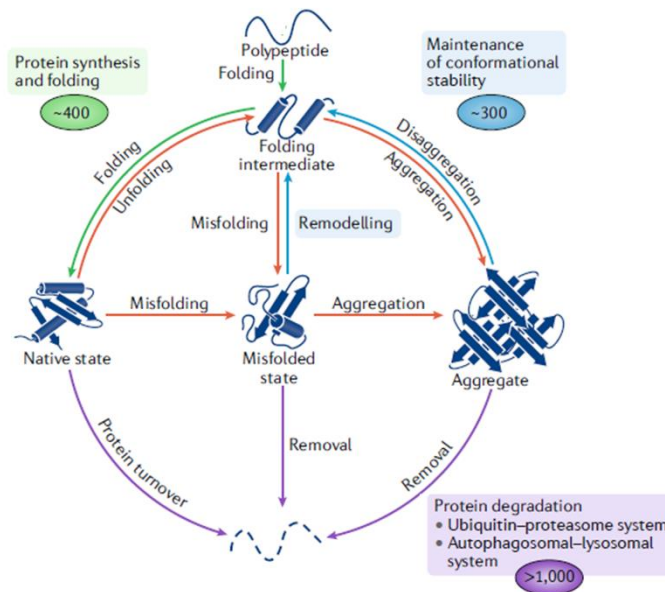


Figure 1 | The proteostasis network includes protein synthesis (green), maintenance of conformational stability (blue) and protein degradation (purple). Reprinted with the permission of Springer Nature (modified from Hipp et al. 2019) (1).

An imbalance of the system is associated with ageing and degenerative diseases e.g. Alzheimer’s disease, Huntington’s disease, Spinal muscular atrophy, and Parkinson’s disease (5,6). To ensure cellular functions, proteins must fold and/or assemble to defined three-dimensional structures (7). In principle, the native conformation of a protein is encoded in its amino acid sequence. Nevertheless, many proteins require assistance during their folding process. Beyond the assurance of correct protein folding, it is important that proteins are expressed at the correct time and cellular location. In case of surplus, proteins need to be removed by autophagy or degradation, mediated by the proteasome (1). Protein abundance needs to be strongly controlled, in order to support cell signaling and stoichiometric complex assembly. Therefore, protein expression is highly variable, from 50 copies to more than 10 million molecules per cell (8).

Protein synthesis and folding

In general, a correctly folded protein is in a thermodynamically stable state. However, during the folding process, proteins must pass through a complex energy landscape including the risk to enter a kinetically stable non-native structure with a local energy minimum (Figure 2).

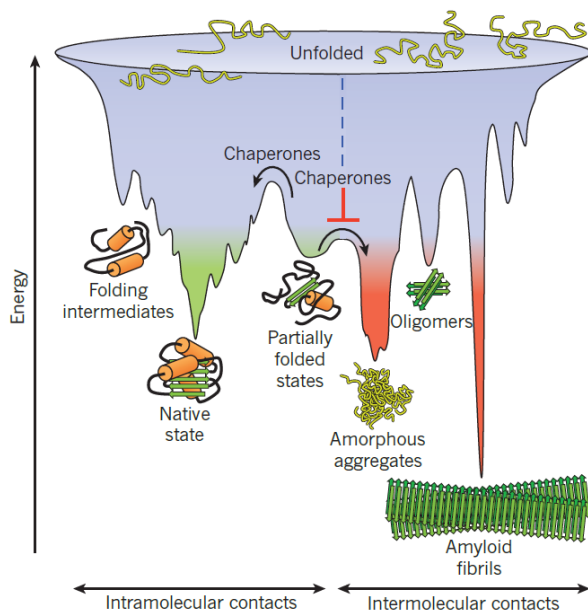


Figure 2 | Energy landscape of the protein folding process. During the folding process, the nascent polypeptides undergo various conformations in order to reach the native conformation. Partially folded intermediates can become trapped in local energy minima and are therefore at risk of aggregation. Molecular chaperones support the formation of native conformation by lowering the free-energy barriers between kinetically stable intermediates (green) whereas intermolecular contacts favor the aggregation process (red). Reprinted with the permission of Springer Nature (Hartl et al. 2011) (9).

Non-native structured proteins tend to generate intermolecular interactions and to form aggregates that may be thermodynamically more stable than the native conformation. To circumvent this event molecular chaperones are required. They lower the free-energy barriers between kinetically stable intermediates and thus promote the achievement of the native state. Most proteins are synthesized in the cytosol, but ~66 % must be transported to their functional location in a specific subcellular compartment (10). Proteins targeted for the endoplasmic reticulum (ER) or mitochondria are prevented from permanent folding by cytosolic chaperones until they reach the correct organelle. For proteins that are located in the nucleus or in the peroxisome, folding occurs before transport. Translocation across the membranes can as well be supported by chaperones (11).

Maintenance of conformational stability

Considering the energy that is necessary for protein synthesis, the maintenance of the correct folding for a functional protein is of high interest for a cell. Many proteins contain highly flexible parts in their native structures. Therefore, functional proteins are in most cases of lower stability. Proteins can be destabilized additionally by the presence of heavy metals, reactive oxygen species, increased temperatures or redox stress. To avoid the accumulation of misfolded proteins in these situations, the transcription of molecular chaperones is induced. The most prominent stress

response is the so-called heat shock response, which is controlled by multiple transcription factors including the heat shock factor 1 (HSF1). Under non-stress conditions, HSF1 is bound to chaperones and thus inactive (12,13). Increasing amounts of non-native proteins demand chaperones for their further handling. Thus, HSF1 gets released from the complex, trimerizes and induces heat shock related gene transcription (14). In contrary, protein transcription in general is attenuated on stress to reduce production of new client proteins. When the stress level diminishes, chaperones are again available for HSF1 complexation and the heat shock response is shut down (15). In a recently published study, Mühlhofer et al. showed that in yeast increased aggregation and degradation during heat stress is compensated by increased protein synthesis and enhanced chaperone activity to maintain a constant protein pool (16).

Protein degradation

Regulation of protein degradation is an important mechanism to maintain cellular functions. By depletion of proteins, copy numbers can be regulated and toxicity of misfolded proteins can be prevented. Protein degradation is mediated by two major proteolytic pathways the ubiquitin-proteasome system (UPS) and the autophagosomal-lysosomal pathway (17). Both of these systems require the support of chaperones to hold the substrates in a degradation-competent state (18). The advantage of the autophagy pathway is the possibility to degrade protein aggregates and whole organelles, whereas UPS requires ATP-dependent unfolding of the substrates. In the UPS, co-chaperones like the E3 ubiquitin ligase CHIP play an important role. As this E3 ligase ubiquitylates proteins that stay too long in contact with chaperones like Hsp90 or Hsp70 and thus targets to the proteasome (19). In the autophagy system Hsc70 and its co-chaperone Bag3 mediate the degradation of aggregates by chaperone-assisted selective autophagy (CASA) (20).

Toxicity of aggregates

Protein aggregate deposits serve as the hallmark of neuro-degenerative diseases and age-dependent pathologies (21). There are two types of protein aggregates known: On the one hand, amyloid fibrils are organized in ordered cross- β structures in parallel or antiparallel β -strands. On the other hand, amorphous aggregates that are also high in β -sheet content but do not show a fibrillar morphology. The most prominent disease of these aggregate deposits is cataract. The mechanism of how aggregates causes cellular dysfunction is still enigmatic. There are only two hypothesis: deformation of lipid membranes and aberrant interactions with membrane-associated proteins and RNA molecules (1). Furthermore, chaperones are prone to sequestration by aggregates because of their ability to recognize and bind misfolded proteins. Therefore, chaperones are depleted from the soluble protein fraction (22).

Prevention of aggregation

There are different mechanisms how chaperones inhibit aggregation. Some chaperones bind to aggregation-prone folding intermediates and process them for refolding or degradation. For some proteins, it is also possible to inhibit the primary nucleation of fibril formation or the fibril elongation (23). Secondary nucleation can also be impaired by coating the fibril surface (24). Another mechanism is the active formation of inclusion bodies to reduce the reactive surface of the aggregated proteins. This so-called ‘aggresome’ function of chaperones depends on a prion-like

intrinsically disordered sequence (25). To lower the concentration of toxic aggregates asymmetrical inheritance of damaged proteins during cell division as well as deposition of aggregates in specific cell compartments was observed (26).

1.2 The guards of the proteome - molecular chaperones

In 1978, molecular chaperones were initially defined as proteins required for correct folding of newly synthesized proteins (27). Later, the definition was extended to any factor that assists in the folding or assembly of proteins without being part of its final structure (28). This evolutionary old protein class can be found in all kingdoms of life (29).

There are four major families classified: small heat shock proteins (sHsps), Hsp60, Hsp70, and Hsp90. Furthermore, there is the Hsp40 family of co-chaperones of the Hsp70 family, several Hsp90 co-chaperones and the Hsp100 family that is not present in higher eukaryotes like animals or humans. The amount of different proteins within one class is highly dependent on the organism and increases drastically with the complexity of the proteome (Table 1).

Table 1 | Chaperome complexity increases from prokaryotes to eukaryotes. The number of members of each major chaperone classes is shown for *E. coli*, *S. cerevisiae*, and *H. sapiens* (30-33).

	<i>E. coli</i>	<i>S. cerevisiae</i>	<i>H. sapiens</i>
sHsp	2	7	10
Hsp60	1	9	14
Hsp70	3	14	17
co-chaperones	6	22	49
Hsp90	1	2	5
co-chaperones	0	11	41

Hsp70s are ATP-dependent chaperones with a molecular mass of about 70 kDa. Its C-terminal domain binds substrates and is allosterically regulated by ATP-binding followed by ATP hydrolysis in the N-terminal ATPase domain. Hsp70 is regulated by cofactors of the Hsp40 class (also called J-proteins), which bind to substrates and recruit Hsp70. Hsp40 stimulates the ATP hydrolysis, and thereby the closing of Hsp70's substrate binding pocket. The Hsp70 system has a broad functionality from initial folding and conformational maintenance to a disaggregase function and to the mediation of degradation (34,35).

About 10 % of the proteome requires the Hsp60 (chaperonins) class chaperone system. These multimeric complexes function by transiently encapsulating substrate proteins so that they cannot aggregate. As for the Hsp70 system, the opening and closing of the folding chamber is regulated by the ATPase domain with or without the presence of its lid-structure-like cofactor (36).

The Hsp90 family works also downstream of the Hsp70 system. The active homodimer of Hsp90, consisting of an N-terminal domain (NTD), a middle domain (MD) and a C-terminal domain (CTD), can be influenced by many different co-chaperones (Table 1). During the ATPase cycle, Hsp90 undergoes large conformational changes. After ATP binding to the NTD, the ATP lid closes

and the domain dimerizes to a closed state with swapped NTDs, exhibiting a more compact MD. This results in the ATPase-competent conformation and the subsequent release of ADP followed by NTD dissociation. Its clients are often in a near-native conformation in order to be prepared for ligand binding for activation e.g. kinases or steroid hormone receptors. Due to these specific substrates, Hsp90 is considered as a therapeutic target for many different diseases (37).

Hsp70 not only cooperates with Hsp60 and Hsp90, but also with the highly diverse small heat shock proteins (sHsps). These comparatively small proteins differ strongly in their size, ranging from 12 to 43 kDa, and sequence, suggesting a large functional diversity (38,39). The family is defined by their α -crystallin domain, which is flanked by a flexible N-terminal domain and a short C-terminal tail. Compared to the other molecular chaperones, sHsps work independent of ATP and do not refold substrates actively (40). As the first line of defense against stress, they protect proteins in non-native states from aggregating by holding them in a refolding competitive conformation. Therefore, they are referred to as ‘holdases’ compared to the ATP-dependent ‘foldases’. Another unique property of sHsps is their ability to form large oligomers of various sizes (41).

1.3 The human small heat shock protein family

The human genome encodes ten different sHsps (HspB1-HspB10) (42). Some of them are ubiquitously expressed, others are tissue-specific like HspB9 (CT51) and HspB10 (ODF1) that are exclusively present in testis (43,44). The members HspB2 (MKBP) and HspB3 (HSPL27) are particularly expressed in neuromuscular tissue and form defined hetero-tetramers in a 3:1 ratio *in vitro* (45). Both of them showed stabilizing effects on cytoskeletal stability under stress and during differentiation although both proteins are not heat shock inducible (46,47). Interestingly, HspB2 was found to be associated with mitochondria upon stress (48). The cardio vascular expressed HspB7 (cvHSP) forms hetero-oligomers with HspB8 (Hsp22) *in vitro* (49). However, *in vivo* both proteins mainly seem to exist as dimers and no further oligomerization was observed (50,51).

Table 2 | Basic overview of human small heat shock protein properties. Adapted from Janowska et al. 2019 (52). Data for *in vitro* oligomer formation are added from Mymrikov et al. 2016 (53).

Name	Alternative name	Oligomer formation <i>in vitro</i>	Tissue distribution	Stress-inducibility	subclass
HspB1	Hsp27, Hsp25	~24mer oligomers	Ubiquitous	HSF-1, HSF-2	I
HspB2	MKBP	Middle size oligomers	Cardiac & skeletal muscle	no	II
HspB3	HSPL27	polydisperse oligomers	Cardiac & skeletal muscle	no	II
HspB4	α A-crystallin	~24mer oligomers	Mainly eye lens	no	II
HspB5	α B-crystallin	~24mer oligomers	Ubiquitous	HSF-1	I
HspB6	Hsp20	Small species	Ubiquitous	no	I
HspB7	cvHsp	Small species	Cardiac & skeletal muscle	no	II
HspB8	Hsp22	Small species	Ubiquitous	HSF-1	I/II
HspB9	CT51	n. d.	Testis	n. d.	II
HspB10	ODF1	n. d.	Testis	n. d.	II

HspB7 was shown not to be heat shock inducible whereas HspB8 was moderate up-regulated upon stress (47). A special feature of HspB8 is its ability to trigger macroautophagy by Bag3-complexation (54). Complex formation with Bag3 was also described for HspB6 (Hsp20) (55). Furthermore, phosphorylated HspB6 interacts with the regulatory 14-3-3 protein to trigger smooth muscle relaxation. Upregulation during heat shock was not observed for HspB6 (52). The members HspB4 (α A-crystallin) and HspB5 (α B-crystallin) are prominent because they encounter over 39 % of the protein in the human eye lens (56,57). They share about 60 % of their amino acid identity. HspB5 in addition is expressed in nearly all other tissues like HspB1 (Hsp27) (58). The first observation of a positive effect of HspB1 overexpression on cell survival was made in 1989 by Landry et al (59). Therefore, it is not surprising that HspB1 and HspB5 are the best-characterized human small heat shock proteins. Both of them ensemble in polydisperse oligomer ensembles typical for sHsps und show holdase function *in vitro* (40).

1.3.1 Structure of small heat shock proteins

Small heat shock proteins are defined by their 90 – 100 amino acids long α -crystallin domain (ACD), flanked by less conserved N-terminal (NTR) and C-terminal region (CTR) (Figure 3, A).

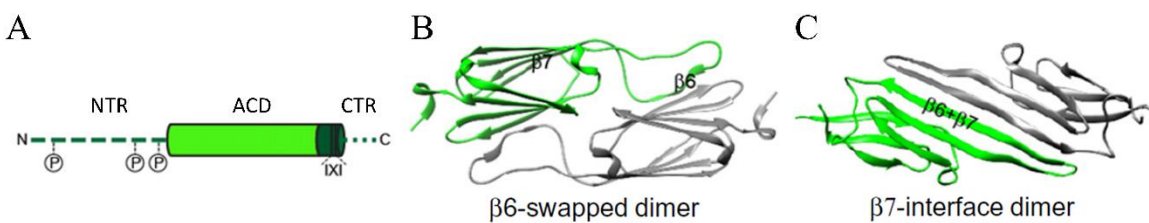


Figure 3 | Structural organization of small heat shock proteins. (A) Dissection structure of sHsp. (B) Three dimensional structure of a β 6-swapped dimer of *M. jannaschii* Hsp16.5 ACD (PDB ID 1SHS)(60). The protomers of the two monomers are colored in green and gray. (C) Three dimensional structure of a β 7-interface dimer of *H. sapiens* HspB5 ACD (PDB ID 2KLR)(61). Modified and reprinted with the permission of Elsevier (Haslbeck et al. 2015) (39).

The N-terminal region (NTR)

The N-terminal domain is much longer than the C-terminal segment, less conserved and highly flexible. The flexibility was predicted based on the absence of structural information from crystal structures and its high susceptibility to proteolysis (62–64). More recent studies give evidence for defined structures within the NTR using NMR or multi-method approaches for HspB1 and HspB5 (61,65,66). These most likely helical structures showed to some extent more than one conformation, but still the flexibility seems to be restricted. The NTRs are enriched in hydrophobic residues, especially phenylalanines and tryptophans (67). Additionally, basic arginines and prolines are overrepresented whereas reactive cysteines and lysines appear less frequently. Phenylalanines have been verified to be important for oligomer assembly and holdase activity suggesting a conserved role of these residues (68–70). The positively charged arginines possibly are involved in oligomer assembly mediated by cation- π interactions with phenylalanine residues (71). Furthermore, arginine can stabilize proteins in solution by its chaotropic side chain (72) and contribution to chaperoning can therefore be hypothesized. Additionally, for most human sHsps several posttranslational modifications are known, especially phosphorylation sites are verified in the NTR (73–75).

More stringent sequence alignments revealed conserved motifs within the NTR. For example, the ‘WDPF’ motif that is supposed to mediate oligomer formation. The effect of this motif was first investigated in HspB1, but later on it was also demonstrated for further human sHsps like HspB5 where even two of these motifs exist (76). Another example is the ‘RLFDQxFG’ motif which was first described as a phenylalanine-rich region in HspB4 and HspB5 (77). Mutations within this motif were shown to affect the assembly and subunit exchange (68,78). Later on the specific effect of arginine within this motif was pointed out to massively influence the protein structure. Substitution of the arginine to alanine led to a change in thermal stability and destabilization of oligomers in HspB1 and HspB5 (79). Overall, one can summarize that multiple regions in the NTR are required for holdase function and oligomer formation.

The investigation of the NTR interactions is still challenging because of its intrinsically disordered character, the high heterogeneity of oligomeric complexes formed in the presence of the NTR, and the fast subunit exchange within these oligomers. Recently, Clouser et al. (2019) determined three different self-interaction sites of the NTR within the ACD using different NMR methods coupled with HDX and a triple phosphor-mimicking HspB1 mutant that includes the NTR but no IXI motif in the CTR. Interactions of the NTR were identified in the ACD, specifically in the loop regions of L3/4 and L5/6, in the dimer interface groove, and, as already postulated before, in the β 4/ β 8 groove (65).

The C-terminal region (CTR)

The short (< 20 aa) and polar C-terminal region is enriched in charged amino acids like glutamate and lysine whereas aromatic residues are of lower frequency. This observation is in opposite to the observed amino acid distribution in the NTR. Furthermore, this region contains for most human sHsps the conserved IXI motif in which ‘X’ is typically a proline residue that participates in the stabilization of the large oligomers (38,80). Especially in vertebrates, the IXI surrounding residues show a palindromic arrangement like in HspB1 ‘EITIPITFE’, in HspB4 ‘ERAIPVSRE’, and in HspB5 ‘ERTIPITRE’. Interestingly, some sHsps also have a IXI motif in their N-terminal region (81). For example, the ³IPVPV⁷ motif of HspB6, which is capable of binding to the ACD β 4/ β 8 groove at either side of the dimer (82) and mediates tetrameric assemblies but no higher oligomeric states (83). Due to the IXI motif, the CTR seems to be much less flexible compared to the NTR. Interactions of the IXI motif with the hydrophobic β 4/ β 8-groove have been observed in crystal structures and solid-state NMR (84). On the contrary, solution NMR studies at more physiological temperatures verified only 2 % of the CTR being in contact with the ACD groove (85).

The α -crystallin domain (ACD)

The ACD is the signature motif of all sHsps. It is a compact β -sheet structure consisting of seven β -sheets (β 2 – β 9) that are organized in two anti-parallel sheets of three and four β -strands respectively similar to the immunoglobulin fold. The β -sheets are connected by short flexible loops (86). There are two possible dimer formations observed. In non-metazoan sHsps an additional β -strand (β 6) was found mediating domain swapping in the ACD dimer. In higher eukaryotes the β 6-sheet is directly connected to the β 7-sheet resulting in a different dimer interface. Originally, the two possible dimer formations were categorized in a bacterial-like fold (B) and a mammalian

like-fold (C). As this termination does not fit for all sHsp structures anymore, the different types were renamed based on their formation in β 6-swapped dimer (B) and β 7-interface dimer (C), respectively (39).

Oligomer assembly

The assembly of the typical oligomers seem to be hierarchically mediated by a series of highly dynamic inter-subunit contacts involving all three sHsp domains (86) (Figure 4). The first building block of higher order structures is the ACD dimer. In human sHsps, this dimer is mediated by the two anti-parallelly oriented prolonged β 6+ β 7 strands. The interaction strength of this interface is relatively low with micro molar affinity (87). Along this interface, the positively charged ACD groove is formed. In the next level, the CTR acts as a flexible ‘cross-linker’ to connect the dimers. For this, the IXI motif of one dimer binds to the β 4/ β 8-groove of the neighboring dimer. Even bidirectional binding of the IXI motif into the groove seem to be possible at least for some sHsp members (65,84,88). The absence of the IXI motif, as it is the case for HspB6 and HspB8, hinders the formation of large oligomers. These sHsps only form dimers or low molecular weight oligomers (53). However, disruption of the IXI motif does not necessarily impedes oligomer formation (89). In the last step, intermolecular NTR interactions induce the association to higher-order assemblies. This dynamic behavior is correlated with the substrate recognition and the holdase activity (90,91).

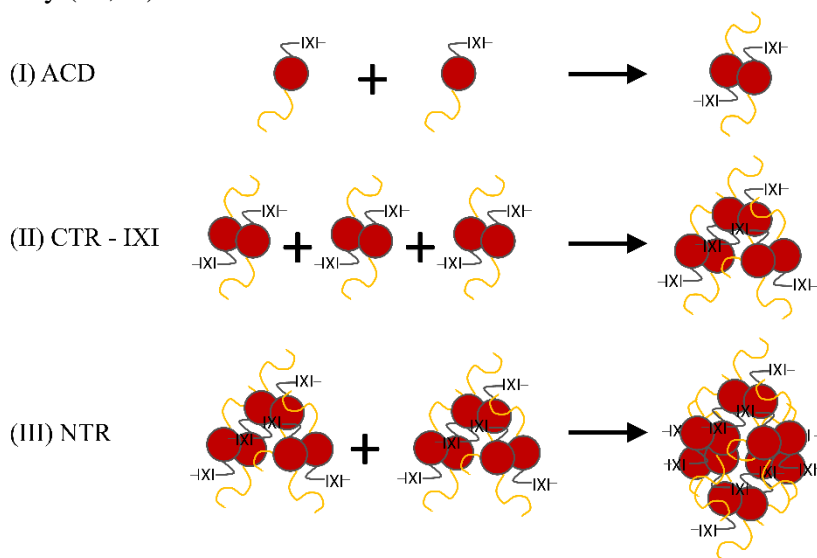


Figure 4 | Hierarchically three-step assembly of sHsp oligomers. In the first step the ACD dimer is formed (I). In the next level, the C-terminal IXI motifs link the dimers to hexamers (II). Higher order oligomers are then mediated by N-terminal interactions (III).

Taken together, the heterogeneity of oligomer complexed formed by sHsps is likely a result of the weak and dynamic inter-subunit interactions. Even though the N-terminal domain seems to play a major role in oligomer organization, not much is known about the mechanism.

Hetero-oligomer formation

The formation of oligomers containing more than one sHsp member was observed early on. The most commonly known hetero-formation is the HspB4-HspB5 (α A- α B) hetero-oligomer in the eye

lens with a well-defined 3:1 ratio (92). Later on hetero-oligomerization of HspB1, HspB5 and HspB6 were obtained during isolation of sHsps from human skeletal muscle tissue. Interestingly, the separation of these three sHsps was possible only in the presence of denaturants (93,94). Another hetero-oligomer of HspB2-HspB3 was discovered during myogenic differentiation of muscle tissue (46). *In vitro* experiments revealed the formation of hetero-oligomer complexes (95-97). Based on their ability to interact, an initial two-hybrid screen divided the human sHsps into two subclasses where only the members within one class can interact with each other (see Table 2). HspB1, HspB5, and HspB6 were determined as first group, whereas HspB2 and HspB3 are members of the second group. Later on, HspB8 was found to interact with members of both classes (49,98). However, studies that are more recent revealed that interactions of HspB8 with group one members are very weak when using untagged proteins (99). Up to date, the exact composition of hetero-oligomer complexes at physiological conditions are not known for most hetero-oligomers.

1.3.2 Functions of small heat shock proteins

In general, sHsp can act as molecular chaperones. They prevent misfolded or unfolded proteins from uncontrolled aggregation by binding them. Refolding from these sHsp/substrate complexes is usually mediated by ATP-dependent chaperones like the Hsp70/Hsp40 system. Therefore sHsps activity was originally termed as ‘holdases’ as they capture efficiently unfolded proteins (40,100). Thus, they generate a pool of refolding-competent proteins for disaggregation after stress survival (Figure 5). Even though sHsps can thus be seen as the first line of stress defense, they are not exclusively expressed under stress conditions.

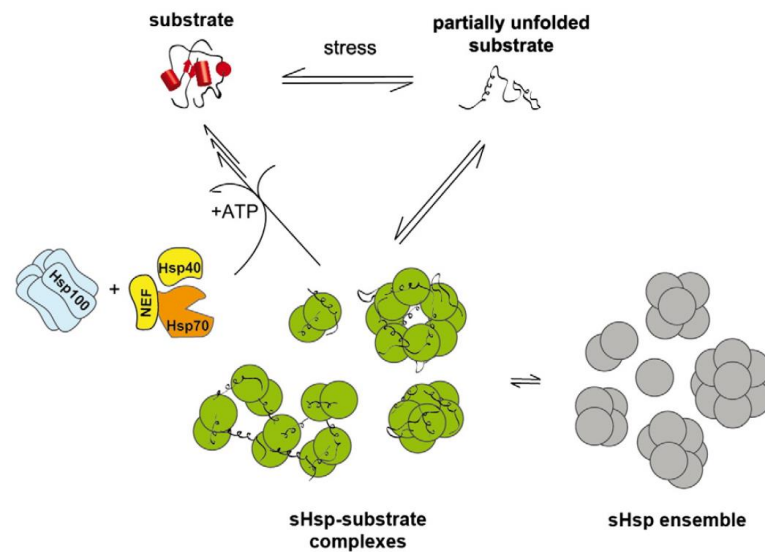


Figure 5 | Mechanism of sHsp chaperone function. sHsps exist as heterogeneous oligomer ensembles (grey). Upon stress conditions substrate proteins (red) can partially unfold (black). sHsps can bind to folding intermediates of substrates in an energy independent fashion and prevent them from aggregation in a sHsp/substrate complex (green). Substrate reactivation from these complexes is mediated with assistance of the Hsp70/Hsp40 and/or Hsp100 system in an ATP-dependent manner (orange). Modified and reprinted with the permission of Elsevier (Haslbeck et al. 2015) (39).

The presence of sHsps during the unfolding of substrate proteins is mandatory to fulfil its function (101,102). Size exclusion chromatography, electron microscopy and mass spectrometry

experiments demonstrated that the sHsp/substrate complexes are enlarged compared to normal oligomer sizes but still soluble species (103-105). The reactivation mechanism from these complexes seems to be dependent on the ratio of sHsp to substrate in the complex. Under substrate excess, sHsp are incorporated into amorphous aggregates of the substrate protein. The formed aggregates differ in size, composition and architecture from amorphous aggregates without incorporated sHsps as they avoid the exposure of hydrophobic surfaces to other cellular components and protect the substrates from proteolysis. Thus, the sequestering of large inclusions is a protective strategy to enhance cellular fitness during stress (106-108). In bacteria, lower eukaryotes and plants the reactivation of substrate protein from these special complexes requires an additional disaggregase (Hsp100 family). In higher eukaryotes like animals or humans this family is not found (109) and disaggregation is mediated by Hsp70/Hsp40 system only (110). Direct interaction of sHsps and Hsp70 has not been reported until now. In addition, a direct interaction would imply a species specificity that is not the case as sHsps can cooperate with Hsp70/Hsp40 systems of different species *in vitro* (101,111,112). Up to now, only an indirect connection via the Hsp70 co-chaperone Bag3 was reported (113). Besides their holdase and disaggregase function, sHsps possibly can mediate aggregation as well (114). For yeast Hsp42 an aggregase functions has been reported, as Hsp42 mediates sequestration of misfolded proteins into cytosolic aggregates, called CytoQ (25). This aggregase activity represents a cytoprotective protein quality control strategy. Substrates can be restored from CytoQ aggregates by Hsp70/Hsp100 disaggregase system for subsequent decision between refolding or degradation pathways (107,114).

Further, some sHsps show interactions with native proteins like the phosphoproteome regulator protein 14-3-3 or cytoskeleton components like actin (115,116). Here, sHsps seem to have a more regulatory function. For example, the phosphorylated form of HspB6 affects the balance of the 14-3-3 interactome and its downstream cellular processes. The interaction of HspB1 with actin regulates functions in a more direct fashion. By blocking the barbed ends of actin HspB1 inhibits the elongation of the polymer (117,118). Furthermore, HspB1 as well as HspB5 were shown to interact with diverse intermediate filaments through stress conditions (119).

Moreover, sHsp also play a role in the regulation of the redox status in cells. In the absence of sHsps, oxidative stress, induced by an increased amount of reactive oxygen species (ROS) leads to depletion of glutathione which results in mitochondrial induced apoptosis by caspase activation (120). sHsp expression significantly decreases the level of ROS in the cell (121,122). For this, glutathione levels are increased up on sHsp expression (123). Additionally, down-regulation of the intracellular iron concentration by HspB1 and HspB5 expression was observed (124,125). In cells free iron molecules catalyze the formation of hydroxyl radicals through the Fenton reaction. Thus, down-regulation of free iron in the cell may be important as a protective mechanism against oxidative stress. How sHsps achieve this mechanistically is still unknown.

1.3.3 Substrate recognition by sHsps

sHsps are omnipotent binders, as they bind to several hundred different proteins under stress conditions (53,126-128). In the literature, there is evidence for substrate capturing via charged

residues as well as via hydrophobic patches (90,129). Many different studies were performed in order to narrow down the interaction sites within sHsps. Early studies on substrate binding using incorporation of a hydrophobic dye suggested short segments in the NTR as important for interactions (130,131). Studies that are more recent confirmed this hypothesis by cross-linking coupled to MS experiments and by using peptide libraries for identification of interaction sites (132,133).

Interestingly, the binding site seem to be strongly dependent on the substrate. The NTR as well as the ACD have been implicated in substrate binding for various sHsp/substrate pairs (52). Binding of amorphous aggregates of lysozyme is mediated by the HspB5 NTR, whereas the amyloid fibril forming A β 1-40 peptide binds to the β 4/ β 8 groove of the HspB5 ACD (134). Consistently, A β 1-42, α -lactalbumin, and κ -casein contacts were observed to the ACD but additional interaction sites in NTR are likely because full activity was only reached in the presence of the full length sHsp (135). In contrary, the isolated ACD revealed enhanced activity towards α -synuclein and tau in absence of NTR and CTR. The presence of the ACD flanking regions can have a self-inhibitory effect on binding (136). Taken together, dependent on the substrate, the NTR or ACD can be involved in substrate recognition. The involvement of the CTR is more likely in an indirect fashion through oligomer and subunit exchange modulation. Substrate recognition with the NTR region might also explain variations in the substrate specificity of different sHsps as this region developed independently during evolution (67).

A potential recognition element in substrates is the IXI motif as this motif is as well commonly present in the CTR and/or NTR of sHsps (52). The sHsp IXI sequence itself binds to the β 4/ β 8 groove. Thus, substrate binding could be a competitive mechanism for binding to the β 4/ β 8 groove. There are characterized sHsp/substrate interactions with substrates containing an IXI sequence like tau. The IXI motif of tau is located within two aggregation-prone motifs and is recognized by HspB1 (137). Further substrate proteins that compete for β 4/ β 8 groove binding are A β 1-40 and α -synuclein, but with divergent motifs likes LVFFA and DVFMK, respectively (134,136). Another protein binding the β 4/ β 8 groove in sHsps is the Hsp70 co-chaperone Bag3. This protein is probably not recognized as a substrate but it still binds via a IXI motif sequence (113). Overall, whether an IXI motif is necessary for sHsp substrate recognition and if other recognition motifs exist remains enigmatic.

1.3.4 The role of sHsps in diseases

In 1986, Petko and Lindquist published a study about Hsp26 deletion in *S. cerevisiae*. Surprisingly, there was no obvious functional consequence of Hsp26 deletion on growth rates and development at 25°C to 55°C (138). In contrary, Landry et al. showed in 1989 that overexpression of HspB1 in cultured cell lines induces a thermo-resistant phenotype (59). Subsequently, crucial discoveries of the involvement of sHsps in severe diseases like cancer, neurological disorders, myopathies and multiple sclerosis were made (139-142). This further illustrated the importance of sHsps for cell survival under physiological conditions.

There are two possibilities how sHsps may influence their environment. They can be involved directly by interference with apoptotic inducers, as HspB1 can directly bind to cytochrome c, released from stress-damaged mitochondria thus preventing apoptosis (143). More often, they influence cell behavior in an indirect way (144). sHsps are not direct disease triggers most of the times, except from diseases based on sHsp mutations. The most prominent sHsp-related disease is the formation of cataract in the human eye lens. Here, the two α -crystallins (HspB4 and HspB5) are supposed to counteract the aggregation processes of the high protein concentrations present in this compartment. In case of their failure, protein aggregates form and the patient develops cataract (141,145). Malfunction of sHsps can result from point mutations that induce loss-of-function or an altered function. In cataract, the R120G point mutant in HspB5 and/or the R116C mutant in HspB4 mainly induce their malfunction. Also in cardiomyopathy, a high abundance of HspB5 R120G was verified (146,147). Furthermore, there are a few mutations that seem to facilitate neuropathy disease development like the Charcot-Marie-Tooth disease (CMT) and the hereditary distal motor neuropathy (HMN) (148,149). For both diseases, mutations in HspB1 and HspB8 are of importance whereas there are more mutations known for HMN. The development of CMT is promoted with HspB1 S135F, R136W and HspB8 K141N (149,150), whereas for HMN additionally HspB1 R127W, T151L and HspB8 K141E facilitate disease development (149,150). This reveals the important roles for these specific sHsps in motor neurons. Furthermore, the HspB8 mutants showed increased aggregation potential in cell culture experiments. Investigations of hetero-oligomer interactions of HspB1-HspB6 and their mutations revealed enhanced or decreased oligomer formation depending on the exact mutation (151). Interestingly, all observed point mutations are located within the ACD. A detailed mechanism how the mutations lead to disease development is still missing (145).

In general, there is the question whether overrepresentation of sHsps has a positive or a negative effect on the human body. On the one hand, increased sHsp levels can protect cells from proteotoxicity (59) and reduced or insufficient levels of sHsps can lead to disease development (152,153). On the other hand, increased sHsp levels support tumor cell growth. Thus, some sHsp members may have health-promoting effects under specific conditions whereas the same members can have the opposite effect under different conditions. In more detail, sHsps mediate chemo- and radiotherapy resistance of tumor cells, can suppress p53 activation and therefore facilitate cancer cell survival. Furthermore, they can induce cytoskeletal remodeling/differentiation (154) and tissue fibrosis (155). Most of these mechanisms are critical for the epithelial-to-mesenchymal transition (EMT) that is crucial for cancer development. At the same time, sHsp show positive effects on healthy tissue like the protection of the eye lens proteome, the protection against cardiac damage related to altered redox metabolism and the prevention of neurodegeneration in neuronal and muscular tissue (156). Taken together, whether positive effects of sHsps overexpression outweigh their possible negative (cancer promoting) effects remains to be elucidated.

Beside the mentioned intracellular effects of sHsps, some extracellular effects are reported. Even though sHsps do not contain a signal sequence for cell export, their extracellular existence has been verified. It is conceivable that the export take place via exosomes or the leakage from dying cells (157). In neuronal tissue that undergoes degeneration the binding of sHsps to extracellular

aggregates can prevent the aggregated species from interacting and damage cellular membranes or even enter cells (158,159). Furthermore, extracellular sHsps may have immune-regulatory functions like triggering the innate immune response or being anti-inflammatory. Some sHsps even show pro-inflammatory functions as an inciting antigen for the adaptive immune response (157).

For development of therapeutic approaches targeting sHsps, more details need to be known about substrate recognition and specificity, the influence of homo-/hetero-oligomerization and especially the impact of post-translational-modifications (PTMs) on the oligomerization. Beyond that, the integration of sHsps in the chaperone network needs to be clarified and the regulation of sHsp gene expression has to be investigated more precisely as some sHsps are HSF-1-dependent but not all.

One possible therapeutic approach may be the upregulation of sHsps. In general, protein overexpression is not used as a therapeutic option because overrepresentation of specific proteins leads to an unphysiological scenario whereas for sHsp temporarily upregulation is an intrinsic property of cells. Therefore HSF-1 is targeted for upregulation by compounds like GGA (160) or BGP-15 (161,162). These compounds reveal some efficacy in protecting against neurodegenerative diseases (162). It remains unclear whether the observed effects are due to sHsp or general Hsp overexpression as HSF-1 regulates many heat response related proteins. An advantage of these compounds is the fact that they do not activate HSF-1, they only boost the already activated heat shock response in stressed cells. Hence, side effects of the compounds in non-stressed cells are minimized. A disadvantage is the ineffectiveness of the HSF-1 controlled members (HspB1, HspB5, and HspB6) on neurodegenerative diseases while other sHsp members like HspB7 or HspB8 are more effective in inhibition of disease development (50,163). Unfortunately, there are no compounds available for boosting specifically HspB7 and/or HspB8.

Another possibility is the specific downregulation of sHsps in cancer cells. Here gene silencing by antisense oligonucleotides or siRNA was reported to decrease tumor cell viability drastically. Phase-I and-II clinical trials are performed to evaluate the applicability of such strategies in humans (164). It remains challenging to distinguish between healthy and cancer cells to affect only cancer cells and to avoid side effects on healthy cells. A further method to use sHsps as therapeutic targets is the direct inhibition of sHsp function by peptide aptamer treatment (165). Until now the mode of action for these aptameric peptides is not clear. Most likely, the peptides interfere with either substrate binding and/or oligomerization, which leads to loss of function.

1.4 The role of the scaffolding protein Bag3

The Bcl-2 associated athanogene 3 (Bag3) protein belongs to the family of BAG proteins. Critical for this family is the BAG domain that mediates Hsp70 interaction. Beside from Bag3, there are six different protein members. The founding family member is Bag1 which binds to Hsc/Hsp70. Bag1 inhibits the nucleotide exchange, impairs the substrate release and can therefore regulate Hsc/Hsp70 activity (166,167). Bag2 appears to be the only family member that enhances rather than suppresses Hsp70 activity (167). Moreover, Bag1 was found to be part of the Hsp70-mediated proteasomal degradation of ubiquitylated proteins (168).

1 INTRODUCTION

For Bag3 there are two isoforms discovered until now. The full length protein with ~70 kDa and a synaptic form with ~40 kDa. Mass spectrometric analysis revealed that the C-terminally shortened synaptic form is missing the BAG domain (169). The full length protein is constitutively expressed whereas upon specific stress conditions relocalization and enhanced expression can be induced (170). At least four different amino acid motifs were identified in the full length Bag3 protein (Figure 6). The N-terminal WW domain participates in the interaction with PXXP repeats (proline-rich) of different proteins and with Bag3 itself. The two conserved IPV motifs, where one is located centrally in the molecule and the other closer to the N-terminus, allow the interaction of Bag3 with sHsps like HspB1, HspB5, HspB6 and HspB8 (51,113,171,172). In the C-terminal part, a PXXP repeat is located that is responsible for interaction with SH3 domain proteins and the name-giving BAG domain providing the interaction with Hsc/Hsp70 and Bcl-2 (173).

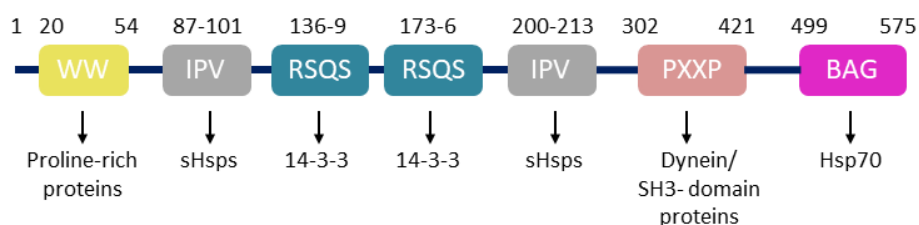


Figure 6 | Domain organization of Bag3. The localization of each domains is indicated in amino acid number and interaction partners of each domain are suggested.

The last domain as well mediates the interaction of Bag3 and HSF-1. In association with the HSF-1 interaction Bag3 was shown to co-translocate to the nucleus upon stress (174). Based on a proteomic approach, the protein 14-3-3 was identified as a prominent interactor for Bag3 (175). Closer investigations revealed this posttranslationally phosphorylated RSQS motifs, one at position 136 and the other at 173 as the interaction sites (176).

Bag3 plays an important role in autophagy induction. There are at least three different types of autophagy: microautophagy, macroautophagy, and chaperone-assisted selective autophagy (CASA). In general, autophagy results in the degradation of intracellular material in lysosomes. Through the material uptake by a phagophore the autophagosome develops. This step is followed by the association of the autophagosome and the lysosome to become the autolysosome. To control the pathway of the chaperone-assisted selective autophagy there are several auxiliary factors and adaptor proteins. Bag3 is one of these auxiliary factors and assists proteins regulating the turnover of protein aggregates. In more detail, Bag3 coordinates the recognition of substrate proteins together with Hsp70 and HspB8 (Figure 7, A). Most likely Bag3 is important to facilitate the physical proximity of Hsp70 and HspB8 (Figure 7, B) (177). STUB1 acts as a chaperone-associated ubiquitin ligase and cooperates with the ubiquitin-conjugating enzyme UBE2D during the ubiquitylation of the chaperone-bound client. Additionally, Bag3 enables autophagosome formation by recruiting SYNPO2 which is important for the fusion of the autophagosome membrane (Figure 7, C). Hence, Bag3 is also called a scaffolding protein that serves as a platform for other proteins.

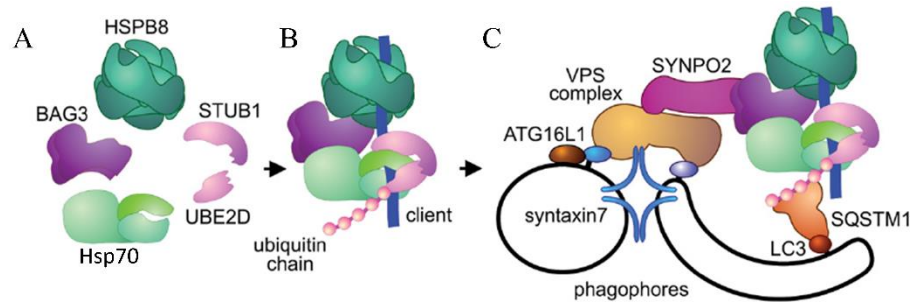


Figure 7 | CASA chaperone complex formation. HspB8, Bag3 and Hsp70 are important for substrate recognition (A). STUB1 and UBE2D mediate the substrate ubiquitylation (B). The formation of the autophagosome is then organized in cooperation with SYNPO2 (C). Modified and reprinted with the permission of Landes Bioscience (Ulbricht et al. 2013) (177).

Bag1 and Bag3 regulate the preferred type of protein turnover. Under physiological conditions, where Bag1 is expressed of higher number than Bag3, Bag1 induces the proteasomal degradation. In contrast, under stress conditions, Bag3 expression levels increases and protein sequestration followed by macroautophagy is induced by Bag3 concluding that the expression level switch is followed by a functional switch to regulate protein turnover in a condition-dependent manner (178).

Most important for the present study is the interaction of Bag3 with sHsps. As described before the interaction of Bag3 and sHsps are probably mediated by the N-terminal IPV motifs of Bag3 to the $\beta 4/\beta 8$ groove of the sHsps. Thus, one Bag3 molecule has potentially two interaction sites for sHsps and can therefore bind one sHsp dimer. At the same time, Bag3 can bind to Hsp70 via its BAG domain and thus facilitate a complex where sHsps and Hsp70 are in close proximity (Figure 8).

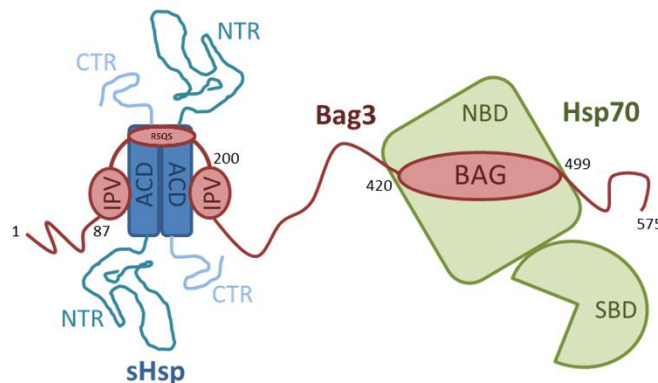


Figure 8 | Scheme of sHsp-Bag3-Hsp70 complex. A sHsp dimer consisting of two promoters is depicted in blue. Bag3 including its two IPV motifs, the RSQS (14-3-3 binding site) sequence and its BAG domain is highlighted in red. Hsp70 containing as nucleotide binding domain (NBD) and a substrate binding domain (SBD) is depicted in green. The figure was kindly provided by Dr. Martin Haslbeck.

Beside from the well-known complex formation with HspB8 to facilitate CASA, interactions with HspB6 were reported which also lead to autophagy *in vivo* (171,179). The corresponding mechanism may be similar for HspB6 and HspB8 as both of them are present only in small oligomer species and do not contain an IXI motif in their CTR. Therefore, their $\beta 4/\beta 8$ groove is not occupied and Bag3 can easily interact. However, interactions of Bag3 with sHsps that form large oligomer species were reported *in vivo* as well, for example the disease-related R120G mutant

of HspB5 (172). In addition, the interaction of HspB1 and Bag3 were characterized *in vitro* by Rauch et al. Here, a shift of the large oligomer species to small oligomer species upon Bag3 addition was observed and enhanced refolding activity was revealed for HspB1/Bag3/Hsp70 complexes compared to experiments without Bag3 (113).

1.5 Regulation of small heat shock proteins

The most obvious regulation mechanism for Hsps is the regulation of expression levels as most of them are upregulated upon stress conditions. This is also valid for sHsps, at least for those that are under control of HSF-1 and/or HSF-2 (see Table 2). In this case enhanced expression levels lead to more active sHsps in the cell. Another general regulation mechanism of Hsps is the transition between low and high affinity states for substrate binding. For ATP-dependent chaperones this can be modulated by nucleotides as the ADP bound state has a low substrate affinity and the ATP-bound state exhibits a high affinity for substrates (29). In the case of the ATP-independent sHsps, the transition is an intrinsic mechanism and results in the ability to form different oligomer states. A transition between a compact and an expanded conformation was reported for yeast Hsp26 (180,181). Here, the activation is induced through a minimal conformational change without disassembly of the oligomeric complex that results in a marginal increase in particle diameter (182). A similar model was proposed for the *E. coli* sHsp IbpB (183).

However, the majority of sHsps requires a shift in the oligomer equilibrium towards smaller species to convert from an inactive storage form to an activated state (80,86,90). This is required because of the involvement of the NTR in substrate binding which is also required for oligomerization and therefore less accessible within the oligomer. The past years of research showed that different conditions can induce the shift towards smaller oligomer species. Additionally, hydrophobic sites that are buried within the oligomer become exposed upon dissociation of oligomers and are therefore accessible for substrate binding. Another change that goes along with the shift to smaller oligomeric species is the increase of subunit exchange rate by a factor of 10 - 100 in terms of sHsp activation (181,184-186). This means sHsps subunits exchange more frequently in their active state. Taken together, the transition from the storage to the active state is not a simple two state mechanism, but a complex process involving several sequential transitions.

There are multiple conditions that can initiate the discussed transition: (1.) presence of substrates, (2.) temperature shift, (3.) change in pH, (4.) phosphorylation, and (5.) hetero-oligomerization (Figure 9). When proteins unfold, they present a more hydrophobic surface. This surface can be recognized by the highly dynamic sHsp oligomers, which functions as a sensor for the presence of unfolded protein parts (129,187,188). By detection of increased hydrophobic surfaces, the sHsp transits to its active state. In terms of evolution, the regulation by a temperature increase is probable one of the oldest mechanisms as it is at a very short time scale and has a high precision of temperature detection (91). Only a few degrees of temperature increase sufficiently activate sHsps, like from 37°C to 42°C for human HspB1 (105,189). The proteome can thus be stabilized rapidly and after the temperature decreases, the activation is reversible within the same time scale.

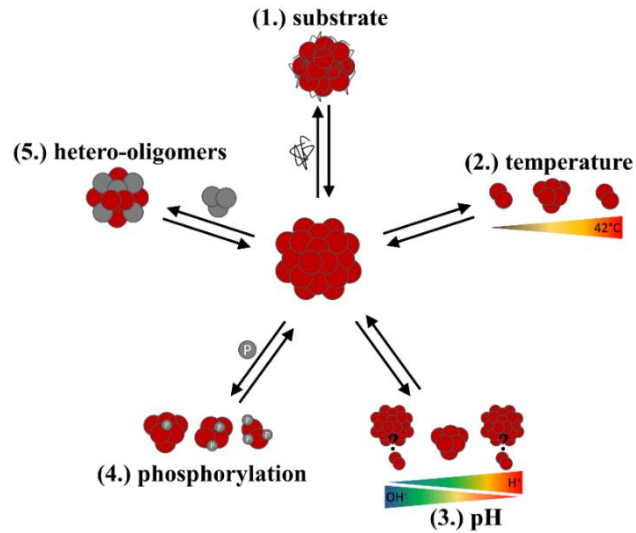


Figure 9 | Regulation of small heat shock proteins. Five different conditions can lead to dissociation of the oligomeric complex (1.-5.). In principle, all of them are reversible whereby dephosphorylation requires the presence of a phosphatase and refolding of substrates from sHsp/substrate complexes is only possible in cooperation with ATP-dependent chaperones.

In *T. gondii* a temperature shock in the opposite direction ('cold shock') was reported. Here, the sHsp was activated by a temperature decrease (186). Temperature-dependent regulation was also observed on the translational level. At least in bacteria an increased temperature led to the melting of the mRNA hairpin structure, which enhances efficiency of translation and therefore increased protein levels (190,191). As the oligomeric complexes of sHsps are highly sensible to charges, it is not surprising that changes in pH can induce structural changes. In humans, two sHsps have been reported to be pH sensitive. For HpB1, acidification leads to oligomer size increase (192). In contrast, for HspB5 destabilization of the dimer interface was reported upon acidification, which led to higher amounts of free monomers (61,86,193). The mechanism was explored for the development-specific sHsp Sip1 from *C. elegans*. The physiological pH in larval and adults *C. elegans* is 7.5, which drops down to 6.3 or below in recovering dauer larvae. In contrast to most other sHsps, Sip1 has a basic pI of 7.9 and gets activated by pH shift from pH 7.5 to pH 6.3. The activation is mediated by an oligomer shift from a 32mer to a 24mer that came along with the dissociation of subunits (126,192).

A condition that is more energy-consuming and also not as easy to reverse, is the insertion of a posttranslational modification. This mechanism has been discovered in mammals but was also reported for yeast Hsp26 (194) and maize Hsp22 (195). It remains unknown whether the effect of phosphorylation is similar for non-mammalian sHsps. Most prominent is the phosphorylation of sHsps in their NTR. All human sHsps can be phosphorylated at their serine/threonine side chains, e.g. HspB1: S15, S78, S832 and HspB5: S19, S45, S59 (58,75,196). Due to the integration of negative charges in the N-terminal domain the oligomeric size shifts in most cases towards smaller species like hexamers, tetramers and/or dimers, as the incorporation of negative charges destabilizes the subunit interfaces. Thus, increasing phosphorylation leads to increase of negative charges and therefore enhanced destabilization. In terms of multiple phosphorylation sites this

mechanism seems to be titratable. It needs to be mentioned that differences in behavior for real phosphorylation and phosphorylation-mimicking mutants were observed. HspB5 tends to form tetramers and dimers upon phosphorylation by MAPKAP2/3 kinase treatment (197) whereas hexamers and dimers were detected for a triple E (S19E, S45E, S59E) mutant (62). The effect of phosphorylation on holdase activity does not seem to be equal under all conditions. For HspB1 substrate interaction was enhanced or reduced depending on the exact experimental conditions and the specific phosphorylation state of HspB1 (58,198-200). Other posttranslational modifications have been reported for sHsps as well, but detailed investigations are still missing. Especially, for HspB4 and HspB5 in the eye lens multiple PTMs like deamination, oxidation, glycation, and methylglyoxal are described (201-204).

A further condition that could induce sHsp activation is the formation of hetero-oligomers. For some organisms hetero-oligomerization is well established like for the *E. coli*. sHsp IbpA, exhibiting very low chaperone activity, but can enhance the chaperone activity of its partner sHsp IbpB by forming hetero-oligomer complexes (205). Whether this mechanism can be generalized for human sHsps is still unclear. In human, the ten sHsps are divided in two groups based on their ability to interact with each other (see Table 2). The best characterized hetero-oligomers are HspB4/HspB5 (class I) in the eye lens (56) and HspB2/HspB3 (class II) in muscular tissue (46). Further hetero-oligomers have been observed for HspB6 with HspB1 and HspB5 resulting in decreased oligomeric size, as well as hetero-oligomers of HspB1 with HspB5 (95,206,207), but a detailed characterization of the effect of their hetero-oligomer formation is still missing. Not all sHsps hetero-oligomerize, even though they exist at the same time in the same compartment. For example, the two members of yeast, Hsp26 and Hsp42, do not interact with each other (208). Furthermore, the incorporation into hetero-oligomers does not necessarily include the complete amount of sHsps. For the incorporation of HspB1 in HspB1-HspB5 hetero-oligomers it was reported that 10 % of HspB1 remains as free homo-oligomer (58). However, hetero-oligomerization does not lead necessarily to smaller species and activation (58). It is as well possible that substrate spectra of single sHsps are modified in hetero assemblies (209).

In summary, the extent to which hetero-oligomerization may regulate sHsp function in man remains to be explored. Additive effects of multiple factors influencing the sHsps at the same time are conceivable e.g. phosphorylation of hetero-oligomeric species. Scenarios like this further increases the complexity of the regulation mechanisms in the cell.

2 OBJECTIVE

Small heat shock proteins (sHsps) are part of the molecular chaperones acting mainly as holdases to keep substrate proteins under stress conditions in a refolding-competitive state and prevent them from irreversible aggregation. A physiological characteristic feature of these ATP-independent chaperones is their ability to form dynamic oligomer structures. To regulate the activity of this ubiquitous and diverse chaperone family, mainly a shift towards smaller oligomeric species is induced by different trigger factors. The principle behind the various effectors is not completely understood. In the present thesis, the effects of three possible regulation mechanisms were characterized in detail: the formation of hetero-oligomers, the function of the N-terminal region, and the potential co-chaperone Bag3.

In man, ten different sHsps exist. Besides from their different expression patterns, it remains inconclusive why multiple sHsps are expressed simultaneously. The presence, composition and performance of hetero-oligomer formation were therefore investigated for human class I sHsps (HspB1, HspB5 and HspB6) in different cell lines. The knowledge from these experiments was then used to further characterize physiological relevant hetero-oligomer assemblies *in vitro* with recombinant proteins. By using five different substrates the effect on the holdase function was investigated in detail. Furthermore, changes in size distribution were analyzed in order to test for a correlation between size and activity.

In the second part the N-terminal region of α B-crystallin (HspB5) was studied to determine the function of its different motifs and the contribution of its aromatic residues. In this context, truncation mutants and point mutants replacing the three different aromatic acids (Phe, Tyr, Trp) were designed, purified and analyzed towards their chaperone activity, size distribution, subunit dynamics and accessibility by *in vitro* assays. To address the question of specific substrate interaction sites within the N-terminal region and a possible interaction sequence motif, crosslink experiments were conducted using two model substrates and mass spectrometry.

The multi-domain protein Bag3 was shown to interact with different sHsps like HspB1, HspB5, HspB6 and HspB8 *in vivo* and/or *in vitro* (113,210). However, the exact interaction sites and the purpose of the interplay are still not clear. In this regard, Bag3 and a shortened mutant were expressed, purified and characterized towards its ability to influence HspB1. In contrast to other heat shock proteins, up to know no co-chaperones of sHsps were identified. As a co-chaperone, Bag3 might have the ability to specifically regulate sHsp stability, subunit dynamics, activity or size distribution. *In vitro* assays were performed to address these questions.

3 MATERIAL AND METHODS

3.1 Material

3.1.1 Chemicals

Chemical	Supplier
2-(4-(2-Hydroxyethyl)-1-piperazinyl)-ethansulfonsäure	Roth
2-Mercaptoethanol	Roth
β -Mercaptoethanol	Sigma
Acetic acid	Roth
Acetonitrile LiChrosolv®	Merck
Acrylamid/Bis solution 38/2 (40% w/v)	Serva
Agar Agar	Serva
Agarose	Serva
Ammonium persulfate	Roth
Ampicilin sodium salt	Roth
Bromphenolblue	Serva
Chloroform	Sigma
Coomassie Brilliant Blue R-250	Serva
Deoxynucleoside triphosphates	Roche
Dipotassium phosphate	Merck
Disodium phosphate	Merck
Disuccinimidyl glutarate	ThermoFisher Scientific
Dithiothreitol	Roth
Dulbecco's Modified Eagle Medium, high/low glucose	Sigma
Ethanol	Merck
Ethylenediaminetetraacetic acid disodium salt	Merck
Extran	Sigma
Fetal bovine serum Gold Plus	Bio&Sell
Formic Acid	Sigma
Glycine	Roth
Guanidinium chloride	Merck
Heavy water	Euriso-top
Hydrochlorid acid 32 %	Merck
Imidazole	Sigma
Iodoacetamide	Merck
Isopropanol	Roth
Isopropyl β -D-1-thiogalaktopyranoside	Serva
Kanamycin sulfate	Roth
LB medium	Serva
Magnesium sulfate	Merck

Methanol	Roth
Minimum Essential Media Eagle (MEME)	Sigma
Milk powder	Roth
Monopotassium phosphate	Merck
Monosodium phosphate	Merck
Non-essential-amino-acids (NEAA)	Gibco
Nonidet P-40 Substitute	Roche
Phenylmethanesulfonyl fluoride	Sigma
Phosphatase inhibitor cocktail 2 and 3	Sigma
Potassium chloride	Roth
Potassium hydroxide	Roth
Protease Inhibitor Mix G	Serva
Protease Inhibitor Mix HP	Serva
Protease Inhibitor Mix M	Serva
Roswell Park Memorial Institute 1640 Medium (RPMI)	Gibco
Sodium chlorid	Merck
Sodium deoxycholate	Merck
Sodium dodecylsulfate	Serva
Sodium hydroxide	Merck
Stain Clear G	Serva
SYPRO Orange	ThermoFisher Scientific
Tetramethylethylenediamine	Roth
Trichloroacetic acid	Sigma
Tri-potassium citrate monohydrate	VWR Chemicals
Triton-X100	Merck
Trizma Base	Sigma
Trypsin, sequencing grade modified	Promega
Trypsin-EDTA solution	Sigma
Tween-20	Merck
Urea	Merck
Water, ultra pure LiChrosolv®	Merck

3.1.2 Consumables

Consumables	Suppliers
Blotting paper	Whatman
Cellstar®, 15 and 50 mL	Greiner Bio One
Centrifuge Filter, 0.22 µm	Merck βipore
Chromacol Closures, 9mm, white Silicone/Red PTFE	Fisher Scientific
Chromacol Vials, 9mm, Polypropylene, 300 µl	Fisher Scientific
Deep well plates, MegaBlock 96-well 2.2 mL PP	Sarstedt
Dialysis membranes Spectra/Por (MWCOs 6-8,000)	Spectrum Laboratories
Glass pasteur pipettes	Labsolute

Nitrocellulose Membrane Roti® NC	Roth
Parafilm M	Roth
PCR tubes	BioRad Laboratories
Petri dishes, PS, 94 mm	Greiner Bio One
Plastic tips	Brand
Protein G Sepharose 4 Fast Flow	GE Healthcare
Reaction tubes for MS preparation	Eppendorf
Reaction tubes, 0.5, 1.5 mL and 2 mL	Sarstedt
Semi-micro cuvette, PS	Brand
serological pipettes 1 mL, 2 mL, 5 mL, 10 mL, 15 mL	Sarstedt
SERVAGel TG PRiME 4-20%, 15 sample wells	Serva
Solid Phase Extraction Disk, C18, 47 mm	Empore
Tissue Culture Flask T25, T75	Sarstedt
Ultracel Ultrafiltration disc 3 kDa NMWL ,76 mm	EMDMillipore

3.1.3 Primers and Plasmids

The recombinant expression for HspB1 the pAK3038-HspB1 Plasmid was used, designed by Jakob et al. in 1993 (40). For HspB5 the expression plasmid from Peschek et al. in 2009 (pET28b-HspB5) (211) and for HspB6 the expression plasmid from Bukach et al. in 2004 (pET23b-HspB6) (212) were utilized. Plasmid design of pET28b-HspB5-Δ28 was performed by Katrin Back (213) and pESUMO-HspB5-Δ40 was produced by Philipp Schmid (214). Due to failure of classical cloning strategies pet28b-HspB5-R11K-R22K-R50K and pET28b-HspB5-R50K were customized synthesized by GeneArt. Additionally, the codon optimized sequences of Bag3 and the Bag3 IPV construct were produced by GeneArt and supplied in pE-SUMOpro plasmid.

Primers	Sequence
aB_Δ20_pESUMO_fw	TTGGTCTCAAGGTATGGCAAGCCGCC
aB_Δ20_pESUMO_rev	CATGGTATATCTCCTTCTTAAAG
aB_Δ51_pESUMO_fw	TTGGTCTTCAAGGTATGGCACCTCCTTCC
aB_Δ51_pESUMO_rev	CATGGTATATCTCCTTCTTAAAG
aB_S35K_fw	CCTGTTGGAGAAAGATCTTTTCCCGAC
aB_S35K_rev	TGCTCTCCGAAGAACTGG
aB_S45K_fw	TACTTCCCTGAAACCCTTCTACC
aB_S45K_rev	GACGTCGGGAAAAGATCAG
aB_R11K_fw	CCCCTGGATCAAACGCCCTTCTTTC
aB_R11K_rev	TGGTGGATGGCGATGTCC
aB_R22K_fw	CTCCCCAGCAAACCTCTTTGACC
aB_R22K_rev	TGGAAAGGAAAGAAGGGG
Bag3_pESUMO_fw	ACGGTCTCAAGGTATGAGCGCCGCCACC
Bag3_pESUMO_rev	ATTCTAGACTACGGTGCTGCTGGGTTACCA
T7	TAATACGACTCACTATAGGG
T7 term	GCTAGTTATTGCTCAGCGG

Plasmid	Resistance	Origin
pE-SUMOpro	Kanamycin	LifeSensors
pET28b	Kanamycin	GeneArt

3.1.4 Substrate proteins

Substrate proteins	Suppliers
Citrate Synthase, pig mitochondrial, UniProt ID P00889	Sigma
Glycerinaldehyd-3-phosphat-Dehydrogenase, bovine liver	Sigma
Insulin, bovine pancreas	Sigma
L-Malate Dehydrogenase, pig heart, Uniprot ID P00346	Roche
Lysozyme, chicken	Sigma

3.1.5 Antibodies

Antibodies	Suppliers
Anti-HspB1, monoclonal, mouse	StressMarq
Anti-HspB1, polyclonal, rabbit	Pineda
Anti-HspB2, monoclonal, mouse	Abcam
Anti-HspB3, polyclonal, rabbit	Sigma
Anti-HspB5, monoclonal, mouse	StressMarq
Anti-HspB5, polyclonal, rabbit	Pineda
Anti-HspB6, monoclonal, mouse	Prof. A. Katrukha
Anti-HspB7, monoclonal, rabbit	Abcam
Anti-HspB8, monoclonal, mouse	Prof. A. Katrukha
Anti-mouse IgG coupled HRP, A9044, produced in rabbit	Sigma
Anti-rabbit IgG coupled HRP, A6154, produced in goat	Sigma

3.1.6 Cell strains

<i>E.coli</i> strain	Genotype	Origin
BL21-CodonPlusR (DE3)	F ⁻ ompT hsdS(r _B ⁻ m _B ⁻) dcm ⁺ Tetr	Stratagene
RIL	gal endA Hte [argU proL Camr]	
Mach1	F ⁻ Φ80lacZΔM15 ΔlacX74 hsdR(r _K ⁻ , m _K ⁺) ΔrecA1398 endA1 tonA	Invitrogen
XL1 Blue	endA1 gyrA96(nal ^R) thi-1 recA1 relA1 lac glnV44 F'[::Tn10 proAB ⁺ lacI ^q Δ(lacZ)M15] hsdR17(r _K ⁻ m _K ⁺)	Stratagene

3 MATERIAL AND METHODS

Human cell line	Tissue	Morphology	Disease	Growth media	Origin
A549 CCL-185	lung	epithelial	carcinoma	DMEM supplemented with 4.5 g/L glucose, 2 mM glutamine and 10 % FBS	ATCC
CaCo-2	colon	epithelial-like	colorectal adenocarcinoma	MEME supplemented with 2 mM glutamine, 0.1 mM NEAA, 1 mM sodium pyruvate and 20 % FBS	Sigma
H460 HTB-177	lung/ pleural effusion	epithelial	carcinoma/ large cell lung cancer	RPMI supplemented with 4.5 g/L glucose, 2 mM glutamine and 10 % FCS	ATCC
HEK293	embryonic kidney	Epithelial	-	DMEM supplemented with 4.5 g/L glucose, 2 mM glutamine and 10 % FBS	Sigma
HeLa	cervix	epithelial	adenocarcinoma	DMEM supplemented with 4.5 g/L glucose, 2 mM glutamine and 10 % FBS	Sigma
HepG2 HB-8065	liver	epithelial	Hepaticellular carcinoma	DMEM supplemented with 1.0 g/L glucose, 2 mM glutamine and 10 % FBS	ATCC
K562	bone marrow	lymphoblast	chronic myelogenous leukemia	RPMI supplemented with 4.5 g/L glucose, 2 mM glutamine and 10 % FBS	Sigma
MCF7	mammary gland	epithelial	adenocarcinoma	DMEM supplemented with 4.5 g/L glucose, 2 mM glutamine and 10 % FBS, 0.1 mM NEAA	Sigma
RD CCL-136	muscle	spindle/ large multinucleated	rhabdomyosarcoma	DMEM supplemented with 4.5 g/L glucose, 2 mM glutamine and 10 % FBS	ATCC
SH-SY5Y CRL-2266	bone marrow	epithelial	neuroblastoma	MEME Ham's F12 media 1:1 mix, 2 mM glutamine and 10 % FBS	ATCC

U138MG HTB-16	brain	polygonal	glioblastoma	DMEM supplemented with 4.5 g/L glucose, 2 mM glutamine and 10 % FBS, 0.1 mM NEAA	ATCC
U373MG	brain	pleomorphic/ astrocytoid	glioblastoma/ astrocytoma	DMEM supplemented with 4.5 g/L glucose, 2 mM glutamine and 10 % FBS, 0.1 Mm NEAA	Sigma

3.1.7 Media, buffer and stock solutions

Buffer	Ingredients
Fairbanks A	25 % (v/v) 2-Propanol 10 % (v/v) Acetic acid 0.05 % (w/v) Coomassie Blue R 250
Fairbanks D	10 % (v/v) Acetic acid
Laemmli Sample Loading buffer (5x)	300 mM Tris-HCl, pH 6.8 10 % (w/v) SDS 50 % (v/v) Glycerol 5 % (v/v) 2-Mercaptoethanol
MS Alkylation Buffer	0.05 % (w/v) Bromphenol bue 50 mM Tris-HCl, pH 7.5 2 M Urea 5 mM IAA
MS Digestion Buffer	50 mM Tris-HCl, pH 7.5 5 ng/μl Trypsin 2 M Urea 1 mM DTT
PBS (1x), pH 7.4	8.1 mM Na ₂ HPO ₄ *2H ₂ O 1.76 mM KH ₂ PO ₄ 137 mM NaCl 2.7 mM KCl
PBST, pH 7.4	4 mM KH ₂ PO ₄ 16 mM Na ₂ HPO ₄ * 2 H ₂ O 115 mM NaCl 0.1 % (v/v) Tween-20
SDS-PAGE-Running buffer (10x)	250 mM Tris-HCl 2 M Glycine 1 % (w/v) SDS
Separating gel buffer (4x)	1.5 M Tris-HCl, pH 8.8 0.8 % (w/v) SDS
Stacking gel buffer (2x)	250 mM Tris-HCl, pH 6.8 0.4 % (w/v) SDS
TAE DNA Gel buffer (50x)	2 M Tris-HCl, pH 1 M acetic acid 50 mM EDTA
Transformation and Storage (TSS) Solution	85 % LB ₀ medium 10 % PEG (w/v)

Tris-EDTA (TE) high salt buffer	5 % DMSO (v/v) 50 mM MgCl ₂ (pH 6.5) 50 mM Tris pH 7.4 – 8.4 1 M NaCl
Tris-EDTA (TE) low salt buffer	2 mM EDTA 50 mM Tris pH 7.4 – 8.4 10 mM NaCl
Western Blot Transfer buffer	2 mM EDTA 48 mM Tris-HCl, pH 9.2 39 mM Glycine 20 % (v/v) Methanol

3.1.8 Reagents, kits and enzymes

Reagents, kits, enzymes	Suppliers
Bradford Reagent (5x)	Serva
BsaI	NEB
CutSmart buffer (10x)	NEB
DNA ladder, 1 kB	PeqLab
DNaseI	AppliChem
DPBS	Gibco
DpnI	NEB
Dual Color protein standard III	Serva
Gel Filtration Standard	BioRad
Gel Loading Dye Purple (6x)	NEB
GoTaq Polymerase	Promega
M-PER	ThermoFisher Scientific
MPer Mammalian Protein Extraction Reagent	ThermoFisher Scientific
Polynucleotide kinase (10,000 u/mL)	Promega
Prestained peqGOLD Protein Marker IV	PeqLab
Protein test Mixture 6 protein standard	Serva
Quick Coomassie Stain	Serva
Quick Ligation KitM2200	NEB
T4 DNA Ligase (40,000 u/mL)	Promega
T4 DNA Ligase buffer (10x)	Promega
UlpI (S. cerevisiae ubiquitin-like-specific protease 1)	Dr. Waldemar Preis, TUM
WesternBright™ ECL-Spray	Advansta
Wizard Plus SV Minipreps DNA Purification System	Promega
Wizard SV Gel and PCR Clean-Up System	Promega
XbaI	NEB

3.1.9 Software

Software

Astra 5.3
 CDNN Spectra Deconvolution, Vers 2.1
 ChemStation Agilent Technologies
 Fasta Tools 9.0
 Image J
 ImageQuant LAS 4000
 MagTran
 MaxQuant Version 1.6.0.16
 Microsoft Office 2010
 OriginPro 2017G 64Bit
 PyMol Molecular Visualization
 RawConverter
 SedFit
 Serial Cloner 2.6.1

3.1.10 Online Tools and databases

Online Tool

DichroWeb	http://dichroweb.cryst.bbk.ac.uk/html/process.shtml
EMBL-EBI Clustal Omega	https://www.ebi.ac.uk/Tools/msa/clustalo/
ExpASY Protparam	https://web.expasy.org/protparam/
National Center for Biotechnology Information/ US National Library of Medicine National Institutes of Health (NCBI/PubMed)	https://www.ncbi.nlm.nih.gov/pubmed
NEW ENGLAND BioLabs Tm Calculator	https://tmcalculator.neb.com/#!/main
PROXL – Protein Cross-linking Database	http://proxl-ms.org/
RCSB Protein Data Bank	https://www.rcsb.org/pdb/home/sitemap.do
UniProt Knowledgebase	https://www.uniprot.org/uniprot/

3.1.11 Devices

Device

Company

Amicon Bioseparations Stirred Cells, 50 mL	EMD Millipore
Autoclave Varioclav EP-Z	H+P
Bead Mill MM400	Retsch
Cell Disruption Apparatus Basic Z	Constant Systems
Centrifuges:	
- Avanti JXN-26/ J26 XP; Rotors: JA-10/JA-25.50	Beckman Coulter
- ProteimeLab XL-I; Rotor: AN-50 Ti	Beckman Coulter
- Rotina 420R; Rotor: R10 4770	Hettich
- Tabletop centrifuge 5418 R, Rotor: FA45-18-11	Eppendorf

3 MATERIAL AND METHODS

- Tabletop centrifuge 5418; Rotor: FA45-18-11	Eppendorf
<u>Chromatography systems:</u>	GE Healthcare
- AKTA PURE 25 equipped with	
- U9-L UV-detector	
- F9-R fraction collector	
- Superloops (150 mL, 10 mL, 5 mL)	
Chirascan Circular dichroism spectrometer	Applied Photophysics
Fastblot chamber, semi-dry western blotting	Biometra, Analytik Jena
<u>High performance liquid chromatography System</u>	Shimadzu
- DGU-20A ₃ Degasser	
- SIL-20AC Autosampler	
- LC-20AT Pump	
- SPD-2A UV Detector	
- RF-10A _{XL} Fluorescence Detector	
- Dawn Helios-II MALS Detector	Wyatt Technologies
ImageQuant LAS4000 system	GE Healthcare
Incubator	mytrom
Incubator CO ₂ 150i	Heracell
Magnetic stirrer Heidolph Hei-Standard	Heidolph
<u>Mass spectrometers</u>	
- LTQ Orbitrap XLTM Hybrid Ion Trap MS	ThermoFisher Scientific
- Orbitrap Fusion Tribrid MS	ThermoFisher Scientific
- Ultraflex II MALDI ToF/ToF	Bruker Daltonics
- SYNAPT G2-Si MS	Waters
- Quadrupole LC-MS 6130	Agilent Technologies
Microscope Leica DM IL	Leica Microsystems
Membrane Vacuum Pump	Vacuubrand
pH meter pH538	WTW
Polymax 2040	Heidolph
Power amplifiers EPS 301	amersham pharmacia
Power amplifiers GPS 200/400	Pharmacia
Rotator SB3	Stuart
Savant TM DNA120 SpeedVac TM Concentrator	ThermoFisher Scientific
<u>Scales:</u>	
- BL1500S	Satorius
- SI-4002	Denver Instrument
- SI-234	Denver Instrument
Thermoblock TB 1	Biometra
Thermomixer compact and comfort	Eppendorf
Ultra-low Freezer C760	New Brunswick Scientific
Ultrasonic cleaner USC-T	VWR
Ultrasonic Homogenizer HD2200-UW220	Bandelin Sonopuls
<u>UV-Vis spectrophotometers:</u>	
Ultrospec 1100 pro and 3100pro	Amersham Biosciences
Varian Cary 50 Bio	Agilent
NanoDrop1000	Peqlab
Vortex Genie 2	Scientific Industries
Water bath F12	Julabo

3.1.12 Cuvettes

Cuvettes	Supplier
High Precision Cell Quartz SUPRASIL 10 mm Light Path, 15 Centre <u>CD cuvette</u>	Hallma Analytics
- QS Suprasil glass path length 0.2 mm, chamber volume 120 μ L	Hallma Analytics
- QS Suprasil glass path length 0.5 mm, chamber volume 200 μ L	Hallma Analytics

3.1.13 Columns

Columns	Supplier
Resource Q, 6 mL	GE Healthcare
Superdex200 26/60	GE Healthcare
Superdex200 16/60	GE Healthcare
Superdex75 16/60	GE Healthcare
Q Sepharose Fast Flow, 75 mL and 40 mL	GE Healthcare
Superdex200 Increase 10/300 GL column	GE Healthcare
Superdex200 5/150 GL	GE Healthcare
HisTrap HP, 5 mL and 1 mL	GE Healthcare
HiTrap Phenyl HP, 5 mL	GE Healthcare
HiTrap Q HP, 5 mL	GE Healthcare

3.2 Methods

3.2.1 Molecular biology

Polymerase chain reaction

To amplify DNA fragments of interest standard PCR was performed with the following settings:

Component		Final volume [μL]	
dNTP-Mix (10 mM each)		1	
5'-primer (1 μ M)		2.5	
3'-primer (1 μ M)		2.5	
template DNA (10 ng/ μ L)		1	
GoTaq buffer (5x)		10	
GoTaq Polymerase (5u/ μ L)		0.5	
nuclease free H ₂ O		32.5	

Cycle	Step	Temperature [$^{\circ}$C]	Time [sec]
1x	Initial denaturation	95	120
30x	Denaturation	95	30
	Annealing	T _m – 5	30
	Extension	72	60
1x	Final extension	72	300
1x	Soak	4	indefinite

After PCR, the size of DNA inserts was validated by agarose gel and inserts of correct size were purified from the gel and digested with corresponding restriction enzymes for 3 h at 37°C. The ligation of the digested inserts and corresponding digested plasmid was performed following the manufacturer instructions from Quick Ligation Protocol (M2200) from NEB.

Agarose gel electrophoresis

To analyze DNA samples by size agarose electrophoresis was conducted. Therefore, samples were mixed with gel loading dye purple (1:6). 1% (w/w) Agarose was dissolved in 100 mL 1xTAE buffer and 3 μ L of stain clear G was added. Depending on the DNA construct size electrophoresis was performed for 15 to 30 min at 120 V. Afterwards DNA bands were detected under UV-light.

DNA purification

If necessary, PCR products were purified from agarose gels or directly from PCR reaction following the Wizard SV Gel and PCR Clean-up System (Promega) protocol.

Site directed mutagenesis

Point mutations were introduced following the Q5 Site-directed mutagenesis protocol and the NEBaseChanger tool from NEW ENGLAND BioLabs (NEB). In brief, Q5 polymerase was used for the PCR and DNA product of successfully performed PCR was treated with Kinase-Ligase-

DpnI (KLD) enzyme mix to eliminate template DNA and ligate the insert into the plasmid. KLD digestion was incubated for 1h at room temperature.

Component	Volume [μL]
PCR product	2
T4 DNA ligase buffer (10x)	1
T4 DNA Ligase (40,000 u/mL)	0.5
Polynucleotide kinase (10,000 u/mL)	0.5
DpnI (10,000 u/mL)	0.5
Nuclease free H ₂ O	5

The entire ligation product was transformed into heat competent XL1 Blue or Mach1 *E. coli* cells. DNA of obtained colonies was enriched and purified for Sanger sequencing at Eurofins Genomics (Erding) or GENEWIZ (Leipzig).

3.2.2 Protein expression

Preparation of chemical competent E. coli

Preculture was inoculated with cells from a glycerol-cryo-stock of the desired *E. coli* strain in LB₀ and cells were incubated at 37°C overnight at 250 rpm. Subsequently a fresh subculture was prepared with a 1:100 dilution in LB₀ and incubated at 37°C and 220 rpm until OD₆₀₀ reached 0.5. Flask was immediately cooled down on ice for 20 min and cells were collected by centrifugation at 5000 rpm (JA-10) for 15 min at 4°C. Pellet was resuspended in 10 mL ice-cold TSS solution and aliquoted in 200 μ L fractions. Competent cells were flash frozen in liquid nitrogen and stored at -80°C until further use.

Transformation of DNA in chemical competent E. coli

To transform plasmid DNA (1 μ L) or ligation products (10 μ L) the desired amount of DNA was incubated on ice with 200 μ L of chemically competent cells for 20 min. The mixture was heat-shocked for 1 min at 42°C, cooled down for 2 min on ice and 1 mL LB₀ was added afterwards. For regeneration cells were incubated at 37°C for 1 h while gentle shaking. Subsequently cells were spun down for 5 min at 5000 rpm (FA45-18-11) and medium was discharged. Cells were resuspended in 200 mL LB₀ and plated on LB₀-Agar plates with 100 μ g/mL ampicillin or 35 μ g/mL kanamycin antibiotic depending on the involved resistance marker or directly transferred into 50 mL LB₀ containing desired antibiotic.

Small scale protein expression test

To test different expression conditions, transformed *E. coli* BL21 cells were incubated overnight in 50 mL LB₀ including corresponding antibiotic at 37°C and 180 rpm. Multiple test expression cultures were inoculated by 1:10 dilution of the preculture in 50 mL LB₀ with corresponding antibiotics and incubated at 37°C and 180 rpm until an OD₆₀₀ of 0.8 was reached. Prior to 1 mM IPTG addition flask were chilled on ice for 20 min and afterwards further incubated at different temperatures (RT, 25°C, 30°C, 37°C) for protein expression. 1 mL samples for analysis were taken before IPTG addition, after 1 h, 4h and overnight. Cells were collected by centrifugation at 5000 rpm (FA45-18-11) for 5 min at RT and cell pellets were resuspended in 200 μ L corresponding TE buffer. 10 μ L whole lysate sample was taken. Then 50 vol-% glass beads were

3 MATERIAL AND METHODS

added and cell lysis was performed by using the bead mill 3x 2 min at 30 s⁻¹ with 2 min breaks to cool down the sample again. To separate cell debris from soluble protein fraction samples were centrifuged for 10 min and 14,000 rpm (FA45-18-11) at 4°C. A 10 µL sample of the soluble protein fraction was taken and SDS-PAGE was performed. By comparing total protein expression and soluble protein expression overtime, the optimal expression condition was selected.

Large scale protein expression

For recombinant protein production, transformed E. coli BL21 cells were incubated overnight in 50 mL LB₀ including corresponding antibiotic at 37°C and 180 rpm. Expression culture was inoculated by 1:200 dilution of the preculture in 2 L LB₀ with corresponding antibiotics and incubated at 37°C and 180 rpm until an OD₆₀₀ of 0.8 was reached. Dependent on optimal expression conditions determined by expression tests 2L flasks were cooled down to desired temperature before addition of 1 mM IPTG for expression induction and incubated for desired time at designated temperature. Afterwards cells were collected by centrifugation 5000 rpm (JA-10) for 12 min at 4°C. If proteins without tag were expressed cell pellets were resuspended in TE low salt buffer at suitable pH. Resuspended pellets were flash frozen in liquid nitrogen and stored at -20°C until purification was performed.

Construct	Theoretical pI with/without SUMO	Expression conditions	Resuspension buffer
His ₆ -SUMO-αB delta20	5.97/6.31	1 mM IPTG, overnight, RT	TE buffer, 7.4
αB delta28	-/6.31	1 mM IPTG, overnight, 30°C	TE buffer, 7.7
His ₆ -SUMO-αB delta40	6.23/8.04	1 mM IPTG, 4 h, RT	TE buffer, 7.8
His ₆ -SUMO-αB delta51	6.12/6.98	1 mM IPTG, overnight, RT	TE buffer, 7.7
αB delta NTR	-/6.98	1 mM IPTG, overnight, RT	TE buffer, 8.3
αB R11K	-/6.76	1 mM IPTG, overnight, 30°C	TE buffer, 8.3
αB R22K	-/6.76	1 mM IPTG, overnight, 30°C	TE buffer, 8.3
αB R50K	-/6.76	1 mM IPTG, overnight, 30°C	TE buffer, 8.3
αB R11KR22kR50K	-/6.76	1 mM IPTG, overnight, 30°C	TE buffer, 8.3
αB S35K	-/7.15	1 mM IPTG, overnight, 30°C	TE buffer, 8.3
αB S45K	-/7.15	1 mM IPTG, overnight, 30°C	TE buffer, 8.3
αB wildtype	-/6.76	1 mM IPTG, overnight, 30°C	TE buffer, 8.3
Hsp27	-/5.98	1 mM IPTG, 4 h, 30°C	TE buffer, 7.8, 100 mM NaCl, 1 mM PMSF, 2 mM DTT
Hsp20	-/5.95	0.5 mM IPTG, overnight, 30°C	TE buffer, 8.0, 100 mM EDTA, 0.5 mM PMSF, 14 mM β-Me
His ₆ -SUMO-Bag3	6.33/6.69	1 mM IPTG, overnight, 30°C	50 mM Tris, pH 7.6, 300 mM NaCl, 20 mM imidazole
His ₆ -SUMO-Bag3-IPV	7.39/9.63	1 mM IPTG, overnight, 30°C	50 mM Tris, pH 7.6, 300 mM NaCl, 20 mM imidazole

3.2.3 Protein purification

Resuspended cell pellets were thawed at room temperature and cell lysis was conducted using a mechanical cell disrupter with 2.2 kbar followed by addition of 1:100 protease inhibitor G and DNase I. In order to separate cell debris from soluble protein fraction lysate was centrifuged at least 45 min and 18,000 rpm (JA-25.50) at 4°C.

Hsp20

Ammonium sulfate (AS) precipitation (0-20 %) of the soluble protein fraction was performed on ice. After 30 min of equilibration the protein solution was centrifuged for 45 min and 18,000 rpm (JA-25.50) at 4°C. Pellet was resuspended in low salt buffer (20 mM Tris, pH 7.6, 10 mM NaCl, 0.1 mM EDTA, 0.1 PMSF, 14 mM β -Me) and applied on a HiTrap Q (5 mL) column with a linear gradient in 25 CV from 10-400 mM NaCl. Fractions containing the protein of interest were defined by SDS-PAGE and dialyzed in no AS buffer (20 mM Na-PB, pH 7.0, 10 mM NaCl, 0.1 mM EDTA, 0.1 mM PMSF). Before protein solution was applied to a HiTrap Phenyl HP column (5 mL) 300 mM AS were added. A linear gradient from 300 mM to 0 mM AS in 25 CV was used to separate the protein of interest from contaminations. Afterwards fractions of interest were again dialyzed in low salt buffer and again applied to a HiTrap Q (5 mL) column. Subsequently fractions containing the protein of interest were concentrated by using a stirred vacuum cell (50 mL) equipped with a 3 kDa filter membrane and loaded on to a superdex75 16/60 equilibrated in 1x PBS pH 7.4. Finally, fractions containing the protein of interest were combined and concentrated up to a concentration of 1-2 mg/mL.

Hsp27

Ammonium sulfate (AS) precipitation (0 - 25 %) of the soluble protein fraction was performed on ice. After 1 h of equilibration the protein solution was centrifuged for 1 h and 20,000 rpm (JA-25.50) at 4°C. The supernatant was again precipitated by using AS (25 – 50 %) and centrifuged retaining the settings. The obtained pellet was resuspended in low salt buffer (10 mM Tris, pH 8.5, 20 mM NaCl, 1 mM DTT, 0.2 mM PMSF, 0.1 mM EDTA) and additionally dialyzed against this buffer overnight at 4°C. Protein solution was applied to Q Sepharose column (75 mL) after a centrifugation step of 45 min and 18,000 rpm (JA-25.50) at 4°C to remove insoluble parts. The elution was induced with a linear gradient of 0 – 300 mM NaCl in 8 CV. Fractions containing the protein of interest were pooled and concentrated by using a stirred vacuum cell (50 mL) equipped with a 3 kDa filter membrane and loaded on to a superdex20 26/60 equilibrated in 1x PBS pH 7.4 and 0.1 mM PMSF. Finally, fractions containing the protein of interest were combined and concentrated up to a concentration of 1 - 5 mg/mL.

α B-crystallin

The protein solution was directly applied to a Q Sepharose column (75 mL) equilibrated in low salt TE buffer at pH 8.3. The elution was induced by a linear gradient from 10 – 500 mM NaCl in 5 CV. Fractions containing the protein of interest were pooled and concentrated by using a stirred vacuum cell (50 mL) equipped with a 3 kDa filter membrane. The protein solution was loaded on to a superdex200 26/60 column equilibrated in 1x PBS pH 7.4. Finally, fractions containing the protein of interest were combined and concentrated up to a concentration of 5 - 20 mg/mL.

His₆-SUMO- α B-crystallin variants

In order to sustain the His₆-tag to protect the NTR from proteolytic degradation the purification was started with a Q Sepharose column (75 mL) in TE buffer with an appropriate pH and a linear gradient from 10 – 300 mM NaCl. Fractions of interest were pooled, concentrated and applied to a Superdex200 16/60 in 1x PBS pH 7.4. Nearly pure fractions were collected and dialyzed in low imidazole buffer (40 mM Na-PB, pH 8.0, 300 mM NaCl, 10 mM imidazole). A HisTrap HP (5 mL) was performed with a four-step elution of 20 mM, 40 mM, 300 mM and 500 mM imidazole. The protein of interest eluted in the 300 mM fraction and was collected for SUMO protease treatment to cleave off the His₆-SUMO-tag in low imidazole buffer overnight at 4°C. Afterwards another HisTrap HP (5 mL) column run was performed to separate His₆-SUMO-tag from the protein of interest. If necessary, a resource Q (5 mL) was additionally used to eliminate further contaminations. Therefore, the protein solution was dialyzed back in low salt TE buffer with adjusted pH for the pI of the protein without His₆-SUMO-tag. A linear gradient was used from 10 - 300 mM NaCl in 25 CV for elution. Fractions contain the protein of interest were collected, concentrated up to 0.5 - 2 mg/mL and dialyzed in 1x PBS pH 7.4. Aliquots were flash frozen and stored at -80°C until further usage.

His₆-SUMO-Bag3 and His₆-SUMO-Bag3-IPV

Bag3 and its IPV mutant were expressed and purified from a pE-SUMOpro plasmid to increase the expression yield. The cell disruption and the separation of the soluble protein fraction were performed as described above and the protein solution was directly applied on a 5 mL HisTrap HP column. After a washing step with 40 mM imidazole the His₆-tagged protein was eluted by increasing imidazole concentration to 300 mM. Fractions containing the protein of interest were dialyzed against 5 mL resuspension buffer overnight at 4°C with Ulp1 protease added in order to cleave off the His₆-SUMO-tag. The reverse HisTrap was performed under the same conditions. The flow through, containing the protein of interest, was collected and the column was regenerated with 500 mM imidazole. The protein samples were again dialyzed overnight at 4°C against 5 L low salt buffer (20 mM Hepes, pH 7.6 (Bag3) or 8.0 (Bag3 IPV) 10 mM NaCl, 5 mM DTT). Afterwards a resource Q (Bag3) or S (Bag3 IPV) was performed. In both cases the protein of interest interacted with the column and was eluted by increasing the NaCl concentration using a linear gradient from 10 – 500 mM NaCl in 25 CV. Fractions containing the protein of interest were collected and concentrated to 5 mL and applied on a superdex200 16/60 in 1x PBS pH 7.4. The pure protein fractions were collected, concentrated to 1 – 2 mg/mL, flash frozen in liquid nitrogen and stored at -80°C until further usage.

3.2.4 Protein biochemistry

Preparation of recombinant protein samples

In general proteins were handled on ice if not designated otherwise. After defrosting, all recombinant protein samples were centrifuged for 10 min at 14,000 rpm (FA45-18-11) at 4°C to separated protein aggregated and artefacts from the protein of interest. Prior to any analysis of sHsps a stock of appropriate concentration was pre-incubated at increased temperatures to ensure formation of their oligomeric structure. For hetero-oligomer investigations proteins were incubated

30 min at 37°C and afterwards 1 h at 42°C while for α B NTR project purposes all samples were incubated for 2 h at 37°C.

SDS-PAGE

In principle SDS-PAGE was performed according to the protocol of Laemmli 1970 (215). Due to the protein molecular mass range between 15 and 32 kDa 12 or 15 % acrylamide for separation gel and 5 % acrylamide for stacking gel were used. Gel samples were treated with 5x Laemmli sample loading buffer and heated for 5 min at 95°C prior to loading. The electrophoresis was carried out at 30 mA per gel for 45 to 50 min at room temperature in 1x SDS-PAGE running buffer. For purification purpose gels were stained with Coomassie R250 using Fairbanks A for staining and Fairbanks D for destaining.

HPLC

Analytical size exclusion chromatography was performed at room temperature using a Shimadzu HPLC system equipped with a superdex200 increase 10/300 GL column or two stacked superdex200 5/150 columns equilibrated in 1x PBS pH 7.4 with 1 mM DTT added freshly every day if not noted differently. All buffers were sterile filtered with a 0.22 μ m filter and degassed before usage. For calibration the BioRad molecular mass standard was used according to the manufacture protocol and 5 μ L were applied onto the column.

In vitro

For *in vitro* analysis of recombinant protein samples a superdex200 increase 10/300 GL column was used with a flow rate of 0.5 mL/min. Usually 50 μ L of a pre-incubated 10 μ M protein sample was applied after a 10 min 14.000 rpm (FA45-18-11) 4°C centrifugation step to remove any aggregates or fine particles that could damage the column. In case of collection 500 μ L were fractionated starting after the void volume of 10 mL.

Ex vivo

For size distribution analysis of lysate samples *ex vivo* two stacked superdex200 5/150 GL columns were used with a flow rate of 0.2 mL/min. Different human cell lines were cultivated in a T75 flask up to 90 % confluency. Prior to cell lysis medium was removed and cells were washed with a sufficient amount of cold 1x PBS pH 7.4. Cells were scraped off in 400 μ L 1x PBS pH 7.4 1 mM DTT in presence of 1:100 protease inhibitor Mix M and phosphatase inhibitor cocktail 2 and 3. Mechanical lysis was induced by passing the cells 5-6 times through a 0.6 mm needle. Cell debris was removed by centrifugation at 14,000 rpm (FA45-18-11) for 10 min at 4°C. Protein concentration of cleared cell lysate was determined by Bradford assay (216) and 0.5 mg were loaded with a volume of about 300 – 500 μ L. In case of collection 300 μ L were fractionated starting after the void volume of 1.5 mL.

TCA-Precipitation

For further analysis of HPLC fractions proteins were precipitated by treating the samples with 1:10,000 10 % NaDoc for 30 min on ice followed by overnight incubation with 10 % TCA at 4°C. Afterwards proteins were pelleted by centrifugation for 10 minutes at 16900 g and pellets were dissolved in 1x Laemmli sample loading buffer diluted in 1 M Tris pH 9.0 for pH neutralization.

Western blot

To visualize specific and/or low abundant proteins on a western blot conventional SDS-PAGE was performed as described above and the gel was equilibrated in WB transfer buffer for 10 min prior to the transfer. Six layers of blotting paper and the nitrocellulose membrane itself were soaked in transfer buffer for a moment before the gel-membrane assembly was arranged in a semi-dry fastblot chamber. Transfer was performed for 2 h at 1.5 mA/cm². The membrane was blocked by 30 min incubation in 1x PBST and 5 % milk powder. After blocking the membrane was incubated overnight with primary antibodies (Pineda antibodies in 1:5,000 dilution and all other antibodies in 1:10,000 dilution) at 4°C. Then the membrane was washed three times with PBST for 10 min and incubated with secondary α -mouse or α -rabbit IgG HRP-coupled antibodies (1:20,000 dilution). After three additional 10 min washing steps bands were visualized with WesternBright ECL Spray (Advansta) and ImageQuant LAS 4000 chemiluminescence detection system (GE Healthcare).

SEC-MALS

Size exclusion chromatography coupled to multi-angle-light-scattering detector was performed using a Shimadzu HPLC system using a superdex200 increase10/300 GL column equilibrated in 1x PBS pH 7.4 with 1 mM DTT added freshly every day if not noted differently. All buffers were sterile filtered with a 0.1 μ m filter and degassed before usage. MALS detector was calibrated by using BSA with approximately 1 mg/mL and 50 μ L injection volume. For investigations protein samples of 50 μ M with 50 μ L injection volume were applied. All runs were carried out at room temperature with a flow rate of 0.5 mL/min.

Crosslinking of sHsp to substrate proteins

All used α B-crystallin variants were pre-incubated as described before for 2 h at 37°C. For crosslinking experiments 50 μ M MDH or 12.5 μ M CS was incubated with 50 μ M α B-crystallin variants in 40 μ L total volume 1x PBS pH 7.4 for 90 min at 45°C. Subsequently, crosslinking was started by addition of 3 mM Disuccinimidyl glutarate (DSG) final concentration from 30 mM stock solution solved in DMSO. Crosslinking was performed for 20 min at 45°C and stopped afterwards immediately with 50 mM Tris. Samples were flash frozen in liquid nitrogen and stored at -20°C until further MS preparation.

Co-Immunoprecipitation

Human cell lines were grown in appropriate media up to approximate 90 % confluence, washed with 1x PBS, and lysed with M-PER cell lysis reagent according to the manufacturer's protocol. About 1 mg lysate, determined by Bradford assay, was used for each co-IP experiment and incubated with 1 μ g of specific antibody for 1 h at 4°C. Due to the low expression level of HspB5 in U138MG cells lysate was pre-incubated for 1 h with 10 μ g recombinant produced HspB5. After addition 20 μ L of protein G sepharose fast flow beads and further incubation for 2 h at 4°C, the sHsp complexes were precipitated by centrifugation for 1 min and 500 rpm (FA45-18-11) at 4°C. Precipitate was washed three times with cold PBST and eluted in 30 μ L 0.5 M glycine pH 3.0. Western blot was performed as described above. About 100 ng recombinant protein served as positive control and Prestained pepGOLD Protein Marker IV (Peqlab) was used as molecular mass standards.

Analysis of sHsp expression in human cell lines

Human cell lines were grown in appropriate media up to approximate 90 % confluence, washed with 1x PBS, and lysed with M-PER cell lysis reagent according to the manufacturer's protocol. For qualitative analysis 50 µg of total protein lysate was loaded on a SDS-PAGE followed by western blotting as described above. To quantify the amount of sHsps in HeLa, MCF7, U373MG, U138MG and H460 we loaded variable amounts of purified sHsps for calibration and a defined amount of cell lysate. The loading of equal amounts of lysate was ensured by total protein concentration determination using Bradford reagent. After SDS-PAGE followed by western blotting we quantified integrated densities of all bands using ImageQuantTL software (GE Healthcare). Calibration curves were accepted with $r^2 \geq 0.95$. Standard conditions (ST) are defined by 37°C and 5 % CO₂ whereas heat stress conditions (HS) equal 2 h at 42°C without supplemented CO₂.

3.2.5 Spectroscopic analysis***Quantification and qualification of DNA samples***

2 µL of DNA sample was measured in a NanoDrop2000 in order to determine the concentration and to check the quality of the sample. A 230:260:280 ratio of 1:1.8:1 for DNA samples was approved to be of high quality.

Protein concentration determination of recombinant proteins

Protein concentration for recombinant proteins was determined by their specific absorbance at 280 nm. The absorption signal at 280 nm is mainly based on aromatic amino acids like Trp and Tyr in proteins. Dependent on the amino acid composition a molar extinction coefficient can be calculated which can be used to quantify the protein of interest applying the Beer-Lambert law:

$$A_{\lambda} = \varepsilon_{\lambda} * c * d \quad (1)$$

A_{λ} = absorbance at specific wavelength; c = concentration [M]; d = optical path length [cm]; ε_{λ} = molar attenuation coefficient at specific wavelength [$M^{-1}cm^{-1}$]

The extinction coefficients were calculated using the ExPASy protparam online tool (217). The absorbance was determined in a NanoDrop2000 or Ultrospec1100 pro.

Protein concentration determination of mixed protein samples

To determine protein concentration of mixed protein samples like lysates a colorimetric Bradford assay was used. The assay bases on the shift of the Coomassie absorption maximum from 470 nm to 595 nm after protein binding at acidic pH (216,218). A calibration curve was conducted using BSA as standard protein and the assay procedure was performed according to the manufactures manual (Serva).

Circular dichroism spectroscopy

To characterize secondary protein structure composition and thermal stability CD spectroscopy was used. Here, the protein sample is exposed to circular polarized light. The differences in absorption of left- and right-handed light, induced by chiral protein components, are detected. The

measured ellipticity can be calculated to mean residue ellipticity which provides information about the secondary structure proportions.

$$\theta_{MRW} = \frac{\theta * 100}{d * c * N_{aa}} \quad (2)$$

Θ_{MRW} = mean residue ellipticity [deg cm² dmol⁻¹]; Θ = measured ellipticity [deg]; d = path length [cm]; c = concentration [M], N_{aa} = number of amino acids

The ellipticity was measured in a Chirascan spectropolarimeter in a QS Suprasil glass path length 0.2 mm or 0.5 mm cuvette with a protein concentration of 10 μ M if not indicated otherwise.

Settings for CD spectrum

Measured signal based on	Absorbance [millidegrees]
Temperature	20°C
Wavelength range	195 – 260 nm
Bandwidth	1.0 nm
Time-per-point	0.25 s
Repeats	10x

Settings for thermal transition

Temperature range	20 – 95 °C
Temperature tolerance	0.2°C
Temperature steps	1°C
Rate	1°C/min

The deconvolution of the recorded CD spectra in the different amounts of secondary structure types was performed by using the CDNN Spectra Deconvolution software.

ANS binding

ANS fluorescence measurements were carried out on a Fluoromax-4 spectrofluorometer in a 25°C temperature-controlled cell holder, using a 2 mm x 10 mm path length cuvette. ANS binding was monitored by exciting the sample at 370 nm and recording the emission from 400 to 600 nm. In this case, 10 μ M of each protein sample was incubated with 100 μ M ANS in PBS for 2 h at room temperature protected from light before recording the spectra.

Settings

Emission wavelength	400 - 600 nm
Excitation wavelength	370 nm
Increment	1 nm
Integration time	0.5 s
Temperature	25°C

Subunit exchange kinetics followed by using FRET

For a fluorescence resonance energy transfer (FRET) system a donor chromophore and an acceptor chromophore are required. The energy transfer between the both is inversely proportional to the

sixth power of the distance between donor and acceptor (3). Therefore, this method is highly sensitive to small changes in distance and can be used to track association and dissociation.

$$E = \frac{1}{1 + \left(\frac{r}{R_0}\right)^6} \quad (3)$$

To analyze the subunit exchange within α B oligomers, two separate batches were labeled at the mutated position S153C with two different Alexa fluorophores Flour350 and Flour488. 1 μ M of a 1:1 ratio of each labeled α B batch was mixed and incubated for 4 h at 37°C to reach equilibrium in oligomer distribution. Subunit exchange was then monitored by recording fluorescence spectra from 380 – 600 nm with an excitation wavelength of 375 nm.

Settings

Data interval	1 nm
Scan speed	200 nm min ⁻¹
Sensitivity	Medium
Response	1 s
Excitation bandwidth	2.5 nm
Emission bandwidth	5 nm

In case of α B mutants the subunit exchange was measured indirectly by addition of 40 μ M unlabeled mutant to the preformed, labeled 1:1 α B protein. The subunit exchange was then recorded overtime at 37°C with an excitation wavelength of 375 nm and a constant emission wavelength of 440 nm. All samples were incubated for 3 h at 37°C separately before measurements for temperature equilibration.

Settings

Time range	0-180 min
Data interval	1 nm
Sensitivity	Medium
Response	2 s
Excitation bandwidth	2.5 nm
Emission bandwidth	5 nm

3.2.6 Functional assays

Activity assay using model substrates

Thermal aggregation of malate dehydrogenase (MDH, 2 μ M), glyceraldehyde 3-phosphate dehydrogenase (GAPDH, 1 μ M), or citrate synthase (CS, 1 μ M) was monitored at 45°C in 1x PBS pH 7.4 containing 1 mM DTT. To determine the chaperone activity of isolated sHsp or hetero-oligomers, sHsp were added to the reaction mix prior to incubation at 45°C. Concentrations of sHsp in 1:1 ratio assays were as follows: 0.5 or 0.25 μ M (per monomer) in MDH aggregation assays, 4 μ M – in GAPDH aggregation assays, and 2.0 or 4.0 μ M – in CS aggregation assays. Chemically induced aggregation of insulin (40 μ M) was initiated by an addition of 20 mM DTT and incubation at 37°C, concentration of sHsps in this assay was 4.0 μ M. Aggregation processes were monitored for 60 to 90 min following the apparent increase of light scattering induced by

substrate unfolding, recording the absorbance at 360 nm in a Cary 50 UV/VIS spectrophotometer equipped with a temperature-adjustable cuvette holder. To estimate the chaperone activity of isolated sHsps or hetero-oligomers the light scattering values at the end point (60 or 90 min) were normalized to the level of spontaneous aggregation of the model substrate in the absence of sHsp. At least three measurements were averaged and processed if necessary by applying Savitzky-Golay smoothing filter. To estimate the chaperone activity of the respective sHsps, the endpoint scattering signal in the respective sample was normalized in comparison to the respective endpoint value of spontaneous aggregation (without sHsp addition) which was set to one. The modulation of chaperone activity was achieved by subtracting these normalized values from one.

Theoretical activity values of hetero-oligomers are defined as the sum of sHsp control activity of both single homo-oligomers. At the end modulation values were calculated by subtracting theoretical activity values from measured activity values. Hence, a negative modulation value refers to a higher activity of homo-oligomers whereas positive modulation values refer to a higher activity of hetero-oligomers.

Substrate-sHsp crosslinking

For thermal aggregation 50 μM sHsp and 50 μM MDH were incubated in 1x PBS pH 7.4 for 90 min at 45°C. 12.5 μM sHsp and 50 μM CS were used for CS respectively. Crosslinking was induced by addition of 3 mM Disuccinimidyl glutarate (DSG) and performed at 45°C for 20 min. The reaction was stopped by addition of 50 mM Tris. 10 μl of each sample were prepared with Laemmli for SDS-PAGE analysis. The remaining sample was flash frozen in liquid nitrogen and stored at -20°C until MS preparation was performed.

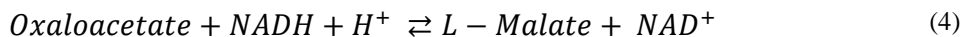
Activity assay using human cell lysate

HEK293 cells were grown up to 90-95 % confluence, washed with DPBS, detached from the flask by trypsinization, pelleted, and mechanically lysed in 1x PBS buffer pH 7.4 with 1 mM DTT in presence of 1:100 protease inhibitor Mix M and phosphatase inhibitor cocktail 2 and 3. Mechanical lysis was induced by passing the cells 5-6 times through a 0.6 mm needle. Cell debris was removed by centrifugation at 14,000 rpm (FA45-18-11) for 10 min at 4°C. Protein concentration of cleared cell lysate was determined by Bradford assay. Cleared cell lysate was depleted for ATP by hexokinase treatment and stored at -80°C. 40 μg of HEK293 cell protein was incubated for 90 min at 45°C without or with addition of 2.0 μM isolated sHsp or pre-formed hetero-oligomers in 1x PBS pH 7.4 containing 1 mM DTT. After heat shock, samples were centrifuged to separate insoluble proteins at 14,000 rpm (FA45-18-11) for 10 min and 4°C. Pellets were washed twice with ice-cold PBS, then dissolved in 1x Laemmli buffer, and analyzed by SDS-PAGE using SERVAGel TG PRiME 4 – 20 %. To generate a more homogeneous background gels were stained with Quick Coomassie Stain instead of using Fairbanks staining. The average amount of insoluble proteins out of at least three experiments was quantified by densitometry using ImageQuantTL software.

MDH refolding assay

Thermal aggregation of 1 μM MDH was performed in presence of 2 μM sHsp at 46°C for 45 min in 20 mM Hepes, pH7.4, 50 mM KCl, 5 mM MgCl₂, 1 mM TCEP. Afterwards the samples were

centrifuged at 4°C for 2 min at 14,000 rpm (FA45-18-11) to remove any big aggregates. Then the samples were mixed 1:1 with a chaperone mix, consisting of 20 µM Hsc70, 4 µM Hdj, and 10 mM ATP. The refolding was performed for 4-5 hour at 30°C. The reactivation was monitored by NADH+H⁺ signal decrease during MDH supported conversion of oxaloacetate to L-malate.



Therefore, 190 µl assay buffer (20 mM Hepes, pH7.4, 50 mM KCl, 5 mM MgCl₂, 1mM TCEP, 0.5 mM Oxaloacetate, 0.1 mM NADH) and 2.5 µl sample were mixed and measured in a Cary50 at 340 nm for 50 min. Endpoint values after 50 min were normalized to native MDH activity and plotted against refolding time. As controls native MDH and sHsp-substrate without Hsp70/40-system were always performed simultaneously.

3.2.7 Transmission electron microscopy

Prior to staining of isolated sHsps or hetero-oligomers were incubated for 10 min at 45°C. 5 µl samples were adsorbed for 30 seconds onto carbon coated grids (glow discharged). Excess protein solution was blotted off and samples were washed with 20 µl water and stained with 5 µl of a 1 % uranyl acetate solution. Micrographs were recorded at 0.6 - 0.8 µm defocus at a nominal magnification of 50k either on a JEOL JEM 100CX or a JEM 1400 plus transmission electron microscope operating at 100 kV or 120 kV respectively. Micrographs on the JEM 1400plus microscope were collected with a JEOL Ruby CCD camera with a pixel size of 0.332 nm/px, while electron micrographs from the JEM 100CX were digitized using a FlexTight X5 scanner resulting in a final pixel size of 0.169 nm/px. For size distributions, ~10,000 particles were selected semi automatically from micrographs using Eman2 (219). These particles were bandpass filtered, centered and normalized with IMAGIC5 (220), followed by multivariate statistical analysis (MSA). Only Eigenvectors indicating size differences within the dataset were used for classification into different classes with an average of 30 particles per class. The Ferret of the class averages was measured with ImageJ (221).

Transmission electron microscopy experiments were performed by Carsten Peters (Center for Integrated Protein Science and Department Chemistry, TUM).

3.2.8 Mass spectrometry

Hydrogen Deuterium Exchange MS

HDX-MS experiments were performed as described before (222,223). In brief, protein samples were measured with a concentration of 30 µM in 1x PBS pH 7.4 followed by 1:20 dilution in deuterium oxide and incubation at 20°C for 10 s, 1 min, 10 min, 30 min, and 2 h to allow hydrogen deuterium exchange. The labeling reaction was stopped and samples were denatured by 1:1 dilution in 200 mM Na₂HPO₄, 200 mM NaH₂PO₄, 250 mM TCEP, 3 M GdnCl, pH 2.2) at 1°C. In order to reduce digestion efficiency and time, the on column pepsin digestion was conducted at 4°C with an increased flowrate of 300 µl/min. Subsequently, the peptides were trapped on a C₁₈ column at 10°C. In order to minimize back exchange trapping and chromatographic separation were performed at 0°C. MS analysis was conducted with an ESI-TOF and before fragmentation by MSE

and mass detection in resolution mode, the peptide ions were additionally separated by drift time within the mobility cell. Obtained data were processed with Waters Protein Lynx Global Server PLGS (version 3.0.3) and DynamX (version 3.0).

Crosslink MS

Cross linked samples were precipitated by Wessel-Flügge precipitation (224), the obtained pellet was resuspended in 25 μ L MS digestion buffer and incubated for 2 h at 25°C. Subsequently, 100 μ L of MS alkylation buffer were added and overnight incubation at 25°C while 450 rpm shaking was performed. The reaction was quenched with 12.5 μ L 10 % formic acid (FA) to a final FA concentration of 1 %. The samples were desalted using self-packed StageTips with double C layer. The stage tips were equilibrated by washing once with 70 μ L MeOH and three times with 70 μ L 0.5 % FA using centrifugation steps at 1,000 g in between without letting the C₁₈ material run dry. Then, the samples were loaded and washed again three times with 70 μ L 0.5 % FA. The elution was performed using two times 30 μ L of 80 % ACN, 0.5 % FA. The samples were dried completely in a SpeedVac concentrator and stored at -80°C. Directly before MS measurement, samples were thawed and resuspended in 24 μ L 0.1 % FA by pipetting up and down and a following ultrasonication step for 15 min in a ultrasonic bath USC-T. The dissolved samples were loaded to a 0.22 μ m centrifuge filter and centrifuged two times at 1,377 g for 2 min. 1 μ L protein sample was injected for each measurement and a linear gradient from 5 – 45 % ACN in 33 min followed by a step elution at 90 % ACN for 10 min on a C₁₈ column to separate the different peptides.

The measurements were performed by Katja Bäuml (Chair of Organic Chemistry II, Department Chemistry, TUM).

Crosslink MS data were converted from .raw-files to .mzXML-files by using the RawConverter software. Afterwards crosslinks were identified with Kojak Software. An example of a utilized configuration file and database are attached in the appendix K and L. To verify the obtained hits, the percolator software was applied. To upload the generated .xml-percolator-files in the RPOXL online tool these files need to be converted into a different .xml-file by using the kojak2PROXLXML converter software. Then files can be uploaded in PROXL for visualization and further evaluation.

Full length LC-MS

An electron spray ionization LC-MS Quadrupole 6130 mass spectrometer was used for protein full length mass determination. Therefore, samples of 20 μ L of 0.1 mg/mL were prepared in 1x PBS pH 7.4 with or without 1 mM DTT. A linear gradient was applied from 5 – 50 % ACN in 15 min to separate the protein of interest from potential degradation products on a C₄ column. 4 μ L protein sample was injected for each measurement. Obtained m/z data were exported from ChemStation software to MagTran (225) for charge state deconvolution to molecular mass and integration of peaks of interest.

Peptide Fingerprint MS

By using a Matrix-Assisted-Laser-Desorption Ionization Imaging coupled to a time-of-flight detector mass spectrometer (MALDI-TOF-MS) a peptide fingerprint of purified recombinant

proteins was measured to proof the correctness of the protein being present. Therefore, protein samples were cut out of a SDS-PAGE. Pellets were then washed two times with 100 μL 10 mM NH_4HCO_3 for 10 min and once with 100 μL acetonitril- 10mM NH_4HCO_3 (1:1) for 10 min. Reduction of the samples were achieved by addition of 100 μL of 80 mM DTT, 0.5 mM GdnCl, 0.8 mM EDTA and 0.1 mM Tris pH 8.2 for 30 min at 37°C. 10 μL of 0.5 M Indol-3-acetic-acid (IAA) and 0.1 M Tris pH 8.2 were added and incubated for another 15 min at 20°C light protected. The Supernatant was discharged whereas 5 μL β -Me and 100 μL 10 mM NH_4HCO_3 were added and incubated for 5 min at 20°C. An alternating washing step of acetonitril- 10 mM NH_4HCO_3 (1:1) and pure 10 mM NH_4HCO_3 was performed three times before pellets were dried by vacuum centrifugation. The trypsin digestion by addition of 2 μL trypsin overnight at 37°C leads to a set of peptides which can be analyzed by MALDI-MS and assigned to a specific proteins by using Mascot database search (226).

The samples for MALDI-TOF-MS were prepared by Bettina Richter (Chair of Biotechnology, Department Chemistry, TUM) and measurements were performed by Florian Rührnößl or Laura Meier (Chair of Biotechnology, Department Chemistry, TUM).

3.2.9 Analytical ultracentrifugation

Size distribution by analytical ultracentrifugation of hetero-oligomer samples was investigated at 20°C at 34,000 rpm (AN-50 Ti) in 1x PBS pH 7.4 1 mM DTT. Sedimentation velocity (SV) experiments were carried out using a ProteomeLab XL-I ultracentrifuge supplied with an absorbance optics. Sedimentation was detected by using the absorbance detection system at 280 nm. Therefore, samples were prepared with a total absorbance between 0.3 and 1.2 at 280 nm. This equals protein concentrations between 25 μM and 6.25 μM . The process of sedimentation velocity is governed by three forces: gravitation, buoyancy and hydrodynamic friction. The balance of these three forces is the basis of the Svedberg equation:

$$s = \frac{v}{\omega^2 r} = \frac{M_w D (1 - \bar{v} \rho)}{RT} \quad (5)$$

S = sedimentation coefficient [s], v = observed radial velocity [ms^{-1}], ω = angular velocity of the rotor [ms^{-2}], $\omega^2 r$ = centrifugal field, M_w = molar weight [gmol^{-1}], D = diffusion coefficient [m^2s^{-1}], \bar{v} = partial specific volume [cm^3g^{-1}], R = gas constant [$8.314472 \text{ JK}^{-1}\text{mol}^{-1}$], T = absolute temperature [K]

Data analysis for molecular mass determination was performed using in the Sedfit software (227) with a non-model based continuous Svedberg distribution method.

4 RESULTS

The behavior of human small heat shock proteins is influenced by multiple parameters. Within this thesis, three of the trigger factors were studied more closely. First, the possibility of the regulation by the formation of hetero-oligomeric complexes of different human sHsps. Second, the influence of different regions of the N-terminal region (NTR) and third, the interaction with the potential co-chaperone Bag3.

4.1 Regulation of small heat shock proteins by hetero-oligomer formation

To evaluate the regulation of sHsps different methods were approached. First of all, hetero-oligomerization needed to be verified and characterized *in vivo* to design a good *in vitro* model system. Next, size distribution and activity of sHsps were investigated in detail by different assays and under stress vs. non-stress conditions.

4.1.1 Expression of sHsps in human cell lines

As described in the introduction (1.5 Regulation of small heat shock proteins), simultaneous expression and hetero-oligomerization of sHsps within one tissue type has been observed long time ago. The question arises whether more than one sHsp is present within one cell type and whether the hetero-oligomerization can occur already within cells. Another possibility is the expression of different sHsps in different cell types and that the observed hetero-oligomerization occurred *ex vivo* after homogenization of the tissue, which leads to a lysate mixture of different cell types. The second scenario is less likely because of the interaction characteristics noted but it is still theoretically possible. To get a better idea of the *in vivo* situation in cells the expression profiles of HspB1, HspB5 and HspB6 were analyzed in different human cell lines by western blot (Figure 10). Cell lines from various tissue types were used to get a representative view of the situation in the human body. U373MG and U138MG are from brain tissue, A549 and H460 from lung, K562 and SH-SY5Y from bone marrow, HeLa from cervix, Caco-2 from colon, MCF7 from mammary gland, HepG2 from liver, RD from skeletal muscle, and HEK293 from kidney.

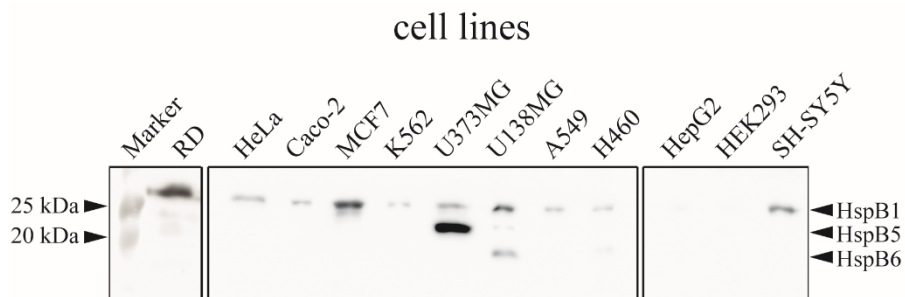


Figure 10 | Endogenous expression of HspB1, HspB5 and HspB6 in different human cell lines analyzed by Western Blot. Modified and reprinted with the permission of American Soc. for Biochemistry & Molecular Biology (Riedl et al. 2020) (228).

Screening these eleven cancer cell lines and one non-cancer cell line (HEK293) for control purposes under physiological conditions we found that HspB1 is widely expressed in different cell

lines whereas HspB5 and HspB6 expression was not observed as frequently. Expression levels of all sHsps vary substantially between cell lines. Surprisingly, in the muscle-derived cell line RD only one type of sHsp (HspB1) was found. Based on previous findings of hetero-oligomers in muscle tissue we expected at least HspB5 to be co-expressed, but this was not the case. Therefore, additionally the expression of HspB3, HspB4 and HspB8 has been tested for this cell line, but no further sHsps were detected (data not shown). Interestingly, HspB5 and HspB6 were exclusively expressed in the presence of HspB1. There are two cell lines expressing two sHsps, which are U373MG (expressing HspB1 and HspB5) and H460 (expressing HspB1 and HspB6). U138MG was the only tested cell line expressing all three sHsp simultaneously. Beside from a very light expression of HspB1 in HepG2 cells, HEK293 cells are the only cell type which did not show detectable HspB1 expression in our Western Blot.

In general, it has been shown before that the expression level of HspB1 and/or HspB5 is increased in cancer tissue leading to higher proliferation rate and resistance of the tumor against cytotoxic compounds (209,229,230). In contrast, the expression of HspB6 is negatively correlated with malignancy in certain cancer tissues (231). In this context, hetero-oligomerization may add to the complexity of the system and could be implicated in the proliferation decision.

Based on the current knowledge, the simultaneous expression of different sHsps in the cytosol of a cell seems to be redundant. Mymrikov et al. (2017) showed that human sHsps have a large overlap in substrate spectra. In their CoIP experiments they were able to verify 109 substrates for HspB1 and 88 for HspB5 whereby 75 substrate proteins were detected for both proteins (53). For HspB6 no significant number of substrate proteins was identified. Hence, the hypothesis was that sHsp hetero-oligomer formation may regulate size and activity by different oligomer compositions. The possible hetero-oligomers within a cell result from the concentrations of each sHsps and the respective ratios. Therefore, the sHsp concentration was quantified in selected cell lines. HeLa and MCF7 cell lines were chosen as reference cell lines because of their moderate HspB1 expression. Furthermore, cell lines expressing more than one sHsp (U138MG, U373MG and H460) were picked for additional investigations.

Table 3 | Quantification of HspB1, HspB5 and HspB6 in five human cancer cell lines by western blotting. sHsp amounts were determined under heat shock conditions (HS) as well as standard conditions (ST). Concentrations were calculated assuming 150 mg/mL total protein concentration in the cells (8). An average of three measurements and corresponding standard deviation are stated. Not detectable sHsp amounts are labeled by n.f. (not found). Modified and reprinted with the permission of American Soc. for Biochemistry & Molecular Biology (Riedl et al. 2020) (228).

Cell line	Protein concentration					
	HspB1 HS [μ M]	HspB1 ST [μ M]	HspB5 HS [μ M]	HspB5 ST [μ M]	HspB6 HS [μ M]	HspB6 ST [μ M]
HeLa	49 \pm 3	30 \pm 2	n.f.	n.f.	n.f.	n.f.
MCF7	50 \pm 3	11 \pm 0.7	n.f.	n.f.	n.f.	n.f.
U373MG	36 \pm 0.5	11 \pm 2	29 \pm 3	29 \pm 3	n.f.	n.f.
U138MG	49 \pm 5	52 \pm 5	7 \pm 0.8	5 \pm 0	33 \pm 4	29 \pm 3
H460	7 \pm 0.2	2 \pm 0.1	n.f.	n.f.	6 \pm 0.3	0.5 \pm 0.2

4 RESULTS

As observed before, an increase of expression based on heat stress is likely for sHsps (40,232). Therefore, the sHsp expression levels in these five cell lines were quantified under heat stress (HS) and standard conditions (ST) (Table 3). For calibration purposes, different amounts of recombinant sHsp and defined amounts of cell lysate were applied on a SDS-PAGE followed by Western Blot (appendix A). Expression levels were quantified by determination of band intensities. The absolute amount of sHsp in one lane was calculated and converted into the concentration value by setting 150 mg/mL as total protein concentration in the cell (8). Under standard conditions, MCF7 and U373MG showed relatively similar expression of HspB1. In H460, the expression was lower whereas HeLa and U138MG showed an increased HspB1 level. As expected, the heat shock induced an almost 2-fold increase of HspB1 expression level for all cell lines, except U138MG. This cell line overall did not show any response to the heat stress condition used. No change in expression pattern of the tested sHsps was detected.

As mentioned before, our main interest was if cells do have the ability to change their ratios of sHsp expression. The ratio in U373MG before the heat treatment was 1:3 for HspB1/HspB5 and shifted during heat treatment to 1:1 due to overexpression of HspB1 and unchanged levels of HspB5. Likewise, a ratio shift was observed for H460 by heat treatment. Starting with a 4:1 (HspB1/HspB6) ratio at standard conditions, the simultaneous stronger expression of HspB1 and HspB6 led to an altered ratio of 1:1. The observed changes in ratio could affect the oligomer ensemble and hetero-oligomerization.

Next, complex formation in the cell lines was analyzed. To this end, co-immunoprecipitation (CoIP) experiments with specific antibodies and cell lysates were performed (Figure 11). By applying one antibody to separate the complexes from the lysate proteins and a second antibody for WB detection, hetero-oligomer formation was tested. By using the same antibody for CoIP and WB detection, homo-oligomer formation was proven.

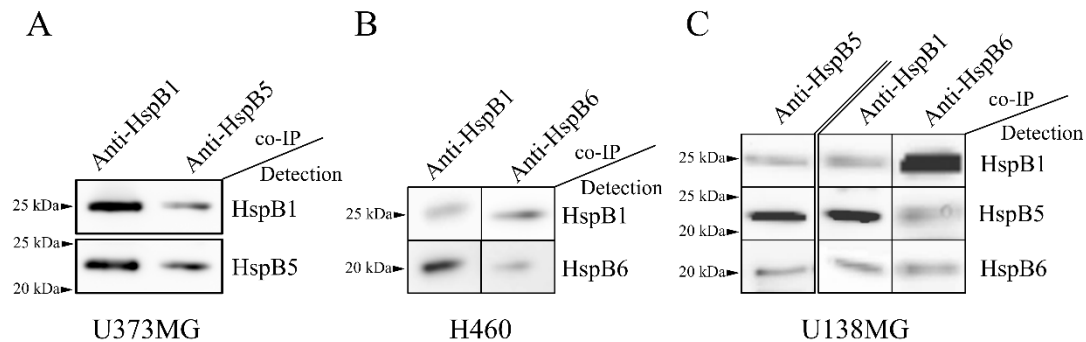


Figure 11 | Analysis of sHsp homo- and hetero-interaction by CoIP of endogenously expressed sHsps in the soluble lysate fraction of different cancer cell lines. The CoIPs were performed independently using specific antibodies against HspB1 and HspB5 in U373MG cell lysate (A). In H460 cell lysate (B) specific antibodies against HspB1 and HspB6 were used instead and in case of U138MG cell lysate (C), CoIPs with anti-HspB1 and HspB6 were performed. For HspB5 CoIPs, 10 μ g recombinant HspB5 was added due to low endogenous expression level. Reprinted with the permission of American Soc. for Biochemistry & Molecular Biology (Riedl et al. 2020) (228).

As can be seen in Figure 11, the interaction of all possible homo- and hetero-oligomers in H460, U373MG and U138MG cells was detected. Because of the low HspB5 expression in U138MG

cells, detection of hetero-oligomer formation was only possible in the presence of slightly increased amounts of recombinant HspB5. Overall, homo- and hetero-oligomers do exist in parallel in the respective cells. As sHsps show high intrinsic dynamics and as subunit exchange is expected to occur constantly, the specific amounts of homo- and hetero-oligomers cannot be estimated from these data. The demonstration of hetero-oligomer complexes within the cells together with the observed shifts in ratios and concentrations, raised the question how this influences the size of sHsp complexes.

4.1.2 Size distribution of sHsps in cancer cells

To investigate the *in vivo* size distribution of sHsps, cells were lysed mechanically to circumvent complex disassembly by harsh lysis buffer e.g. containing detergents. To further stabilize the lysate, protease inhibitor as well as phosphatase inhibitor was added and the procedure was performed on ice. Lysis was directly followed by size-exclusion chromatography. The fractions were precipitated and analyzed by Western Blot. The blots were then quantified densitometrically and data were plotted against the elution volume (Figure 12).

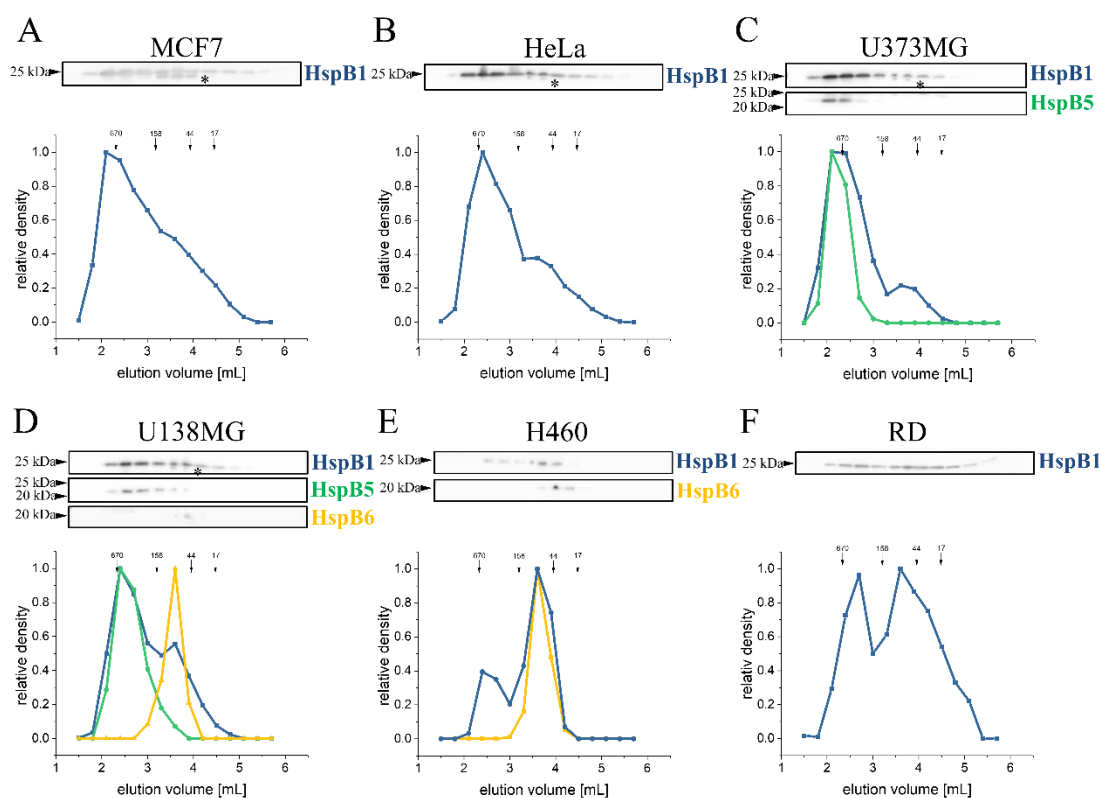


Figure 12 | Size distribution of endogenously expressed sHsps under standard conditions (ST) in six human cancer cell lines. The soluble lysate fraction of different cancer cell lines was applied directly after mechanical lysis onto a size-exclusion chromatography column. Subsequently, the fractions were analyzed by Western Blot. The relative content of the sHsp was quantified by densitometry blots depicted as graphs. MCF7 (A), HeLa (B), and (F) RD are expressing only HspB1 (blue). Elution profiles of sHsps from U373MG cells expressing HspB1 and HspB5 (green) (C), U138MG cells expressing HspB1, HspB5 and HspB6 (yellow) (D), H460 cells expressing HspB1 and HspB6 (E), and RD cells expressing HspB1 only (F). Positions of molecular mass standards (MW in kDa) are indicated with arrows. Double bands of HspB1, labeled with an asterisk, are commonly observed.

4 RESULTS

Modified and reprinted with the permission of American Soc. for Biochemistry & Molecular Biology (Riedl et al. 2020) (228).

As expected for the reference cell lines MCF7 and HeLa, HspB1 showed a broad distribution with two maxima corresponding to apparent molecular masses (MW) of ~400 – 600 kDa and ~70 kDa, as reported before (233). The smaller oligomers probably represent phosphorylated species, as a shift from big oligomer to small oligomer has been shown before *in vitro* using phosphorylation-mimicking mutants of HspB1 (232). For smaller oligomers (158 kDa – 44 kDa), a commonly observed double band is visible in the blots (233). Presumably, this double band is a degradation product as it can also be observed during purification of recombinant protein expressed in *E. coli*, which excludes posttranslational modifications as its origin. The double band during recombinant purification has been verified to consist of HspB1 by MALDI fingerprint MS analysis. The third cell line, which was selected to investigate the sHsp size distribution, was RD. We specifically chose this cell line because sHsp expression seems to be of particular interest in muscle tissue (93,94,234). The elution profile of HspB1 in this cell line resembles the distribution of HspB1 in other cell lines like MCF7 and HeLa. As before two peaks were observed one at high oligomer size (~400 – 600 kDa) and one at decrease oligomer size (~70 kDa). Interestingly, the two fractions are of similar amount whereas for MCF7 and HeLa a higher amount of large oligomers was detected.

In U373MG cells, which express HspB1 and HspB5, a similar elution profile of HspB1 with two maxima at ~400-600 kDa and ~70 kDa was found. In contrast, HspB5 co-eluted in the high oligomeric fraction only (Figure 12C). It is possible that HspB5 is not phosphorylated under standard conditions and does therefore not show any smaller species. Another option is a higher stability of HspB5 oligomers compared to HspB1. Concentration dependent dissociation of HspB1 has been observed *in vitro* (data not shown), whereas in the same concentration range HspB5 did not show any dissociation. In U138MG cells, additional expression of HspB6 did not change the elution profile of HspB1 and HspB5. Interestingly, HspB6 co-eluted with the smaller HspB1 peak (~70 kDa) only. This is surprising because interaction of HspB6 with HspB1 and HspB5 has been proven in CoIP experiments before, while the size distribution data did not show incorporation into the high oligomers. This hints to an interaction within small oligomer assemblies. *In vitro* HspB6 alone elutes in an even smaller species, probably monomeric or dimeric (53). The size increase may also be an evidence for interactions of HspB6 particular with HspB1 or even with HspB5 as a low abundant species. In H460 cells the evidence for an interaction of HspB1 and HspB6 in the absence of HspB5 is even stronger, as the fraction of small HspB1 species and co-eluted HspB6 was more pronounced.

Based on the findings of sHsp ratio shifts in U373MG and H460 cells upon heat treatment, the size distribution analysis was repeated with heat shocked cells (Figure 13). Therefore, cells were grown at 42°C for 2 h without CO₂ addition as for determination of expression levels. Generally speaking, the sHsp distribution was not significantly changed upon HS within the accuracy limits of the applied method. In more detail, the smaller HspB1 fraction shifted slightly to even smaller species in MCF7, HeLa and U373MG.

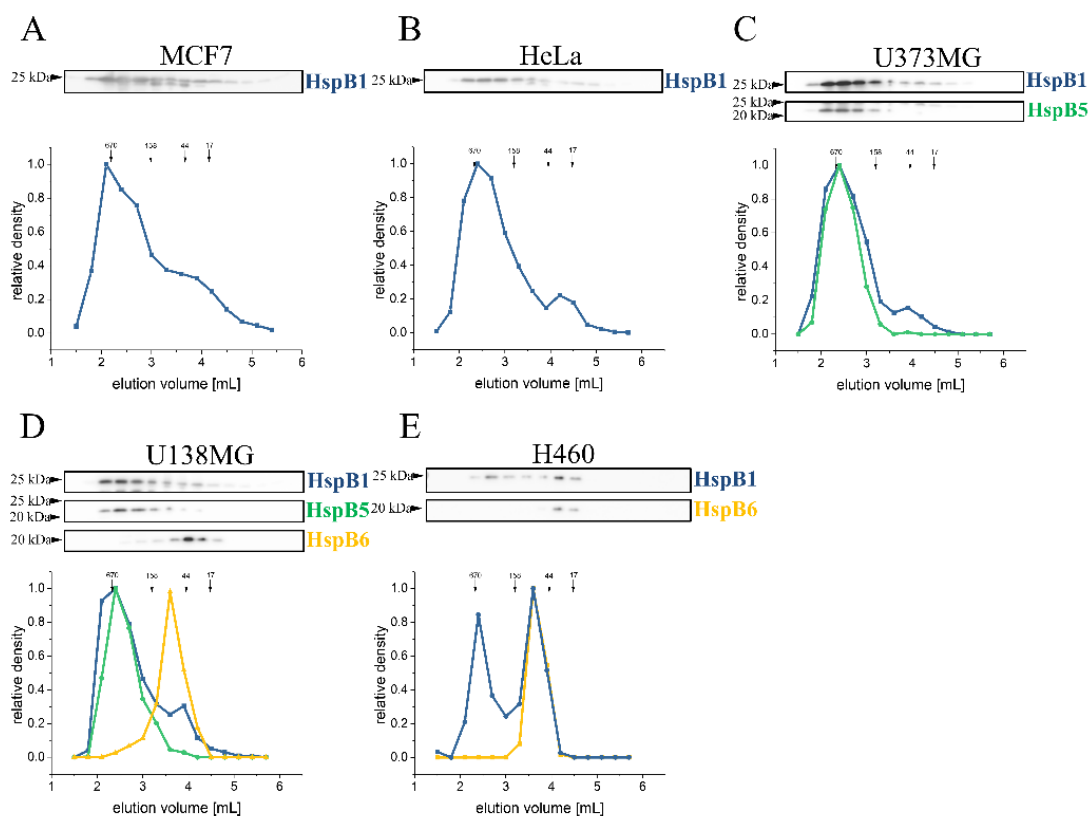


Figure 13 | Size distribution of endogenously expressed sHsps after heat shock (HS) in five human cancer cell lines. As before, the soluble lysate fraction of different cancer cell lines was applied directly after mechanical lysis onto a SEC column. Subsequently, the fractions were analyzed by Western Blot and signal intensities plotted against elution volume. MCF7 (A) and HeLa (B) are expressing only HspB1 (blue). Elution profiles of sHsps from U373MG cells expressing HspB1 and HspB5 (green) (C), U138MG cells expressing HspB1, HspB5 and HspB6 (yellow) (D), and H460 cells expressing HspB1 and HspB6 (E). Positions of molecular mass standards (MW in kDa) are indicated with arrows. Double bands of HspB1, labeled with an asterisk, are commonly observed. Reprinted with the permission of American Soc. for Biochemistry & Molecular Biology (Riedl et al. 2020) (228).

In the presence of HspB6, this shift could not be observed. Additionally, in H460 cells the amount of HspB1 high oligomer fraction seemed to be increased. The shift towards smaller species may be explained by the stress-related increase of HspB1 phosphorylation. The higher amount of large oligomers in H460 cells may result from the increased overall HspB1 concentration in H460 during heat shock (Table 3). As mentioned before a concentration dependent equilibrium of HspB1 of small and large oligomers was observed for HspB1 *in vitro*. It is quite conceivable that this effect can be observed in this assay as well.

Arrigo et al. (1988) evaluated the effect of different kinds of stresses on HspB1 solubility in HeLa cells. They showed that under normal conditions 20 % of HspB1 was found in the pellet fraction whereas 80 % stay in the supernatant. After heat treatment for 90 min at 43°C, 40 % was obtained in the supernatant and 60 % precipitated in the pellet fraction (235). Hence, one needs to keep in mind that only the soluble cell lysate was analyzed in the present assay. Furthermore, the presence of other proteins like interaction partners or substrates within a cell lysate may induce specific complexes e.g. sHsp-substrate complexes. These complexes are predicted to be even larger than

the high oligomer fraction and may sediment during centrifugation (103,111). To characterize the size distribution of hetero-oligomers without any further interaction partners the experiment was repeated *in vitro* with recombinant proteins.

4.1.3 Size distribution of hetero-oligomers *in vitro*

To visualize the size distribution of proteins *in vitro*, size exclusion chromatography coupled to multi-angle-light-scattering (SEC-MALS), analytical ultracentrifugation (AUC), and transmission electron microscopy (TEM) experiments were employed as complementary methods. For SEC-MALS experiments a dilution of the lysate samples and the occurrence of shear forces during the run need to be considered (236). This concern can be circumvented by using analytical ultracentrifugation as here no shear forces or sample dilution occur. However, the sHsp concentration range is restricted for AUC because of the signal detection at 280 nm. In TEM experiments, the resolution of small oligomers is highly restricted.

Due to the expected widely dispersed molecular masses of the complexes, SEC-MALS was performed using a Superdex200 increase column (Figure 14). This column is suitable for protein sizes between 10 – 600 kDa according to GE Healthcare manufacturer specifications. By using the MALS and the RI detector apparent molecular mass (MW) of hetero-oligomer complexes were calculated independently of the elution volume. HspB1 and HspB5 co-eluted in a high oligomer fraction ranging from 400 – 600 kDa (Figure 14, A). The smallest species observed were HspB5 and HspB1 homo-oligomers whereas hetero-oligomers were slightly increased in size for all ratios.

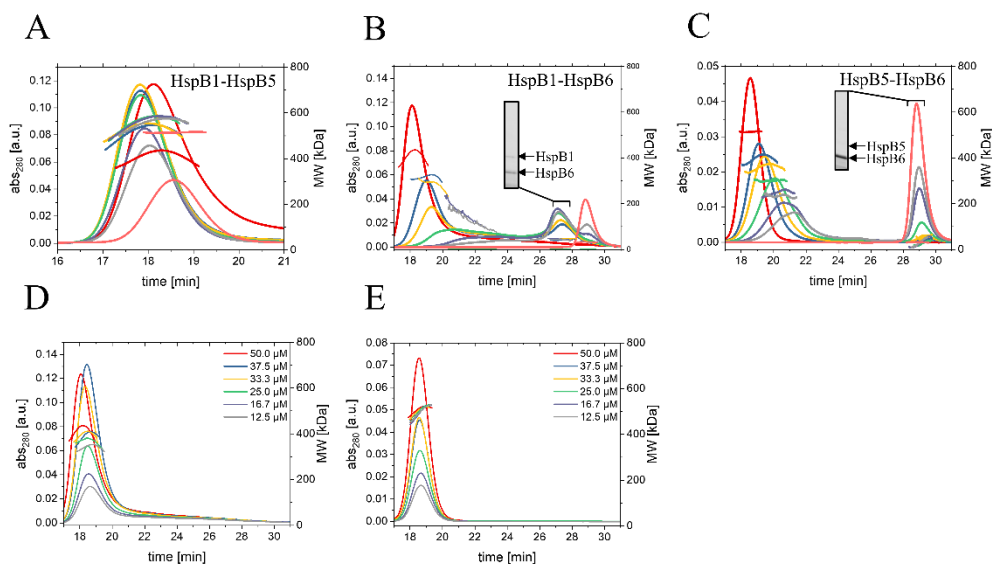


Figure 14 | Size distribution of sHsp hetero-oligomers formed at different ratios *in vitro* determined by size exclusion chromatography coupled to multi-angle light scattering (SEC-MALS). Left Y-axis: UV absorption at 280 nm, right Y-axis: molecular mass determined by MALS using RI signal. SDS-PAGE analysis of peak fractions is depicted as inserts. In (A) to (C) colors indicate varying ratios of sHsps at constant total protein concentration (red – 1:0; blue – 3:1; yellow - 2:1; green – 1:1; purple – 1:2; gray – 1:3; pink – 0:1). (D) and (E) are homo-oligomer controls of HspB1 and HspB5 respectively. Colors indicate varying concentrations as outlined in the graphics. Modified and reprinted with the permission of American Soc. for Biochemistry & Molecular Biology (Riedl et al. 2020) (228).

HspB6 alone appeared as a very small sized complex (< 30 kDa), most likely a dimer. Together with HspB1, the high oligomer complex dissociated into smaller species decreasing in size with the increasing amount of HspB6 (200 – 400 kDa) and an additional species around 45 kDa was formed (Figure 14, B). In the case of HspB5, addition of HspB6 resulted in dissociation of the high oligomer complex as well but no additional intermediate sized complex was formed (Figure 14, C). When HspB6 was added in excess, it was not completely integrated into the hetero-oligomers, and a peak at 32 kDa corresponding to free HspB6 dimer was detected. Comparing the apparent molecular masses of HspB6 homo-dimer and HspB1 monomer (22.783 kDa), it is likely that the identified 45 kDa species represents a hetero-dimer of HspB1 and HspB6. Because of this surprising result, the components of the small size peaks were analyzed by SDS-PAGE (inserts and appendix B). The presence of both proteins were verified for HspB1-HspB6 but only the presence of HspB6 in the case of HspB5-HspB6.

For transient interactions and highly dynamic complexes like sHsp oligomers, the shear forces which appear during a chromatography may dissociate the complexes or influence their apparent mass. Moreover, analytical ultracentrifugation (AUC) was performed additionally (Figure 15).

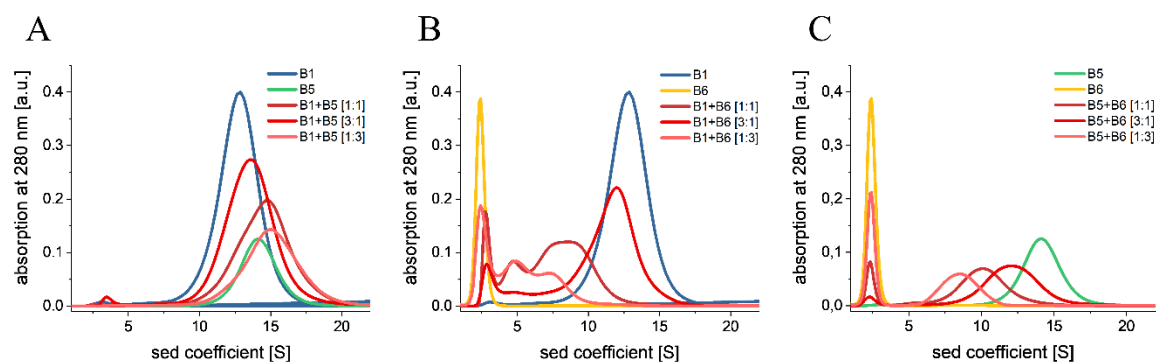


Figure 15 | Size distribution of sHsp hetero-oligomers formed at different ratios in vitro determined by analytical ultracentrifugation (AUC). The sedimentation of different complexes was sensed by detection of the UV absorption signal at 280 nm during the run. Hetero complexes are depicted in different shades of red according to their composition (3:1 – dark red; 1:1 – red; 1:3 – light red). (A) HspB1-HspB5 complexes with 25 μ M HspB1 alone (blue) and 25 μ M HspB5 alone (green). (B) HspB1-HspB6 complexes with 25 μ M HspB1 alone (blue) and 25 μ M HspB6 alone (yellow) and (C) HspB5-HspB6 complexes with 25 μ M HspB5 (green) and 25 μ M HspB6 alone (yellow).

The results of AUC experiments confirmed the data obtained by SEC-MALS experiments. The HspB1-HspB5 complex size was increased by hetero-oligomer formation from 12.5 S to 15 S whereas HspB1-HspB6 and HspB5-HspB6 showed a shift to smaller oligomer species up on hetero-oligomerization between 7.5 – 12.5 S. Furthermore, the previously described ~45 kDa species of HspB1-HspB6 hetero-oligomers was observed by AUC as well at ~5 S. This species was again not observed for HspB5-HspB6 assemblies. As for SEC-MALS experiments, when present in excess, HspB6 was not completely integrated into the hetero-oligomers, and a peak at 2.5 S was detected in addition.

Due to the relative large size of the complexes, transmission electron microscopy (TEM) could be conducted as well. Micrographs of homo-oligomers and hetero-oligomers in three different ratios

4 RESULTS

were taken (Figure 16, A) and for size distributions $\sim 10,000$ particles were selected semi automatically from micrographs for each complex (Figure 16, B). To cover the ratios observed *in vivo*, the sHsps were varied from 3:1 to 1:3. As expected from earlier studies, we detected HspB1 and HspB5 homo-oligomers in heterogeneous populations of large oligomeric species with diameters between 11 - 17 nm, with HspB1 being more heterogeneous than HspB5. The mean diameter of HspB5 homo-oligomers (14 nm) was slightly larger than that of HspB1 homo-oligomers (13 nm). At the same time, the particle distribution for HspB1 was more disperse ranging from 11 - 17 nm whereas the HspB5 distribution was narrower, ranging from 12 – 16 nm. Particle size distributions of the hetero-oligomers was similar to that of HspB5 or slightly enlarged in mean diameter. In HspB6 samples, large oligomers were absent. The dimeric species were too small to be clearly discerned under our experimental conditions (Figure 16, A) therefore no size distributions are included for HspB6 alone and for HspB1-HspB6 in a 1:3 ratio (Figure 16, B).

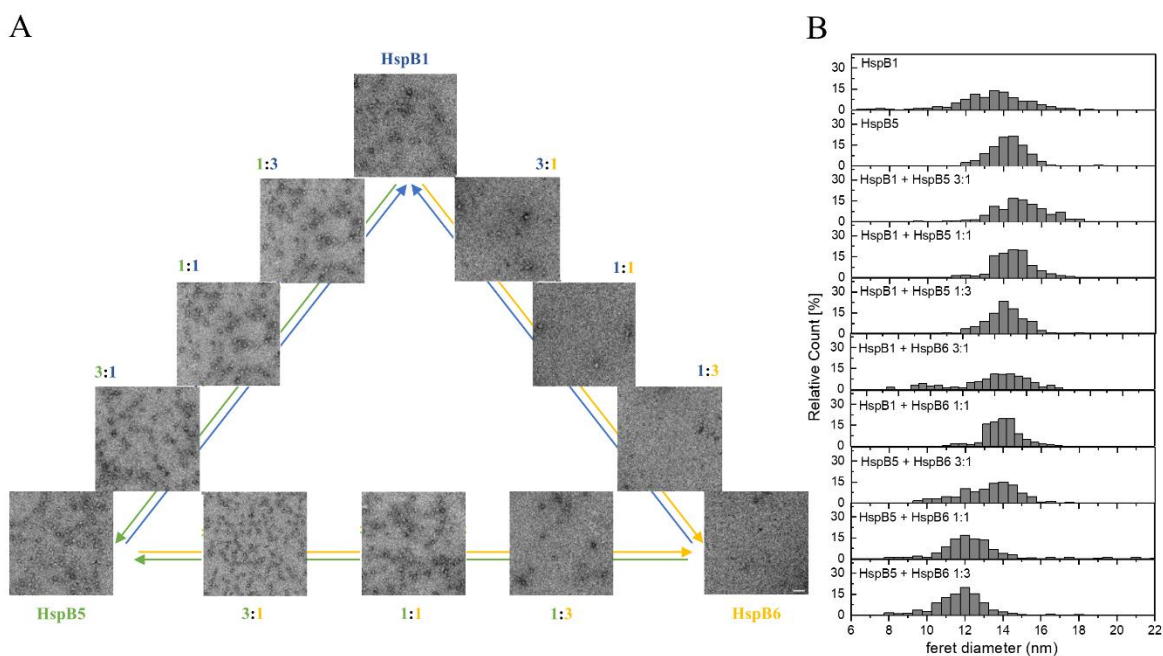


Figure 16 | Size distribution of sHsp homo- and hetero-oligomers formed at different ratios *in vitro* determined by transmission electron microscopy (TEM). Electron micrographs of negatively stained hetero-oligomeric complexes formed at a constant total protein concentration of 1 μM . Proteins and ratios are colour coded, with HspB1 - blue, HspB5 - green and HspB6 - yellow. Scale bar: 50 nm. (B) Size distributions of homo-oligomers formed at different ratios determined from the feret diameters. HspB6 alone and HspB1-HspB6 hetero-oligomers formed at 1:3 ratios are not included as they are too small to be discerned. Modified and reprinted with the permission of American Soc. for Biochemistry & Molecular Biology (Riedl et al. 2020) (228).

Overall, both HspB1 and HspB5 oligomers decreased in size upon addition of HspB6 and the size distribution became broader. Especially hetero-oligomers formed by HspB1 and HspB6 are heterogeneous and show a high content of small species. It should be noted that hetero-dimers as observed in AUC and SEC-MALS experiments of HspB1-HspB6 hetero-samples cannot be resolved with TEM due to their small size.

Taken together, these results show that HspB6 decreases the size of both the HspB1 and HspB5 large oligomers in a concentration-dependent manner resulting in intermediate sized

(200-400 kDa) hetero-oligomers. Surprisingly, HspB6 forms stable hetero-dimers exclusively with HspB1 but not with HspB5 as shown by SEC-MALS and AUC.

4.1.4 Prevention of aggregation of cellular proteins by sHsps

In the current model of sHsp activity regulation, a shift to smaller oligomer species leads to an activity increase in most cases (41,80,86,90,237). There are a few exceptions like Hsp26 from *S. cerevisiae* where transition to a state of increased substrate binding affinity and therefore higher chaperone activity is induced by conformational changes which can occur without perturbation of the oligomeric state (180,181). To investigate how the observed changes in oligomeric size influence the chaperone activity of human hetero-oligomers, a lysate protein aggregation assay was used. Here, thermal aggregation of HEK293 lysate proteins after incubation at 45°C was tracked by loading the pellet fraction on a SDS-PAGE (Figure 17).

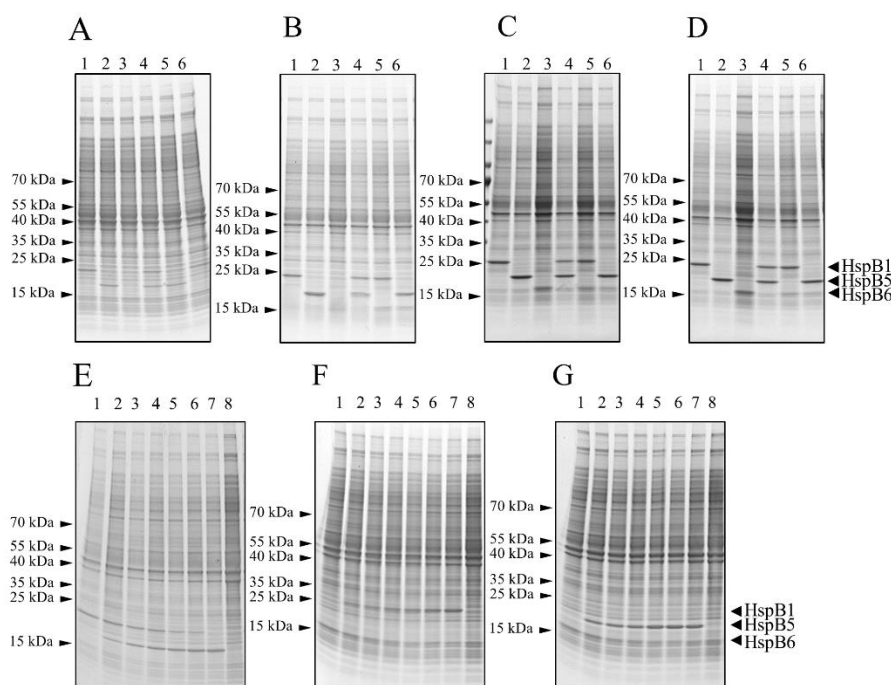


Figure 17 | Suppression of aggregation of HEK293 lysate proteins at different concentrations and different ratios of HspB1, HspB5, HspB6 or hetero-oligomers. The sHsps were added to soluble HEK293 lysate proteins in various amounts and the mixture was heat-treated. Afterwards insoluble proteins were separated by centrifugation and analyzed by SDS-PAGE. (A) - (D) are performed at 1:1 ratio with A – 1 μ M, B – 2 μ M, C - 4 μ M and D - 6 μ M total sHsp concentration. Lane 1 – HspB1, lane 2 - HspB5, lane 3 - HspB6 and lane 4 to 6 -hetero-oligomers. Whereas (E) - (G) are performed at 2 μ M of total sHsp in ratios 1:0, 3:1, 2:1, 1:1, 1:2, 1:3 and 0:1 (lane 1 – 7) with E – HspB1-HspB5, F – HspB1-HspB6 and G – HspB5-HspB6. Lysate without any sHsp is depicted in lane 8. Modified and reprinted with the permission of American Soc. for Biochemistry & Molecular Biology (Riedl et al. 2020) (228).

To evaluate the influence of different sHsp complexes on the lysate proteins during heat shock, recombinant produced sHsps were added at different concentrations (A-D) or at different ratios (E-F) to the lysate. In Figure 17 A–D it can be seen that for low sHsp concentrations the aggregation of lysate proteins was not affected but with increasing sHsp concentration a decrease of proteins in the pellet was observed. As observed before by Mymrikov et al. (53), HspB6 showed a reduced

4 RESULTS

holdase like activity in this assay (A - D, lane 3). Furthermore, the ability of sHsps to hold lysate proteins in solution appears to have a maximum of 60 % inhibition starting at around 4 μM sHsp concentration. An increase of sHsp concentrations to 6 μM did not show increased inhibition (D).

In order to quantify the results, the lanes were densitometrically scanned using ImageQuant software. A lane without any sHsp addition (lane 8) was set as 1 and all other values were normalized based on this value (Figure 18). The quantification of the pellet fraction shows equal values for HspB1, HspB5 and HspB1-HspB5 hetero-oligomers in a 1:1 ratio. However, in 1:1 hetero complexes with HspB6 the activity of HspB1 and HspB5 seem to be slightly increased considering the reduced activity of HspB6 alone. Here the hetero-complexes showed nearly the same activity compared to homo-oligomers of HspB1 or HspB5 alone at equal total sHsp concentrations (Figure 18, A).

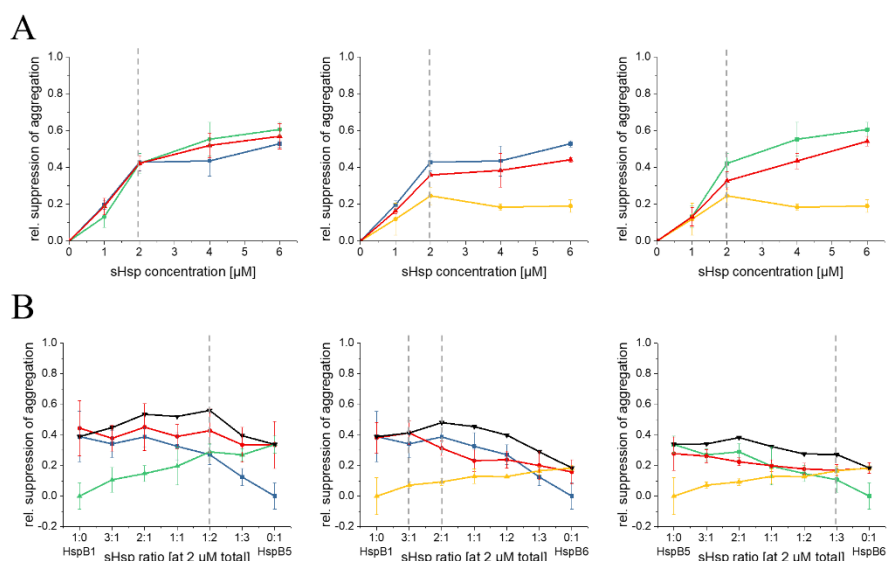


Figure 18 | Chaperone activity of hetero-oligomers formed at different ratios of sHsp towards HEK293 lysate. Hetero-oligomers (HspB1-HspB5, HspB1-HspB6 or HspB5-HspB6) were formed at (A) a constant ratio of 1:1 at different total sHsp concentrations ranging from 1 – 6 μM or at (B) a constant total sHsp concentration of 2 μM with different hetero-sHsp ratios varied from 3:1 to 1:3. The color code refers to the respective hetero-oligomers – red, HspB1 – blue, HspB5 – green, HspB6 – yellow, and theoretical activities values – black. Gray dotted lines indicate (A) sHsp concentration chosen for ratio dependent experiments and (B) physiological ratios according to Table 3. Modified and Reprinted with the permission of American Soc. for Biochemistry & Molecular Biology (Riedl et al. 2020) (228).

Therefore, the influence of HspB6 on HspB1 and HspB5 was investigated in more detail by testing different hetero-oligomer ratios. As the total sHsp concentration 2 μM was chosen to make sure not to reach activity saturation (Figure 18, B). To simplify the interpretation, we calculated a theoretical activity value (black) which equals the sum of homo-oligomer activities at each ratio.

$$\text{theor. hetero activity} = \text{measured sHsp activity 1} + \text{measured sHsp activity 2} \quad (6)$$

If no activity modulation occurs, the calculated theoretical activity value (black) equals the measured hetero-oligomer activity value (red). As observed for 1:1 ratio experiments, HspB1-HspB5 hetero-oligomer complexes did not show pronounced changes in activity. The

measured hetero-oligomer activity and the calculated theoretical hetero activity are within the same range considering the relative high error bars which are justified by the technical complexity of this assay. As for HspB1-HspB6 and HspB5-HspB6 of an activating influence of HspB6 on HspB1 and HspB5 activity could not be verified. The measured activity value did not differ strongly from the calculated theoretical activity values. The lack of strong modulating effects of hetero-oligomer formation on the heat-induced aggregation of the cytosolic proteome leaves the possibility that hetero-oligomers may exhibit specific differences towards individual substrate proteins.

4.1.5 Chaperone activity of human sHsp hetero-oligomers on model substrates

To test whether hetero-oligomers have a specific behavior towards individual substrates, *in vitro* experiments with four different model substrates were performed. Malate dehydrogenase (MDH), citrate synthase (CS) and glyceraldehyde-3-phosphate dehydrogenase (GAPDH) were destabilized by heat whereas insulin aggregation was induced by addition of a reducing agent. For these *in vitro* experiments the optimal sHsp-substrate ratio is strongly dependent on the model substrate and the experimental conditions used (e.g. buffer system, pH, and temperature). Additionally, the used substrate concentration is dependent on the generated light scattering signal to track the aggregation at 360 nm. After optimization of specific substrate and sHsp concentrations for all sHsp-substrate pairs, measurements at different sHsp concentrations and a 1:1 ratio were performed and the increase of light scattering was detected over time (appendix C).

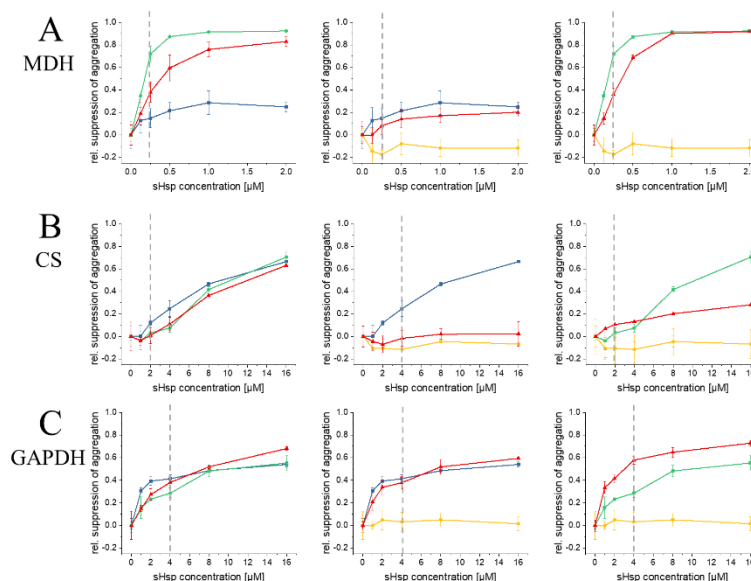


Figure 19 | Chaperone activity of hetero-oligomers on different model substrates and HEK293 lysate at varying concentrations. Malate dehydrogenase (A; MDH), citrate synthase (B; CS), and glyceraldehyde-3-phosphate dehydrogenase (C; GAPDH) aggregation was induced by heat at 45°C for 60 to 90 minutes. sHsp ratio of hetero-oligomers (HspB1-HspB5, HspB1-HspB6 and HspB5-HspB6) was fixed at 1:1 ratio for all measurements shown. Hetero-sHsp are depicted in red whereas HspB1 - blue, HspB5 - green, HspB6 - yellow and theoretical activities values - black. Gray dotted lines indicate the respective sHsp concentrations used in Figure 20. Modified and reprinted with the permission of American Soc. for Biochemistry & Molecular Biology (Riedl et al. 2020) (228).

Light scattering end point values were plotted versus different sHsp concentrations. The data for homo-oligomer controls and the corresponding hetero-oligomer were depicted in one graph for each model substrate (Figure 19). From these data the optimal sHsp concentrations for assays, in which the ratios were varied, were determined (Figure 20). As before the chosen concentration has to be in the middle of the activity range to circumvent activity saturation within an experiment. The defined sHsp concentrations are highlighted in Figure 19 as grey dotted lines. For MDH aggregation, a sHsp concentration of 0.25 μM was selected which equals a sHsp/substrate ratio of 1:4 implying an excess of substrate for this pair. In contrast for GAPDH 4 μM sHsp was used which resulted in a 4:1 sHsp/substrate ratio with an excess of sHsp. For CS two different concentrations were used because of enhanced effects for different hetero-oligomers at different concentrations. 2 μM sHsp was selected for HspB5 experiments (2:1 sHsp/substrate ratio) whereas 4 μM sHsp was used for HspB1-HspB6 hetero-oligomer experiments (4:1 sHsp/substrate ratio). This optimization step was not performed for insulin assays because modulation effects have already been seen at a concentration of 4 μM sHsp for all hetero-oligomer pairs (1:10 sHsp/substrate ratio).

For the following aggregation experiments, the concentrations of model substrate as well as the total concentration of sHsp were kept constant but the ratios of sHsps were varied from 3:1 to 1:3 to cover the *in vivo* situation as determined in Table 3 for each hetero sHsp pair (red) (Figure 20).

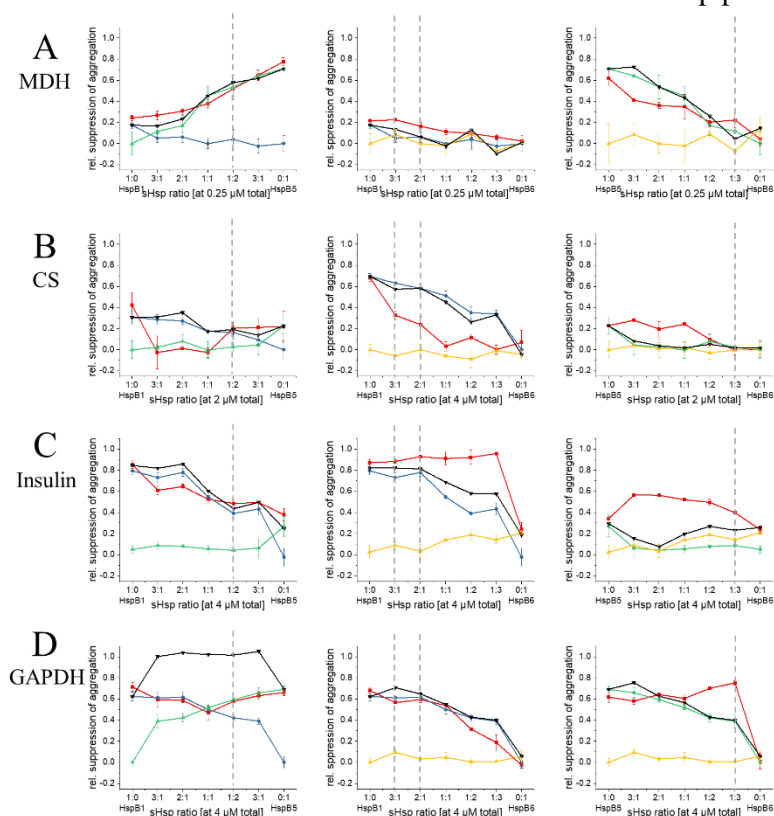


Figure 20 | Chaperone activity of hetero-oligomers formed at different ratios of sHsp towards model substrates. Hetero-oligomers (HspB1-HspB5, HspB1-HspB6 or HspB5-HspB6) were formed at the constant total sHsp concentration indicated. Ratios of sHsp for hetero-oligo formation varied from 3:1 to 1:3. Chaperone activity was measured for different model substrates like malate dehydrogenase (A; MDH), citrate synthase

(B; CS), insulin (C), and glyceraldehyde-3-phosphate dehydrogenase (D; GAPDH). The color code refers to the respective hetero-oligomers – red, HspB1 – blue, HspB5 – green, HspB6 – yellow, and theoretical activities values – black. Gray dotted lines indicate physiological ratios according to Table 3. Modified and reprinted with the permission of American Soc. for Biochemistry & Molecular Biology (Riedl et al. 2020) (228).

The respective *in vivo* ratios of the hetero-oligomer are indicated with gray dotted lines. As controls homo-oligomers alone were measured at corresponding concentrations (HspB1-blue, HspB5-green, and HspB6-yellow). The corresponding light scattering over time plots are attached in the appendix C. The most prominent observation was the absence of HspB6 activity on its own (yellow) for all model substrates tested. HspB6 was only able to slightly prevent insulin aggregation (Figure 20, C). On the contrary, HspB1 and HspB5 showed well pronounced substrate-specific activities. HspB1 was highly competent to inhibit aggregation of CS, insulin and GAPDH but not the aggregation of MDH. HspB5 showed a huge impact on MDH, CS, and GAPDH aggregation but not on insulin (53). It needs to be mentioned that for the present study GAPDH from a different supplier had to be used. As this GAPDH batch displayed decreased stability, buffer conditions had to be optimized. This resulted in an altered HspB1 activity for this substrate compared to previously published data (53). For all present experiments the same GAPDH batch was used. Thus all data are comparable within this thesis.

As before, hetero-oligomer activities (red) were compared to calculated theoretical activities (black). For HspB1-HspB5 hetero-oligomers, the measured hetero-oligomer activity was slightly lower compared to the theoretical activity in all cases tested. For substrates like CS and insulin where HspB1 and HspB5 showed differences in activity, the less active sHsp seems to negatively affect the aggregation suppression of the more active one. However, in the case of GAPDH, where HspB1 and HspB5 alone showed similar activities, the hetero-oligomer samples exhibited strongly decreased activities compared to the theoretical values (Figure 20, column 1).

The most striking effects were observed for HspB6 hetero-oligomers. HspB5 activity was enhanced upon addition of HspB6 for all substrates tested at ratios close to the physiological conditions (gray dotted line). Even though the extent of influence varies between different substrates, the effect was overall consistent. The situation was different for HspB6 added to HspB1. Here the influence seemed to be more dependent on the substrate used. The aggregation of MDH and GAPDH was prevented by the hetero-oligomer as effectively as in the absence of HspB6. A huge but contradictory effect was observed for insulin where the presence of HspB6 improved HspB1 activity and for CS where HspB6 induced lower activity of HspB1.

4.1.6 Comparison of chaperone activities

For comparison of all chaperone activity, data modulation values were calculated. This value refers to the difference between the measured activity and the theoretical activity.

$$\text{modulation value} = \text{measured activity} - \text{theoretical activity} \quad (7)$$

Positive modulation values indicate an increase in activity of the hetero-oligomer compared to the corresponding homo-oligomers whereas negative modulation values indicate a decrease in activity. For visualization of the results a heat map was created including all obtained modulation values.

The exact calculated values are attached in appendix D. Positive modulation values are depicted in red and negative modulation values are highlighted in blue (Figure 21).

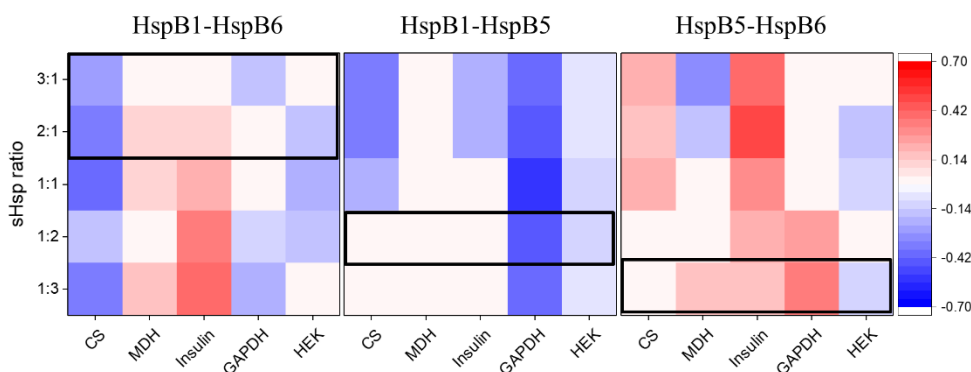


Figure 21 | Modulation of aggregation suppression ability of sHsp hetero-oligomers. The heat map shows negative modulation (indicating inhibition) in blue and positive modulation (indicating activation) in red. Modulation values equate to the difference of real activity and theoretical activity whereas theoretical activity is defined as the sum of single sHsp control chaperone activities. For all experiments the cut off for color conditional formatting was set to 0.1 which equals the averaged standard deviation. Outlined boxes indicate physiological relevant ratios of the specific hetero-oligomers according to Table 3. Reprinted with the permission of American Soc. for Biochemistry & Molecular Biology (Riedl et al. 2020) (228).

This analysis shows that the modulation by a sHsp depends both on the interaction partner and the substrate. For HspB1 and HspB5 the observed decrease in activity upon hetero-oligomerization follows the common model of sHsps chaperone activity where an enrichment of higher oligomers leads to less activity (41). As hetero-oligomerization of HspB5 and HspB6 enriches smaller oligomers, a general increase in activity fits the scheme. The specific appearance of a hetero-dimer of HspB1-HspB6, however, renders the influence on the chaperone activity substrate-specific. Notable, in the range of *in vivo* ratios (Figure 21, boxes) at ST and HS conditions the overall direction of the regulation effect (positive or negative) is consistent for all substrates.

4.1.7 Disaggregase activity of sHsp hetero-oligomers

Another function of sHsps is their support of refolding processes. If proteins aggregate in the presence of a sHsp, sHsp-substrate complexes are formed which remain refolding-competent suggesting that ATP-dependent chaperones can trigger the release of the substrate (238). Like for aggregation assays, the re-activation mechanism appears to be largely dependent on the sHsp/substrate ratio and the used ATP-dependent refolding machinery. For the following experiments human Hsc70, Hdj1 and MDH as substrate were used combined with hetero- oligomeric sHsps at *in vivo* ratios or homo-oligomeric at the corresponding concentrations (Figure 22). The reactivation of MDH was measured by recording turnover of the NADH to NAD photometrically. The Hsc70/Hdj1 was only able to refold the substrate if sHsps were present during aggregation. The release and refolding of non-native proteins trapped in sHsp/substrate complexes did not occur spontaneously (dashed lines).

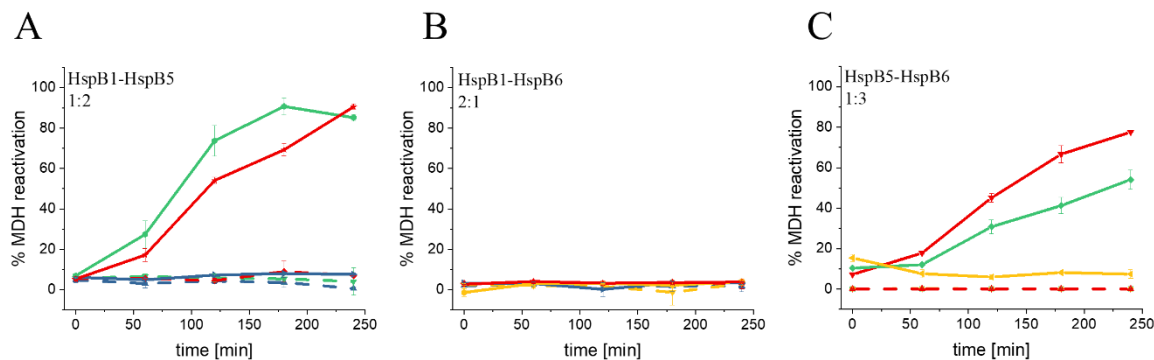


Figure 22 | Influence on MDH reactivation of sHsp homo – and hetero-oligomers at *in vivo* ratios. The total amounts of MDH (0.5 μ M), Hdj1 (2 μ M), Hsc70 (10 μ M), and sHsp (1 μ M) were equal for all measurements. Dashed lines depict control measurements without Hsc70 and Hdj1. HspB1 - blue, HspB5 - green, HspB6 - yellow, and hetero complexes - red are depicted in (A) HspB1-HspB5 (1:2) with HspB1 control (0.67 μ M) and HspB5 control (1.33 μ M), (B) HspB1-HspB6 (2:1) with HspB1 control (1.33 μ M) and HspB6 control (0.67 μ M), and (C) HspB5-HspB6 (1:3) with HspB5 control (0.5 μ M) and HspB6 control (1.5 μ M).

As observed in the aggregation assays HspB6 did not show any influence on the reactivation of MDH on its own. In the presence of HspB5 alone and of HspB1-HspB5 MDH showed very similar reactivation. This indicates that there was no regulation in terms of HspB1-HspB5 hetero-oligomers. For HspB5-HspB6 the picture was different. The effect of the hetero-oligomer on MDH in this case was significantly reduced and a positive modulation of HspB5 by HspB6 can be postulated here. Surprisingly, HspB1 alone did not support MDH refolding under our conditions. Combined with the low activity of HspB1 in MDH aggregation prevention assays this may have a substrate-specific reason. This needs to be investigated in more detail by using different model substrates.

4.2 Regulation of sHsps by their N-terminal region

To investigate the influence of the N-terminal region (NTR) of a sHsp on its behavior, human α B-crystallin (α B) was chosen as a model protein. Its NTR consists of 60 - 70 amino acids depending where the beginning of the ACD is defined. As mentioned in the introduction the NTR of sHsps is little conserved (1.3.1 Structure of small heat shock proteins) whereas the sequence of α B-crystallin itself is well conserved between different mammals (rat, mouse, human, bovine) and even vertebrates (chicken, zebrafish) (Figure 23).

aBNTR_zebrafish	MEISIQHPWYRRPLFGFFPYRIFDQYFGEHLSDDPFSPFY--TMFYYPYLWRFP	57
aBNTR_chicken	MDITIHNPILIRPLFSWLTSPSRIFDQIFGEHLQSELLPTSPSLSPFLMRSP-FFRMP	59
aBNTR_rat	MDIAIHHPWIRRPFFPFHSPRLFDQFFGEHLLSDLFSTATSLSPFYLRPPSFLR	60
aBNTR_mouse	MDIAIHHPWIRRPFFPFHSPRLFDQFFGEHLLSDLFSTATSLSPFYLRPPSFLR	60
aBNTR_human	MDIAIHHPWIRRPFFPFHSPRLFDQFFGEHLLSDLFPTSTSLSPFYLRPPSFLR	60
aBNTR_bovine	MDIAIHHPWIRRPFFPFHSPRLFDQFFGEHLLSDLFPASTSLSPFYLRPPSFLR	60
	::*:*:* **:* * *:* ** * ** *:* : * * : * **	

Figure 23 | Amino acid sequence alignment of different α B-crystallin sequences form different species. The alignment was performed using the Clustal Omega Online Tool. The color code divides the amino acids in categories based on their properties (acidic = blue; basic = pink; hydrophobic = red; polar = green).

The aim was to characterize a possible regulatory effect of the NTR on chaperone activity, size distribution of complexes, surface accessibility and oligomeric dynamics. To assign the different effects on specific characteristics of the NTR, the sequence was analyzed using different mutants. On the one hand, distinct regions may have special functions for regulation of substrate recognition, size distribution, and activity. On the other hand, specific residues with special properties may play a crucial role for the NTR like hydrophobic or aromatic amino acids. Firstly, the NTR was subdivided into short stretches and the sequence was truncated based on these segments until the whole NTR was deleted. Second, aromatic residues of the NTR were replaced by alanine systematically to analyze their effect on α B-crystallin.

4.2.1 The influence of N-terminal truncated mutants

The secondary structure predictions in the pseud-atomic α B model of Braun et al. (2011) based on a triple hybrid approach combining data from cryoelectron microscopy, NMR spectroscopy, and structural modeling the NTR was subdivided in five different regions (Figure 24) (66). The amino acid sequences of all mutants are attached in appendix E. There are three predicted helices in the NTR, which vary in size depending on the prediction method used. The results of an earlier study showed that the deletion of the first 15 aa does not affect the quaternary structure and chaperone activity significantly (213). Therefore, the first truncation mutant investigated in this study was Δ 20. For this mutant the first helix (α 1) including the flexible loop before and after this helix was deleted. The second mutant (Δ 28) includes the deletion of the second helix (α 2) additionally.

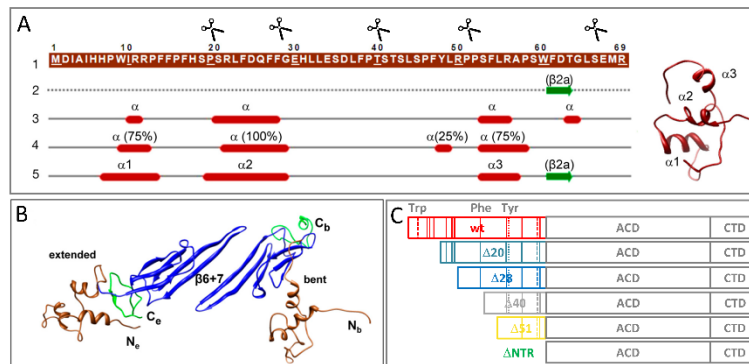


Figure 24 | Secondary structure prediction and structural model of the α B NTR. (A) First lane: Primary sequence of the NTR of human α B. Second lane: Secondary structure elements observed in the NMR structure of α B (PDB 2KLR). Third and fourth lanes: Secondary structure elements predicted by the I-Tasser and Phyre, respectively. Fifth lane: secondary structure elements included in the pseud-atomic model of human α B. Scissors indicate the positions of truncation mutants. (B) Predicted 3D models of two protomers with the N- (brown), C-terminal (green) domains and the NMR structure of the dimeric ACD (blue). The figure was modified from Braun et al. 2011 (66).

The biggest flexible loop is between the helices $\alpha 2$ and $\alpha 3$. This 20 aa long section was divided at position 40 which led to a rather instable mutant in terms of solubility and degradation during purification. In the first attempts the construct was expressed and purified by using a pet28 plasmid (Figure 25). The expected full length molecular mass of the $\Delta 40$ construct from pet28 plasmid is 15,515 Da, including an additional alanine residue after the primary methionine. The obtained molecular mass of 15,366 Da (A) corresponds to this construct lacking the primary Met (149 Da). Full length ESI-MS measurements revealed that 30 – 35 % of the protein was degraded (A). The degradation products could be identified as $\Delta 53$ (13,714 Da) and $\Delta 54$ (13,860 Da).

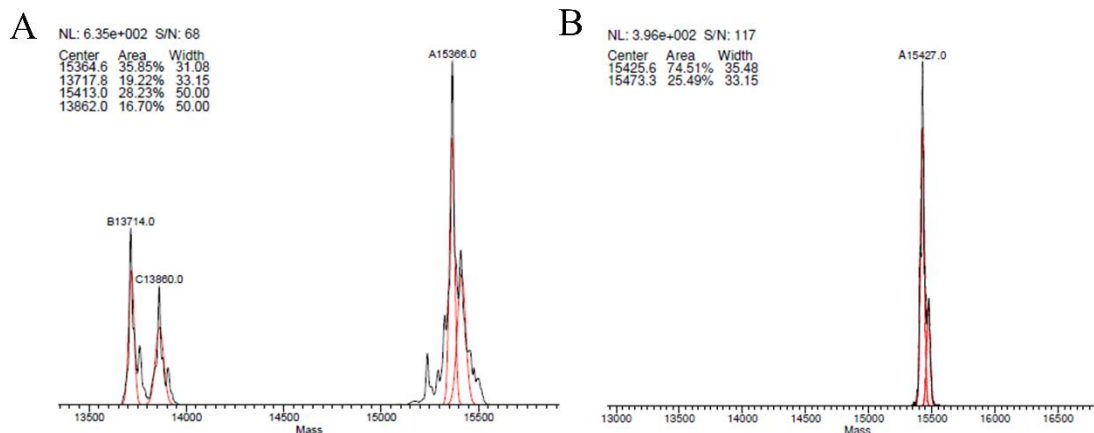


Figure 25 | Full length ESI-MS analysis of α B $\Delta 40$ purification products. The protein was expressed from different plasmids: (A) pet28 and (B) pE-SUMOpro.

Optimization of expression conditions with this plasmid did not lead to a protein preparation without degradation products. To protect the N-terminal segment from degradation, the $\Delta 40$ sequence was cloned into a pE-SUMOpro vector resulting in the addition of an N-terminal His₆-SUMO-tag. Additionally, expression conditions were optimized resulting in a shorter expression time (4h instead of overnight) at lower temperature (25°C instead of 30°C). Under these

conditions the solubility of the protein during expression was improved. After purification pure protein was obtained without degradation products (B). The molecular mass of 15,427 Da includes the methionine which was protected by the His₆-SUMO-tag, but does not contain an additional alanine. Still the yield of this construct remained low with about 0.5 mg per liter *E. coli* culture. The attempt to generate more stable variants at positions in proximity failed. The fourth mutant ($\Delta 51$) showed again better solubility, presumably because of the absence of the entire flexible loop, and therefore better yields. But difficulties with degradation during expression were observed for the $\Delta 51$ mutant as well. It seems recommended to express this construct from pE-SUMOpro plasmid to avoid degradation. The last used truncation mutant studied is missing the NTR completely and has been already described by Mainz et al. (2015) (134). Initially, for all truncation mutants the purity was checked via SDS-PAGE, their correct sequence was verified to be αB by MALDI footprint MS, and their integrity was demonstrated by full length ESI-MS. For further characterization, the content of secondary structure was measured by CD spectroscopy followed by thermal transitions from 20 – 90°C (Figure 26).

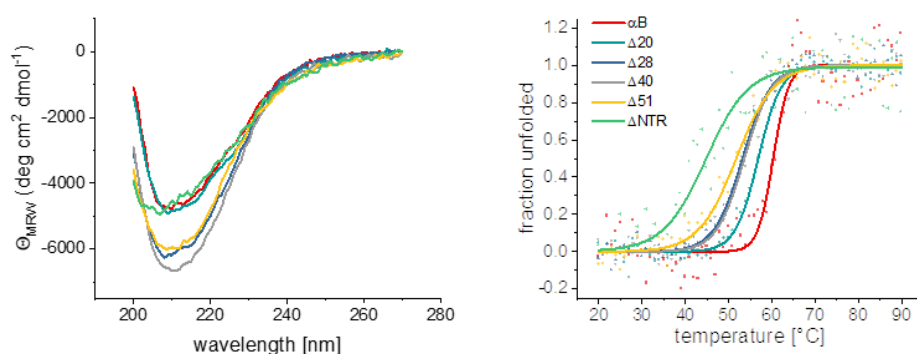


Figure 26 | Secondary structure and thermal stability investigations of truncation mutants of αB . The far-UV spectra are shown in the left panel. Thermal transitions followed at 205 nm and fitted with a sigmoidal Boltzmann fit are depicted in the right panel.

In principle, the curve spectra of all truncation mutants were similar. Differences only occurred in the intensity of molar ellipticity. Due to the fact that all truncations contain the IgG-like folded ACD a β -sheet characteristic CD spectrum with a minimum at 215 nm was expected. The comparable small amount of helical content in the N-terminal region did not result in significant differences between the truncations. On the contrary, the thermal transitions and calculated melting points showed significant differences. The highest stability was obtained for the wildtype protein (αB) with a melting temperature of 60.3°C and the lowest stability was observed for the protein with the longest truncation, ΔNTR ($T_m^{\Delta NTR} = 44.7^\circ C$). The mutants showed decreasing melting temperatures depending on the truncation length ($T_m^{\Delta 20} = 56.8^\circ C$; $T_m^{\Delta 28} = 53.2^\circ C$; $T_m^{\Delta 40} = 53.6^\circ C$; and $T_m^{\Delta 51} = 51.7^\circ C$). Thus, a decrease in the NTR length destabilizes the protein.

Next, the chaperone activity was analyzed for MDH as a model substrate and HEK293 lysate presenting a broad range of substrates (Figure 27). The ability of αB to prevent MDH aggregation and to keep a significant amount of HEK293 lysate proteins in a soluble conformation was characterized before in detail (53). Nevertheless, the wildtype protein was always included for comparison.

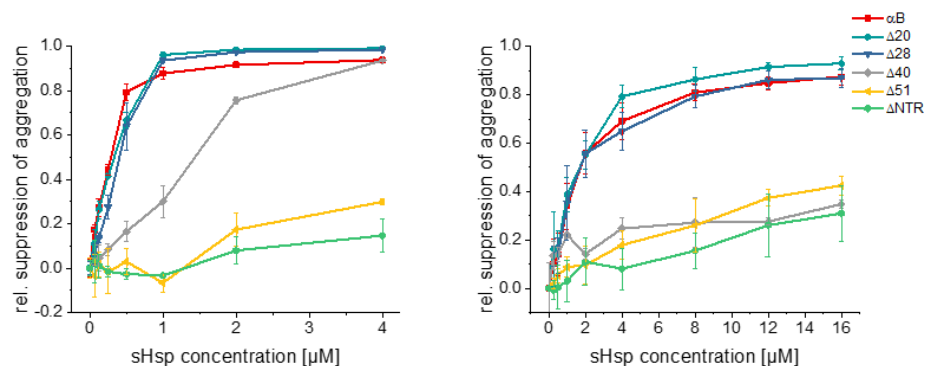


Figure 27 | Chaperone activity of α B truncation mutants towards the model substrate MDH (left) and HEK293 lysate (right). The thermal aggregation at 42°C of 4 μ M MDH was followed by detection of light scattering at 360 nm whereas for HEK293 lysate the soluble and insoluble part of the samples were separated by centrifugation after thermal denaturation at 45°C and analyzed by SDS-PAGE.

Complete suppression of MDH aggregation was observed for α B wildtype, Δ 20 and Δ 28. The truncation mutants Δ 51 and Δ NTR showed nearly complete inactivity, whereas the activity of Δ 40 was diminished but not totally inhibited. Interestingly, the picture was very similar for HEK293 lysate assays except for Δ 40, which was even more impaired in this assay. These results suggest the region between position 28 and 51 to be of importance for the holdase activity.

During different assays, it was observed that the mutants behave differently at distinct temperatures. Aggregation temperatures for MDH (42°C) and HEK293 lysate (45°C) were selected based on the optimal signal intensity range. To evaluate whether the increased temperature in the HEK293 lysate assays led to the decreased ability of Δ 40 to prevent aggregation, MDH and CS aggregation assays were performed at three different temperatures. CS was chosen as a second model substrate because HEK293 lysate aggregation was not possible at various temperatures to a comparable extent (Figure 28).

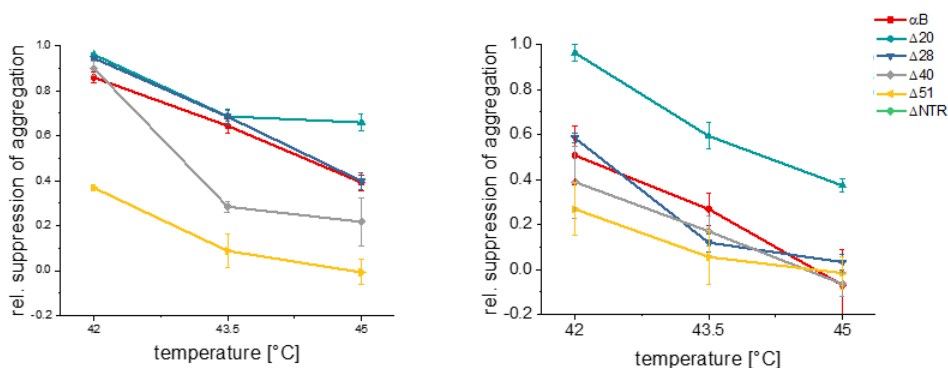


Figure 28 | The influence of α B truncation mutants on MDH (left) and CS (right) aggregation was tested at three different temperatures. The molar concentration of model substrate and sHsp were kept constant in a 4:1 ratio for MDH/sHsp and a 1:2 ratio for CS/sHsp.

The ability of sHsps to suppress the thermal aggregation of model substrates seemed to be temperature-dependent. In general, the α B constructs were more capable to inhibit substrate aggregation at lower temperatures. This may be based on the slower substrate unfolding and therefore prolonged possibilities of sHsp to interact with the substrate. Another possibility is that

4 RESULTS

the α B variants may be more binding-competent at lower temperatures. It is quite feasible that the α B variants show different size distributions, subunit exchange, or surface accessibility at different temperatures. In more detail, the ability to hold MDH in solution was similar for all truncation mutants at 42°C, except Δ 51, but at 43.5°C, Δ 40 did not show comparable activity anymore. A second interesting fact is the higher activity of Δ 20 at 45°C compared to wildtype α B and Δ 28. For CS aggregation the trend was similar: The higher the temperature, the lower the activity. More precisely, the holdase function of α B and its mutants, except Δ 20, was impaired completely at 45°C for CS aggregation and the activity increased gradually with decreasing temperature. Surprisingly, the Δ 20 mutant showed increased activity compared to wildtype at all tested temperatures. Overall, the reduced ability of Δ 40 to inhibit protein aggregation in the HEK293 lysate assay may be due to the higher aggregation temperature.

To check whether the observed changes in chaperone activity are based on changes in size distribution, SEC-MALS and AUC were conducted (Figure 29). SEC-MALS analysis revealed the presence of small sized oligomers for Δ 28 to Δ NTR with ~20 - 40 kDa corresponding to ~2.5 S in AUC. For the Δ 40 mutant a very broad distribution was detected in SEC-MALS ranging from 20 - 100 kDa. In the AUC experiments, its size distribution was narrower (2.5 – 5 S). α B wildtype has a size of ~500 kDa which equals ~15 S. The truncation mutant Δ 20 showed oligomeric species with a size of about 200 kDa, which is significantly decreased, compared to the wildtype but still a large oligomer.

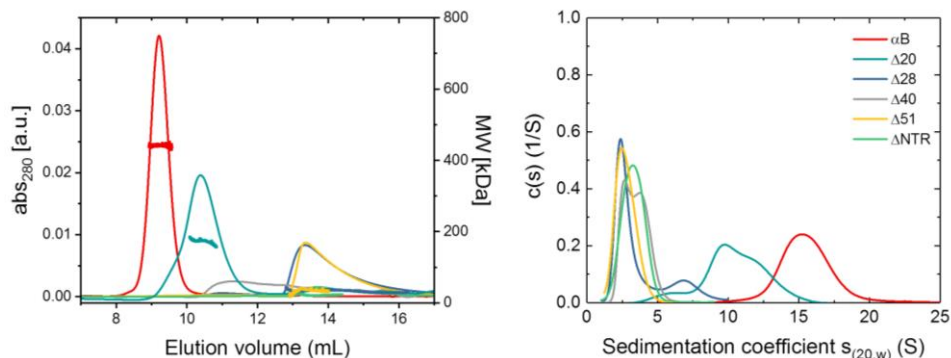


Figure 29 | Size distribution of α B truncation mutants analyzed by SEC-MALS and AUC. Size exclusion chromatography coupled to multi angle light scattering (left) was performed with 25 μ M sHsp at room temperature. Analytical ultracentrifugation (right) was performed with 2 μ M sHsp at room temperature. The SEC-MALS measurements were carried out by Nicole Lim, Ph.D. and the AUC experiments were performed by Dr. P. W. Schmid.

Overall, the size distributions obtained by SEC-MALS and AUC were in good agreement. In the current model of sHsp regulation, correlation of small active and bigger more inactive species does not fit the behavior of the mutants. The small oligomer sizes of Δ 28, Δ 51 and Δ NTR do not correlate with increased chaperone activity, and bigger oligomers of Δ 20 and α B wildtype did not show decreased activity.

Another property of sHsps is their highly dynamic behavior due to the constant exchange of subunits. This ability can be tested using a fluorescence resonance energy transfer (FRET) system within the α B oligomer. A single mutation at position S135 to cysteine was introduced to label the

protein specifically at this position. Due to the absence of further cysteines in α B, this is the most straightforward method. In order to generate a FRET system, two different labels (donor and acceptor) were covalently linked to the position in two separate attempts. The mutant proteins were measured indirectly by addition of an unlabeled mutant to the FRET system. The signal decrease due to subunit displacement with unlabeled subunits was then recorded and exchange rates were calculated based on a single exponential fit (Figure 30).

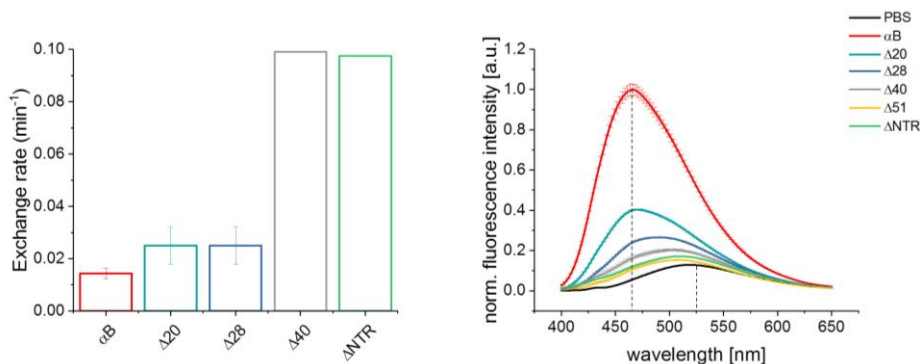


Figure 30 | Further characterization of α B truncation mutants by subunit exchange (left) and ANS binding (right) measurements. Loss of FRET efficiency was measured over time at 37°C at an excitation wavelength of 375 nm and a constant emission wavelength of 440 nm. The subunit exchange measurements were performed by Dr. P. W. Schmid. ANS binding was detected at 25°C after 2 h equilibration using 380 nm as excitation wavelength and recording spectra from 400 – 650 nm. Experiments were carried out by Nicole Lim, Ph.D..

Strikingly, the observed exchange rates correlate with the sHsp’s ability to hold proteins in solution during heat treatment. The wildtype α B protein as well as the active truncation mutants ($\Delta 20$ and $\Delta 28$) showed relatively slow subunit exchange rates of $\sim 0.02 \text{ min}^{-1}$ whereas $\Delta 40$ and Δ NTR showed strongly increased exchange rates of $\sim 0.1 \text{ min}^{-1}$. Based on the location of the fluorescence label (S135C), which is in the $\beta 8$ -sheet of the ACD, it is likely that subunit exchange within a dimer is detected only. Following this hypothesis, the dynamics of monomers are observed and slower exchange would mean a higher stability of the dimer.

Surprisingly, during data evaluation enhanced deviation of the one-phase exponential decay function (ExpDec1) used was observed for some fits. It seems like a one-phase fit is improper to represent the dynamics of subunit exchange especially for the bigger sHsp complexes. For the wildtype α B protein as well as for the $\Delta 20$ mutant even a two-phase exponential decay function (ExpDec2) did not result in suitable fit quality. Here, good fit deviations were only gained by using a three-phase exponential decay function (ExpDec3). This observation suggests a multi-step mechanism of subunit exchange, implying that FRET can also be observed between different protomers, and not only within a dimer as stated before. A three-step mechanism for subunit exchange may be explained by the three-fold symmetry axis of the α B 24mer structure (66). Based on this model, in the first step dimers are formed, in the second step hexamers are assembled which then serve as building blocks for the big oligomer. Although $\Delta 20$ oligomers are much smaller compared to the wildtype they still reached the size of a 12mer and a three-step mechanism does fit here as well. The size of all other mutants was smaller and a one-phase fit was suitable.

4 RESULTS

Another thing that needs to be kept in mind is the postulated competitive binding of the NTR to the substrate binding groove near the ACD interface (65). On the one hand, a shortened NTR may not be able to bind to this interface, which would increase the accessibility of this area to substrates. On the other hand, the NTR seems to be important for substrate recognition itself and the absence of distinct areas probably impairs the ability to interact with substrates (130-133,239). The binding of sHsps to substrates is mediated by hydrophobic patches (90,130,240). Therefore, it is likely that mutations especially in the highly hydrophobic NTR may lead to changes in the interaction ability. Furthermore, the observation of increased instability and decreased solubility of truncation mutants during recombinant expression and purification supports this hypothesis. A possibility to measure the amount of accessible hydrophobic patches of a protein is to quantify the binding of the fluorescence probe 8-anilinobaphthalene-1-sulfoic acid (ANS). This compound changes its fluorescence properties as it binds to hydrophobic protein surfaces. Upon binding, the fluorescence signal shows a hypsochromic shift (blue shift) and an increase in intensity. In Figure 30 (right panel), a clear shift and a strong intensity increase can be seen comparing the buffer control (black) and the α B wildtype (red). The trend holds true for all truncation mutants. The shorter the NTR is, the lower the fluorescence intensity and the less pronounced the observed hypsochromic shift was. This means the accessible surface hydrophobicity decreases with the amount of truncated NTR. Due to the hydrophobic and highly flexible characteristics of the NTR a binding of ANS especially to this region is likely. It does not seem like the NTR (or other hydrophobic patches) are ‘covered’ in the 24-mer of α B wildtype.

Hydrogen-deuterium exchange coupled to mass spectrometry (HDX-MS) is a sophisticated method to gain insight into overall surface accessibility of proteins narrowed down to their primary structure (Figure 31).

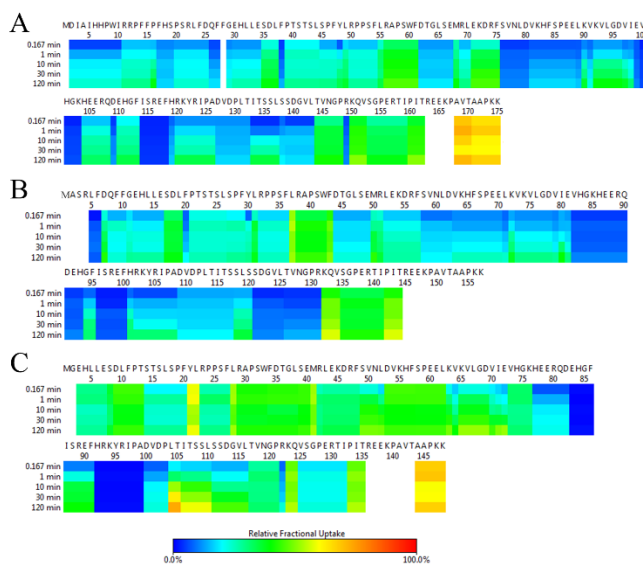


Figure 31 | Hydrogen-deuterium-exchange coupled to MS analysis of α B (A), its truncation mutants Δ 20 (B), and Δ 28 (C). The relative fractional deuterium uptake is color coded from blue (0 % uptake) to red (100% uptake). Peptide coverage maps of all measurements are attached in the appendix F.

This method may help to define whether the hydrophobicity of the NTR itself or other parts of the protein induce the decreased ANS intensity signal for the truncation mutants. Interestingly, the

hydrogen exchange in the wildtype and the $\Delta 20$ mutant is highly similar in the ACD as well as in the NTR. Even though the two proteins did not show oligomeric complexes of exactly the same size, both of them exist as oligomeric complexes bigger than 200 kDa. The strong changes in ANS intensity cannot be explained by a general higher accessibility of hydrophobic residues in $\Delta 20$. It is more likely that the absence of the first 20 amino acids is the reason for the decrease in the ANS signal as these do have a very high content of hydrophobic residues ($> 50\%$). The situation is different for the $\Delta 28$ mutant. Here, the hydrogen exchange rate was significantly increased for the NTR and even for the ACD. This again fits well to the size distribution data, as $\Delta 28$ was detected exclusively as a dimer. Taken together, the HDX-MS experiments revealed high dynamics of the NTR and also increased dynamics for the ACD in the case of dimeric species, whereas oligomeric complexes show comparable exchange rates even though their oligomer size is not exactly the same.

4.2.2 The influence of aromatic substituted mutants

The aromatic amino acid content in the N-terminal region is about 19%. This value is strongly increased compared to the average amount of aromatic amino acids in the UniProtKB/TrEMBL database of 8.1% (F = 3.91%; W = 1.3%; Y = 2.89%). Also in comparison to the remaining αB sequence, which has 10% aromatic amino acid content, it is significantly higher. Especially the phenylalanine content is increased from 3.5% in average proteins to 13% in the αB NTR. To gain further insight into the function of the N-terminal region of αB , the aromatic residues within the NTR were substituted by alanine in three different ways. First, only tryptophan residues (W9 and W60) were replaced by alanine (Trp free). Second, only phenylalanine residues (F14, F15, F17, F24, F27, F28, F38, F47, F54, and F61) were exchanged to alanine (Phe free) and third, tryptophans, phenylalanines and tyrosines (Y49) were substituted to alanine (aromats free). The design of all mutants is depicted in Figure 32.

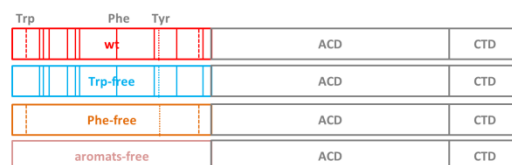


Figure 32 | Overview of aromatic substituted mutants of αB . In the Trp free mutant, tryptophan residues (W9 and W60) were replaced by alanine, in the Phe free mutant phenylalanine residues (F14, F15, F17, F24, F27, F28, F38, F47, F54, and F61) were exchanged to alanine, and in the aromats free mutant tryptophans, phenylalanines and tyrosines (Y49) were substituted to alanine.

The integrity of the recombinantly produced and purified proteins was shown by fingerprint MALDI-MS, SDS-PAGE, and full length ESI-MS, the secondary structure and the thermal stability were analyzed by CD spectroscopy (Figure 33). The secondary structure contents of wildtype αB and the Trp free mutant were very similar whereas the Phe free and aromats free mutants showed a strong increase of random coil with a more pronounced minimum and a minimum shift from 215 nm to 205 nm (left figure). Nevertheless, the basic structure for sHsp, which is the typical β -sheet from the IgG like folded ACD, could be verified for all mutants and CDNN analysis demonstrated very similar secondary structure proportions (appendix G).

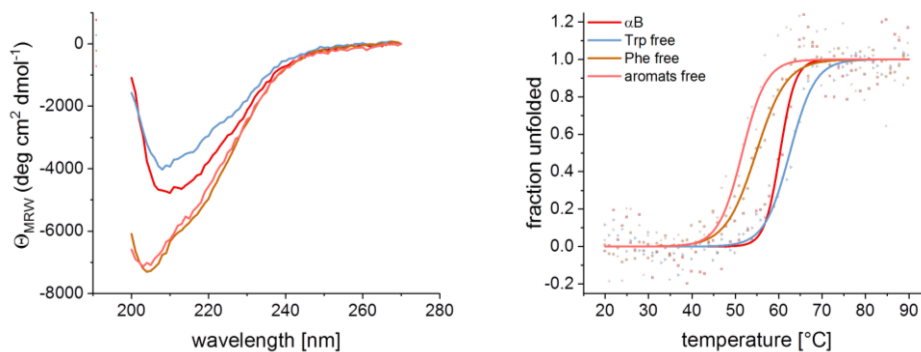


Figure 33 | Secondary structure and thermal stability investigations of aromatic mutants of α B. The far-UV spectra are shown in the left panel. Thermal transitions followed at 205 nm and fitted with a sigmoidal Boltzmann fit are depicted in the right panel.

The thermal transitions revealed the high similarity of the Trp free mutant ($T_m^{\text{Trp free}} = 62.5^\circ\text{C}$) and the wildtype ($T_m^{\alpha\text{B}} = 60.3^\circ\text{C}$). For the Phe free and the aromats free mutant a decreased thermal stability was observed with melting temperatures of 54.8°C and 51.6°C , respectively. The changes in the secondary structure, obtained in the far-UV spectra, led to a decrease in protein stability. Hence, particularly the deletion of N-terminal phenylalanines destabilizes the protein.

To test the holdase activity of the constructs MDH aggregation assays and HEK293 lysate aggregation assays were performed as described before (Figure 34).

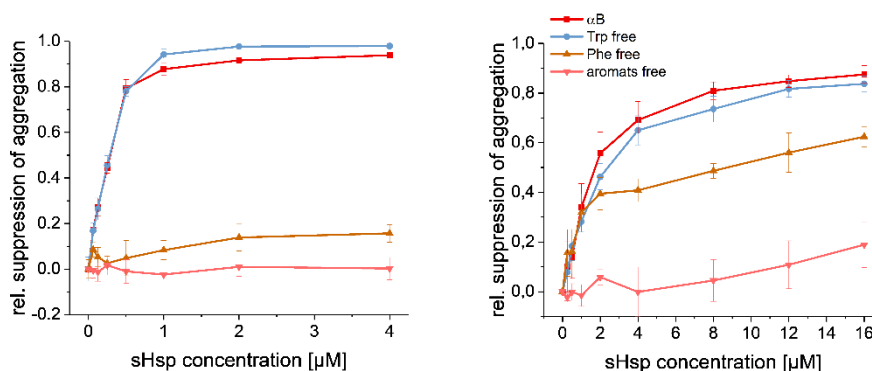


Figure 34 | Chaperone activity of α B aromatic mutants towards the model substrate MDH (left) and HEK293 lysate (right). The thermal aggregation at 42°C of $4\ \mu\text{M}$ MDH was followed by detection of light scattering at $360\ \text{nm}$ whereas for HEK293 lysate the soluble and insoluble part of the samples were separated by centrifugation after thermal denaturation at 45°C and analyzed by SDS-PAGE.

No difference in activity was detected for wildtype and the Trp free mutant whereas the aromats free mutant was completely inhibited and the Phe free mutant showed a strong decrease of activity for MDH but only slightly impaired activity in HEK293 lysate assay. Here again the strongest impact was observed for the deletion of the phenylalanines. To test whether the observed behavior can be traced back to the oligomer size of the mutants, size distribution analysis by SEC-MALS and AUC were performed (Figure 35). SEC-MALS and AUC showed consistent small species ($< 45\ \text{kDa}$) for the aromats free and the Phe free mutants. Hence, these two mutants lost their ability to form oligomeric species completely.

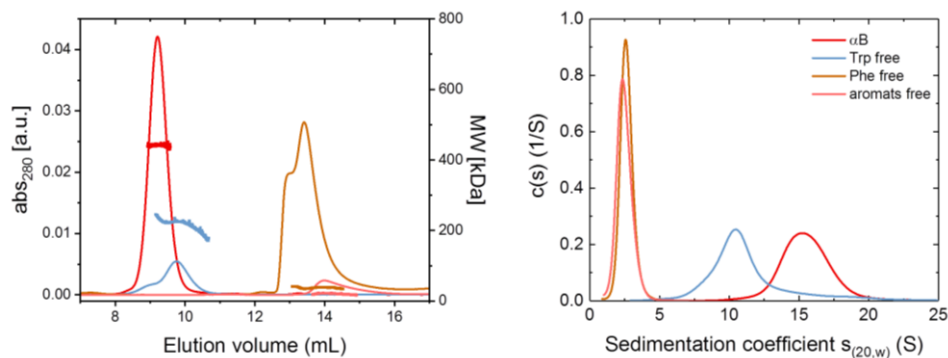


Figure 35 | Size distribution of α B aromatic mutants analyzed by SEC-MALS and AUC. Size exclusion chromatography coupled to multi angle light scattering (left) was performed with 25 μ M sHsp at room temperature. Analytical ultracentrifugation (right) was performed with 2 μ M sHsp at room temperature. The SEC-MALS measurements were carried out by Nicole Lim, Ph.D. and the AUC experiments were provided by Dr. P. W. Schmid.

For the Trp free mutant the variance of the obtained sizes was higher. The SEC-MALS analysis determined 300 – 200 kDa and in AUC the calculated mass was slightly higher with ~375 kDa (10.5 S). As observed before for the truncation mutants the chaperone activity did not correlate with the size distribution. Therefore, subunit exchange and surface hydrophobicity was analyzed by FRET and ANS binding (Figure 36).

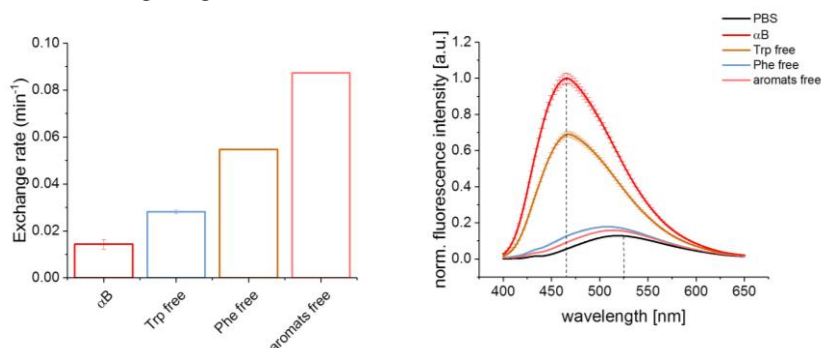


Figure 36 | Characterization of α B truncation mutants by subunit exchange (left) and ANS binding (right). The ANS binding experiments were provided by Nicole Lim, Ph.D. and the subunit exchange measurements were performed by Dr. P. W. Schmid.

For the aromatic mutants a gradually increasing subunit exchange rate was detected where less aromatic residues led to higher exchange rates. Apparently the slightly increased exchange rate of the Trp free mutant ($\sim 0.028 \text{ min}^{-1}$) did not impair its holdase capacity but a stronger increase of the exchange rate in case of the Phe free mutant ($\sim 0.054 \text{ min}^{-1}$) did impair the activity at least for HEK293 lysate substrates. The exchange rate for the aromats free mutant was comparable to the exchange rates of inactive truncation mutants ($\Delta 40$ and ΔNTR) and led to inactivity in this case as well. Hence, a correlation between subunit exchange rate and chaperone activity can be observed for the aromatic mutants as well whereas size distribution did not correlate.

As expected, an ANS signal decrease was observed for mutants with substituted aromatic residues compared to the wildtype signal. The exchange of the two tryptophanes reduced the intensity around 35 % but did not shift the maximum of the observed peak. Hence, the influence of the

4 RESULTS

tryptophanes on the hydrophobic surface seems to be small. The Phe free and the aromats free mutants showed similar results with an intensity decrease of over 80 % and a significant shift of the maximum. Here, a change in surface hydrophobicity was definitely induced by the mutations. In order to verify with results and to determine changes in structure dynamics, hydrogen-deuterium-exchange was performed (Figure 37).

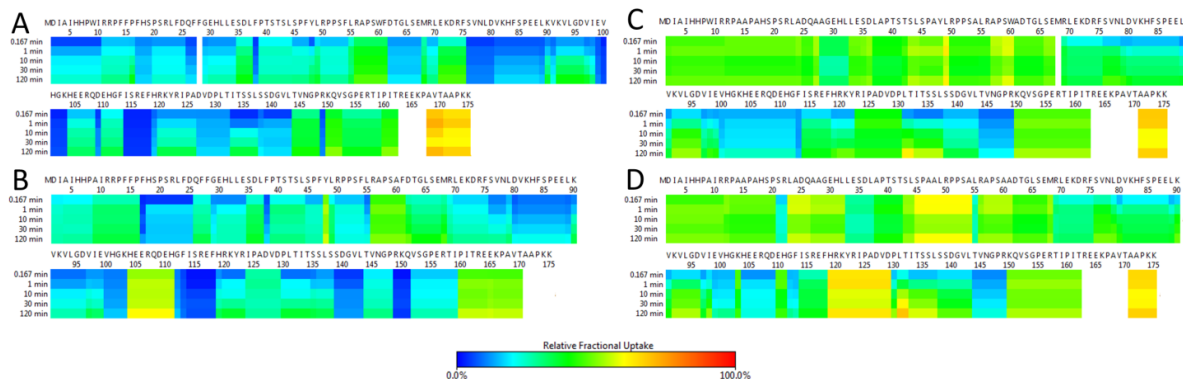


Figure 37 | Hydrogen-deuterium-exchange coupled to MS analysis of α B (A) and its aromatic mutants (B) Trp free, (C) Phe free, and (D) aromats free. The relative fractional deuterium uptake is color coded from blue (0 % uptake) to red (100% uptake). Peptide coverage maps of all measurements are attached in the appendix H.

The HDX-MS results presented in Figure 37 include different incubation times with deuterium (10 s; 1 min; 10 min; 30 min and 2 h) for each mutant. The most prominent difference between the four experiments is the overall higher relative fractional uptake of deuterium of the Phe free and the aromats free mutants (C+D). For these two mutants only the peptides of the ACD (70 - 150) displayed an uptake below 50 %. Even within the ACD there is an area (120-130) showing increased uptake for the aromats free mutant (D). This region belongs to the end of the β 6+7 strands and the following loop region which may be important for NTR and/or substrate binding as it is likely part of the substrate binding groove near the ACD (65). The same region appeared as well in the Trp free mutant (B) with a relative high deuterium uptake. Compared to the wildtype protein, this mutant also revealed a slightly higher uptake in the NTR, but not as obvious as the other two mutants. The CTR region cannot be analyzed reliable because of too few available peptides (see appendix H).

Taken together, the dynamics of the mutants with pronounced changes in the primary sequence was higher within the NTR as well as in the ACD. Nevertheless, increased accessibility was also observed for the double point mutant (Trp free) in both regions although to a smaller extent.

4.2.3 Substrate-sHsp interaction analyzed by cross linking experiments

Crosslinking experiments have been performed before with sHsps to gain information about their structure and function (66,241,242). The simplest way to crosslink proteins in aqueous solution under physiological conditions (moderate temperature, pH 7.4, reducing conditions) is an amine reactive chemical reaction. Therefore, NHS ester compounds which react with primary amines are used. Within a protein sequence primary amines can be found in lysines (K) and at the N-terminal end of the protein sequence. Unfortunately, the N-terminal region of α B does not contain any lysine

residues. Point mutations needed to be introduced distributed over the first 60 aa because the first native lysine of α B is located at position 72 (Figure 38).

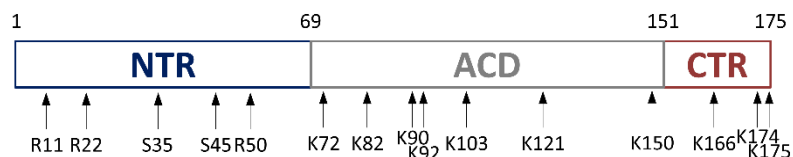


Figure 38 | Overview of amino acid positions within primary structure of α B which were mutated to lysine for crosslinking experiments. As indicated the ACD and the CTR contain even distributed native lysine residues.

Lysines ($pK = 10.28$) are positively charged under physiological conditions. Thus, the position needs to be selected with care. Amino acids with a comparable pK value are arginine ($pK = 13.2$), asparagine ($pK = 13.2$) or tyrosine ($pK = 10.02$). As arginines occur frequently within the NTR, these positions were chosen for point mutations (R11K, R22K and R50K). Furthermore, two serine positions (S35K and S45K) were chosen because of a general sterically similarity of serine and lysine and the absence of residues with higher similarity between position 22 and 50. Last, a triple lysine mutant (R3xK) including R11K, R22K, and R50K was designed to increase the crosslinking within one construct. The model substrates of choice (MDH and CS) showed well distributed lysine residues in nearly all regions. Hence, no point mutations needed to be introduced.

To ensure the wildtype-like behavior of the mutants in terms of substrate interactions, their chaperone activity towards MDH and CS were tested (Figure 39).

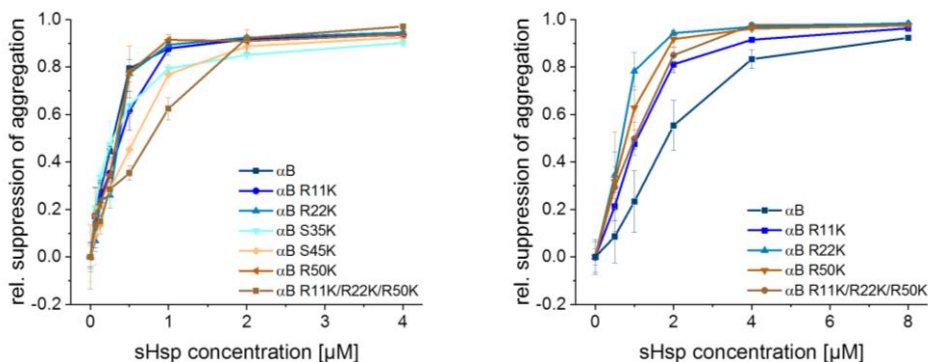


Figure 39 | Chaperone activity of α B crosslinking mutants towards the model substrate MDH (left) and CS (right). The thermal aggregation at 42°C of 4 μ M MDH was followed by detection of light scattering at 360 nm whereas for CS the thermal aggregation was performed with 1 μ M substrate at 45°C.

In case of holdase activity towards thermal MDH aggregation almost all mutants behaved wildtype-like. A significantly decreased activity was obtained for the triple lysine mutant (R3xK) only. Moreover, this deviation from wildtype activity appeared only at 8:1 and 4:1 substrate/sHsp ratio. At higher sHsp concentrations, the mutant exhibited similar activity. Therefore, crosslink experiments were performed at 1:1 substrate/sHsp ratios. For CS as model substrate all mutants showed slightly increased holdase activities. Nevertheless, as the activities are still in the same range, especially at higher sHsp concentrations, crosslink experiments were performed at 1:4 substrate/sHsp ratio.

4 RESULTS

Further requirements that need to be determined are the length of the crosslinker and the possibility of cleavable or non-cleavable crosslinker. The advantage of a cleavable crosslinker is the improved identification of crosslinked peptides by different types of gas phase fragmentation and levels of tandem MS. These datasets require more intense data analysis. Therefore, a non-cleavable crosslinker was chosen. The length of the crosslinker defines the specificity because it limits the spatial area of possible interaction partners. A short crosslinker is therefore preferred but may diminish the crosslink reactions per se. To aim for highly specific crosslinks, a crosslinker (DSG) with a spacer arm of only 7.7 Å was chosen (Figure 40, A).

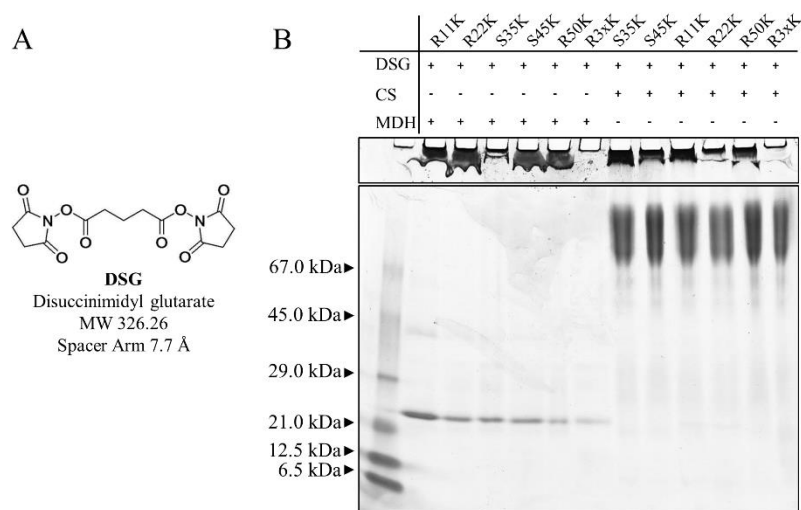


Figure 40 | (A) Chemical structure of the DSG crosslinker compound used and (B) SDS-PAGE of crosslinking experiments of different α B lysine mutants with MDH and CS using DSG as crosslinker. For optimal resolution of high molecular mass crosslinks and monomeric species a precast 4-20 % SERVAGel TG PrIME was used and separation was performed under reducing conditions at low current (20 mA).

After pre-incubation of the sHsps, the samples were mixed with substrate and thermal aggregation was performed. Subsequently, the crosslinker was added and crosslinking was stopped with Tris after further incubation. All crosslink experiments were analyzed by SDS-PAGE in addition to check for successful crosslinking (Figure 40, B). For MDH crosslinking, sHsps were not incorporated in substrate/sHsp complex completely. The remaining sHsp can be seen at around 22 kDa. The substrate/sHsp complex itself did not enter the separation gel because of too huge complex size, which indicates a high crosslink rate. For CS experiments, no remaining sHsps were observed at monomer size, but complexes were observed between 100 – 200 kDa in the separation gel and additionally again huge complexes, which did not enter the separation gel. Surprisingly, for the R3xK mutant no huge complexes in the pockets of the stacking gel were found. It needs to be mentioned that all used proteins (α B, CS and MDH) form oligomers on their own. Therefore, intermolecular crosslinking within one species is likely as well as intramolecular crosslinking. All three types of crosslinks are visualized on the SDS-PAGE whereas for MS crosslink data analysis self-crosslinks were excluded.

MS data of crosslink experiments were analyzed using the program Kojak and hits were verified by the percolator software. For visualization and further evaluation, results were uploaded to the PROXL online tool. The generated crosslink maps are attached in the appendix I and J. The

intermolecular hits of all mutants were counted for the sequence of CS, MDH, and α B separately, normalized for better comparison and summarized in Figure 41. The reduced amount of crosslinks observed for CS (A) can be explained by not fully optimized crosslinking conditions and the lower lysine content of 5.7 % in CS compared to 8.3 % in MDH and 9.1 % in α B including all mutations.

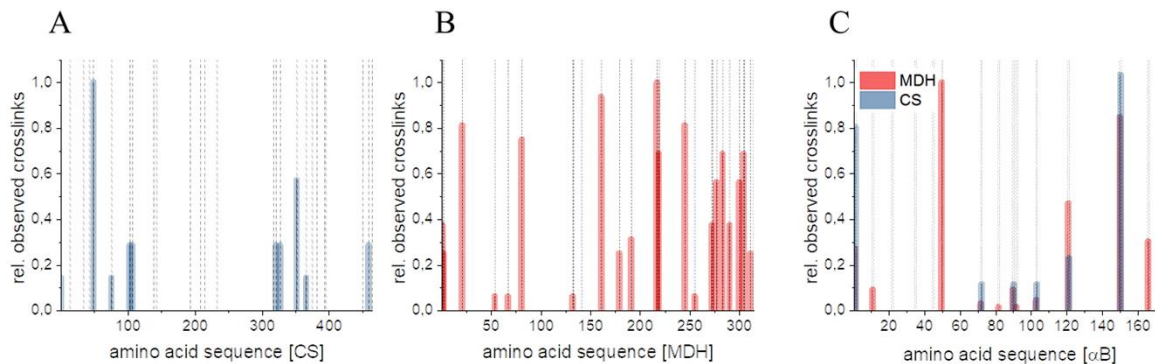


Figure 41 | Distribution of all verified crosslinks in (A) the CS sequence, (B) the MDH sequence, and (C) the α B sequence. The sum of the counted hits per position was normalized for better comparison between the different proteins. For α B, crosslinks of CS (blue) and MDH (red) are depicted in the same figure. Gray dotted lines visualize the positions of lysine residues.

It can be expected that substrates are at least partially or even completely unfolded in the substrate/sHsp complexes after thermal aggregation. Therefore, it can be assumed that all lysines are accessible for crosslinks. Noticeable, for both substrates the crosslink distribution was not homogeneous. For CS (A) no crosslinks were observed in the middle part of the protein whereas for MDH (B) crosslinks accumulated at the C-terminal part. The occurrence of preferred regions indicates that crosslink positions within the substrates were not random and specific sites of interaction do exist. Using self-designed CelluSpots chips with immobilized substrate-derived peptides, Dr. K. Back showed as well that α B has selective binding affinities for substrate regions (213). Here, aromatic/non-polar residues like leucine, phenylalanine, alanine, valine, tyrosine, glycine and arginine were identified as amino acids improving the binding whereas negatively charged amino acids particularly glutamic acid and aspartic acid. As sHsps bind to a lot of different proteins, it is not surprising that no clear motif was determined (213). Therefore, effectively crosslinked regions were highlighted in the primary sequences of CS and MDH (Figure 42). Crosslinks of lysines were increased in close proximity to arginine (R) or proline (P). Even though proline is not classified per se as positively charged residue the face of the proline ring is partially positively charged (243). The presence of negatively charged residues can possibly be compensated by the increased presence of positively charged residues (K, R, and P). This may pertain to the crosslink region in CS around K321/K327 and in MDH towards the C-terminal end from K272-K314.

For the sHsp accessibility of all lysines was not expected as α B should not unfold or even aggregate at 45°C. However, a high accessibility of the NTR and CTR regions is expected whereas the residues of the ACD are possibly hidden in the protein core through its IgG-like β -sheet structure and the dimer interactions. Unexpectedly, the crosslink distribution on α B (Figure 41, C) showed clearly a high number of interaction sites in the CTR (150-175) followed by the ACD (70-150)

4 RESULTS

although lysines were distributed evenly by using the designed mutants. Noteworthy, only the N-terminal end itself showed high crosslinking for CS and the position R50K for MDH, respectively.

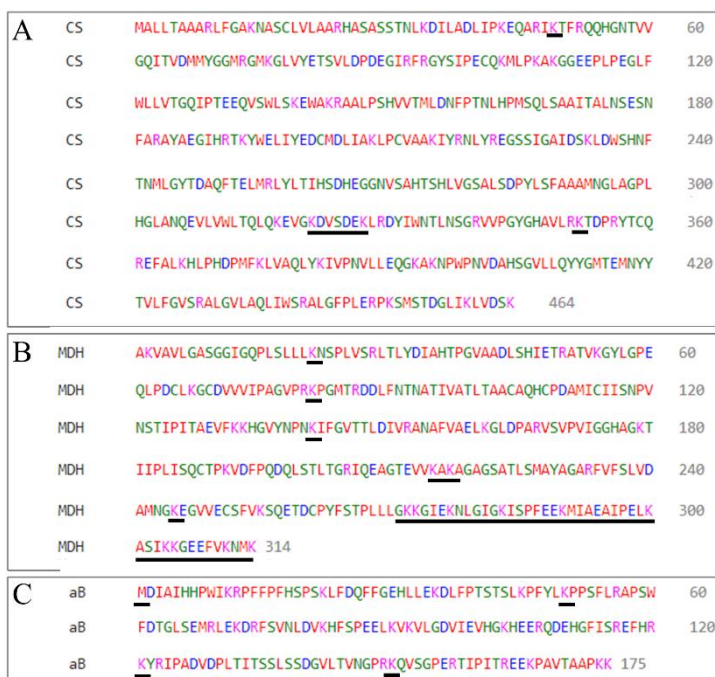


Figure 42 | Amino acid sequences of model substrates (A) CS and (B) MDH as well as of α B (C). Residues are color-coded based on their properties: non-polar (red), polar (green), negatively charged (blue), or positively charged (pink). Figures are created using the Clustal Omega online tool from EMBL-EBI. Highly crosslinked regions/lysines are highlighted by an underlining.

Previous studies suggest predominantly the NTR and the CTR as the regions of substrate interaction (64,133,239,240,244). However, there is also evidence for the ACD being involved in substrate binding (131,134,245). In α A and α B a short sequence was found that can work as a chaperone on its own. The sequence, named ‘mini-chaperone’, is located in the β 3-sheet of the ACD (131,245). Thus, substrate interaction must also be possible in the ACD domain. Other studies reported the preferred interaction of the fibril-forming Alzheimer’s disease A β 1–40 peptide with the ACD, whereas the amorphously aggregating lysozyme was captured by the NTR of α B (134). Overall, there are indications for all three domains being substrate interaction sites for substrate proteins. In terms of a possible amino acid motif in α B for substrate recognition, opposite characteristics compared to the features in the model substrates could be assumed. However, this is not the case: all observed crosslink regions in α B show very similar properties like arginines or prolines in proximity and the absence of negatively charged amino acids (Figure 42, C).

Taking all these findings together, the crosslinking of model substrates and sHsps per se works using DSG as crosslinker under the mentioned conditions. The generated data together with the outcome of previous studies suggest a selective way of substrate/sHsp interaction. As positively charged amino acids in particular seem to play an important role, it is recommended to use a lysine-independent crosslinking mechanism.

4.3 Regulation of sHsps by the postulated co-chaperone Bag3

Since Bag3 is postulated to be a co-chaperone of sHsps (113), we wanted to investigate its influence on sHsps. Bag3 contains at least seven domains including an N-terminal WW domain, which mediates binding to proline-rich regions, or its own PXXP domain, two IPV domains that interact with sHsps, two RSQS motifs mediating 14-3-3 interactions, a PXXP domain that cooperates with dynein and SH3-domain proteins, and a BAG domain, for Hsp70 interaction (Figure 43). Based on the BAG domain Bag3 is classified to be a nucleotide exchange factor of Hsp70.

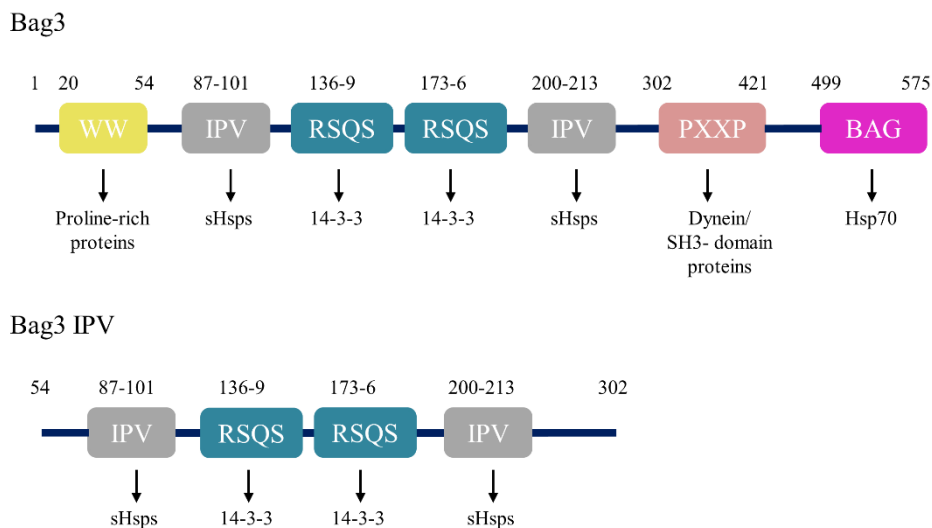


Figure 43 | Protein domain composition of Bag3 and the Bag3 IPV mutant. Arrows indicate interactions with specific protein types. Numbers in the figure depicts amino acid positions.

Parts of the *in vitro* interaction of Bag3 with different sHsps was investigated by Rauch et al. (2017) by ITC. To narrow down the exact interaction site multiple mutants of Bag3 with deletions of each domain one by one were generated. Additionally, a separated BAG domain and full length constructs with point mutations in the IPV motif to GPG were used. A separate IPV construct including only the two IPV motifs to prove the interactions of sHsp to this motif only was designed and characterized in the present study. Even though the IPV motifs per se are very short stretches of about 13-14 aa long, the surrounding regions were included for the first construct to ensure the intact structure of the interacting regions.

4.3.1 Production of recombinant Bag3 protein from *E. coli*

First expression tests with a pet28 plasmid including a human Bag3 sequence insert isolated by PCR from a cDNA database did not result in high expression efficiency. Therefore, the insert was cloned into the pE-SUMOpro plasmid. As it can be seen in Figure 44, the amount of the expressed protein was still low under all conditions tested. Obviously, the low expression amount was not due to poor solubility, as the protein amount in the total cell suspension (C) was very similar to the protein amount in the soluble protein fraction (S).

The human and the bacterial translation machinery differ in the relative preference of using specific codons. For each organism specific so-called major codons are defined that occur in highly

expressed proteins whereas low expressed proteins contain codons that are rarely used. (246). In case of differences in codon usage between bacteria and man, protein expression can be enhanced by codon optimization (CO) in the DNA sequence.

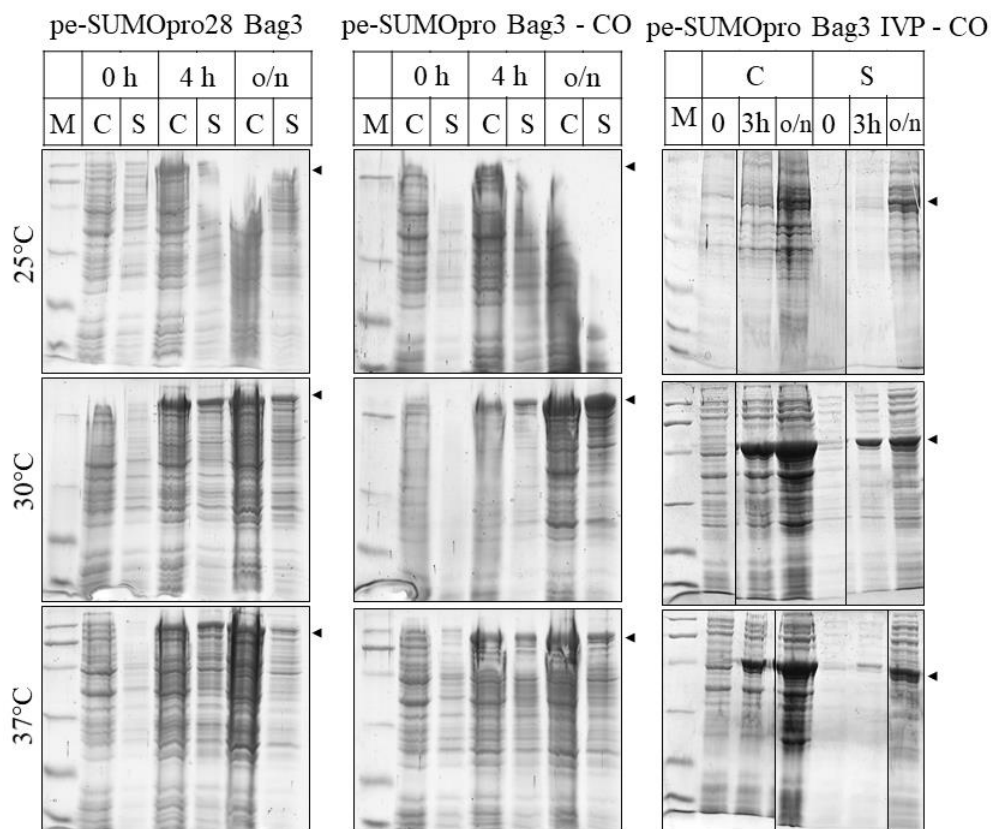


Figure 44 | Test expression of Bag3 constructs from pE-SUMOpro plasmids in BL21 *E. coli* cells. The total cell suspension (C) as well as the soluble protein fraction after lysis (S) were analyzed by SDS-PAGE before induction (0 h), after 3 h/4 h of expression (3 h/4 h) and after overnight expression (o/n). Plasmids with codon-optimized sequences are marked with 'CO'. Arrows indicate the size of the expressed construct. M indicates the position of the marker proteins.

Fortunately, the expression level of Bag3 increased using an optimized DNA sequence for Bag3 and also the Bag3 IPV mutant was expressed in a satisfactory amount despite some degradation bands at 37°C. Hence, protein expression was performed at 30°C overnight for both constructs using the codon-optimized pE-SUMOpro plasmids. Compared to the published purification protocol by Rauch et al. (2017) the purification procedure was slightly optimized (Figure 45) (113). Nevertheless, after the nickel-affinity chromatography and cleavage of the tag, two further columns (ion exchange and SEC) were necessary to produce highly pure Bag3 or Bag3 IPV. The two constructs differ strongly in their pI especially after cleavage of the SUMO-tag (see 3.2.2 Protein expression). Thus, an anion exchange chromatography (resource Q) was included for Bag3 purification and a cation exchange chromatography was used for the Bag3 IPV protein. Finally, a size exclusion chromatography was performed to separate the last contaminations and transfer the proteins into storage buffer (PBS pH 7.4).

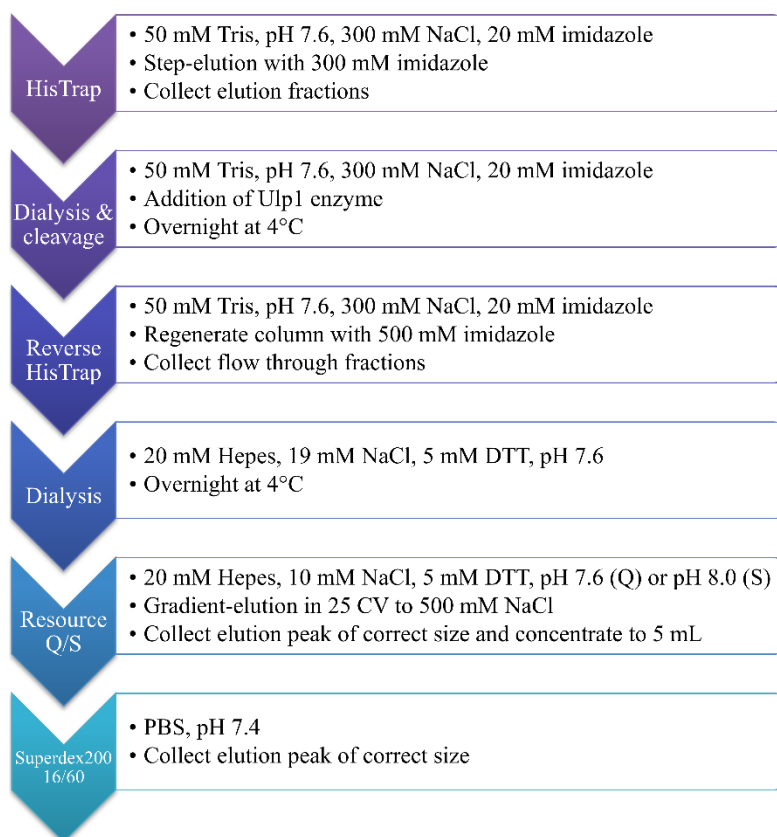


Figure 45 | Schematic purification protocol for Bag3 and Bag3 IPV proteins. Due to a strong difference in their pI values, Bag3 (pI 6.46) was purified by using an anion exchange column (ResQ) whereas for Bag3 IPV (pI 9.63) a cation exchange column was used (ResS).

The correct protein content was verified by MALDI fingerprint MS and the protein purity was checked by SDS-PAGE (Figure 46). It was verified that both proteins are present at high purity without any degradation products or contaminations. Especially, no contamination by DnaK or other bacterial chaperones was observed, which is of importance for chaperone activity assays.

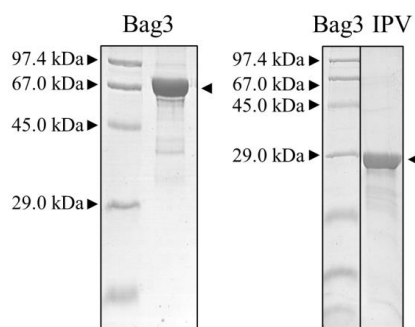


Figure 46 | Quality control of purified Bag3 and Bag3 IPV proteins on SDS-PAGE. 5 μ g of recombinant purified protein was applied on a 12.5 % SDS-PAGE. Arrows indicate the size of the target protein for Bag3 (61.595 kDa) and Bag3 IPV (26.838 kDa).

However, the apparent size of both proteins was increased on the SDS-PAGE as Bag3 appeared at 67 kDa and Bag3 IPV at 29 kDa compared to the theoretical molecular mass (UniProtKB ID O95817) and the results of full length mass analysis.

4.3.2 Basic characterization of Bag3 and Bag3 IPV

In order to gain insight into the secondary structure of the not yet characterized IPV part of Bag3, CD spectroscopy was performed for both proteins (Figure 47). The published structure of the BAG domain consists of α -helices (247) whereas the WW domain contains β -sheets only (248). Additionally, the structure prediction tool Phyre2 postulated an increased α -helix content in the PXXP domain as expected because of the high proline content. CDNN evaluations of the recorded far-UV spectra at 20°C showed indeed a significant content of α -helices (> 20 %) and a lower amount of β -sheet (< 10 %), but also a huge amount of random coil (> 40 %) for the full length protein (appendix O). As it can be clearly seen from the CD graph (Figure 47, left), the Bag3 IPV mutant showed an even increased amount of random coil (> 45 %) and a decrease in the α -helix proportion. The β -sheet amount was calculated to be similar (appendix O). The decrease in the α -helix percentage can be explained by the absence of the BAG and the PXXP domain. Whereas the constant amount of β -sheet is surprising due to the depletion of the WW domain. This hints to secondary structure parts within the IPV region itself.

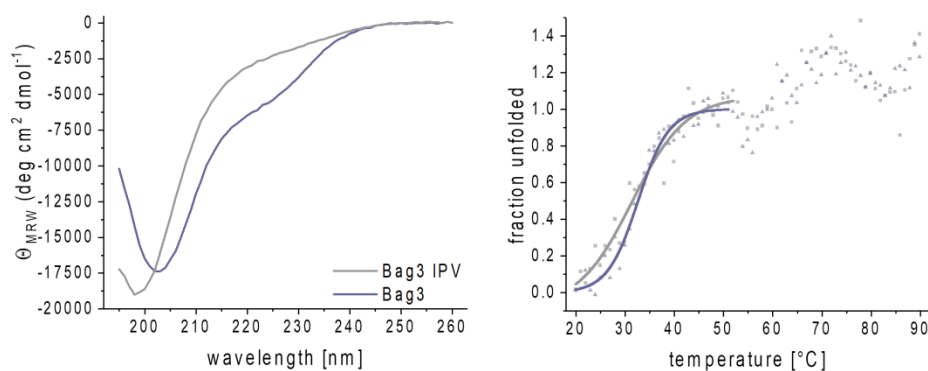


Figure 47 | Secondary structure and stability analysis of Bag3 and Bag3 IPV. Thermal transition was followed at 205 nm and fitted with a sigmoidal Boltzmann fit is depicted. Full spectra data of the thermal transitions are attached in the appendix N.

Thermal transition experiments were performed using CD spectroscopy to compare the protein stabilities. In Figure 47 the transition is visualized at 205 nm and fitted with a sigmoidal Boltzmann fit. The melting temperature T_m is defined as the inflection point (x_0) of the Boltzmann equation. The fit only represents the first part of the transition. Further transitions at higher temperatures are not considered. The determined melting temperature was highly similar for Bag3 and Bag3 IPV with 32.6°C and 31.4°C, respectively. As both proteins are derived from humans, which do have a core body temperature of 37°C (249), a melting temperature of about 32°C is relative low. However, the effect of proteins *in vitro* without any interaction partners may explain this value. More important is the observation of an equal behavior of Bag3 and Bag3 IPV. Due to the high deviation of the dataset at higher temperatures it was impossible to determine the exact temperature of the second transition with a fit function. The transition was roughly observed between 60°C and 70°C. A second transition indicates another part of the protein which is more stable and therefore transits at higher temperatures. This additional domain seems to be located within the Bag3 IPV sequence as this behavior was observed for both proteins. Surprisingly, although the shorter Bag3 IPV mutant showed little secondary structure compared to the full length Bag3 protein, the thermal transitions were almost equal.

Size exclusion chromatography coupled to multi-angle-light-scattering (MALS) detector was performed to gain insight into the quaternary structure of Bag3 and Bag3 IPV. To be able to measure sHsps and Bag3 proteins on the same column, a Superdex200 Increase was chosen. The measurements were performed at room temperature whereas the proteins were injected after incubation either on ice or at 37°C for 90 min (Figure 48).

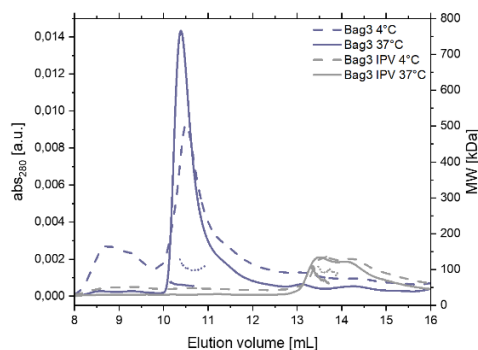


Figure 48 | Size distribution of Bag3 and Bag3 IPV mutant analyzed by SEC-MALS. Size exclusion chromatography coupled to multi angle light scattering was performed with 10 μ M Bag3 or Bag3 IPV at room temperature using a superdex200Increase 10/300 GL column.

As observed before for the sHsps, the incubation at 37°C led to a decrease of the high molecular weight fraction (\sim 9 mL elution volume). Hence, for all following experiments proteins were pre-incubated at 37°C for 90 min. The Bag3 full length protein eluted at an elution volume of 10.5 mL in a single peak and the apparent molecular mass calculated from the light scattering detector was \sim 57 kDa which equals the mass of a monomer (61.6 kDa). The IPV mutant eluted in a double peak between 13 – 14.5 mL corresponding to an apparent molecular mass of 30 – 60 kDa. As the mass of a monomer is 26.838 kDa, it can be concluded that the IPV mutant exists as a dimer/monomer mixture in a 1:1 ratio under the experimental conditions.

4.3.3 Bag3 influence on sHsp chaperone activity

The influence of Bag3 on sHsp activities has been described before *in vivo* (51,172). Especially, effects have been observed in the context of autophagy processes (54,179,250). In the present study the influence on the holdase activity of sHsp was investigated. Since Rauch et al. (2017) observed the tightest interactions between HspB1 and Bag3, HspB1 was selected for the following experiments (113). The most likely binding ratio of HspB1/Bag3 is 2:1 as Bag3 contains two IPV motifs. This indication was confirmed by ITC experiment (113). Due to low accessible Bag3 concentrations CS and insulin assays were performed with a 4:1 ratio while for MDH it was possible to work with a 2:1 HspB1/Bag3 ratio. On the one hand, citrate synthase (CS; A) and insulin (B) were chosen because HspB1 shows strong activity for these substrates. On the other hand, malate dehydrogenase (MDH; C) was tested, trying to induce chaperone activity of HspB1 for this unfavored HspB1 substrate (Figure 49). Bag3 on its own (purple) did not show any ability to suppress the thermal aggregation of CS and MDH. Surprisingly, for the reduction-induced aggregation of insulin, Bag3 showed about 40 % of aggregation suppression up on high concentrations. Although, Bag3 was observed to be unstable at increased temperatures, co-aggregation of Bag3 was not observed during the performed assays.

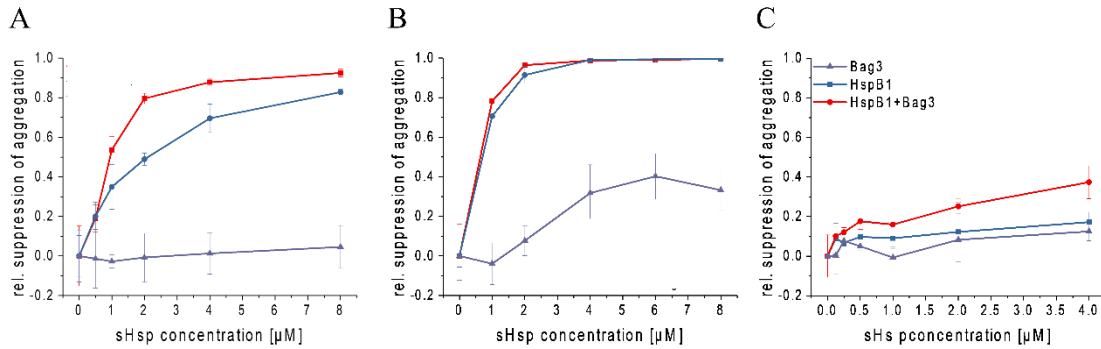


Figure 49 | Influence of Bag3 on HspB1 chaperone activity on (A) CS, (B) insulin and (C) MDH aggregation. For CS and insulin experiments, a 4:1 HspB1/Bag3 ratio was used. In the case of MDH, experiments were performed using a 2:1 HspB1/Bag3 ratio.

In the case of CS and MDH, HspB1 activity was slightly increased upon Bag3 addition. For CS, the effect was observed particularly before reaching the saturation at around 4 μM sHsp concentration. The aggregation of insulin was prevented by HspB1 effectively already at HspB1 concentrations of 2 μM . It is likely that an enhancing effect of Bag3 cannot be observed here because total aggregation inhibition was reached by HspB1 alone. In general, no inhibiting effect was observed in any assay. In contrary, for two out of three model substrates a slight increase of chaperone activity was observed.

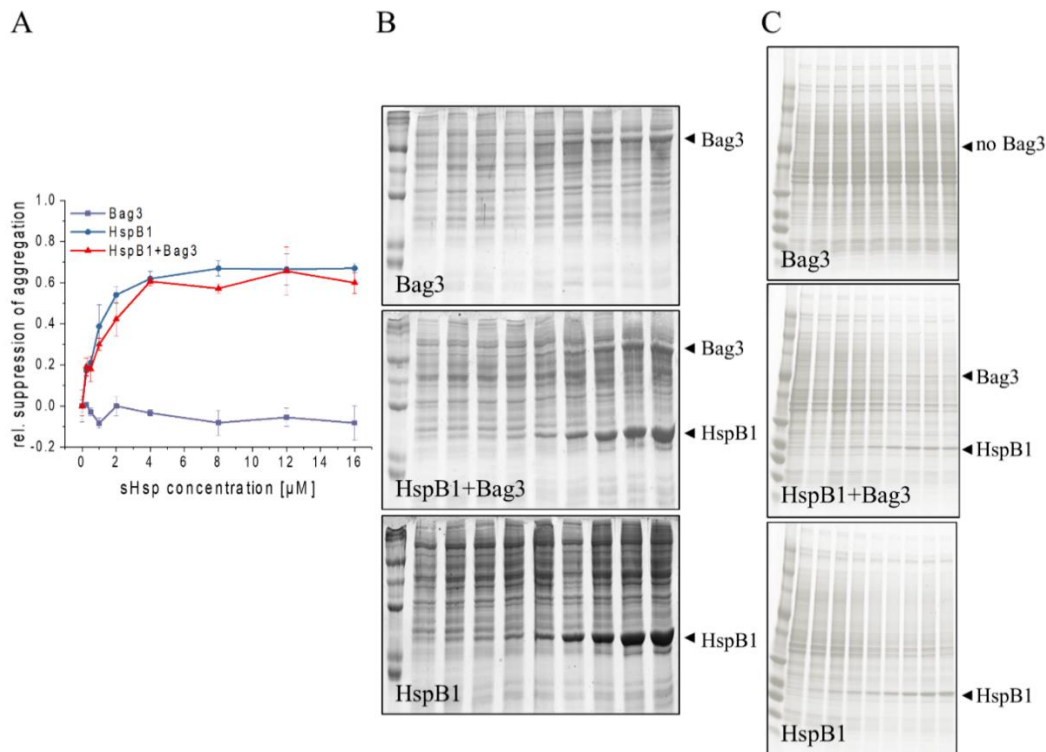


Figure 50 | Influence of Bag3 on HspB1 chaperone activity on HEK lysate aggregation. (A) Quantification of SDS-PAGE read-out, (B) SDS-PAGE of soluble fraction, and (C) SDS-PAGE of insoluble fraction. The HspB1/Bag3 ratio was 4:1.

Since the observed effects differ between different model substrates, HEK lysate was used as a more heterogeneous substrate mixture (Figure 50). Here again Bag3 did not show any holdase

activity on its own (purple) whereas HspB1 alone was active (blue). Here, Bag3 did not influence the activity of HspB1 (red) (Figure 50, A). Evaluating the results in more detail, the two proteins were found in the soluble protein fraction in the mixed samples as well as in the single control samples (Figure 50, B). As expected, HspB1 was also present in the pellet protein fraction as it precipitates in complex with its substrates. In contrary, Bag3 alone was not found in the pellet protein fraction. When HspB1 and Bag3 were present at the same time, Bag3 precipitated in the pellet fraction as well. This strengthens the hypothesis of an interaction of HspB1 and Bag3. The question arises whether this interaction is due to a co-chaperone/chaperone interaction or because HspB1 recognizes Bag3 as a substrate. However, the fact that Bag3 alone does not precipitate during the experiment strongly indicates that it is stable at 45°C. A recognition of substrates by sHsps conversely is only expected in case of an unfolding event followed by exposure of hydrophobic patches. Thus a co-chaperone/chaperone interaction is more likely.

4.3.4 Bag3 influence on sHsp size distribution

The influence of Bag3 on the sHsp size distribution was of interest to figure out whether the effects on activity modulation are connected to the size of sHsps. As two complementary methods TEM and SEC-MALS were performed (Figure 51 and Figure 52).

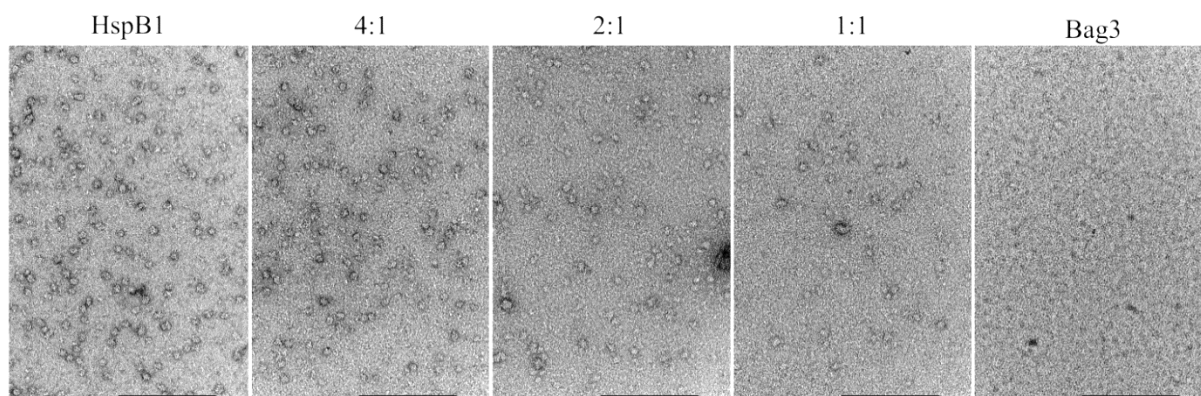


Figure 51 | Influence of Bag3 on HspB1 size distribution analyzed by TEM. 10 μ M HspB1 was used and Bag3 was added in different amounts to generate the depicted HspB1/Bag3 ratios. As a control 10 μ M Bag3 is depicted alone. Scale bars indicate 100 nm. The TEM measurements were carried out by Dr. Beate Rockel, Chair of electron microscopy, TUM.

Although the same concentration of HspB1 was used for all experiments, the number of big oligomers decreased significantly. The size of the oligomers seemed to be constant within the resolution limits of TEM. Bag3 alone did not show oligomers in the range of TEM detection. These observations are in good agreement to the previous SEC-MALS experiments of Bag3 (4.3.2 Basic characterization of Bag3). All SEC-MALS experiments were performed at room temperature with pre-incubated protein samples at 37°C (Figure 52). To enhance a possible shift in size, a 1:1 HspB1/Bag3 ratio was applied (Figure 52, A). Additionally, the same experiment was conducted with the Bag3 IPV mutant (Figure 52, B). As observed before, Bag3 eluted as a monomer at an elution volume of 10.5 mL (purple). The HspB1 elution profile was more heterogeneous, between 8.5 – 9.5 mL, which equals an apparent molecular mass of 400 – 500 kDa. HspB1/Bag3 eluted in two peaks whereas one peak clearly corresponded to a Bag3 monomer as the calculated apparent

4 RESULTS

molecular mass matches exactly the size of the Bag3 run. The second peak was observed in the range of HspB1 but was significant smaller. The determined apparent molecular mass was decreased by ~50 kDa. In addition, the UV signal of the Bag3 monomer peak decreased about 15 %, indicating that Bag3 was incorporated in the HspB1 complex.

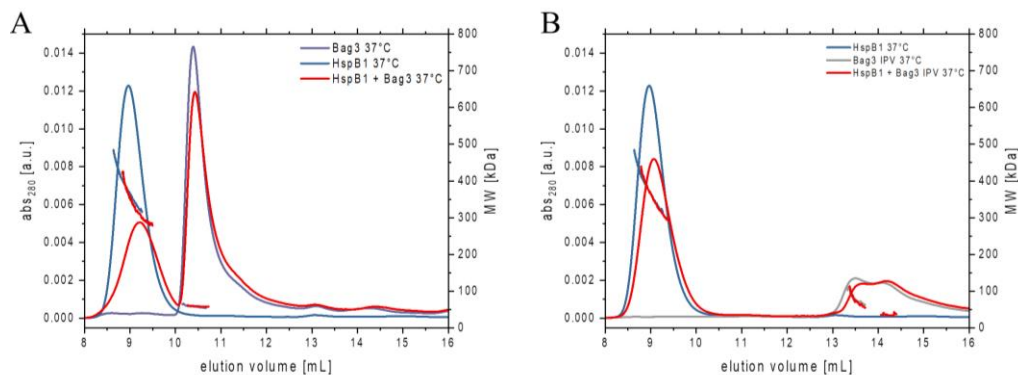


Figure 52 | Influence of Bag3 (A) and Bag3 IPV (B) on HspB1 distribution in SEC-MALS. The ratio of HspB1/Bag3 or HspB1/Bag3 IPV respectively was 1:1. All samples were pre-incubated at 37°C for at least 90 min.

HspB1/Bag3 IPV eluted in two peaks as well (Figure 52, B). The double peak equals the elution profile of Bag3 IPV alone and again the calculated apparent molecular masses match exactly. The dimer peak of Bag3 IPV decreased slightly in the UV signal whereas the monomer peak did not change. The calculated apparent molecular mass of the second peak again equals the size of HspB1 but was reduced by about 50 kDa. To ensure the presence of Bag3 and Bag3 IPV in the oligomeric complex SDS-PAGE of the SEC fractions needs to be performed.

Taken together, the TEM as well as the SEC-MALS experiments revealed a reduction in the size of the oligomeric complexes. This observation supports the hypothesis of a co-chaperone interaction since a size increase of the sHsp-substrate complexes has been verified for various model substrates like CS, insulin, rhodanese and luciferase (103,111). The reduction in oligomeric size and the increase in chaperone activity confirm the expectations of Bag3 acting as a co-chaperone for sHsps. The fact that Bag3 IPV alone can induce the oligomeric size decrease even strengthens the hypothesis.

5 SUMMARY AND DISCUSSION

Small heat shock proteins are ubiquitous molecular chaperones acting mainly as holdases to prevent substrate proteins from irreversible aggregation. A key feature of these small molecular chaperones is their ability to form highly dynamic oligomeric structures. To transfer the ATP-independent sHsps in an active conformation a shift of the oligomer size towards smaller species needs to be induced. The present study investigated three different effectors to shift the equilibrium in more detail: Hetero-oligomer formation, the influence of their N-terminal region, and the effects of the co-chaperone Bag3.

5.1 Regulation of sHsps by hetero-oligomer formation

In principle hetero-oligomerization may be a by-product of evolution of the multi-member sHsp system without functional consequences (251). However, it is remarkable that multi-cellular organisms like human and animals maintained the redundant proteins, if they are of no additional benefit. Proteomic analysis of substrate spectra of different human sHsps revealed that they do have a high overlap in substrate spectra, but also show unique specificity for several substrates (53). It is quite plausible that hetero-oligomers may exhibit unique modulated substrate spectra. A primary sequence analysis of different sHsps uncovered that NTRs and CTRs developed independently in evolution (67). Hence, the sHsp multi-member system in human may not be the simple result of gene duplications without improved and specialized functions. First reports concerning hetero-oligomerization in terms of disease association have been published. For example specific amino acids in HspB1 are crucial for the interaction with HspB6 and specific point mutations can interrupt or force HspB1-HspB6 hetero-oligomer formation leading to development of Marie-Tooth disease (CMT) (151).

In this study eleven different cell lines were analyzed for class I sHsp members (HspB1, HspB5 and HspB6) and the expression profiles as well as size distribution of the oligomeric complexes were characterized in detail for specific cell lines of interest. Among all tested cell lines ten of them expressed HspB1. HspB5 and/or HspB6 expression was exclusively found in presence of HspB1. Interestingly, sHsp expression levels varied substantially between the different cell lines (Table 3). Three out of eleven cell lines expressed more than one sHsp simultaneously (U373MG, U138MG, H460). Although co-expression of HspB1 and HspB5 was observed before in cell lines (252), this general principle could not be confirmed for the tested cell lines. In the present study, HspB1 and HspB6 co-expression was observed as well (H460 and U138MG). Co-immunoprecipitation experiments confirmed the existence of all possible hetero-oligomer formations (Figure 11). Furthermore, the study shows distinct changes in sHsp expression patterns upon heat shock. HspB1 and HspB6 exhibited enhanced protein levels in the soluble protein fraction during heat shock whereas levels of HspB5 were negligible (Table 3). Therefore, sHsp ratios shifted in the cell lines containing more than one sHsp member and a change of the activity profile is possible. Under non-stress conditions, HspB5 was present in excess whereas during heat shock HspB1 increased and this resulted in an equimolar concentration of both sHsps. It is possible that some HspB1 does

not incorporate in the hetero-oligomer complex (58). When no further HspB5 is available for hetero-oligomerization, additional HspB1 will form homo-oligomers. Free HspB1 should increase with increasing HspB1 concentrations, because HspB5 concentrations did not increase under heat stress. Hence, under stress conditions a higher amount of free HspB1 homo-oligomers would be present and thus be more active. Furthermore, it has been observed that oligomerization of HspB1 is concentration-dependent. A higher HspB1 concentration under stress conditions probably stabilizes the oligomeric HspB1 complex. Size exclusion chromatography experiments of this study revealed that the increased HspB1 concentration led to enhanced formation of oligomers in H460 cells under stress conditions (Figure 13). It is conceivable that oligomeric complexes have an important role for the interactions with the cytoskeleton and fibrils at stress conditions (158,253,254). Polymers, like cytoskeletal proteins, are in the insoluble fraction of cellular lysate and therefore excluded from the HEK lysate assay used. Recognition of polymeric, cytosolic proteins is not sufficiently described by the current model of sHsp function. This is of specific interest as especially large sHsp-oligomers seem to act on these polymers (253-255).

In general, co-expression of HspB1 and HspB5 seem to be upregulated in cancer cell lines, while HspB6 is often reduced (209,229,230,256,257). Hetero-oligomerization might influence the decision between proliferation and apoptosis in these cells in a distinct way (258,259). When HspB1 and HspB6 coexisted in the cell, under non-stressed conditions, HspB1 was present in excess (Table 3). Under stress conditions, the ratio shifted to equimolar concentration of both sHsps again. *In vitro* aggregation assays revealed that HspB6 acts like a HspB1 modulator (Figure 21). Under stress conditions most likely an altered substrate spectrum is developed and therefore a substrate-dependent modulation of the HspB1 activity would be beneficial.

The only cell line containing HspB1, HspB5 and HspB6 (U138MG) in this study did not show any heat shock inducible change of sHsp expression (Table 3). Nevertheless, the influence of HspB6 on HspB1 and HspB5 in this cell line may be of importance. The change of substrate spectra and/or the activity state of the sHsps might also be induced by phosphorylations or by temperature increase itself. Altered hetero-oligomer assembly by mutations and/or phosphorylation has been reported before (151,260). For example, the disease-associated HspB1 mutations R127W and S135F enhance hetero-oligomer formation, whereas HspB1 R136W disrupts hetero-oligomer formation. Additional phosphorylation of HspB1 reduced oligomer formation and thus decreased hetero-oligomer formation further (151). In HspB5 the disease-related R120G mutation leads to an increase of oligomer size. Incorporation in these enlarged oligomers was demonstrated for HspB1 wildtype and phosphorylated species, although phosphorylated HspB1 forms dimers only in absence of Hsp5 (260). In another study, a stabilizing effects of HspB5 by HspB1 upon hetero-oligomer formation was demonstrated (261). Similar to phosphorylation, the increase of temperature can disrupt the oligomeric structure of sHsps. Thus, hetero-oligomers might be disrupted and small homo-oligomeric species can fulfill altered functions. The outcome of this event depends on the ability or inability of the hetero-oligomer complexes to form small hetero-species as well.

Even though the ratio between the three sHsps does not change in the U138MG cells, it is conceivable that hetero-oligomer formation changes. For example, a higher amount of HspB1-HspB5 hetero-oligomers can be formed under non-stress conditions or HspB6 incorporation may increase under stress conditions to activate the complexes. The performed size distribution analysis of soluble lysate fraction did not show major changes between standard and heat stress conditions. Nevertheless, the HspB1 oligomer fractions of nearly all tested cell lines (MCF7, HeLa, U373MG) tend to form slightly decreased species possibly due to stress induced enhanced phosphorylation (Figure 13). However, the interplay of phosphorylation, temperature dependent activation, changes in expression patterns and hetero-oligomerization *in vivo* needs to be analyzed in more detail.

To focus on the formation of different hetero-oligomers, size distribution and activity were analyzed *in vitro*. Thus, it could be ensured that any changes are induced by altered formation of hetero-oligomers in the absence of phosphorylation and conditions like temperature, substrates, and pH are constant for all measurements. Taken together, size distribution analysis showed a clear increase in size of HspB1-HspB5 hetero-oligomers that came along with an overall impaired holdase activity for model substrates (Figure 21 and Figure 53). In contrast, HspB1 and HspB5 size decreased upon addition of HspB6. Strikingly, the mechanism of this modulation seem not to be identical for both proteins as HspB1 forms a defined hetero-dimer with HspB6, whereas HspB5 is not incorporated in the small species. Furthermore, HspB6 was not incorporated completely upon excess (Figure 14). Different influence of HspB6 was also found in the ability of HspB6 to modulate the holdase activity of HspB1 and HspB5 (Figure 53).

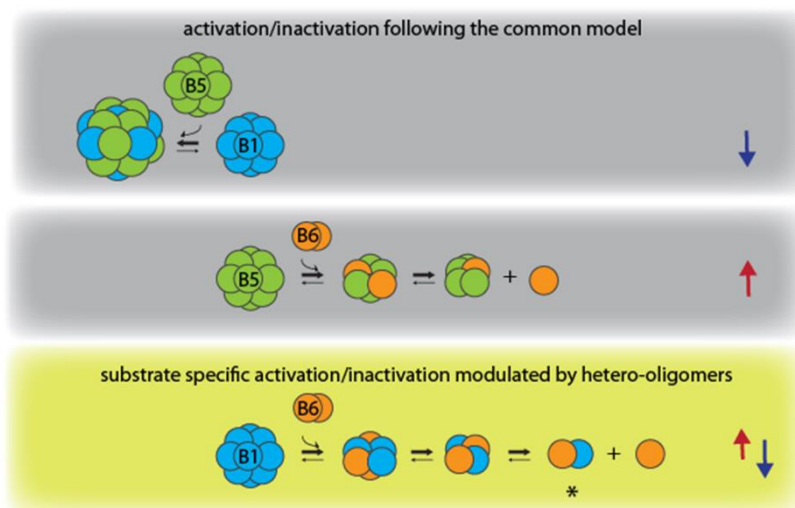


Figure 53 | Model of activity modulation by hetero-oligomerization between HspB1 (blue), HspB5 (green) and HspB6 (orange). The hetero-oligomer assemblies of HspB1-HspB5 and HspB5-HspB6 follow the common model of activity modulation with increasing activity (red) for decreasing oligomer size (grey). The HspB1-HspB6 hetero-oligomer showed a specific type of regulation as the size of oligomers were decreased but the activity was up-(red) or down-regulated (blue) dependent on the used substrate protein. The arrow marks the uniquely formed hetero-dimer of HspB1-HspB6. Reprinted with the permission of American Soc. for Biochemistry & Molecular Biology (Riedl et al. 2020) (228).

In case of HspB5, where no hetero-dimers were observed, HspB6 showed an overall enhancement of HspB5 activity. For HspB1 the influence is more precise in terms of substrate specificity. For some tested substrates HspB6 enhances the HspB1 activity, whereas for others even an impaired activity was detected (Figure 21 and Figure 53).

The obtained results in this thesis show that there is no defined effect of hetero-oligomer formation on the chaperone activity of sHsps in general. Rather several distinct regulatory principles become obvious. The mechanism of HspB6 on HspB1 and HspB5 is strikingly different whereas HspB6 itself seem not to be actively part participating in aggregation suppression, rather it seems to have a regulatory role only. *In vivo* an additional layer of complexity is introduced by phosphorylation, pH changes, and changing substrate spectra. All these conditions are known to affect the oligomeric state of HspB1 and HspB5 in cells (Figure 9). After duplication of a sHsp gene, hetero-oligomers should be a natural species. Based on the fact that sHsps evolved different substrate specificities there might be an evolutionary pressure against hetero-oligomer formation. In this context, activity modulation through hetero-oligomer formation is counter intuitive in an evolutionary setting that is restricted to avoiding hetero-oligomers (251). Overall, hetero-oligomer formation is beneficial for survival of the organism by adding another layer of regulation and functional specialization to the already known repertoire of the fascinating family of sHsps.

5.2 Regulation of sHsps by their N-terminal region

The N-terminal region (NTR) of sHsps has been under investigations for a long time and still little is known about the structure and the function of this non-conserved region. The region is one out of three domains and represents about 35 % of the total protein sequence. Thus, its influence on the structure and function on sHsps is massive. Several properties make the N-terminal region particularly challenging for characterization. First, the amount of secondary structure content is very low and the intrinsically disordered regions are highly flexible (66). In the ordered regions heterogeneity is a challenge as most regions show more than one structured state (65). Additionally, the sequence contains many hydrophobic residues, therefore an isolated characterization of the region *in vitro* is not possible. Second, the N-terminal region mediates the oligomerization to multimers. Thus, its physiological function can only be analyzed in this oligomeric state, which is problematic for many methods (NMR, FRET, CX-MS). Third, subunits of the oligomer structure are highly dynamic and exchange frequently during experiments, making it difficult to capture a single oligomeric state or even a narrow distribution of states. Finally, intermolecular interactions with the ACD as well as intermolecular interactions with substrates or other protomers of the sHsp oligomer are highly transient, which makes it challenging to capture complexes. In the present study the full length α B-crystallin (α B) was truncated from the N-terminus to gain insight into individual functions of NTR parts. Further, aromatic residues were replaced by alanine to characterize the influence of this highly abundant amino acids. Last, *in vitro* crosslink experiments of different N-terminal α B lysine point mutants with CS and MDH as model substrates were conducted. The obtained crosslinks were used to localize preferred interaction sites in the NTR as well as in the substrate sequences.

The NTR was divided in five parts based on secondary structure predictions (66) deleting stepwise α -helices and the connecting loops (Figure 24). In addition, the long loop between α 2 and α 3 was divided at position 40, resulting in an unstable and degradation prone construct. The analyzed degradation products showed cleavage sites at position 53 and 54 equaling the beginning of the next α -helix (Figure 25). Thermal stability decreased with increasing truncation length. Thus, the N-terminal domain is important to stabilize the structure of the whole protein (Figure 26). The NTR is involved in the oligomer assembly, as it participates in inter-dimer and in particular in inter-hexamer interaction (91). In absence of the NTR, only dimer formation via the β 6+ β 7 sheet is still possible (134). Most likely the flexible NTR and CTR loose proportions of their defined structure upon oligomer disruption. Δ 20 can form hexamers, thus parts of the NTR are still mediating the inter-dimer contact even though inter-hexamer interaction seems to be disrupted. Not much difference between the wildtype melting temperature and Δ 20 was observed ($\Delta T_m = 3^\circ\text{C}$), whereas the melting temperature of Δ 28, Δ 40, and Δ 51 are reduced by $\sim 8^\circ\text{C}$ compared to wildtype. The complete deletion of the NTR resulted in a decrease of the melting temperature by $\sim 15^\circ\text{C}$. Apparently, the residues between 51 – 70 still have a major impact on the temperature stability. Unstructured parts of a protein can initiate aggregation due to the exposure of hydrophobic amino acid residues (1). As the NTR contains many hydrophobic residues, aggregation is favored upon exposure of the NTR sequence.

Activity assays showed that the first 28 amino acids are not necessarily required to fulfill aggregation inhibition functions towards MDH and HEK lysate whereas the deletion of 51 aa or more led to a complete loss-of-function. In MDH assays the activity could be sustained at high sHsp concentrations. In contrary, for HEK lysate $\Delta 40$ was not competent under any conditions (Figure 27). It turned out that the difference in temperature applied for the two assays might be the reason for the divergence in behavior, as αB in general seems to be less active for substrates aggregating at higher temperatures (Figure 28 and Figure 54, C). The turning point in activity of the $\Delta 40$ mutant could not be reproduced in size distribution analysis. While $\Delta 20$ still showed oligomers larger than 200 kDa, $\Delta 28$ was already drastically decreased in size. Similar to all other truncation mutants, $\Delta 28$ lost the ability to form large oligomeric complexes and appeared between 20-45 kDa (Figure 29). The first 20 amino acids seem to be important to mediate full oligomer formation, whereas without these amino acids at least middle size oligomers can still be formed. This hints towards a multistep assemble mechanism as reported before (66). The results of FRET experiments to characterize subunit exchange rates of the different mutants strengthen this observation. For the wildtype protein and oligomeric $\Delta 20$ mutant, one-phase exponential decay fits resulted in high deviations and seem to be inappropriate. Even two-phase fits were only suitable for small oligomeric systems. A three-phase exponential decay function led to an adequate fit quality. The current three step assembly mechanism including first the dimer formation mediated by the ACD, second the hexamer formation mediated by the CTR IXI motif and third the oligomer formation mediated by NTR can be confirmed in terms of the number of steps, but clearly the NTR is essential already for the second step whereas the third step is mediated by the first 20 amino acids (Figure 54, D).

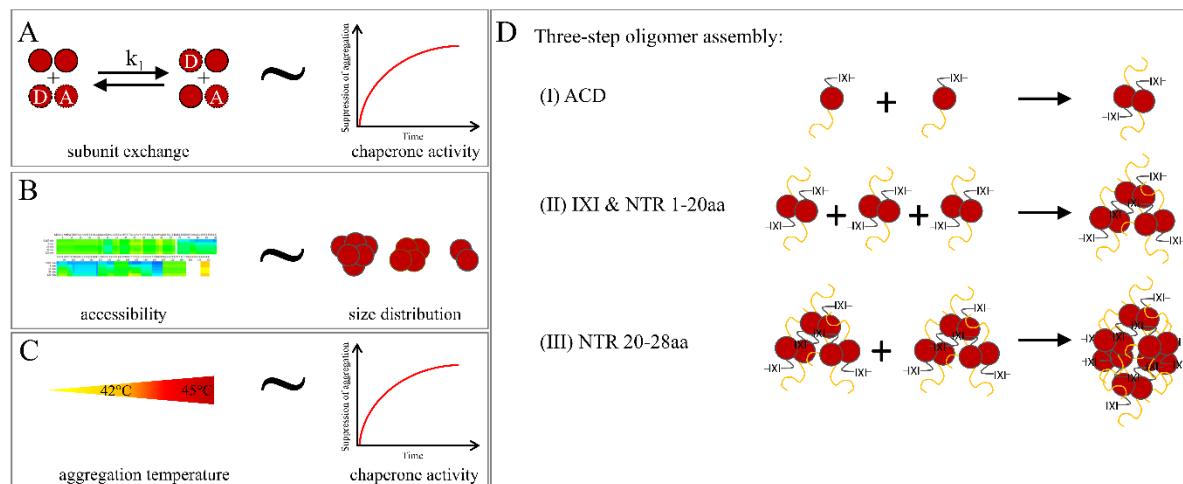


Figure 54 | Summary of N-terminal influence on sHsp behavior. ACDs are depicted in red, NTRs in yellow and CTRs including the IXI motif in black. (A) Subunit exchange is correlated with chaperone activity, (B) Exchange rates of hydrogen to deuterium are correlated with size distribution, (C) the extent of chaperone activity is correlated with the aggregation temperature, and (D) the three-step oligomer assembly is influenced by the NTR at specific steps.

Exchange rates of the subunits correlate with the observed holdase activities (Figure 54, A). Strikingly, strongly increased exchange rates correlate with impaired chaperone activity and slower exchange rates in the range of the full length protein lead to full chaperone functionality. In the literature exchange rates are discussed controversially. On the one hand, polydispersity of sHsps is

connected with lower exchange rates and monodisperse sHsps with increased exchange rates (181,184,186,262). On the other hand, exchange rates are postulated to increase chaperone activity whereas substrate binding seem to reduce the rates (91). If substrate binding reduces the exchange rates it is conceivable that interactions of the NTR with the ACD decrease the exchange in a similar way. Therefore, mutants with a longer NTR, exhibiting a higher ability for self-interactions, have a slower exchange rate. Another study postulated the absence of a correlation between subunit exchange rates and chaperone activity (263) and even crosslinked proteins lacking the ability to exchange subunits exhibit chaperone activity (264). However, in the present study subunit exchange rates of the α B truncation mutants negatively correlate with chaperone activity, independent of their size distribution. Moreover, HDX-MS experiments reveal a direct correlation between dynamics and oligomeric size but not with chaperone activity (Figure 54, B). ANS experiments seem not to be suitable to make a statement concerning the surface hydrophobicity of truncation mutants as a NTR deletion itself lead to a drastic decrease of hydrophobicity based on the high aromatic acid content in the NTR. With 19 % aromatic amino acids, the content is clearly increased in the human α B-crystallin NTR compared to 8 % in the human proteome. Especially, phenylalanines are strongly enriched by 10 %. Phenylalanines probably play an important role for oligomer assembly by mediating cation- π interactions with positively charged arginines, which are as well overrepresented in the NTR (71). Besides its intramolecular contacts, phenylalanines are also reported to be involved in holdase activity (68-70). To elucidate the effects of these amino acids, three mutants were generated deleting tryptophans only (Trp free), phenylalanines only (Phe free) or all aromatic amino acids (aromats free) within the NTR.

Thermal stability investigations showed that depletion of phenylalanines and all aromats destabilizes the entire protein and the melting temperatures were decreased by about 5 and 10°C, respectively. Additionally, the mutations lead to a reduction in secondary structure assuming an influence of the NTR on the secondary structure of the ACD and/or a disruption of N-terminal secondary structure in the absence of phenylalanines (Figure 33). A similar picture arises for the chaperone activity which is not impaired upon deletion of tryptophans, but strongly reduced by phenylalanine deletion (Figure 34). The deletion of all aromatic residues inhibits the chaperone activity even further. Surprisingly, chaperone activity for the Phe free mutant was partially maintained only for HEK lysate, indicating a substrate-specific loss of chaperoning ability for the Phe free mutant. As reported before, different substrates have different requirements for the chaperone (134). Apparently, for inhibition of MDH aggregation, phenylalanines have an important role, but in the soluble fraction of HEK lysate about 60 % of the aggregation can be inhibited by α B without N-terminal phenylalanines. The size distribution upon tryptophan replacement leads to a partial disruption of the oligomer from a ~400 kDa complex to a ~200 kDa complex. Notably, one of the two deleted tryptophans is located within the first 20 aa (W9) and postulated to be involved in the high order oligomer organization from the results obtained for the truncation mutants. Deletion of phenylalanines and tyrosines leads to further disruption to dimeric species (Figure 35). Even though the CTR is completely intact, the postulated connection of the dimers to hexamers by the C-terminal IXI motif cannot be mediated in the absence of these aromatic residues (66,84,88). Subunit exchange experiments confirm a correlation between increased exchange rate and decreased activity, whereas exchange rates in the range of the wildtype

protein are correlated with complete maintenance of activity (Figure 36). HDX-MS measurements validated a high dynamic of the non-oligomeric mutants Phe free and aromats free. The oligomeric mutant Trp free again showed high similarity to the wildtype protein. Moreover, a region with increased deuterium uptake between position 120 and 130 was found in all aromatic mutants. This region equals the end of the $\beta_6+\beta_7$ sheet including the following loop region. As a part of the ACD groove, this region has been predicted before to interact with the NTR (65). An increase of deuterium incorporation might implicate a disruption of this interaction followed by higher flexibility of this region. The correlation between increasing deuterium exchange rates with decreasing oligomer size can be confirmed for the aromatic mutants. Again, ANS binding experiments to determine the amount of accessible hydrophobic surfaces are not suitable for these type of mutations as the deletion of aromatic amino acids per se leads to a strong decrease independent of the conformation.

There are several crosslink experiments reported in the literature for sHsps. Older studies simply verify interactions within their oligomeric structure (265-268) and others prove the transient interaction of sHsps with substrate proteins or further interaction partners (99,244,269,270). Specifically introduced crosslinks in the ACD were used to covalently link ACD dimers and investigate the effect of impaired subunit flexibility (242). A few studies used multimethod approaches to gain structural insights of sHsp/substrate or sHsp oligomeric complexes (133,244,271). Exceedingly few studies use crosslink experiments coupled to MS in order to narrow down the exact interaction sites (66,207,271). In the present study, lysine residues were introduced, evenly distributed over the NTR, to gain information about site-specific binding preferences (Figure 38). The lysine mutants were crosslinked with MDH or CS to learn about specific binding motifs in the substrate protein. All mutants were tested for altered chaperone activity towards the used model substrates MDH and CS (Figure 39). Overall, all mutants showed wildtype like holdase activity for both substrates. Therefore, crosslinking of all lysine mutants with DSG was performed and analyzed by MS. In general, the interaction mechanism of αB with MDH seem to differ from the CS interaction. First, even though a four times lower sHsp/substrate ratio was used for MDH experiments, αB was not 100 % incorporated in the sHsp/substrate complex and second, for CS crosslinks, species between 100 – 200 kDa were observed, which were not present in MDH experiments. Surprisingly, no large crosslinked complexes were found for the triple lysine mutant (3xK). Whether this is due to an inability of the 3xK mutant to form oligomeric complexes or due to a different sHsp/complex formation still needs to be clarified. However, crosslinked peptides were obtained by MS for all mutants. Surprisingly, an uneven crosslinking distribution on substrate proteins was observed. This might be because of remaining secondary structure and only partially unfolding of the substrates and therefore inaccessible areas, or because of preferred interaction sites of the sHsp and the substrate.

Previous studies using peptide chips showed preferences for interactions of αB with aromatic/non-charged amino acids like leucine, phenylalanine, alanine, valine, tyrosine, glycine and the positively charged amino acid arginine (213). Additionally, the absence of negatively charged amino acids like glutamic and aspartic acid was observed while arginine and other positively charged amino acids like proline and lysine were found to be enriched in close proximity

to the crosslink positions (Figure 42). In accordance with the peptide chip experiments, negatively charged amino acids were identified as non-binders. However, as positively charged amino acids seem to play an essential role, it is recommended to repeat crosslink experiments with a lysine-independent crosslinker as lysines comprise a positive charge. The crosslink distribution within α B displayed mainly crosslinks in the ACD and CTR (Figure 41 and Figure 55).

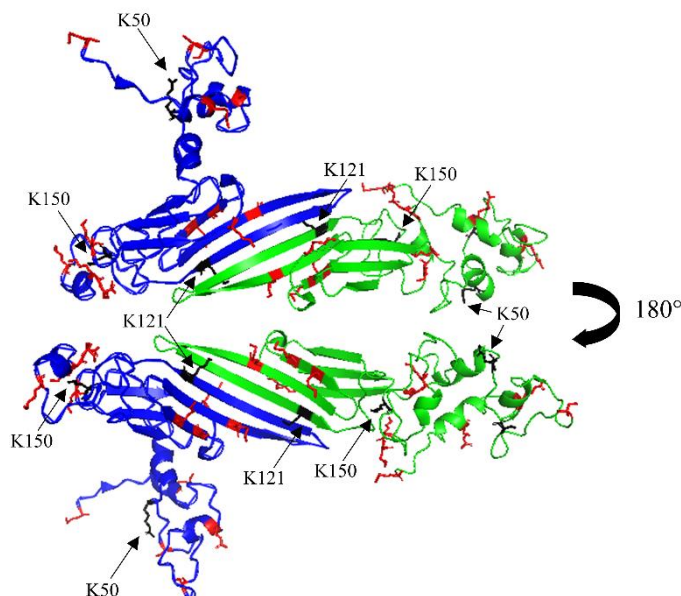


Figure 55 | Localization of crosslink positions in the dimeric three dimensional α B-crystallin structure. An isolated dimer from the 24mer structure (PDB ID 2ygd) is depicted (66). The two monomers are represented in blue and green. Lysine residues are colored in red, whereas important crosslink positions (K50, K121, K150) are highlighted in black.

Substrate binding to the ACD has been reported for amyloid fibril forming A β 1-42 and amorphous aggregating α -lactalbumin and κ -casein. Especially, binding to the β 4/ β 8 groove and the ACD groove was assumed. The results of the crosslink experiments confirm a high crosslink potential at the end of the β 6+7 sheet (position K121). This fits well to the high flexibility in this region induced in the aromatic mutants, as already small structure rearrangements in the NTR can lead to an increase of flexibility in this region. Thus, it is likely that upon substrate binding the region becomes more dynamic exhibiting a higher crosslink potential. The N-terminus itself and position K50 were the only two positions yielding in a high crosslink accumulation within the NTR, whereas no crosslinks were observed for position 22, 35 and 45 at all. Surprisingly high number of crosslinks were identified additionally at the very end of the ACD (position K150). The importance of this region in α B for substrate binding has been demonstrated before by Mainz et al. using solution-state ^1N - ^{15}N -HSQC (134).

Taking together, it is rather difficult to define a substrate interaction motif by crosslink studies using primary amines for covalent crosslinking. Strikingly, position K50 in the NTR was found to be highly interactive. This position is of special interest as it is located towards the end of the long flexible loop between the predicted helices α 2 and α 3 that was predicted to be of special importance in the truncation mutant study and seem to have a high influence on the stability and activity of α B-crystallin.

5.3 Regulation of sHsps by the possible co-chaperone Bag3

Beside from its interactions with Bcl-2 (272), Bag3 was characterized largely as a nucleotide exchange factor for Hsp70 (173). However, the Bag3 knockout in mice resulted in severe myopathy and skeletal muscle defects that cannot be explained by its nucleotide exchange factor function (273). Significant advances have been made to develop a new model suggesting a significant role of Bag3 in the regulation of macroautophagy depending on the interaction with the sHsps HspB6 and/or HspB8 (171). The sHsp/Bag3 complex seem to be involved in the stimulation of the autophagic process after Bag3 upregulation by HSF-1 during stress conditions (167). Furthermore, Bag3 seem to be able to physically connect the two chaperone systems Hsp70 and sHsps via its multi domain structure. The separation of the Bag3 IPV motifs and the BAG domain probably allow Bag3 to bind both chaperone classes simultaneously and support their interplay (113). Certainly, up to now there is no direct proof for the existence of this multi-complex. On the sHsp side, it seems that Bag3 can enhance the oligomer formation of its binding partners HspB6 and HspB8 and might generate chaperone activity of these largely inactive sHsps (Figure 56, A). On the other side, the interaction of Bag3 was reported for oligomeric sHsp members like HspB1 and HspB5 whereas the physiological function of their interplay is not clear yet (113).

To gain new insights into the cooperation of Bag3 with oligomeric sHsps, the expression and purification of Bag3 full length protein and a truncated IPV mutant were established and optimized followed by a basic *in vitro* characterization of the obtained recombinant proteins. The analysis of the secondary structure revealed a high random coil content, 20 % α -helixes and 10 % β -sheets. The IPV mutant showed much less secondary structure as it is missing the structured WW, PXXP and BAG domains (Figure 47). Nevertheless, for both proteins a similar thermal stability with a melting point of 32°C was determined by CD thermal transition experiments. This value is obviously relatively low for a protein that is involved in autophagy processes even under stress conditions, but this might be explained by the *in vitro* conditions used. Furthermore, for both proteins an additional transition was observed between 60°C and 70°C. Later on, heat shock experiments were performed at 45°C in cell lysate where Bag3 remained intact and soluble. A higher melting temperature was as well confirmed for Bag3 by DSF measurements using a different buffer system (274). Quaternary structure investigations by SEC-MALS confirmed a monomeric structure of Bag3 as reported before by Meister-Broekema et al. (2018) (274). The Bag3 IPV mutant forms monomers and dimers in a 1:1 ratio (Figure 48).

Bag3 showed a slightly positive impact on the HspB1 holdase function for the model substrates CS and MDH (Figure 49). In contrary, this modulation was not observed for insulin or HEK lysate as substrates. Surprisingly, regardless of the absence of an influence on activity, the behavior of Bag3 in HEK lysate assays changed upon addition of HspB1. In the absence of HspB1, Bag3 was found exclusively in the soluble protein fraction, whereas in the presence of HspB1, Bag3 precipitated in the pellet fraction (Figure 50). This hints towards an interaction of sHsp and Bag3 regardless of the type of interaction (direct vs indirect). In a cell lysate, multiple other cell component might influence the cooperation of sHsp and Bag3. Therefore, *in vitro* SEC-MALS experiments were performed with recombinant HspB1 and Bag3 or its IPV mutant. In both cases,

the addition of Bag3 induced a shift of HspB1 oligomers towards smaller species (Figure 52). As the effect was not strong, TEM images were generated and proofed the reduction of the large oligomeric species (Figure 51).

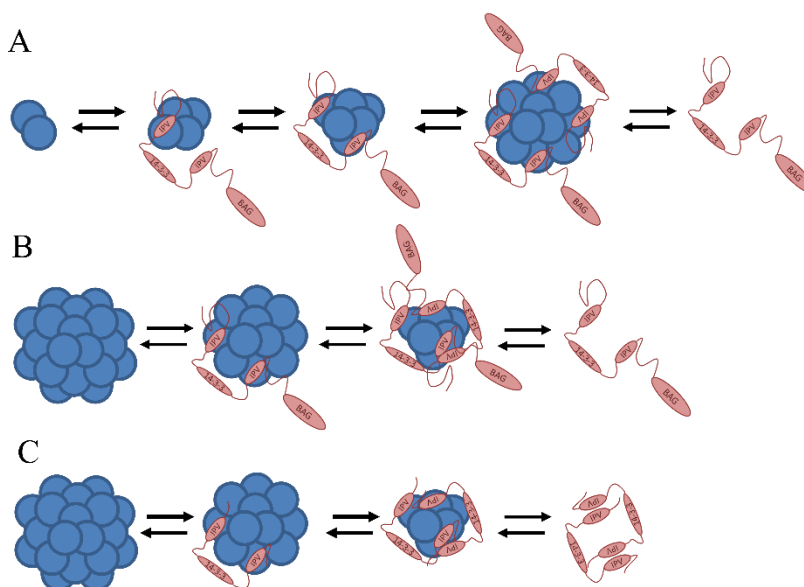


Figure 56 | Model of the influence of the co-chaperone Bag3 on sHsp oligomerization. The small heat shock proteins are depicted in blue and Bag3 is visualized in red. One circle does not necessarily represent a sHsp monomer. (A) Effect of Bag3 on dimeric/monomeric sHsps. (B) Effect of Bag3 on oligomeric sHsps. (C) Effect of the Bag3 IPV mutant on oligomeric sHsps.

A direct interaction between Hsp1 and Bag3 or Bag3 IPV can still be of various nature. On the one hand, the function of a holdase is to bind partially unfolded proteins, that expose hydrophobic surfaces. From the CD data a high content of random coil is known for Bag3 and Bag3 IPV. For proteins with low secondary structure content and limited stability, the interaction with sHsps is favored as they probably present hydrophobic patches. This type of contact is referred as sHsp/substrate interaction. On the other hand, Bag3 might actively bind to HspB1 as a co-chaperone. The term ‘co-chaperone’ can be loosely defined as a non-substrate protein that binds and affects the activity of a chaperone (167). As there are no co-chaperones for sHsps reported until now, there is no clear definition to distinguish between a co-chaperone and a substrate. In general, sHsp/substrate complexes are increased in size and depending on the ratio they switch between soluble and insoluble fractions (103,111). All sHsp/Bag3 complexes in the present study were found to be soluble and reduced in size (Figure 52 and Figure 56, B). Additionally, the hypothesis of a co-chaperone interaction is strengthened by the fact, that even the Bag3 IPV mutant, which has an increased amount of random coil, was able to induce the oligomeric shift (Figure 56, C).

To characterize the interaction of oligomeric sHsps with Bag3 in more detail, further experiments are required. It remains unclear whether sHsps bind to Bag3 and substrate protein simultaneously or competitively. As Bag3 IPV was able to induce a similar size shift, it would be of interest which part of the IPV construct fulfills this function. To generalize the mode of action and to exclude a HspB1 unique feature, the interactions need to be proven for further oligomeric sHsps like HspB5.

In human there are two nucleotide exchange factors of Hsp70 known to be disease-associated; the ER specific SIL1 and Bag3 (274). The most prominent disease-related mutant of Bag3 is the point mutation P209L that induces myofibrillar myopathy (MFM). The mutation is located in the second IPV motif of Bag3. Thus, there is a strong suspicion that the possibly disruption of the interaction of sHsps and Bag3 may cause the disease. Indeed, *in vitro* experiments revealed a reduced binding affinity of HspB1 to Bag3^{P209L} (274). Further experiments in cell lines showed an only slight decrease of HspB8 binding to Bag3^{P209L} (274). Upon deletion of both Bag3 IPV motifs, the HspB8/Bag3 complex could no longer form. However, Bag3^{P209L} leads to cytosolic puncta formation, which could not be reproduced by deletion of both IPV motifs. Thus a loss of sHsp binding to Bag3 was insufficient to induce the phenotype (274). In more detailed investigations, a correlation between Hsp70/Bag3 interaction and the loss of solubility of Bag3 was reported. Here, the interaction of Hsp70 and Bag3 was disrupted by the formation of higher oligomers of the P209L mutant. Deletion mutants of the BAG domain did not lead to puncta formation, even though Hsp70 interaction was disrupted (274). Based on the presented monomer/dimer formation of the Bag3 IPV mutant it would be interesting to see if this mutant still causes the observed phenotype. Furthermore, HspB1 co-localizes with Bag3^{P209L} in the cytosolic puncta pointing towards an involvement of oligomeric sHsps in their function. However, it is also possible that in this case the interplay of Bag3 and sHsp is of a different nature and HspB1 co-localizes in order to fulfill its holdase function.

A complete deletion of Bag3 in knock-out mice strains was reported to induce decreased protein stability and enhanced sHsp (HspB5, HspB6 and HspB8) degradation (275). Therefore, the overall insoluble protein amount increased. For HspB7 no increase in degradation was reported, which is logical as no interaction of HspB7 with Bag3 was reported (50). Unfortunately, the behavior of HspB1 was not tested in this study (275). The results obtained suggest strongly a protection from degradation of sHsps by Bag3. At least for the non-oligomeric species HspB6 and HspB8 this seems convincing as instability of these proteins in lysate has been observed before (53).

Taken together, the interplay between Bag3, sHsps and Hsp70 needs to be analyzed in more detail. *In vitro* and *in vivo* experiments can help to generate a big picture of how this tripartite system works. Beyond that, a possible difference of the effect of Bag3 binding to monomeric/dimeric sHsps (HspB6, HspB8) and oligomeric sHsps (HspB1, HspB5) should be taken into account. The Bag3 IPV mutant can be of help to narrow down interaction sites of the huge multi-domain protein.

6 REFERENCES

1. Hipp, M. S., Kasturi, P., and Hartl, F. U. (2019) The proteostasis network and its decline in ageing. *Nature Reviews* **20**, 421-435
2. Powers, E. T., Morimoto, R. I., Dillin, A., Kelly, J. W., and Blach, W. E. (2009) Biological and Chemical Approaches to Diseases of Proteostasis Deficiency. *Annu. Rev. Biochem.* **78**, 959-991
3. Kulak, N. A., Geyer, P. E., and Mann, M. (2017) Loss-less nano-fractionator for high sensitivity, high coverage proteomics. *Molecular & Cellular Proteomics* **16**, 694-705
4. Klaipts, C. L., Jayaraj, G. G., and Hartl, F. U. (2018) Pathways of cellular proteostasis in aging and disease. *Journal of Cell Biology* **217**, 51-63
5. Taylor, R. C., and Dillin, A. (2011) Aging as an Event of Proteostasis Collapse. *Cold Spring Harbor Perspectives in Biology* **3**, 1-19
6. Labbadia, J., and Morimoto, R. I. (2015) The Biology of Proteostasis in Aging and Disease. *Annu. Rev. Biochem.* **84**, 1-32
7. Anfinsen, C. B. (1973) Principles that Govern the Folding of Protein Chains. *Science (New York, N.Y)* **181**, 223-230
8. Geiger, T., Wehner, A., Schaab, C., Cox, J., and Mann, M. (2012) Comparative proteomic analysis of eleven common cell lines reveals ubiquitous but varying expression of most proteins. *Molecular & cellular proteomics : MCP* **11**, 1-11
9. Hartl, F. U., Bracher, A.-., and Hayer-Hartl, M. (2011) Molecular chaperones on protein folding and proteostasis. *Nature* **475**, 324-332
10. Thul, P. J., Åkesson, L., Wiking, M., Mahdessian, D., Geladaki, A., Ait Blal, H., Alm, A., Asplund, A., Björk, L., Breckels, L. M., Bäckström, A., Danielsson, F., Fagerberg, L., Fall, J., Gatto, L., Gnann, C., Hober, S., Hjelmare, M., Johansson, F., Lee, S., Lindskog, C., Mulder, J., Mulvey, C. M., Nilsson, P., Oksvold, P., Rockberg, J., Schutten, R., Schwenk, J. M., Sivertsson, Å., Sjöstedt, E., Skogs, M., Stadler, C., Sullivan, D. P., Tegel, H., Winsnes, C., Zhang, C., Zwahlen, M., Mardinoglu, A., Pontén, F., von Feilitzen, K., Lilley, K. S., Uhlén, M., and Lundberg, E. (2017) A subcellular map of the human proteome. *Science (New York, N.Y)* **356**, 1-12
11. Schneider, H.-C., Berthold, J., Bauer, M. F., Diemeier, K., Guiard, B., Brunner, M., and Neupert, W. (1994) Mitochondrial Hsp70/MIM44 complex facilitates protein import. *Nature* **371**, 768-774
12. Zou, J., Guo, Y., Guettouche, T., Smith, D. F., and Voellmy, R. (1998) Repression of Heat Shock Transcription Factor HSF1 Activation by HSP90 (HSP90 complex) that Forms a Stress-Sensitive Complex with HSF1. *Cell* **94**, 471-480
13. Zheng, X., Krakowiak, J., Patel, N., Beyzavi, A., Ezike, J., Khalil, A. S., and Pincus, D. (2016) Dynamic control of Hsf1 during heat shock by a chaperone switch and phosphorylation. *eLIFE* **5**, 1-26
14. Ankar, J., and Sistonen, L. (2011) Regulation of HSF1 Function in the Heat Stress Response: Implications in Aging and Disease. *Annu. Rev. Biochem.* **80**, 1089-1115
15. Gomez-Pastor, R., Burchfiel, E. T., and Thiele, D. J. (2018) Regulation of heat shock transcription factors and their roles in physiology and disease. *Nat Rev Mol Cell Biol.* **19**, 4-19
16. Mühlhofer, M., Berchtold, E., Stratil, C. G., Csaba, G., Kunold, E., Bach, N. C., Sieber, S. A., Haslbeck, M., Zimmer, R., and Buchner, J. (2019) The Heat Shock Response in Yeast Maintains Protein Homeostasis by Chaperoning and Replenishing Proteins. *Cell Reports* **29**, 4593-4607
17. Dikic, I. (2017) Proteasomal and Autophagic Degradation Systems. *Annu. Rev. Biochem.* **86**, 193-224

18. Arndt, V., Rogon, C., and Höhfeld, J. (2007) To be, or not to be - molecular chaperones in protein degradation. *Cell. Mol. Life Sci.* **64**, 2525-2541
19. Esser, C., Alberti, S., and Höhfeld, J. (2004) Cooperation of molecular chaperones with the ubiquitin/proteasome system. *Biochimica et Biophysica Acta* **1695**, 171-188
20. Arndt, V., Dick, N., Tawo, R., Dreiseidler, M., Wenzel, D., Hesse, M., Furst, D. O., Saftig, P., Saint, R., Fleischmann, B. K., Hoch, M., and Hohfeld, J. (2010) Chaperone-assisted selective autophagy is essential for muscle maintenance. *Curr Biol* **20**, 143-148
21. Iadanza, M. G., Jackson, M. P., Hewitt, E. W., Ranson, N. A., and Radford, S. E. (2018) A new era for understanding amyloid structures and disease. *Nature Reviews* **19**, 755-773
22. Olzscha, H., Schermann, S. M., Woerner, A. C., Pinkert, S., Hecht, M. H., Tartaglia, G. G., Venduscolo, M., M., H.-H., Hartl, F. U., and Vabulas, R. M. (2011) Amyloid-like Aggregates Sequester Numerous Metastable Proteins with Essential Cellular Functions. *Cell* **144**, 67-78
23. Muchowski, P. J., Schaffar, G., Sittler, A., Wanker, E. E., Hayer-Hartl, M. K., and Hartl, F. U. (2000) Hsp70 and Hsp40 chaperones can inhibit self-assembly of polyglutamine proteins into amyloid-like fibrils. *PNAS* **97**, 7841-7846
24. Cohen, S. I. A., Arosio, P., Presto, J., Kurudenkandy, F. R., Biverstål, H., Dolfe, L., Dunning, C., Yang, X., Frohm, B., Vendruscolo, M., Johansson, J., Dobson, C. M., Fisahn, A., Knowles, T. P. J., and Linse, S. (2015) A molecular chaperone breaks the catalytic cycle that generates toxic A β oligomers. *Nature Structural & Molecular Biology* **22**, 207-216
25. Grousl, T., Ungelenk, S., Miller, S., Ho, C.-T., Khokhrina, M., Mayer, M. P., Bukau, B., and Mogk, A. (2018) A prion-like domain in Hsp42 drives chaperone-facilitated aggregation of misfolded proteins. *Journal of Cell Biology* **217**, 1269-1285
26. Sontag, E. M., Samant, R. S., and Frydman, J. (2017) Mechanisms and Functions of Spatial Protein Quality Control. *Annu. Rev. Biochem.* **86**, 97-122
27. Laskey, R. A., Honda, B. M., Mills, A. D., and Finch, J. T. (1978) Nucleosomes are assembled by an acidic protein which binds histones and transfers them to DNA. *Nature* **275**, 416-420
28. Hartl, F. U. (1996) Molecular chaperones in cellular protein folding. *Nature* **381-580**, 571-
29. Walter, S., and Buchner, J. (2002) Molecular Chaperones - Cellular Machines for Protein Folding. *Angewandte Chemie* **41**, 1098-1113
30. Genevoux, P., Georgopoulos, C., and Kelley, W. L. (2007) The Hsp70 chaperone machines of Escherichia coli: a paradigm for the repartition of chaperone functions. *Molecular Microbiology* **66**, 840-857
31. Vos, M. J., Hageman, J., Carra, S., and Kampinga, H. H. (2008) Structural and functional diversities between members of the human HSPB, HSPH, HSPA, and DNAJ chaperone families. *Biochemistry* **47**, 7001-7011
32. Brehme, M., Voisine, C., Rolland, R., Wachi, S., Soper, J. H., Zhu, Y., Orton, K., Vilella, A., Garza, D., Vidal, M., Ge, H., and Morimoto, R. I. (2014) AChaperome Subnetwork Safeguards Proteostasis in Aging and Neurodegenerative Disease. *Cell Reports* **9**, 1135-1150
33. Rizzolo, K., Huen, J., Kumar, A., Phanse, S., Vlasblom, J., Kakihara, Y., Zeineddine, H. A., Minic, Z., Snider, J., Wang, W., Pons, C., Seraphim, T. V., Boczek, E. E., Alberti, S., Costanzo, M., Myers, C. L., Stagljar, I., Boone, C., Babu, M., and Houry, W. A. (2017) Features of the Chaperone Cellular Network Revealed through Systematic Interaction Mapping. *Cell Reports* **20**, 2735-2748
34. Kampinga, H. H., and Craig, E. A. (2010) The HSP70 chaperone machinery: J proteins as drivers of functional specificity. *Nature Reviews* **11**, 579-592
35. Clerico, E. M., Tilitky, J. M., Meng, W., and Giarasch, L. M. (2015) How Hsp70 Molecular Machines Interact with Their Substrates to Mediate Diverse Physiological Functions. *J Mol Biol* **427**, 1575-1588
36. Hayer-Hartl, M., Bracher, A., and Hartl, F. U. (2015) The GroEL–GroES Chaperonin Machine: A Nano-Cage for Protein Folding. *Trends in biochemical sciences* **41**, 62-76

37. Biebl, M. M., and Buchner, J. (2019) Structure, Function, and Regulation of the Hsp90 Machinery. *Cold Spring Harbor Perspectives in Biology* **11**, 1-34
38. de Jong, W. W., Leunissen, J. A., and Voorte, C. E. M. (1993) Evolution of the α -Crystallin / Small Heat-Shock Protein Family *Mol. Biol. Evol.* **10**, 103-126
39. Haslbeck, M., and Vierling, E. (2015) A first line of stress defense: small heat shock proteins and their function in protein homeostasis. *J Mol Biol* **427**, 1537-1548
40. Jakob, U., Gaestel, M., Engel, K., and Buchner, J. (1993) Small heat shock proteins are molecular chaperones. *The Journal of biological chemistry* **268**, 1517-1520
41. Haslbeck, M., Weinkauff, S., and Buchner, J. (2019) Small heat shock proteins: Simplicity meets complexity. *The Journal of biological chemistry* **295**, 2121-2132
42. Kappé, G., Franck, E., Verschuure, P., Boelens, W. C., Leunissen, J. A., and de Jong, W. W. (2003) The human genome encodes 10 α -crystallin-related small heat shock proteins: HspB1-10. *Cell stress & chaperones* **8**, 53-61
43. Kappé, G., Verschuure, P., Philipsen, R. L., Staaldin, A. A., Van de Boogaart, P., Boelens, W. C., and De Jong, W. W. (2001) Characterization of two novel human small heat shock proteins: protein kinase-related HspB8 and testis-specific HspB9. *Biochim Biophys Acta* **1520**, 1-6
44. Gastmann, O., Burfeind, P., Gunther, E., Hameister, H., Szpirer, C., and Hoyer-Fender, S. (1993) Sequence, expression, and chromosomal assignment of a human sperm outer dense fiber gene. *Molecular reproduction and development* **36**, 407-418
45. Clark, A. R., Egberts, W. V., Kondrat, F. D. L., Hilton, G. R., Ray, N. J., Cole, A. R., Carver, J. A., Benesch, J. L. P., Keep, N. H., Boelens, W. C., and Slingsby, C. (2018) Terminal Regions Confer Plasticity to the Tetrameric Assembly of Human HspB2 and HspB3. *J Mol Biol* **430**, 3297-3310
46. Sugiyama, Y., Suzuki, A., Kishikawa, M., Akutsu, R., Hirose, T., Waye, M. M., Tsui, S. K., Yoshida, S., and Ohno, S. (2000) Muscle develops a specific form of small heat shock protein complex composed of MKBP/HSPB2 and HSPB3 during myogenic differentiation. *The Journal of biological chemistry* **275**, 1095-1104
47. Mymrikov, E. V., Seit-Nebi, A. S., and Gusev, N. B. (2011) Large potentials of small heat shock proteins. *Physiological reviews* **91**, 1123-1159
48. Nakagawa, M., Tsujimoto, N., Nakagawa, H., Iwaki, T., Fukumaki, Y., and Iwaki, A. (2001) Association of HSPB2, a Member of the Small Heat Shock Protein Family, with Mitochondria. *Experimental Cell Research* **271**, 161-168
49. Sun, X., Fontaine, J. M., Rest, J. S., Shelden, E. A., Welsh, M. J., and Benndorf, R. (2004) Interaction of human HSP22 (HSPB8) with other small heat shock proteins. *The Journal of biological chemistry* **279**, 2394-2402
50. Vos, M. J., Zijlstra, M. P., Kanon, B., van Waarde-Verhagen, M. A., Brunt, E. R., Oosterveld-Hut, H. M., Carra, S., Sibon, O. C., and Kampinga, H. H. (2010) HSPB7 is the most potent polyQ aggregation suppressor within the HSPB family of molecular chaperones. *Hum Mol Genet* **19**, 4677-4693
51. Carra, S., Seguin, S. J., Lambert, H., and Landry, J. (2008) HspB8 chaperone activity toward poly(Q)-containing proteins depends on its association with Bag3, a stimulator of macroautophagy. *The Journal of biological chemistry* **283**, 1437-1444
52. Janowska, M. K., Baughman, H. E. R., Woods, C. N., and Klevit, R. E. (2019) Mechanisms of Small Heat Shock Proteins. *Cold Spring Harbor Perspectives in Biology* **11**
53. Mymrikov, E. V., Daake, M., Richter, B., Haslbeck, M., and Buchner, J. (2017) The Chaperone Activity and Substrate Spectrum of Human Small Heat Shock Proteins. *Journal of Biological Chemistry* **292**, 672-684
54. Carra, S., Seguin, S. J., and Landry, J. (2008) HspB8 and Bag3: a new chaperone complex targeting misfolded proteins to macroautophagy. *Autophagy* **4**, 237-239

55. Carra, S. (2009) The stress-inducible HspB8-Bag3 complex induces the eIF2 α kinase pathway: implications for protein quality control and viral factory degradation? *Autophagy* **5**, 428-429
56. Horwitz, J. (2003) Alpha-crystallin. *Exp Eye Res* **76**, 145-153
57. Slingsby, C., Wistow, G. J., and Clark, A. R. (2013) Evolution of crystallins for a role in the vertebrate eye lens. *Protein Science* **22**, 367-380
58. Arrigo, A. P. (2013) Human small heat shock proteins: protein interactomes of homo- and hetero-oligomeric complexes: an update. *FEBS Lett* **587**, 1959-1969
59. Landry, J., Chrétien, P., Lambert, H., Hickey, E., and Weber, L. A. (1989) Heat shock resistance conferred by expression of the human HSP27 gene in rodent cells. *J Cell Biol* **109**, 7-15
60. Kim, K. K., Kim, R., and Kim, S. H. (1998) Crystal structure of a small heat-shock protein. *Nature* **394**, 595-599
61. Jehle, S., Vollmar, B. S., Bardiaux, B., Dove, K. K., Rajagopal, P., Gonen, T., Oschkinat, H., and Klevit, R. E. (2011) N-terminal domain of alphaB-crystallin provides a conformational switch for multimerization and structural heterogeneity. *Proceedings of the National Academy of Sciences of the United States of America* **108**, 6409-6414
62. Peschek, J., Braun, N., Rohrberg, J., Back, K. C., Kriehuber, T., Kastenmuller, A., Weinkauff, S., and Buchner, J. (2013) Regulated structural transitions unleash the chaperone activity of alphaB-crystallin. *Proceedings of the National Academy of Sciences of the United States of America* **110**, E3780-3789
63. Jiao, W., Qian, M., Li, P., Zhao, L., and Chang, Z. (2005) The Essential Role of the Flexible Termini in the Temperature-responsiveness of the Oligomeric State and Chaperone-like Activity for the Polydisperse Small Heat Shock Protein IbpB from Escherichia coli. *J. Mol. Biol.* **347**, 871-884
64. Aquilina, J. A., and Watt, S. J. (2007) The N-terminal domain of α B-crystallin is protected from proteolysis by bound substrate. *Biochemical and Biophysical Research Communications* **353**, 1115-1120
65. Clouser, A. F., Guttman, M., Baughman, H. E., Nath, A., Klevit, R. E., and Basanta, B. (2019) Interplay of disordered and ordered regions of a human small heat shock protein yields an ensemble of 'quasiordered' states. *eLIFE* **8**
66. Braun, N., Zacharias, M., Peschek, J., Kastenmuller, A., Zou, J., Hanzlik, M., Haslbeck, M., Rappsilber, J., Buchner, J., and Weinkauff, S. (2011) Multiple molecular architectures of the eye lens chaperone alphaB-crystallin elucidated by a triple hybrid approach. *Proceedings of the National Academy of Sciences of the United States of America* **108**, 20491-20496
67. Kriehuber, T., Rattei, T., Weinmaier, T., Bepperling, A., Haslbeck, M., and Buchner, J. (2010) Independent evolution of the core domain and its flanking sequences in small heat shock proteins. *Faseb J* **24**, 3633-3642
68. Horwitz, J., Huang, Q. L., Ding, L., and Bova, M. P. (1998) Lens alpha-crystallin: chaperone-like properties. *Methods in enzymology* **290**, 365-383
69. Hanazono, Y., Takeda, K., Oka, T., Abe, T., Tomonari, T., Akiyama, N., Aikawa, Y., Yohda, M., and Miki, K. (2013) Nonequivalence Observed for the 16-Meric Structure of a Small Heat Shock Protein, SpHsp16.0, from Schizosaccharomyces pombe. *Structure* **21**, 220-228
70. Kelley, P. B., and Abraham, E. C. (2003) Thermally induced disintegration of the oligomeric structure of α B-crystallin mutant F28S is associated with diminished chaperone activity. *Molecular and Cellular Biochemistry* **252**, 273-278
71. Shah, D., Li, J., and Shaikh, A. R. (2012) Arginine-Aromatic Interactions and Their Effects on Arginine-Induced Solubilization of Aromatic Solutes and Suppression of Protein Aggregation. *Biotechnol Prog.* **28**, 223-231

72. Arakawa, T., Ejima, D., Tsumoto, K., Obeyama, N., Tanaka, Y., Kita, Y., and Timasheff, S. N. (2007) Suppression of protein interactions by arginine: A proposed mechanism of the arginine effects. *Biophys Chem* **127**, 1-8
73. Beall, A. C., Kato, K., Goldenring, J. R., Rasmussen, H., and Brophy, C. M. (1997) Cyclic nucleotide-dependent vasorelaxation is associated with the phosphorylation of a small heat shock-related protein. *The Journal of biological chemistry* **272**, 11283-11287
74. Voorter, C. E. M., Mulders, J. W. M., Bloemendal, H., and De Jong, W. W. (1986) Some aspects of the phosphorylation of α -crystallin A. *Eur. J. Biochem.* **160**, 203-210
75. van den IJssel, P. R. L. A., Overkamp, P., Bloemendal, H., and de Jong, W. W. (1998) Phosphorylation of α B-Crystallin and HSP27 Is Induced by Similar Stressors in HeLa Cells. *Biochemical and Biophysical Research Communications* **247**, 518-523
76. Lambert, H., Charette, S. J., Bernier, A. F., Guimond, A., and Landry, J. (1999) HSP27 multimerization mediated by phosphorylation-sensitive intermolecular interactions at the amino terminus. *The Journal of biological chemistry* **274**, 9378-9385
77. Crabbe, M. J. C., and Goode, D. (1994) α -Crystallin: chaperoning and aggregation. *Biochem. J.* **297**, 653-654
78. Derham, B. K., van Boekel, M. A. M., Muchowski, P. J., Clark, J. I., Horwitz, J., Scott, H. W. H., de Jong, W. W., Crabbe, M. J. C., and Harding, J. J. (2001) Chaperone function of mutant versions of α A- and α B-crystallin prepared to pinpoint chaperone binding sites. *Eur. J. Biochem.* **268**, 713-721
79. Shatov, V. M., Weeks, S. D., Strelkov, S. V., and Gusev, N. B. (2018) The Role of the Arginine in the Conserved N-Terminal Domain RLFDQxFG Motif of Human Small Heat Shock Proteins HspB1, HspB4, HspB5, HspB6, and HspB8. *Int. J. Mol. Sci.* **19**
80. Garrido, C., Paulb, C., Seigneuric, R., and Kampinga, H. H. (2012) The small heat shock proteins family: The long forgotten chaperones. *The International Journal of Biochemistry & Cell Biology* **44**, 1588-1592
81. Heirbaut, M., Beelen, S., Strelkov, S. V., and Weeks, S. D. (2014) Dissecting the Functional Role of the N-Terminal Domain of the Human Small Heat Shock Protein HSPB6. *PLoS One* **9**, e105892
82. Sluchanko, N. N., Beelen, S., Kulikova, I. A., Weeks, S. D., Antson, A. A., Gusev, N. B., and Strelkov, S. V. (2017) Structural Basis for the Interaction of a Human Small Heat Shock Protein with the 14-3-3 Universal Signaling Regulator. *Structure* **25**, 305-316
83. Weeks, S. D., Baranova, E. V., Heirbaut, M., Beelen, S., Shkumatov, A. V., Gusev, N. B., and Strelkov, S. V. (2014) Molecular structure and dynamics of the dimeric human small heat shock protein HSPB6. *Journal of Structural Biology* **185**, 342-354
84. Jehle, S., Rajagopal, P., Bardiaux, B., Markovic, S., Kuhne, R., Stout, J. R., Higman, V. A., Klevit, R. E., van Rossum, B. J., and Oschkinat, H. (2010) Solid-state NMR and SAXS studies provide a structural basis for the activation of α B-crystallin oligomers. *Nature structural & molecular biology* **17**, 1037-1042
85. Baldwin, A. J., Hilton, G. R., Lioe, H., Bagneris, C., Benesch, J. L., and Kay, L. E. (2011) Quaternary dynamics of α B-crystallin as a direct consequence of localised tertiary fluctuations in the C-terminus. *J Mol Biol* **413**, 310-320
86. Delbecq, S. P., and Klevit, R. E. (2013) One size does not fit all: the oligomeric states of α B crystallin. *FEBS Lett* **587**, 1073-1080
87. Hilton, G. R., Hochberg, G. K., Laganowsky, A., McGinnigle, S., Baldwin, A. J., and Benesch, J. L. (2013) C-terminal interactions mediate the quaternary dynamics of α B-crystallin. *Philos Trans R Soc Lond B Biol Sci.* **368**, 20110405
88. Laganowsky, A., Benesch, J. L., Landau, M., Ding, L., Sawaya, M. R., Cascio, D., Huang, Q., Robinson, C. V., Horwitz, J., and Eisenberg, D. (2010) Crystal structures of truncated α A and α B crystallins reveal structural mechanisms of polydispersity important for eye lens function. *Protein Sci* **19**, 1031-1043

89. Treweek, T. M., Ecroyd, H., Williams, D. M., Meehan, S., Carver, J. A., and Walker, M. J. (2007) Site-Directed Mutations in the C-Terminal Extension of Human α B-Crystallin Affect Chaperone Function and Block Amyloid Fibril Formation. *PLoS ONE* **2**
90. Basha, E., O'Neill, H., and Vierling, E. (2012) Small heat shock proteins and alpha-crystallins: dynamic proteins with flexible functions. *Trends in biochemical sciences* **37**, 106-117
91. Haslbeck, M., Weinkauff, S., and Buchner, J. (2015) Regulation of the Chaperone Function of Small Hsps. in *The big book on small heat shock proteins* (Tanguay, R. M., and Hightower, L. E. eds.), Springer International Publishing AG. pp
92. Groenen, P. J., Merck, K. B., de Jong, W. W., and Bloemendal, H. (1994) Structure and modifications of the junior chaperone alpha-crystallin. From lens transparency to molecular pathology. *Eur. J. Biochem.* **225**, 1-19
93. Kato, K., Shinohara, H., Goto, S., Inaguma, Y., Morishita, R., and Asano, T. (1992) Copurification of small heat shock protein with alpha B crystallin from human skeletal muscle. *The Journal of biological chemistry* **267**, 7718-7725
94. Kato, K., Goto, S., Inaguma, Y., Hasegawa, K., Morishita, R., and Asano, T. (1994) Purification and characterization of a 20-kDa protein that is highly homologous to alpha B crystallin. *The Journal of biological chemistry* **269**, 15302-15309
95. Aquilina, J. A., Shrestha, S., Morris, A. M., and Ecroyd, H. (2013) Structural and functional aspects of hetero-oligomers formed by the small heat shock proteins alphaB-crystallin and HSP27. *The Journal of biological chemistry* **288**, 13602-13609
96. Datskevich, P. N., Mymrikov, E. V., and Gusev, N. B. (2012) Utilization of fluorescent chimeras for investigation of heterooligomeric complexes formed by human small heat shock proteins. *Biochimie* **94**, 1794-1804
97. den Engelsman, J., Boros, S., Dankers, P. Y., Kamps, B., Vree Egberts, W. T., Bode, C. S., Lane, L. A., Aquilina, J. A., Benesch, J. L., Robinson, C. V., de Jong, W. W., and Boelens, W. C. (2009) The small heat-shock proteins HSPB2 and HSPB3 form well-defined heterooligomers in a unique 3 to 1 subunit ratio. *J Mol Biol* **393**, 1022-1032
98. Fontaine, J. M., Sun, X., Benndorf, R., and Welsh, M. J. (2005) Interactions of HSP22 (HSPB8) with HSP20, alphaB-crystallin, and HSPB3. *Biochem Biophys Res Commun* **337**, 1006-1011
99. Mymrikov, E. V., Seit-Nebi, A. S., and Gusev, N. B. (2012) Heterooligomeric complexes of human small heat shock proteins. *Cell stress & chaperones* **17**, 157-169
100. Horwitz, J. (1992) Alpha-crystallin can function as a molecular chaperone. *Proceedings of the National Academy of Sciences of the United States of America* **89**, 10449-10453
101. Bepperling, A., Alte, F., Kriehuber, T., Braun, N., Weinkauff, S., Groll, M., Haslbeck, M., and Buchner, J. (2012) Alternative bacterial two-component small heat shock protein systems. *Proceedings of the National Academy of Sciences of the United States of America* **109**, 20407-20412
102. Mchaourab, H. S., Dodson, E. K., and Koteiche, H. A. (2002) Mechanism of Chaperone Function in Small Heat Shock Proteins: Two-mode binding of the excited states of T4 Lysozyme mutants by α A-crystallin. *The Journal of biological chemistry* **277**, 40557-40566
103. Stromer, T., Ehrnsperger, M., Gaestel, M., and Buchner, J. (2003) Analysis of the interaction of small heat shock proteins with unfolding proteins. *The Journal of biological chemistry* **278**, 18015-18021
104. Stengel, F., Baldwin, A. J., Painter, A. J., Jaya, N., Basha, E., Kay, L. E., Vierling, E., Robinson, C. V., and Benesch, J. L. P. (2010) Quaternary dynamics and plasticity underlie small heat shock protein chaperone function. *PNAS* **107**, 2007-2012
105. Haslbeck, M., Walke, S., Stromer, T., Ehrnsperger, M., White, H. E., Chen, S., Saibil, H. R., and Buchner, J. (1999) Hsp26: a temperature-regulated chaperone. *The EMBO Journal* **18**, 6744-6751

106. Specht, S., Miller, S. B. M., Mogk, A., and Bukau, B. (2011) Hsp42 is required for sequestration of protein aggregates into deposition sites in *Saccharomyces cerevisiae*. *The Journal of Cell Biology* **195**
107. Ungelenk, S., Moayed, F., Ho, C. T., Grousl, T., Scharf, A., Mashaghi, A., Tans, S., Mayer, M. P., Mogk, A., and Bukau, B. (2016) Small heat shock proteins sequester misfolding proteins in near-native conformation for cellular protection and efficient refolding. *Nat Commun* **7**, 13673
108. Escusa-Toret, S., Vonk, W. I. M., and Frydman, J. (2012) Spatial sequestration of misfolded proteins by a dynamic chaperone pathway enhances cellular fitness during stress. *Nature Cell Biology* **15**, 1231-1243
109. Zolkiewski, M., Zhang, T., and Nagy, M. (2012) Aggregate reactivation mediated by the Hsp100 chaperones. *Arch Biochem Biophys.* **520**
110. Mogk, A., Bukau, B., and Kampinga, H. H. (2018) Cellular Handling of Protein Aggregates by Disaggregation Machines. *Molecular cell* **69**, 214-226
111. Friedrich, K. K., Giese, K. C., Buan, N. R., and Vierling, E. (2004) Interactions between Small Heat Shock Protein Subunits and Substrate in Small Heat Shock Protein-Substrate Complexes. *The Journal of Biological Chemistry* **279**, 1080-1089
112. Mogk, A., Schlieker, C., Friedrich, K. L., Schönfeld, H.-J., Vierling, E., and Bukau, B. (2003) Refolding of Substrates Bound to Small Hsps Relies on a Disaggregation Reaction Mediated Most Efficiently by ClpB/DnaK. *The Journal of biological chemistry* **278**
113. Rauch, J. N., Tse, E., Freilich, R., MoK, S.-A., Makley, L. N., Southworth, D. R., and Gestwicki, J. E. (2017) BAG3 Is a Modular, Scaffolding Protein that physically Links Heat Shock Protein 70 (Hsp70) to the Small Heat Shock Proteins. *JMB* **429**, 128-141
114. Mogk, A., and Bukau, B. (2017) Role of sHsps in organizing cytosolic protein aggregation and disaggregation. *Cell Stress and Chaperones* **22**, 493-502
115. Pozuelo Rubio, M., Geraghty, K. M., Wong, B. H., Wood, N. T., Campbell, D. G., Morrice, N., and Mackintosh, C. (2004) 14-3-3-affinity purification of over 200 human phosphoproteins reveals new links to regulation of cellular metabolism, proliferation and trafficking. *The Biochemical journal* **379**, 395-408
116. Mounier, N., and Arrigo, A. P. (2002) Actin cytoskeleton and small heat shock proteins: how do they interact? *Cell stress & chaperones* **7**, 167-176
117. Miron, T., Vancompernelle, K., Vandekerckhove, J., Wilchek, M., and Geiger, B. (1991) A 25-kD Inhibitor of Actin Polymerization Is a Low Molecular Mass Heat Shock Protein. *J Cell Biol.* **114**, 255-261
118. Benndorf, R., Hayess, K., Ryazantsev, S., Wieske, M., Behlke, J., and Lutsch, G. (1994) Phosphorylation and supramolecular organization of murine small heat shock protein HSP25 abolish its actin polymerization-inhibiting activity. *The Journal of biological chemistry* **269**, 20780-20784
119. Liang, P., and MacRae, T. H. (1997) Molecular chaperones and the cytoskeleton. *Journal of Cell Science* **110**, 1431-1440
120. Zucker, B., Hanusch, J., and Bauer, G. (1997) Glutathione depletion in fibroblasts is the basis for apoptosis-induction by endogenous reactive oxygen species. *Cell Death and Differentiation* **4**, 288-295
121. Arrigo, A. P. (2007) The cellular "networking" of mammalian Hsp27 and its functions in the control of protein folding, redox state and apoptosis. *Adv Exp Med Biol* **594**, 14-26
122. Arrigo, A.-P. (2001) Hsp27: Novel Regulator of Intracellular Redox State. *IUBMB Life.* **52**, 303-307
123. Mehlen, P., Kretz-Remy, C., Preville, X., and Arrigo, A. P. (1996) Human hsp27, Drosophila hsp27 and human alphaB-crystallin expression-mediated increase in glutathione is essential for the protective activity of these proteins against TNFalpha-induced cell death. *Embo J* **15**, 2695-2706

124. Arrigo, A.-P., Firdaus, W. J. J., Mellier, G., Moulin, M., Paul, C., Diaz-latoud, C., and Kretz-remy, C. (2005) Cytotoxic effects induced by oxidative stress in cultured mammalian cells and protection provided by Hsp27 expression. *Methods* **35**
125. Arrigo, A.-P., Virost, S., Chaufour, S., Firdaus, W., Kretz-Remy, C., and Diaz-Latoud, C. (2005) Hsp27 consolidates intracellular redox homeostasis by upholding glutathione in its reduced form and by decreasing iron intracellular levels. *Antioxidants & Redox Signaling* **7**
126. Fleckenstein, T., Kastenmuller, A., Stein, M. L., Peters, C., Daake, M., Krause, M., Weinfurter, D., Haslbeck, M., Weinkauff, S., Groll, M., and Buchner, J. (2015) The Chaperone Activity of the Developmental Small Heat Shock Protein Sip1 Is Regulated by pH-Dependent Conformational Changes. *Molecular cell* **58**, 1067-1078
127. Basha, E., Lee, G. J., Breci, L. A., Hausrath, A. C., Buan, N. R., Giese, K. C., and Vierling, E. (2004) The Identity of Proteins Associated with a Small Heat Shock Protein during Heat Stress in Vivo Indicates That These Chaperones Protect a Wide Range of Cellular Functions. *The Journal of biological chemistry* **279**, 7566-7575
128. Fu, X., Shi, X., Yan, L., Zhang, H., and Chang, Z. (2013) In vivo substrate diversity and preference of small heat shock protein IbpB as revealed by using a genetically incorporated photo-cross-linker. *The Journal of biological chemistry* **288**, 31646-31654
129. Treweek, T. M., Meehan, S., Ecroyd, H., and Carver, J. A. (2015) Small heat-shock proteins: important players in regulating cellular proteostasis. *Cell. Mol. Life Sci.* **72**, 429-451
130. Lee, G. J., Roseman, A. M., Saibil, H. R., and Vierling, E. (1997) A small heat shock protein stably binds heat-denatured model substrates and can maintain a substrate in a folding-competent state. *EMBO J* **16**, 659-671
131. Sharma, K. K., Kumar, G. S., Murphy, A. S., and Kester, K. (1998) Identification of 1,1'-bi(4-anilino)naphthalene-5,5'-disulfonic acid binding sequences in alpha-crystallin. *The Journal of biological chemistry* **273**, 15474-15478
132. Ghosh, J. G., Shenoy, A. K., Jr., and Clark, J. I. (2007) Interactions between important regulatory proteins and human alphaB crystallin. *Biochemistry* **46**, 6308-6317
133. Jaya, N., Garcia, V., and Vierling, E. (2009) Substrate binding site flexibility of the small heat shock protein molecular chaperones. *PNAS* **106**, 15604-15609
134. Mainz, A., Peschek, J., Stavropoulou, M., Back, K. C., Bardiaux, B., Asami, S., Prade, E., Peters, C., Weinkauff, S., Buchner, J., and Reif, B. (2015) The chaperone alphaB-crystallin uses different interfaces to capture an amorphous and an amyloid client. *Nature structural & molecular biology* **22**, 898-905
135. Hochberg, G. K. A., Ecroyd, H., Liud, C., Cox, D., Cascio, D., Sawaya, Michael R., Collier, M. P., Stroud, J., Carver, J. A., Baldwin, A. J., Robinson, C. V., Eisenberg, D. S., Benesch, J. L. P., and Laganowsky, A. (2014) The structured core domain of alphaB-crystallin can prevent amyloid fibrillation and associated toxicity. *Proc Natl Acad Sci U S A.* **111**
136. Liu, Z., Wang, C., Li, Y., Zhao, C., Li, T., Li, D., Zhang, S., and Liu, C. (2018) Mechanistic insights into the switch of B-crystallin chaperone activity and self-multimerization. *J Biol Chem.* **293**, 14880-14890
137. Baughman, H. E. R., Clouser, A. F., Klevit, R. E., and Nath, A. (2018) HspB1 and Hsc70 chaperones engage distinct tau species and have different inhibitory effects on amyloid formation. *J Biol Chem.* **293**, 2687-2700
138. Petko, L., and Lindquist, S. (1986) Hsp26 is not required for growth at high temperatures, nor for thermotolerance, spore development, or germination. *Cell* **45**, 885-894
139. Mymrikov, E. V., and Haslbeck, M. (2015) Medical implications of understanding the functions of human small heat shock proteins. *Expert Rev Proteomics* **12**, 295-308
140. Sun, Y., and MacRae, T. H. (2005) The small heat shock proteins and their role in human disease. *FEBS J* **272**, 2613-2627
141. Bakthisaran, R., Tangirala, R., and Rao Ch, M. (2015) Small heat shock proteins: Role in cellular functions and pathology. *Biochim Biophys Acta* **1854**, 291-319

142. Arrigo, A.-P., and Gibert, B. (2014) HspB1, HspB5 and HspB4 in Human Cancers: Potent Oncogenic Role of Some of Their Client Proteins. *Cancers* **6**, 333-365
143. Bruey, J. M., Ducasse, C., Bonniaud, P., Ravagnan, L., Susin, S. A., Diaz-Latoud, C., Gurbuxani, S., Arrigo, A. P., Kroemer, G., Solary, E., and Garrido, C. (2000) Hsp27 negatively regulates cell death by interacting with cytochrome c. *Nat Cell Biol* **2**, 645-652
144. Acunzo, J., Katsogiannou, M., and Rocchi, P. (2012) Small heat shock proteins HSP27 (HspB1), α B-crystallin (HspB5) and HSP22 (HspB8) as regulators of cell death. *The International Journal of Biochemistry & Cell Biology* **44**, 1622-1631
145. Kampinga, H. H., and Garrido, C. (2012) HSPBs: Small proteins with big implications in human disease. *The International Journal of Biochemistry & Cell Biology* **44**, 1706-1710
146. Perng, M. D., Muchowski, P. J., van Den, I. P., Wu, G. J., Hutcheson, A. M., Clark, J. I., and Quinlan, R. A. (1999) The cardiomyopathy and lens cataract mutation in α B-crystallin alters its protein structure, chaperone activity, and interaction with intermediate filaments in vitro. *The Journal of biological chemistry* **274**, 33235-33243
147. Vicart, P., Caron, A., Guicheney, P., Li, Z., Prevost, M. C., Faure, A., Chateau, D., Chapon, F., Tome, F., Dupret, J. M., Paulin, D., and Fardeau, M. (1998) A missense mutation in the α B-crystallin chaperone gene causes a desmin-related myopathy. *Nat Genet* **20**, 92-95
148. Perng, M. D., and Quinlan, R. A. (2004) Neuronal Diseases: Small Heat Shock Proteins Calm Your Nerves. *Current Biology* **14**, R625–R626
149. Evgrafov, O. V., Mersiyanova, I., Irobi, J., Van Den Bosch, L., Dierick, I., Leung, C. L., Schagina, O., Verpoorten, N., Van Impe, K., Fedotov, V., Dadali, E., Auer-Grumbach, M., Windpassinger, C., Wagner, K., Mitrovic, Z., Hilton-Jones, D., Talbot, K., Martin, J. J., Vasserman, N., Tverskaya, S., Polyakov, A., Liem, R. K., Gettemans, J., Robberecht, W., De Jonghe, P., and Timmerman, V. (2004) Mutant small heat-shock protein 27 causes axonal Charcot-Marie-Tooth disease and distal hereditary motor neuropathy. *Nat Genet* **36**, 602-606
150. Irobi, J., Van Impe, K., Seeman, P., Jordanova, A., Dierick, I., Verpoorten, N., Michalik, A., De Vriendt, E., Jacobs, A., Van Gerwen, V., Vennekens, K., Mazanec, R., Tournev, I., Hilton-Jones, D., Talbot, K., Kremensky, I., Van Den Bosch, L., Robberecht, W., Van Vandekerckhove, J., Van Broeckhoven, C., Gettemans, J., De Jonghe, P., and Timmerman, V. (2004) Hot-spot residue in small heat-shock protein 22 causes distal motor neuropathy. *Nat Genet* **36**, 597-601
151. Weeks, S. D., Muranova, L. K., Heirbaut, M., Beelen, S., Strelkov, S. V., and Gusev, N. B. (2018) Characterization of human small heat shock protein HSPB1 α -crystallin domain localized mutants associated with hereditary motor neuron diseases. *Scientific Reports* **8**
152. Ojha, J., Karmegam, R. V., Masilamoni, J. G., Terry Jr., A. V., and Cashikar, A. G. (2011) Behavioral Defects in Chaperone-Deficient Alzheimer's Disease Model Mice. *PLoS One* **6**
153. Andley, U. P., Song, Z., Wawrousek, E. F., Brady, J. P., Bassnett, S., and Fleming, T. P. (2001) Lens epithelial cells derived from α B-crystallin knockout mice demonstrate hyperproliferation and genomic instability. *The FASEB Journal* **15**, 221-229
154. Morrow, G., and Tanguay, R. M. (2012) Small heat shock protein expression and functions during development. *Int J Biochem Cell Biol* **44**, 1613-1621
155. Wettstein, G., Bellaye, P. S., Micheau, O., and Bonniaud, P. (2012) Small heat shock proteins and the cytoskeleton: An essential interplay for cell integrity? *The International Journal of Biochemistry & Cell Biology* **44**, 1680–1686
156. Carra, S., Crippa, V., Rusmini, P., Boncoraglio, A., Minoia, M., Giorgetti, E., Kampinga, H. H., and Poletti, A. (2012) Alteration of protein folding and degradation in motor neuron diseases: Implications and protective functions of small heat shock proteins. *Progress in Neurobiology* **97**, 83-100
157. van Noort, J. M., Bsibsi, M., Nacken, P., Gerritsen, W. H., and Amor, S. (2012) The link between small heat shock proteins and the immune system. *The International Journal of Biochemistry & Cell Biology* **44**, 1670-1679

158. Shammass, S. L., Waudby, C. A., Wang, S., Buell, A. K., Knowles, T. P. J., Ecroyd, H., Welland, M. E., Carver, J. A., Dobson, C. M., and Meehan, S. (2011) Binding of the molecular chaperone α B-crystallin to A β amyloid fibrils inhibits fibril elongation. *Biophysical journal* **101**, 1681-1689
159. Krueger-Naug, A. M., Emsley, J. G., Myers, T. L., Currie, R. W., and Clarke, D. B. (2003) Administration of brain-derived neurotrophic factor suppresses the expression of heat shock protein 27 in rat retinal ganglion cells following axotomy. *Neuroscience* **116**, 49-58
160. Hirakawa, T., Rokutan, K., Nikawa, T., and Kishi, K. (1996) Geranylgeranylacetone Induces Heat Shock Proteins in Cultured Guinea Pig Gastric Mucosal Cells and Rat Gastric Mucosa. *Gastroenterology* **111**, 345-357
161. Haldimann, P., Muriset, M., Vigh, L., and Goloubinoff, P. (2011) The Novel Hydroxylamine Derivative NG-094 Suppresses Polyglutamine Protein Toxicity in *Caenorhabditis elegans*. *The Journal of biological chemistry* **286**, 18784–18794
162. Gombos, I., Crul, T., Piotto, S., Gungör, B., Török, Z., Balogh, G., Péter, M., Slotte, J. P., Campana, F., Pilbat, A.-M., Hunya, Á., Tóth, N., Literati-Nagy, Z., Vigh Jr., L., Glatz, A., Brameshuber, M., Schütz, G. J., Hevener, A., Febbraio, M. A., Horváth, I., and Vigh, L. (2011) Membrane-Lipid Therapy in Operation: The HSP CoInducer BGP-15 Activates Stress Signal Transduction Pathways by Remodeling Plasma Membrane Rafts. *PLoS One* **6**
163. Boncoraglio, A., Minoia, M., and Carra, S. (2012) The family of mammalian small heat shock proteins (HSPBs): Implications in protein deposit diseases and motor neuropathies. *The International Journal of Biochemistry & Cell Biology* **44**, 1657– 1669
164. Zoubeidi, A., and Gleave, M. (2012) Small heat shock proteins in cancer therapy and prognosis. *The International Journal of Biochemistry & Cell Biology* **44**, 1646– 1656
165. Gibert, B., Hadchity, E., Czekalla, A., Aloy, M.-T., Colas, P., Rodriguez-Lafresse, C., Arrigo, A.-P., and Diaz-Latoud, C. (2011) Inhibition of heat shock protein 27 (HspB1) tumorigenic functions by peptide aptamers. *Oncogene* **30**, 3672–3681
166. Bimston, D., Song, J., Winchester, D., Takayama, S., Reed, J. C., and Morimoto, R. I. (1998) BAG-1, a negative regulator of Hsp70 chaperone activity, uncouples nucleotide hydrolysis from substrate release. *The EMBO Journal* **17**, 6871-6878
167. McCollum, A. K., Casagrande, G., and Kohn, E. C. (2010) Caught in the middle: the role of Bag3 in disease. *The Biochemical journal* **425**, e1-3
168. Alberti, S., Esser, C., and Höhfeld, J. (2003) BAG-1—a nucleotide exchange factor of Hsc70 with multiple cellular functions. *Cell Stress and Chaperones* **8**, 225-231
169. Bruno, A. P., Festa, M., Dal Piaz, F., Rosati, A., Turco, M. C., Giuditta, A., and Marzullo, L. (2008) Identification of a synaptosome- associated form of BAG3 protein. *Cell Cycle* **7**, 3104-3105
170. Gamerdinger, M., Hajieva, P., Kaya, A. M., Wolfrum, U., Hartl, F. U., and Behl, C. (2009) Protein quality control during aging involves recruitment of the macroautophagy pathway by BAG3. *The EMBO Journal* **28**, 889-901
171. Fuchs, M., Poirier, D. J., Seguin, S. J., Lambert, H., Carra, S., Charette, S. J., and Landry, J. (2010) Identification of the key structural motifs involved in HspB8/HspB6-Bag3 interaction. *The Biochemical journal* **425**, 245-255
172. Hishiya, A., Salman, M. N., Carra, S., Kampinga, H. H., and Takayama, S. (2011) BAG3 Directly Interacts with Mutated α B-Crystallin to Suppress Its Aggregation and Toxicity. *PLoS One* **6**
173. Behl, C. (2016) Breaking BAG: The Co-Chaperone BAG3 in Health and Disease. *Trends in Pharmacological Sciences* **37**
174. Jin, Y.-H., Ahn, S.-G., and Kim, S.-A. (2015) BAG3 affects the nucleocytoplasmic shuttling of HSF1 upon heat stress. *Biochemical and Biophysical Research Communications* **464**, 561-567

175. Chen, Y., Yang, L.-N., Cheng, L., Tu, S., Guo, S.-J., Le, H.-Y., Xiong, Q., Mo, R., Li, C.-Y., Jeong, J.-S., Jiang, L., Blackshaw, S., Bi, L.-J., Zhu, H., Tao, S.-C., and Ge, F. (2013) Bcl2-associated Athanogene 3 Interactome Analysis Reveals a New Role in Modulating Proteasome Activity. *Molecular & Cellular Proteomics* **12**, 2804-2819
176. Xu, Z., Graham, K., Foote, M., Liang, F., Rizkallah, R., Hurt, M., Wang, Y., Wu, Y., and Zhou, Y. (2013) 14-3-3 protein targets misfolded chaperone-associated proteins to aggresomes. *Journal of Cell Science* **126**, 4173-4186
177. Ulbricht, A., Arndt, V., and Höhfeld, J. (2013) Chaperone-assisted proteostasis is essential for mechanotransduction in mammalian cells. *Communicative & Integrative Biology* **6**, e24925
178. Stürner, E., and Behl, C. (2017) The Role of the Multifunctional BAG3 Protein in Cellular Protein Quality Control and in Disease. *Frontiers in Molecular Neuroscience* **10**
179. Ulbricht, A., Gehlert, S., Leciejewski, B., Schiffer, T., Bloch, W., and Höhfeld, J. (2015) Induction and adaptation of chaperone-assisted selective autophagy CASA in response to resistance exercise in human skeletal muscle. *Autophagy* **11**, 538-546
180. Franzmann, T. M., Wühr, M., Richter, K., Walter, S., and Buchner, J. (2005) The activation mechanism of Hsp26 does not require dissociation of the oligomer. *J. Mol. Biol.* **350**, 1083-1093
181. Franzmann, T. M., Menhorn, P., Walter, S., and Buchner, J. (2008) Activation of the Chaperone Hsp26 Is Controlled by the Rearrangement of Its Thermosensor Domain. *Molecular cell* **29**, 207-216
182. White, H. E., Orlova, E. V., Chen, S., Wang, L., Ignatiou, A., Gowen, B., Stromer, T., Franzmann, T. M., Haslbeck, M., Buchner, J., and Saibil, H. R. (2006) Multiple Distinct Assemblies Reveal Conformational Flexibility in the Small Heat Shock Protein Hsp26. *Structure* **14**, 1197-1204
183. Fu, X., Chang, Z., Shi, X., Bu, D., and Wang, C. (2014) Multilevel structural characteristics for the natural substrate proteins of bacterial small heat shock proteins. *Protein Sci* **23**, 229-237
184. Bova, M. P., McHaourab, H. S., Han, Y., and Fung, B. K. (2000) Subunit exchange of small heat shock proteins. Analysis of oligomer formation of alphaA-crystallin and Hsp27 by fluorescence resonance energy transfer and site-directed truncations. *The Journal of biological chemistry* **275**, 1035-1042
185. Basha, E., Jones, C., Wysocki, V., and Vierling, E. (2010) Mechanistic differences between two conserved classes of small heat shock proteins found in the plant cytosol. *The Journal of biological chemistry* **285**, 11489-11497
186. de Miguel, N., Braun, N., Bepperling, A., Kriehuber, T., Kastenmüller, A., Buchner, J., Angel, S. O., and Haslbeck, M. (2009) Structural and functional diversity in the family of small heat shock proteins from the parasite *Toxoplasma gondii*. *Biochimica et Biophysica Acta* **1793**, 1738-1748
187. Benesch, J. L., Ayoub, M., Robinson, C. V., and Aquilina, J. A. (2008) Small heat shock protein activity is regulated by variable oligomeric substructure. *The Journal of biological chemistry* **283**, 28513-28517
188. Shi, J., Koteiche, H. A., McDonald, E. T., Fox, T. L., Stewart, P. L., and McHaourab, H. S. (2013) Cryoelectron microscopy analysis of small heat shock protein 16.5 (Hsp16.5) complexes with T4 lysozyme reveals the structural basis of multimode binding. *The Journal of biological chemistry* **288**, 4819-4830
189. Ehrnsperger, M., Lilie, H., Gaestel, M., and Buchner, J. (1999) The dynamics of Hsp25 quaternary structure. Structure and function of different oligomeric species. *The Journal of biological chemistry* **274**, 14867-14874
190. Krajewski, S. S., Joswig, M., Nagel, M., and Narberhaus, F. (2014) A tricistronic heat shock operon is important for stress tolerance of *Pseudomonas putida* and conserved in many environmental bacteria. *Environmental Microbiology* **16**, 1835-1853

191. Cimdin, A. B., Klinkert, Aschke-Sonnenborn, U., Kaiser, F. M., Kortmann, J., and Narberhaus, F. (2014) Translational control of small heat shock genes in mesophilic and thermophilic cyanobacteria by RNA thermometers. *RNA Biology* **11**, 594-608
192. Chernik, I. S., Panasencko, O. O., Li, Y., Marston, S. B., and Gusev, N. B. (2004) pH-induced changes of the structure of small heat shock proteins with molecular mass 24/27kDa (HspB1). *Biochem Biophys Res Commun* **324**, 1199-1203
193. Baldwin, A. J., Lioe, H., Hilton, G. R., Baker, L. A., Rubinstein, J. L., Kay, L. E., and Benesch, J. L. (2011) The polydispersity of alphaB-crystallin is rationalized by an interconverting polyhedral architecture. *Structure* **19**, 1855-1863
194. Bodenmiller, B., Wanka, S., Kraft, C., Urban, J., Campbell, D., Pedrioli, P. G., Gerrits, B., Picotti, P., Lam, H., Vitek, O., Brusniak, M.-Y., Roschitzki, B., Zhang, C., Shokat, K. M., Schlapbach, R., Colman-Lerner, A., Nolan, G. P., Nesvizhskii, A. I., Peter, M., Loewith, R., von Mering, C., and Aebersold, R. (2010) Phosphoproteomic Analysis Reveals Interconnected System-Wide Responses to Perturbations of Kinases and Phosphatases in Yeast. *Science Signaling* **153**
195. Lund, A. A., Rhoads, D. M., Lund, A. L., Cerny, R. L., and Elthon, T. E. (2001) In Vivo Modifications of the Maize Mitochondrial Small Heat Stress Protein, HSP22. *The Journal of biological chemistry* **276**
196. Gaestel, M. (2002) sHsp-Phosphorylation: Enzymes, Signaling Pathways and Functional Implications. in *Small Stress Proteins* (Arrigo AP., M. W. E. G. e. ed.), Springer, Berlin, Heidelberg, Progress in Molecular and Subcellular Biology. pp
197. Ito, H., Kamei, K., Iwamoto, I., Inaguma, Y., Nohara, D., and Kato, K. (2001) Phosphorylation-induced change of the oligomerization state of alpha B-crystallin. *The Journal of biological chemistry* **276**, 5346-5352
198. Hayes, D., Napoli, V., Mazurkie, A., Stafford, W. F., and Graceffa, P. (2009) Phosphorylation dependence of hsp27 multimeric size and molecular chaperone function. *The Journal of biological chemistry* **284**, 18801-18807
199. Lelj-Garolla, B., and Mauk, A. G. (2005) Self-association of a small heat shock protein. *J Mol Biol* **345**, 631-642
200. Shashidharamurthy, R., Koteiche, H. A., Dong, J., and McHaourab, H. S. (2005) Mechanism of chaperone function in small heat shock proteins: dissociation of the HSP27 oligomer is required for recognition and binding of destabilized T4 lysozyme. *The Journal of biological chemistry* **280**, 5281-5289
201. Gupta, R., and Srivastava, O. P. (2004) Deamidation Affects Structural and Functional Properties of human α A-Crystallin and its Oligomerization with α B-Crystallin. *The Journal of biological chemistry* **279**, 44258-44269
202. Chen, S.-J., Sun, T.-X., Akhtar, N. J., and Liang, J. J.-N. (2001) Oxidation of human lens recombinant α A-crystallin and cysteine-deficient mutants. *Journal of Molecular Biology* **305**, 969-976
203. Kumar, M. S., Mrudula, T., Mitra, N., and Reddy, G. B. (2004) Enhanced degradation and decreased stability of eye lens α -crystallin upon methylglyoxal modification,. *Experimental Eye Research* **799**, 577-583
204. Kumar, P. A., Kumar, M. S., and Reddy, G. B. (2007) Effect of glycation on alpha-crystallin structure and chaperone-like function. *The Biochemical journal* **408**, 251-258
205. Ratajczak, E., Ziętkiewicz, S., and Liberek, K. (2009) Distinct Activities of Escherichia coli Small Heat Shock Proteins IbpA and IbpB Promote Efficient Protein Disaggregation. *Journal of Molecular Biology* **386**, 178-189
206. Bukach, O. V., Glukhova, A. E., Seit-Nebi, A. S., and Gusev, N. B. (2009) Heterooligomeric complexes formed by human small heat shock proteins HspB1 (Hsp27) and HspB6 (Hsp20). *Biochim Biophys Acta* **1794**, 486-495

207. Heirbaut, M., Lermyte, F., Martin, E. M., Beelen, S., Sobott, F., Strelkov, S. V., and Weeks, S. D. (2017) Specific sequences in the N-terminal domain of human small heat-shock protein HSPB6 dictate preferential hetero-oligomerization with the orthologue HSPB1. *The Journal of biological chemistry* **292**, 9944-9957
208. Haslbeck, M., Braun, N., Stromer, T., Richter, B., Model, N., Weinkauff, S., and Buchner, J. (2004) Hsp42 is the general small heat shock protein in the cytosol of *Saccharomyces cerevisiae*. *The EMBO Journal* **23**, 638-649
209. Arrigo, A. P., and Gibert, B. (2013) Protein interactomes of three stress inducible small heat shock proteins: HspB1, HspB5 and HspB8. *International journal of hyperthermia : the official journal of European Society for Hyperthermic Oncology, North American Hyperthermia Group* **29**, 409-422
210. Fuchs, M., Poirier, D. J., Seguin, S. J., Lambert, H., Carra, S., Charette, S. J., and Landry, J. (2010) Identification of the key structural motifs involved in HspB8/HspB6-Bag3 interaction. *Biochem. J.* **425**, 245-255
211. Peschek, J., Braun, N., Franzmann, T. M., Georgalis, Y., Haslbeck, M., Weinkauff, S., and Buchner, J. (2009) The eye lens chaperone alpha-crystallin forms defined globular assemblies. *Proceedings of the National Academy of Sciences of the United States of America* **106**, 13272-13277
212. Bukach, O. V., Seit-Nebi, A. S., Marston, S. B., and Gusev, N. B. (2004) Some properties of human small heat shock protein Hsp20 (HspB6). *European journal of biochemistry* **271**, 291-302
213. Back, K. C. (2016) *Substrate recognition determinants of the small heat shock protein α B-crystallin and its role in cataractogenesis*, Technische Universität München
214. Schmid, P. W. N. (2019) *Untersuchungen zu den molekularen Determinanten der Kataraktentstehung und der Substratbindung von α B-Kristallin*, Technischen Universität München
215. Laemmli, U. K. (1970) Cleavage of structural proteins during the assembly of the head of bacteriophage T4. *Nature* **227**, 680-685
216. Bradford, M. M. (1976) A rapid and sensitive method for the quantitation of microgram quantities of protein utilizing the principle of protein-dye binding. *Anal Biochem* **72**, 248-254
217. Gasteiger, E., Hoogland, C., Gattiker, A., Duvaud, S., Wilkins, M. R., Appel, R. D., and Bairoch, A. (2005) Protein Identification and Analysis Tools on the ExpASY Server. in *The Proteomics Protocols Handbook* (Walker, J. M. ed.), Humana Press. pp 571-607
218. Compton, S. J., and Jones, C. (1985) Mechanism of Dye Response and Interference in the Bradford Protein Assay. *ANALYTICAL BIOCHEMISTRY* **151**, 369-374
219. Ludtke, S. J., Baldwin, P. R., and Chiu, W. (1999) EMAN: Semiautomated Software for High-Resolution Single-Particle Reconstructions. *Journal of Structural Biology* **128**, 82-97
220. Van Heel, M., Harauz, G., Orlova, E. V., Schmidt, R., and Schatz, M. (1995) A New Generation of the IMAGIC Image Processing System. *Journal of Structural Biology* **116**, 17-24
221. Schneider, C. A., Rasband, W. S., and Eliceiri, K. W. (2012) NIH Image to ImageJ: 25 years of image analysis. *Nature Methods* **9**, 671-675
222. Weber, B., Brandl, M. J., Pulido Cendales, M. D., Berner, C., Pradhan, T., Feind, G. M., Zacharias, M., Reif, B., and Buchner, J. (2018) A single residue switch reveals principles of antibody domain integrity. *The Journal of biological chemistry* **293**, 17107-17118
223. Zhang, A., Hu, P., MacGregor, P., Xue, Y., Fan, H., Suchecki, P., Olszewski, L., and Liu, A. (2014) Understanding the Conformational Impact of Chemical Modifications on Monoclonal Antibodies with Diverse Sequence Variation Using Hydrogen/Deuterium Exchange Mass Spectrometry and Structural Modeling. *Anal. Chem.* **86**, 3468-3475
224. Wessel, D., and Flügge, U. I. (1984) A method for the quantitative recovery of protein in dilute solution in the presence of detergents and lipids. *ANALYTICAL BIOCHEMISTRY* **138**, 141-143

225. Zhang, Z., and Marshall, A. G. (1998) A Universal Algorithm for Fast and Automated Charge State Deconvolution of Electrospray Mass-to-Charge Ratio Spectra. *Journal of American Society for mass Spectrometry* **9**, 225-233
226. Perkins, D., Pappin, D., Creasy, D., and Cottrell, J. (1999) Probability-based protein identification by searching sequence databases using mass spectrometry data. *Electrophoresis*. **20**, 3551-3567
227. Schuck, P. (2000) Size-distribution analysis of macromolecules by sedimentation velocity ultracentrifugation and lamm equation modeling. *Biophysical journal* **78**, 1606-1619
228. Mymrikov, E. V., Riedl, M., Peters, C., Weinkauff, S., Haslbeck, M., and Buchner, J. (2020) Regulation of small heat shock proteins by hetero-oligomer formation. *Journal of Biological Chemistry* **295**, 158-169
229. Assimakopoulou, M., Sotiropoulou-Bonikou, G., Maraziotis, T., and Varakis, I. (1997) Prognostic significance of Hsp-27 in astrocytic brain tumors: an immunohistochemical study. *Anticancer Res* **17**, 2677-2682
230. Ciocca, D. R., and Calderwood, S. K. (2005) Heat shock proteins in cancer: diagnostic, prognostic, predictive, and treatment implications. *Cell stress & chaperones* **10**, 86-103
231. Nagasawa, T., Matsushima-Nishiwaki, R., Toyoda, H., Matsuura, J., Kumada, T., and Kozawa, O. (2014) Heat shock protein 20 (HSPB6) regulates apoptosis in human hepatocellular carcinoma cells: Direct association with Bax. *Oncology Reports* **32**, 1291-1294
232. Rogalla, T., Ehrnsperger, M., Preville, X., Kotlyarov, A., Lutsch, G., Ducasse, C., Paul, C., Wieske, M., Arrigo, A. P., Buchner, J., and Gaestel, M. (1999) Regulation of Hsp27 oligomerization, chaperone function, and protective activity against oxidative stress/tumor necrosis factor alpha by phosphorylation. *The Journal of biological chemistry* **274**, 18947-18956
233. Gibert, B., Eckel, B., Fasquelle, L., Moulin, M., Bouhallier, F., Gonin, V., Mellier, G., Simon, S., Kretz-Remy, C., Arrigo, A.-P., and Diaz-Latoud, C. (2012) Knock Down of Heat Shock Protein 27 (HspB1) Induces Degradation of Several Putative Client Proteins. *PLoS One* **7**, e29719
234. Golenhofen, N., Perng, M. D., Quinlan, R. A., and Drenckhahn, D. (2004) Comparison of the small heat shock proteins alphaB-crystallin, MKBP, HSP25, HSP20, and cvHSP in heart and skeletal muscle. *Histochem Cell Biol* **122**, 415-425
235. Arrigo, A. P., Suhan, J. P., and Welch, W. J. (1988) Dynamic changes in the structure and intracellular locale of the mammalian low-molecular-weight heat shock protein. *Mol Cell Biol* **8**, 5059-5071
236. Wu, C.-s. (2003) *Handbook of Size Exclusion Chromatography and Related Techniques*, CRC Press
237. McHaourab, H. S., Godar, J. A., and Stewart, P. L. (2009) Structure and mechanism of protein stability sensors: chaperone activity of small heat shock proteins. *Biochemistry* **48**, 3828-3837
238. Ehrnsperger, M., Graber, S., Gaestel, M., and Buchner, J. (1997) Binding of non-native protein to Hsp25 during heat shock creates a reservoir of folding intermediates for reactivation. *Embo J* **16**, 221-229
239. Ahrman, E., Lambert, W., Aquilina, J. A., Robinson, C. V., and Emanuelsson, C. S. (2007) Chemical cross-linking of the chloroplast localized small heat-shock protein, Hsp21, and the model substrate citrate synthase. *Protein Science* **16**, 1464-1478
240. Van Montfort, R. L., Slingsby, C., and Vierling, E. (2001) Structure and function of the small heat shock protein/alpha-crystallin family of molecular chaperones. *Adv Protein Chem.* **59**, 105-156
241. Mymrikov, E. V., Bukach, O. V., Seit-Nebi, A. S., and Gusev, N. B. (2010) The pivotal role of the beta 7 strand in the intersubunit contacts of different human small heat shock proteins. *Cell stress & chaperones* **15**, 365-377

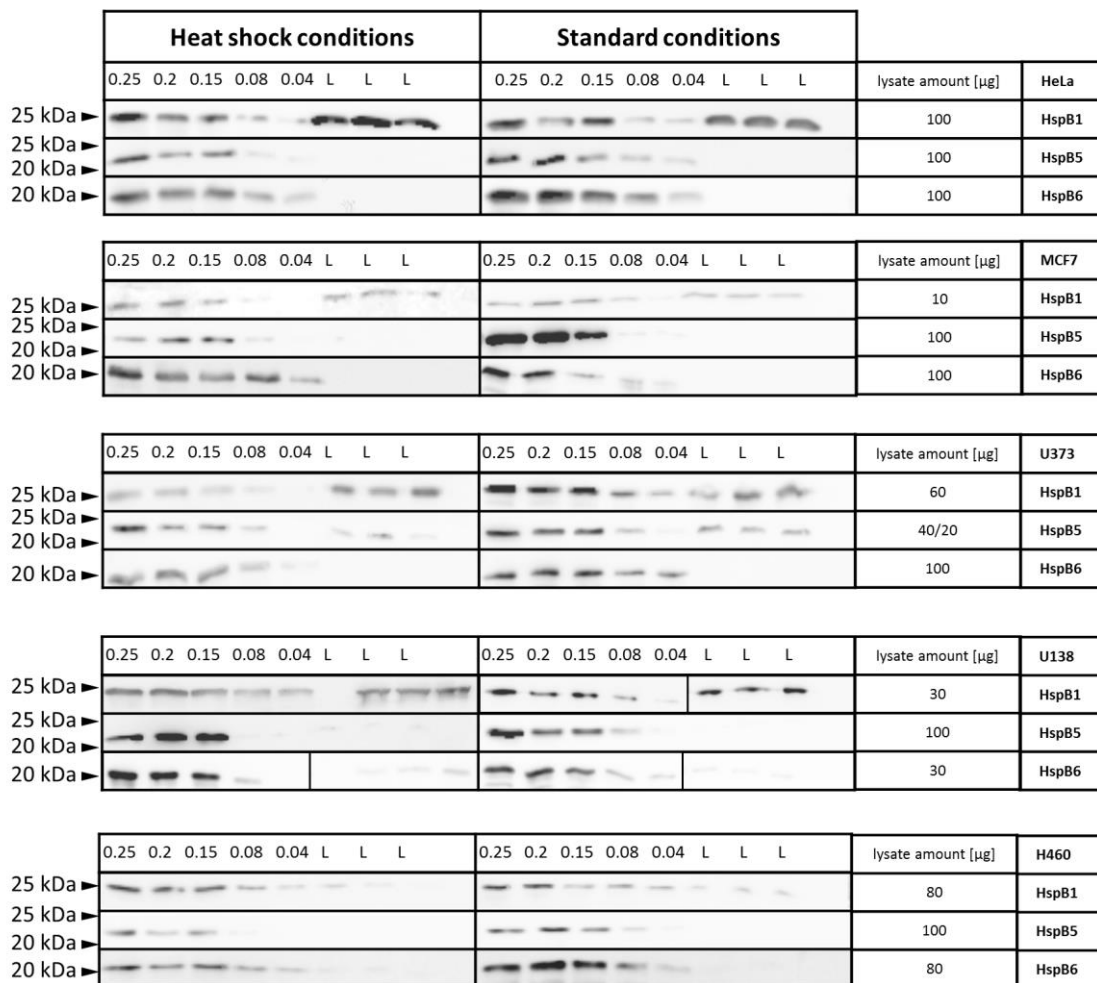
242. Chalova, A. S., Sudnitsyna, M. V., Semenyuk, P. I., Orlov, V. N., and Gusev, N. B. (2014) Effect of disulfide crosslinking on thermal transitions and chaperone-like activity of human small heat shock protein HspB1. *Cell stress & chaperones* **19**, 963-972
243. Zondlo, N. J. (2013) Aromatic-Proline Interactions: Electronically Tunable CH/ π Interactions. *Acc Chem Res.* **46**, 1039-1049
244. Lambert, W., Rutsdottir, G., Hussein, R., Bernfur, K., Kjellström, S., and Emanuelsson, C. (2013) Probing the transient interaction between the small heat-shock protein Hsp21 and a model substrate protein using crosslinking mass spectrometry. *Cell Stress and Chaperones* **18**, 75-85
245. Bhattacharyya, J., Udupa, E. G. P., Wang, J., and Sharma, K. K. (2006) Mini-aB-Crystallin: A Functional Element of aB-Crystallin with Chaperone-like Activity. *Biochemistry* **45**, 3069-3076
246. Nakamura, Y., Gojobori, T., and Ikemura, T. (2000) Codon usage tabulated from the international DNA sequence databases. *Nucl. Acids Res.* **28**
247. Sondermann, H., Scheufler, C., Schneider, C., Höhfeld, J., Hartl, F.-U., and Moarefi, I. (2001) Structure of a Bag/Hsc70 complex: convergent functional evolution of Hsp70 nucleotide exchange factors. *Science (New York, N.Y)* **291**
248. Macias, M. J., Hyvönen, M., Baraldi, E., Schultz, J., Sudol, M., Saraste, M., and Oschkinat, H. (1996) Structure of the WW domain of a kinase-associated protein complexed with a proline-rich peptide. *Letters to Nature* **382**
249. Obermeyer, Z., Samra, J. K., and Mullainathan, S. (2017) Individual differences in normal body temperature: longitudinal big data analysis of patient records. *BMJ* **359**
250. Ganassi, M., Mateju, D., Bigi, I., Mediani, L., Poser, I., Lee, H. O., Seguin, S. J., Morelli, F. F., Vinet, J., Leo, G., Pansarasa, O., Cereda, C., Poletti, A., Alberti, S., and Carra, S. (2016) A Surveillance Function of the HSPB8-BAG3-HSP70 Chaperone Complex Ensures Stress Granule Integrity and Dynamism. *Molecular cell* **63**, 796–810
251. Hochberg, G. K. A., Shepherd, D. A., Marklund, E. G., Santhanagoplan, I., T. Degiacomi, M., Laganowsky, A., Allison, T. M., Basha, E., Marty, M. T., Galpin, M. R., Struwe, W. B., Baldwin, A. J., Vierling, E., and Benesch, J. L. P. (2018) Structural principles that enable oligomeric small heat-shock protein paralogs to evolve distinct functions. *Science (New York, N.Y)* **359**, 930-935
252. Zantema, A., Verlaan-De Vries, M., Maasdam, D., Bol, S., and van der Eb, A. (1992) Heat Shock Protein 27 and aB-Crystallin Can Form a Complex, Which Dissociates by Heat Shock. *The Journal of biological chemistry* **267**, 12936-12941
253. Song, S., Landsbury, A., Dahm, R., Liu, Y., Zhang, Q., and Quinlan, R. A. (2009) Functions of the intermediate filament cytoskeleton in the eye lens. *The Journal of Clinical Investigation* **119**, 1837-1848
254. Nefedova, V. V., Sudnitsyna, M. V., and Gusev, N. B. (2017) Interaction of small heat shock proteins with light component of neurofilaments (NFL). *Cell stress & chaperones* **22**, 467-479
255. Perng, M. D., Cairns, L., van den, I. P., Prescott, A., Hutcheson, A. M., and Quinlan, R. A. (1999) Intermediate filament interactions can be altered by HSP27 and alphaB-crystallin. *J Cell Sci* **112** 2099-2112
256. Li, F., and Yang, H. X. F. Z. H. B. (2017) Study of HSPB6: Insights into the Properties of the Multifunctional Protective Agent. *Cellular Physiology and Biochemistry* **44**, 314-332
257. Ju, Y. T., Kwag, S. J., Park, H. J., Jung, E. J., Jeong, C. Y., Jeong, S. H., Lee, Y. J., Choi, S. K., Kang, K. R., Hah, Y. S., and Hong, S. C. (2015) Decreased expression of heat shock protein 20 in colorectal cancer and its implication in Tumorigenesis. *J Cell Biochem* **116**, 277-286
258. Rouse, J., Cohen, P., Trigon, S., Morange, M., Alonso-Llamazares, A., Zamanillo, D., Hunt, T., and Nebreda, A. R. (1994) A novel kinase cascade triggered by stress and heat shock that stimulates MAPKAP kinase-2 and phosphorylation of the small heat shock proteins. *Cell* **78**, 1027-1037

259. Blagosklonny, M. (2002) Hsp-90-associated oncoproteins: Multiple targets of geldanamycin and its analogs. *Leukemia* **16**, 455-462
260. Simon, S., Dimitrova, V., Gibert, B., Virost, S., Mounier, N., Nivon, M., Kretz-Remy, C., Corset, V., Mehlen, P., and Arrigo, A. P. (2013) Analysis of the dominant effects mediated by wild type or R120G mutant of alphaB-crystallin (HspB5) towards Hsp27 (HspB1). *PLoS One* **8**, e70545
261. Fu, L., and Liang, J. J.-N. (2003) Enhanced stability of alphaB-crystallin in the presence of small heat shock protein Hsp27. *Biochemical and Biophysical Research Communications* **302**, 710-714
262. Bova, M. P., Ding, L. L., Horwitz, J., and Fung, B. K. (1997) Subunit exchange of alphaA-crystallin. *The Journal of biological chemistry* **272**, 29511-29517
263. Aquilina, J. A., Benesch, J. L., Ding, L. L., Yaron, O., Horwitz, J., and Robinson, C. V. (2005) Subunit Exchange of Polydisperse Proteins: Mass Spectrometry Reveals Consequences of AlphaA-Crystallin Truncation. *The Journal of biological chemistry* **280**, 14485-14491
264. Augusteyn, R. C. (2004) Dissociation is not required for alpha-crystallin's chaperone function. *Experimental Eye Research* **79**, 781-784
265. Kasakov, A. S., Bukach, O. V., Seit-Nebi, A. S., Marston, S. B., and Gusev, N. B. (2007) Effect of mutations in the beta5-beta7 loop on the structure and properties of human small heat shock protein HSP22 (HspB8, H11). *FEBS J* **274**, 5628-5642
266. Morrow, G., Inaguma, Y., Kato, K., and Tanguay, R. M. (2000) The Small Heat Shock Protein Hsp22 of *Drosophila melanogaster* Is a Mitochondrial Protein Displaying Oligomeric Organization. *The Journal of biological chemistry* **275**, 31204-31210
267. Leroux, M. R., Ma, B. J., Batelier, G., Melki, R., and Candido, E. P. (1997) Unique structural features of a novel class of small heat shock proteins. *The Journal of biological chemistry* **272**, 12847-12853
268. Leroux, M. R., Melki, R., Gordon, B., Batelier, G., and Candido, E. (1997) Structure-Function Studies on Small Heat Shock Protein Oligomeric Assembly and Interaction with Unfolded Polypeptide. *The Journal of biological chemistry* **272**, 24646-24656
269. Shemetov, A. A., and Gusev, N. B. (2011) Biochemical characterization of small heat shock protein HspB8 (Hsp22)-Bag3 interaction. *Arch Biochem Biophys* **513**, 1-9
270. Chernik, I. S., Seit-Nebi, A. S., Marston, S. B., and Gusev, N. B. (2007) Small heat shock protein Hsp20 (HspB6) as a partner of 14-3-3gamma. *Mol Cell Biochem* **295**, 9-17
271. Cheng, G., Basha, E., Wysocki, V. H., and Vierling, E. (2008) Insights into small heat shock protein and substrate structure during chaperone action derived from hydrogen/deuterium exchange and mass spectrometry. *The Journal of biological chemistry* **283**, 26634-26642
272. Doong, H., Vrailas, A., and Kohn, E. C. (2002) What's in the 'BAG'? – a functional domain analysis of the BAG-family proteins. *Cancer Letters* **188**, 25-32
273. Homma, S., Iwasaki, M., Shelton, G. D., Engvall, E., Reed, J. C., and Takayam, S. (2006) BAG3 Deficiency Results in Fulminant Myopathy and Early Lethality. *Am J Pathol.* **169**, 761-773
274. Meister-Broekema, M., Freilich, R., Jagadeesan, C., Rauch, J. N., Bengoechea, R., Motley, W. W., Kuiper, E. F. E., Minoia, M., Furtado, G. V., van Waarde, M. A. W. H., Bird, S. J., Rebelo, A., Zuchner, S., Pytel, P., Scherer, S. S., Morelli, F. F., Carra, S., Weihl, C. C., Bergink, S., Gestwicki, J. E., and Kampinga, H. H. (2018) Myopathy associated BAG3 mutations lead to protein aggregation by stalling Hsp70 networks. *Nature Communications* **9**, 5342
275. Fang, X., Bogomolovas, J., Wu, T., Zhang, W., Liu, C., Veevers, J., Stroud, M. J., Zhang, Z., Ma, X., Mu, Y., Lao, D. H., Dalton, N. D., Gu, Y., Wang, C., Wang, M., Liang, Y., Lange, S., Ouyang, K., Peterson, K. L., Evans, S. M., and Chen, J. (2017) Loss-of-function mutations in co-chaperone BAG3 destabilize small HSPs and cause cardiomyopathy. *The Journal of Clinical Investigation* **127**, 3189-3200

7 APPENDIX

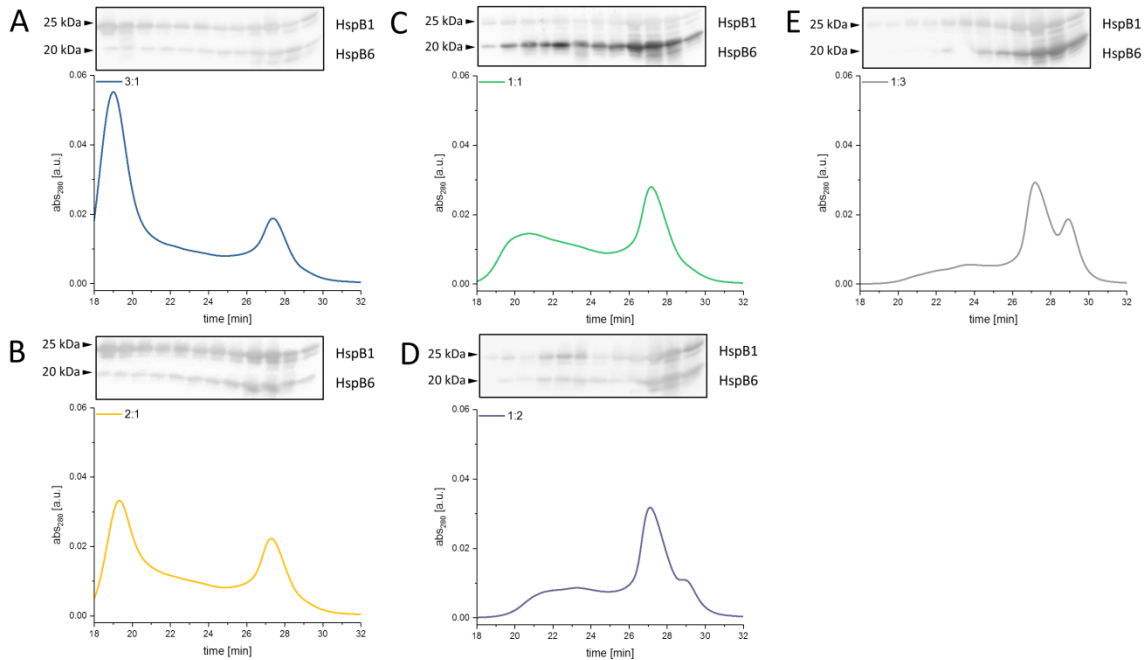
A | Quantification of endogenous expressed sHsp amounts in five human cancer cell lines (HeLa, MCF7, U373MG, U138MG and H460) by western blotting under heat shock and standard conditions.

Increasing amounts of purified recombinant proteins (0.25 – 0.04 μg) were loaded on the first five lanes for calibration. Triplicates of fixed, total protein amounts of cell lysates (L) were loaded on lane 6 to 8. The total protein amounts analyzed for the respective cell line are indicated on the right.

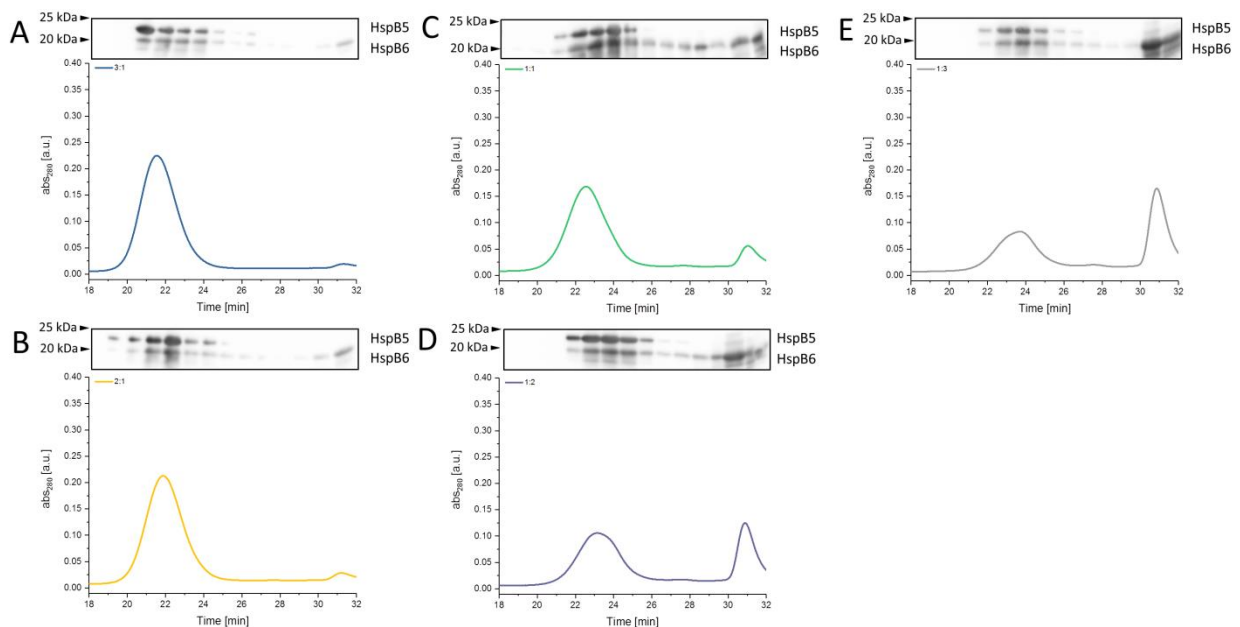


B | Western blot analysis of size exclusion chromatography fractions of HspB1-HspB6 and HspB5-B6 hetero-oligomers obtained at different ratios but constant total sHsp amount.

Identical concentrations and conditions are applied as in Figure 14. The use of a different HPLC system resulted in a slight shift in elution time (due to differences in length and diameters of tubing and detector cells). 50 μ l of a 50 μ M HspB1-HspB6 sample with (A) 3:1; (B) 2:1; (C) 1:1; (D) 1:2 and (E) 1:3 ratio were separated on a superdex200 increase column



Respectively, 50 μ l of a 50 μ M HspB5-HspB6 sample with (A) 3:1; (B) 2:1; (C) 1:1; (D) 1:2 and (E) 1:3 ratio were separated on a superdex200 increase column.

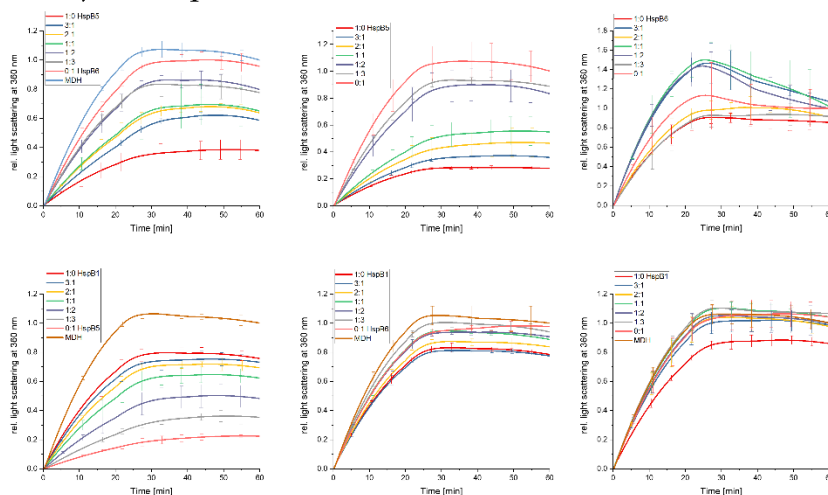


C | Chaperone activity of hetero-oligomers formed at different ratios of HspB1-HspB6, HspB1-HspB5 or HspB5-HspB6

Malate dehydrogenase (A, MDH and 0.25 μM total sHsp; B, MDH and 0.5 μM total sHsp), citrate synthase (C, CS and 2 μM total sHsp; D, CS and 4 μM total sHsp), insulin (E) and glyceraldehyde-3-phosphate dehydrogenase (F, GAPDH) were used as substrates. Endpoint values are depicted with HspB1 – blue, HspB5 – green, HspB6 – yellow and hetero-oligomers – red. Theoretical value indicating the sum of the activity of sHsp homo-oligomers at the respective concentration are depicted in black.

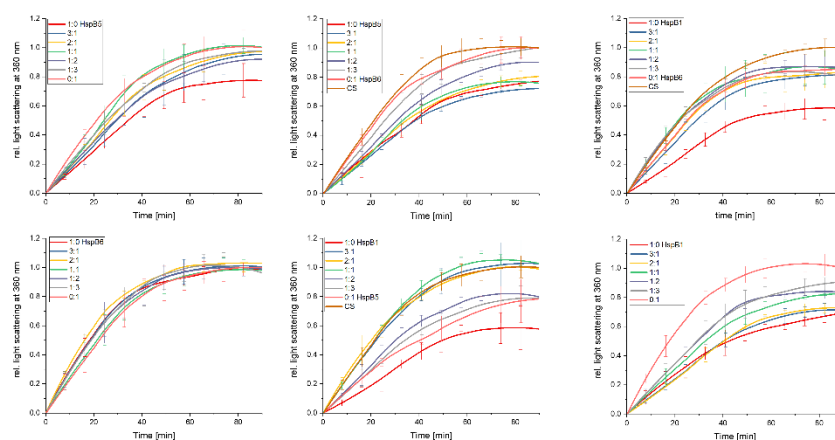
MDH

0.25 μM sHsp concentration

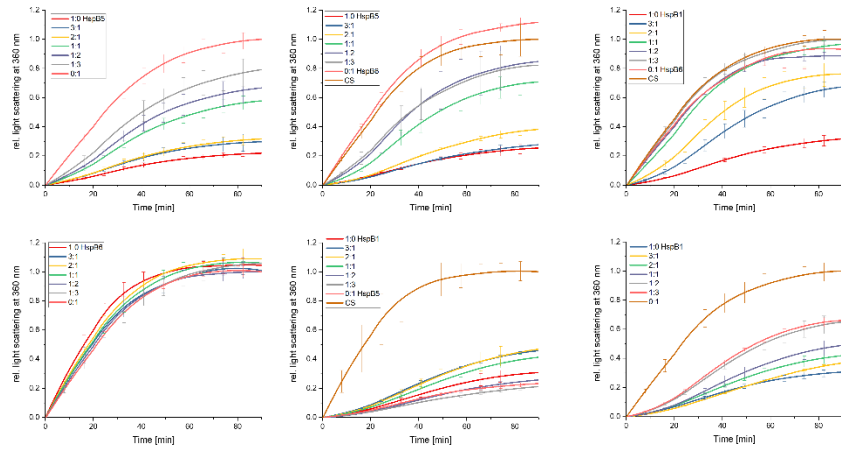


CS

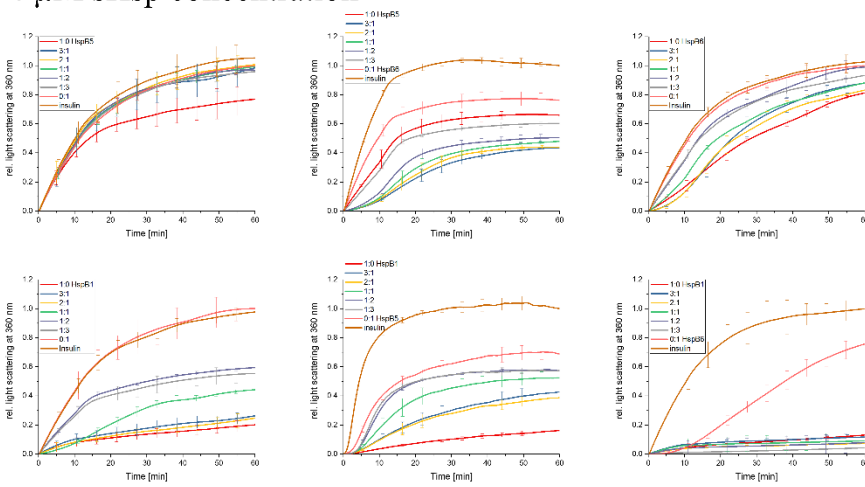
2 μM sHsp concentration



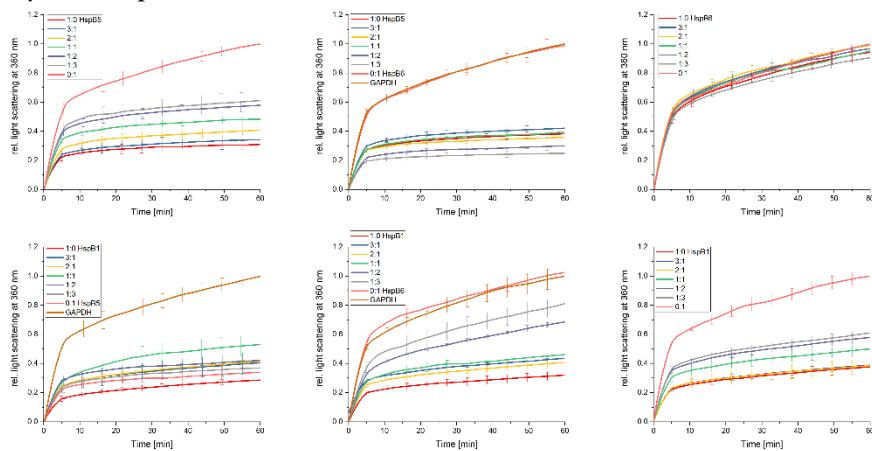
CS

4 μM sHsp concentration

Insulin

4 μM sHsp concentration

GAPDH

4 μM sHsp concentration

D | Modulation values of aggregation suppression ability for the respective sHsp hetero-oligomers.

The table shows the calculated modulation values corresponding to the heat map in Fig. 6. Negative values indicate inhibition, positive values indicate activation. Modulation values were calculated as difference of the measured activity value and the theoretical activity value whereas the theoretical activity value is defined as the sum of both homo-oligomeric (single) sHsp activities. Measured activity values represent the suppression of aggregation capacity calculated as 1 subtracted by the normalized endpoint aggregation values according to Figure 21.

	HspB1-HspB6					HspB1-HspB5					HspB5-HspB6				
	MDH	CS	Insulin	GAPDH	HEK	MDH	CS	Insulin	GAPDH	HEK	MDH	CS	Insulin	GAPDH	HEK
1:0	0.04	-0.01	0.05	0.06	0.03	0.07	0.12	0.01	0.09	0.12	-0.09	0.00	0.05	-0.07	-0.07
3:1	0.09	-0.25	0.06	-0.14	0.08	0.10	-0.34	-0.21	-0.40	0.20	-0.31	0.20	0.41	-0.09	-0.04
2:1	0.10	-0.34	0.11	-0.05	0.09	0.07	-0.34	-0.21	-0.45	0.11	-0.18	0.16	0.48	0.02	-0.03
1:1	0.14	-0.42	0.22	-0.01	-0.05	-0.07	-0.20	-0.08	-0.55	0.05	-0.08	0.23	0.32	0.04	-0.02
1:2	-0.04	-0.15	0.34	-0.11	0.06	-0.06	0.01	0.05	-0.44	0.16	-0.06	0.05	0.23	0.27	-0.10
1:3	0.16	-0.33	0.38	-0.21	0.09	0.03	0.07	0.00	-0.42	0.15	0.18	-0.02	0.17	0.35	-0.03
0:1	0.01	0.11	0.06	-0.08	0.05	0.07	-0.01	0.13	-0.03	-0.03	-0.10	-0.01	-0.02	-0.05	-0.04

E | Overview of amino acid sequences of αB mutants

αB

MDIAIHHPWIRRPFFPFHSPSRLFDQFFGEHLLESDFPTSTSLSPFYLRPPSFLRAPSWFDT
GLSEMRLEKDRFSVNLDVKHFSPEELKVKVLGDVIEVHGKHEERQDEHGFISREFHRKY
RIPADVDPLTITSSLSSDGVLTVNGPRKQVSGPERTIPITREEKPAVTAAPKK

$\Delta 20$

MASRLFDQFFGEHLLESDFPTSTSLSPFYLRPPSFLRAPSWFDTGLSEMRLEKDRFSVNLD
DVKHFSPEELKVKVLGDVIEVHGKHEERQDEHGFISREFHRKYRIPADVDPLTITSSLSSD
GVLTVNGPRKQVSGPERTIPITREEKPAVTAAPKK

$\Delta 28$

MGEHLLESDFPTSTSLSPFYLRPPSFLRAPSWFDTGLSEMRLEKDRFSVNLDVKHFSPEE
LKVKVLGDVIEVHGKHEERQDEHGFISREFHRKYRIPADVDPLTITSSLSSDGVLTVNGPR
KQVSGPERTIPITREEKPAVTAAPKK

$\Delta 40$

MASTSLSPFYLRPPSFLRAPSWFDTGLSEMRLEKDRFSVNLDVKHFSPEELKVKVLGDVI
EVHGKHEERQDEHGFISREFHRKYRIPADVDPLTITSSLSSDGVLTVNGPRKQVSGPERTI
PITREEKPAVTAAPKK

$\Delta 51$

MAPSFLRAPSWFDTGLSEMRLEKDRFSVNLDVKHFSPEELKVKVLGDVIEVHGKHEERQ
DEHGFISREFHRKYRIPADVDPLTITSSLSSDGVLTVNGPRKQVSGPERTIPITREEKPAV
TAAAPKK

ΔNTR

MEMRLEKDRFSVNLDVKHFSPEELKVKVLGDVIEVHGKHEERQDEHGFISREFHRKYRI
PADVDPLTITSSLSSDGVLTVNGPRKQVSGPERTIPITREEKPAVTAAPKK

Trp free

MDIAIHHPAIRRPFPPFHSPSRLFDQFFGEHLLESDFPTSTSLSPFYLRPPSFLRAPS AFDTG
LSEMRLEKDRFSVNLDVKHFSPEELKVKVLGDVIEVHGKHEERQDEHGFISREFHRKYRI
PADVDPLTITSSLSSDGVLTVNGPRKQVSGPERTIPITREEKPAVTAAPKK

Phe free

MDIAIHHPWIRRPAAHAHSPSRLADQAAGEHLLESDFLAPTSTSLSPAYLRPPSALRAPS W
ADTGLSEMRLEKDRFSVNLDVKHFSPEELKVKVLGDVIEVHGKHEERQDEHGFISREFH
RKYRIPADVDPLTITSSLSSDGVLTVNGPRKQVSGPERTIPITREEKPAVTAAPKK

Aromats free

MDIAIHHPAIRRPAAPAHSPSRLADQAAGEHLLESDFLAPTSTSLSPAALRPPSALRAPS AA
DTGLSEMRLEKDRFSVNLDVKHFSPEELKVKVLGDVIEVHGKHEERQDEHGFISREFHR
KYRIPADVDPLTITSSLSSDGVLTVNGPRKQVSGPERTIPITREEKPAVTAAPKK

 α B R11K

MDIAIHHPWIKRPFPPFHSPSRLFDQFFGEHLLESDFPTSTSLSPFYLRPPSFLRAPS WFD T
GLSEMRLEKDRFSVNLDVKHFSPEELKVKVLGDVIEVHGKHEERQDEHGFISREFHRKY
RIPADVDPLTITSSLSSDGVLTVNGPRKQVSGPERTIPITREEKPAVTAAPKK

 α B R22K

MDIAIHHPWIRRPFFPFHSPSKLFDQFFGEHLLESDFPTSTSLSPFYLRPPSFLRAPS WFD T
GLSEMRLEKDRFSVNLDVKHFSPEELKVKVLGDVIEVHGKHEERQDEHGFISREFHRKY
RIPADVDPLTITSSLSSDGVLTVNGPRKQVSGPERTIPITREEKPAVTAAPKK

 α B S35K

MDIAIHHPWIRRPFFPFHSPSRLFDQFFGEHLLKDLFPTSTSLSPFYLRPPSFLRAPS WFD T
GLSEMRLEKDRFSVNLDVKHFSPEELKVKVLGDVIEVHGKHEERQDEHGFISREFHRKY
RIPADVDPLTITSSLSSDGVLTVNGPRKQVSGPERTIPITREEKPAVTAAPKK

 α B S45K

MDIAIHHPWIRRPFFPFHSPSRLFDQFFGEHLLESDFPTSTSLKPFYLRPPSFLRAPS WFD T
GLSEMRLEKDRFSVNLDVKHFSPEELKVKVLGDVIEVHGKHEERQDEHGFISREFHRKY
RIPADVDPLTITSSLSSDGVLTVNGPRKQVSGPERTIPITREEKPAVTAAPKK

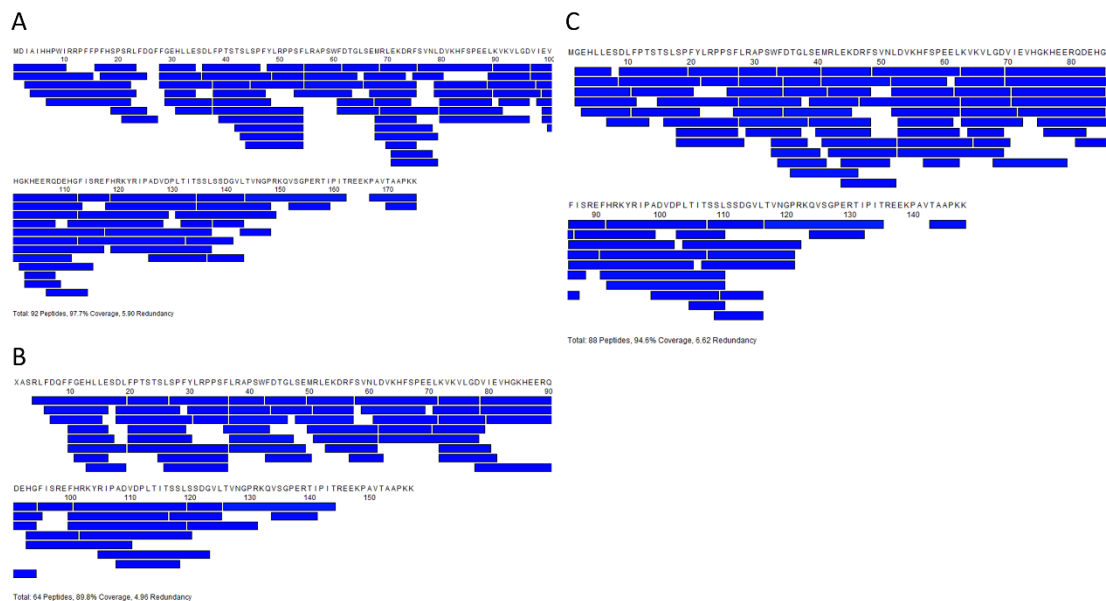
 α B R50K

MDIAIHHPWIRRPFFPFHSPSRLFDQFFGEHLLESDFPTSTSLSPFYLRPPSFLRAPS WFD T
GLSEMRLEKDRFSVNLDVKHFSPEELKVKVLGDVIEVHGKHEERQDEHGFISREFHRKY
RIPADVDPLTITSSLSSDGVLTVNGPRKQVSGPERTIPITREEKPAVTAAPKK

 α B R11K R22KR50K

MDIAIHHPWIKRPFPPFHSPSKLFDQFFGEHLLESDFPTSTSLSPFYLRPPSFLRAPS WFD T
GLSEMRLEKDRFSVNLDVKHFSPEELKVKVLGDVIEVHGKHEERQDEHGFISREFHRKY
RIPADVDPLTITSSLSSDGVLTVNGPRKQVSGPERTIPITREEKPAVTAAPKK

F | Peptide Coverage for HDX-MS measurements of α B (A) and its truncation mutants Δ 20 (B), and Δ 28 (C).

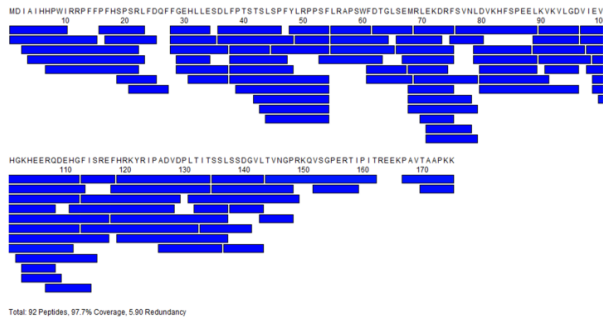


G | CDNN results of CD spectroscopy experiments of α B aromatic mutants.

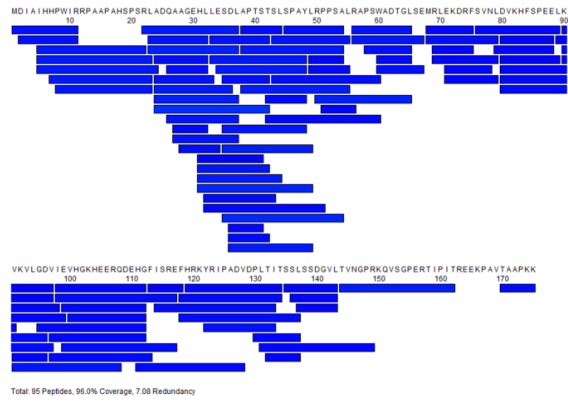
	WT	Trp free	Phe free	aromats free
Helix	13.10%	13.20%	13.10%	13.10%
Antiparallel	20.00%	19.80%	20.00%	20.00%
Parallel	18.80%	18.70%	18.80%	18.80%
Beta-Turn	22.20%	22.10%	22.20%	22.20%
Rndm. Coil	52.90%	52.70%	52.80%	52.80%
Total Sum	127.00%	126.50%	127.00%	127.00%

H | Peptide Coverage for HDX-MS measurements of α B (A) and its aromatic mutants (B) Trp free, (C) Phe free, and (D) aromats free.

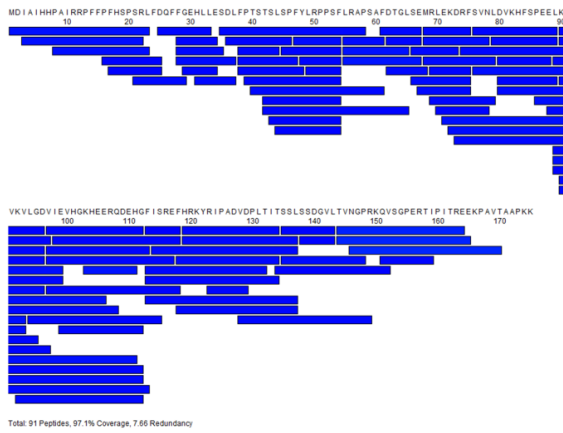
A



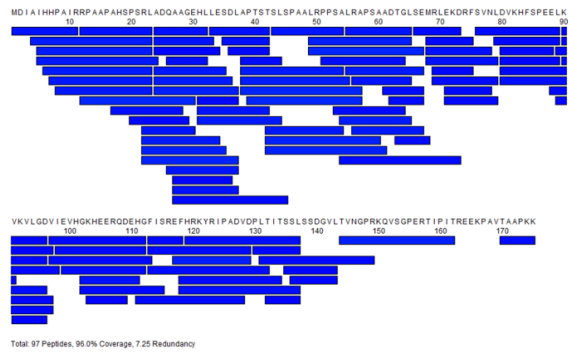
C



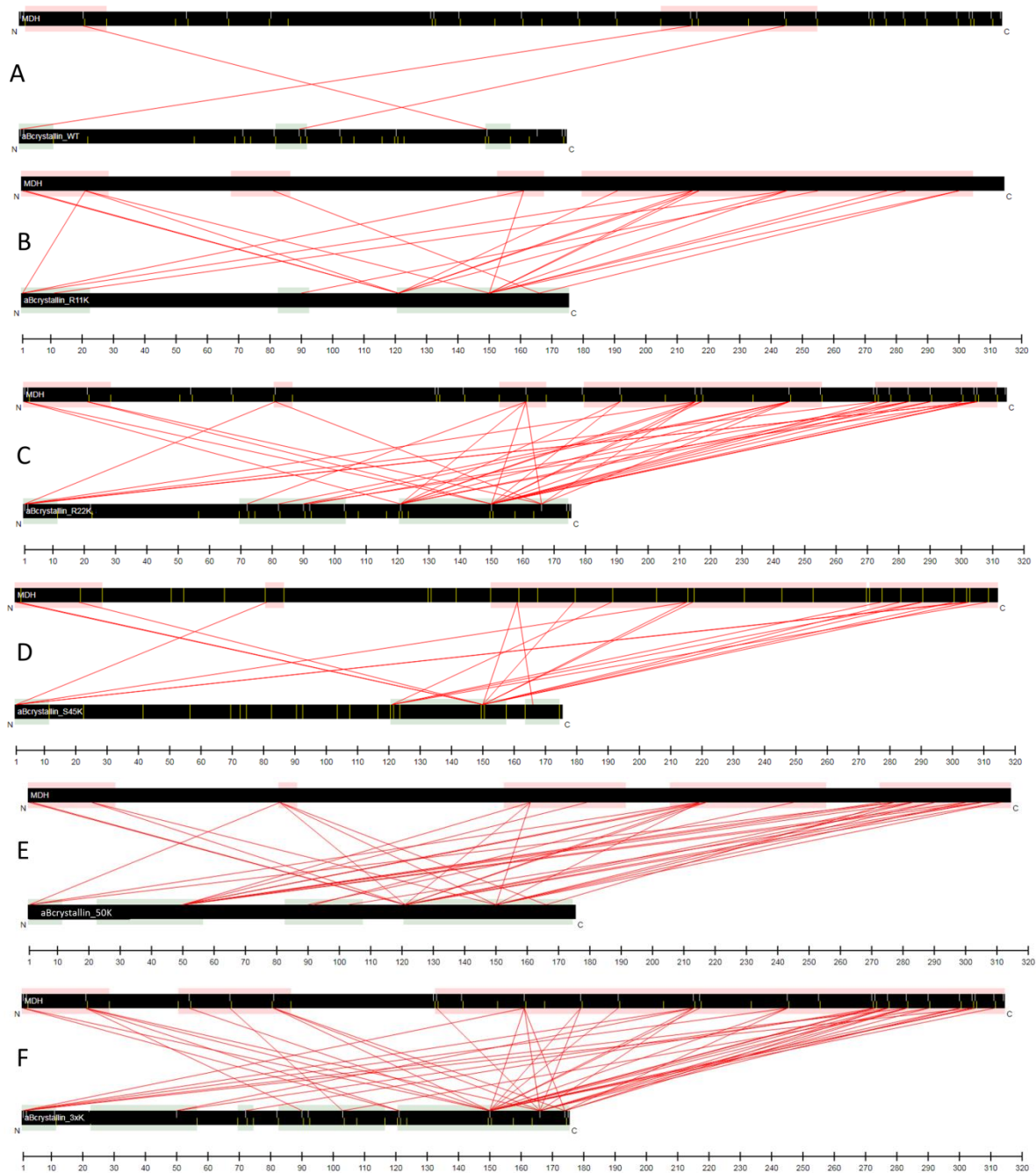
B



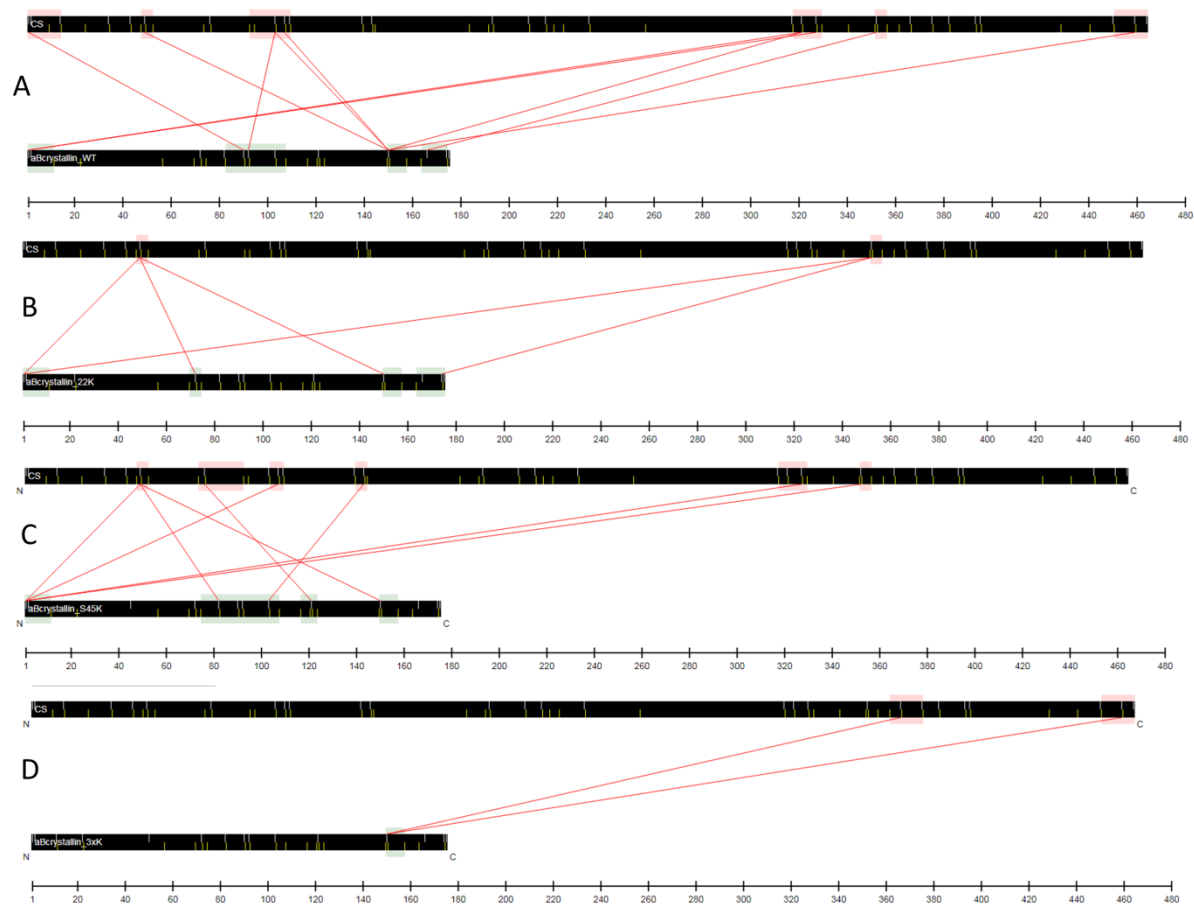
D



I | Crosslinks of MDH with α B (A) and its lysine mutants (B) R11K, (C) R22K, (D) S45K, (E) R50K, and (F) R11KR22KR50K. DSG was used as crosslinker. Data are analyzed by Kojak, verified by percolator and visualized by PROXL. No results were obtained for S35K mutant.



J | Crosslinks of CS with α B (A) and its lysine mutants (B) R22K, (C) R45K, and (D) R11KR22KR50K. DSG was used as crosslinker. Data are analyzed by Kojak, verified by percolator and visualized by PROXL. No data were obtained for R11K and S35K.



K | Configuration settings for Kojak crosslink analysis. The text-file is exemplary for a dataset of R22K mutant crosslinked to MDH. The file location for the database (.fasta) and the MS (.mzXML) needs to be adjusted for each evaluation.

```

# Kojak version 1.5.5 parameter file
# Please see online documentation at:
# http://www.kojak-ms.org/param
# All parameters are separated from their values by an equals sign ('=')
# Anything after a '#' will be ignored for the remainder of the line.
# Computational resources
threads = 4 #increase to use more cores/nodes
# Data input files: include full path if not in current working directory
database = H:\MS\crosslinking_V4\ab22K_MDH\Kojak_MM_database_aBR22K_MDH.fasta # adjust
export_percolator = 1
export_pepXML = 1
MS_data_file = H:\MS\crosslinking_V4\ab22K_MDH\20190810_MR_8.mzXML # adjust
percolator_version = 2.08
# Parameters used to described the data being input to Kojak
enrichment = 0 #Values between 0 and 1 to describe 180 APE.
#For example, 0.25 equals 25 APE.
instrument = 0 #Values are: 0=Orbitrap, 1=FTICR (such as Thermo LTQ-FT)
MS1_centroid = 0 #0=no, 1=yes
MS2_centroid = 1 #0=no, 1=yes
MS1_resolution = 70000 #Resolution at 400 m/z, value ignored if data are
#already centroided
MS2_resolution = 17500 #Resolution at 400 m/z, value ignored if data are
#already centroided
# Cross-link and mono-link masses allowed. May have more than one of each parameter.
# Format for cross_link is [amino acids] [amino acids] [mass mod] [identifier]
# Format for mono_link is [amino acids] [mass mod]
# One or more amino acids (uppercase only!!) can be specified for each linkage moiety
# Use lowercase 'n' or 'c' to indicate protein N-terminus or C-terminus
cross_link = nk nk 96.021130 DSG #DSG_di
mono_link = nk 114.031695 #DSG_mono
# Fixed modifications. Add as many as necessary.
fixed_modification = C 57.02146
fixed_modification_protC = 0
fixed_modification_protN = 0
# Differential modifications. Add as many as necessary. Uppercase only for amino acids!
# n = peptide N-terminus, c = peptide C-terminus
# If more than one modification is possible for an amino acid,
# list all modifications on separate lines
modification = M 15.9949
modification_protC = 0
modification_protN = 0
diff_mods_on_x1 = 1
max_mods_per_peptide = 2
mono_links_on_x1 = 1
# Digestion enzyme rules.
# See http://www.kojak-ms.org/param/enzyme.html
enzyme = [KR][P] #Trypsin
# Scoring algorithm parameters
# fragment_bin_offset and fragment_bin_size influence algorithm precision and memory usage.
# They should be set appropriately for the data analyzed.
# For ion trap ms/ms: 1.0005 size, 0.4 offset
# For high res ms/ms: 0.03 size, 0.0 offset
fragment_bin_offset = 0.4 #between 0.0 and 1.0
fragment_bin_size = 0.03 #in Thomsons
ion_series_A = 0
ion_series_B = 1
ion_series_C = 0
ion_series_X = 0
ion_series_Y = 1
ion_series_Z = 0 #Z-dot values are used
# Additional parameters used in Kojak analysis
decoy_filter = decoy #identifier for all decoys in the database.
#Default value is "random" (without quotes)
isotope_error = 1 #account for errors in precursor peak identification.
#Searches this number of isotope peak offsets.
#Values are 0,1,or 2.
max_misclavages = 2 #number of missed trypsin cleavages allowed evt1 hoeher setzen
max_peptide_mass = 4000.0 #largest allowed peptide mass in Daltons
min_peptide_mass = 500.0 #lowest allowed peptide mass in Daltons
max_spectrum_peaks = 0 #top N peaks to use during analysis. 0 uses all peaks.
modification = M 15.9949
modification_protC = 0
modification_protN = 0
diff_mods_on_x1 = 1
max_mods_per_peptide = 2
mono_links_on_x1 = 1
# Digestion enzyme rules.
# See http://www.kojak-ms.org/param/enzyme.html
enzyme = [KR][P] #Trypsin

```

```

# Scoring algorithm parameters
# fragment_bin_offset and fragment_bin_size influence algorithm precision and memory usage.
# They should be set appropriately for the data analyzed.
# For ion trap ms/ms: 1.0005 size, 0.4 offset
# For high res ms/ms: 0.03 size, 0.0 offset
fragment_bin_offset = 0.4 #between 0.0 and 1.0
fragment_bin_size = 0.03 #in Thomsons
ion_series_A = 0
ion_series_B = 1
ion_series_C = 0
ion_series_X = 0
ion_series_Y = 0
ion_series_Z = 1 #Z-dot values are used
# Additional parameters used in Kojak analysis
decoy_filter = decoy #identifier for all decoys in the database.
#Default value is "random" (without quotes)
isotope_error = 1 #account for errors in precursor peak identification.
#Searches this number of isotope peak offsets.
#values are 0,1,or 2.
max_miscelevages = 2 #number of missed trypsin cleavages allowed evt1 hoeher setzen
max_peptide_mass = 4000.0 #largest allowed peptide mass in Daltons
min_peptide_mass = 500.0 #lowest allowed peptide mass in Daltons
max_spectrum_peaks = 0 #top N peaks to use during analysis. 0 uses all peaks.
ppm_tolerance_pre = 15.0 #mass tolerance on precursor when searching
prefer_precursor_pred = 2 #prefer precursor mono mass predicted by
#instrument software
# 0 = ignore previous predictions
# 1 = use only previous predictions (Thermo Orbitrap predicts)
# 2 = supplement predictions with additional analysis
spectrum_processing = 0 #0=no, 1=yes
top_count = 50 #number of top scoring single peptides to combine evt1. auf 300 erhoehen
#in relaxed analysis
truncate_prot_names = 0 #Max protein name character to export, 0=off
turbo_button = 1 #Generally speeds up analysis. Special cases cause reverse
#effect, thus this is allowed to be disabled. 0=off

```

L | Database used for Kojak crosslink analysis.

The depicted fasta-file is exemplary for a R22K mutant crosslinked to MDH analysis.

```

>aBcrystallin_R22K
MDIAIHHPWIRPPFFPFHSPSKLFDQFFGEHLLESDFPTSTLSPPFYLRPPSFLRAPSW
FDTGLSEMRELEKDRFSVNLVVKHFSPEELKVKVLGDVIEVHGKHEERQDEHGFISREFFHR
KYRIPADVDPILTITSSLSDDGVLTVNGPRKQVSGPERTIPITREEKPAVTAAPKK

>decoy_aBcrystallin_wT
KKPAATVAPKEERTIPITREPGSVQKRPQNVTLVGDSSLSSTITLDPVDAPIRYK
RHFERSIFGHEDQREEHKGHVEIVDGLVVKLEEPSFHKVDLVNVSFRDKELRMESLGTDF
WSPARLFSPPRLYFPSLSTSTPFLDSELLHEGFFQDFLRSPSHFFPPRRRIWPHHIAIDM

>MDH
AKVAVL GASGGIGQPLSLLLNKNSPLVSRLTLYDIAH
TPGVAADLSHIETRAIVKGYLGPEQLPDCLKGCDDVVIPAGVPRKPGMTRDDL FNTNATI
VATLTAACAQHC PDAMCIIISNPVNSTIPITAEVFKKHGVYVNPKNIFGVTTLDIVRANAF
VAELKGLDPARVSVPIGGHAGKTIIP LISQCTPKVDFPQDQLSTLTGRIQEAAGTEVVK
KAGAGSATLSMAYAGARVFSLV DAMNGKEGVVCEFSVFKSQETDCPYFSTPLLLGKKGIE
KNLGIKGISPFEEKIAEAIPEL KASIKKGEFVKMK

>decoy_MDH
KMNKVFEEGKKISAKLEPIAEAIMKEEFPKIGILNK
EIGKKGLLLPTSFYPCDTEQSKVFSCEVVGEGKNMADVLSFVFRAGAYAMSLTASGAGAK
AKVVE TGAEQIRGTLTSLQDQFPDKVPTCQSILPIITKGAHGGIVPVSVRAPDLGKLEAV
FANARVIDLTTVGF IKNPNYVGHKFFVEATIPITSNVPSIICIMADPCHQACAATLTV
ITANTNFLDDRTMGPKRPVGAIVVDCGKLC DPLQEPGLYGVKVTARTEIHSLDAAVGPT
HAIDYLT LRSVLP SNKLLLSLQPGIGGSAGLVAVKA

```

M | Overview of amino acid sequences of human Bag3 and Bag3 IPV

Bag3 (1-574)

```

MSAATHSPMMQVASGNDRDPLPPGWEIKIDPQTGWPFVVDHNSRTTTWNDPRVPSEGPKETPSSAN
GPSREGSRLPPAREGHPVYPQLRPGYIPIVPLHEGAENRQVHPFHVYPQPMQRFRTTEAAAAAPQRSQS
PLRGMPE TTQPKQCGQVAAAAAQQPASHGPERSQSPAASDCSSSSSSASLPSSGRSSLGSHQLPRGYI
SIPVIHEQNVTRPAAQPSFHQAQKTHYPAQQGEYQTHQPVYHKIQGDDWEPRPLRAASPFRSSVQGAS
SREGSPARSSTPLHSPSPIRVHTVVD RPQQPMT HRETAPV SQPENK PESKPGPVGPELPPGHIPIQVIRKE
VDSKPV SQKPPPSEKVEVKVPPAPVPCPPSPGPS AVSSPKSVATEERAAPSTAPAEATPPKPGAEAEAP
PKHPGV LKVEAILEKVQGLEQAVDNFEGKKTDKKYL MIEEYLT KELLALDSVDPEGRADVRQARRDG
VRKVQTILEKLEQKAIDVPGVQVYELQPSNLEADQLQAIMEMGAVAADKGGKNAGNAEDPHTETQ
QPEATAAATSNPSSMTDTPGNPAA

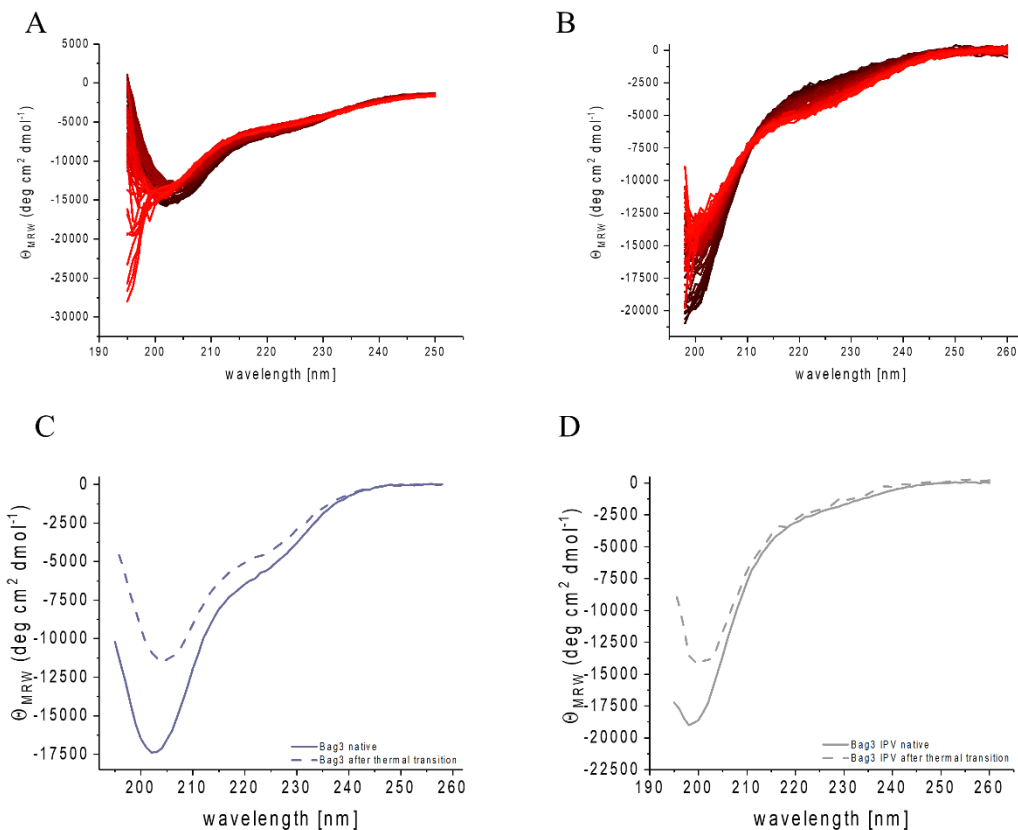
```

Bag3 IPV (54-302)

MVPSEGPKETPSSANGPSREGSRLPPAREGHPVYPQLRPGYIPIVVLHEGAENRQVHPFHVYPQPGMQR
 FRTEAAAAAPQRSQSPLRGMPETTQPDKQCGQVAAAAAAQPPASHGPERSQSPAASDCSSSSSSASLPS
 SGRSSLGSHQLPRGYISIPVIHEQNVTRPAAQPSFHQAQKTHYPAAQQGEYQTHQPVYHKIQGDDWEPRP
 LRAASPFRRSSVQGASSREGSPARSSSTPLHSPSPIRVHTVVDPRP

N | Full spectra data of thermal transition experiments of Bag3 (A) and Bag3 IPV (B).

Additionally, CD spectra were recorded before and after the thermal transition experiment of Bag3 (C) and Bag3 IPV (D).

**O | CDNN results of CD spectroscopy experiments of Bag3 and Bag3 IPV.**

	Bag3	Bag3 IPV
Helix	23.8 %	18.9 %
Antiparallel	10.6 %	12.6 %
Parallel	12.6 %	15.3 %
Beta-Turn	18.6 %	19.7 %
Rndm. Coil	41.1 %	46.2 %
Total Sum	106.6 %	112.7 %

Abbreviations

aa	Amino acid
ACD	A-crystallin domain
ACN	Acetonitril
Amp	Ampicillin sodium salt
ANS	8-Anilinonaphthalene-1-sulfonic acid
APS	Ammonium persulfate
AS	Ammoniumsulfate
AUC	Analytical ultracentrifugation
BSA	Bovine serum albumin
CD	Circular dichroism
CS	Citrate Synthase
CTD	C-terminal domain
CTR	C-terminal region
CV	Column volume
D ₂ O	Heavy water
DMEM	Dulbecco's Modified Eagle Medium
dNTPs	Deoxynucleoside triphosphates
DSG	Disuccinimidyl glutarate
DTT	Dithiothreitol
EDTA	Ethylenediaminetetraacetic acid disodium salt
ER	Endoplasmic reticulum
ESI	Electron spray ionization
FA	Formic acid
FBS	Fetal bovine serum Gold Plus
GAPDH	Glyceraldehyd-3-phosphat-Dehydrogenase
GdnCl	Guanidinium chloride
HDX-MS	hydrogen-deuterium exchange coupled to MS
HEPES	4-(2-hydroxyethyl)-1-piperazineethanesulfonic acid
HPLC	High performance liquid chromatography
IAA	Iodoacetamide
IPTG	Isopropyl β -D-1-thiogalaktopyranoside
ITC	Isothermal Titration Calorimetry
Kana	Kanamycin sulfate
KCl	Potassium chlorid
K ₂ HPO ₄	Dipotassium phosphate
KH ₂ PO ₄	Monopotassium phosphate
KLD	Kinase-Ligase-Digestion
KOH	Potassium hydroxide
L-MDH	L-Malate Dehydrogenase
MALDI-TOF-MS	Matrix-Assisted-Laser-Desorption Ionization Imaging coupled to a time-of-flight detector mass spectrometer

MEME	Minimum Essential Media Eagle
Na ₂ HPO ₄ *2H ₂ O	Disodium phosphate
NaCl	Sodium chlorid
NaDoc	Sodium deoxycholate
NaH ₂ PO ₄	Monosodium phosphate
NaOH	Sodium hydroxide
NEAA	Non-essential-amino-acids
NP-40	Nonidet P-40 Substitute
NTD	N-terminal domain
NTR	N-terminal region
PBS	Phosphate-buffered saline
PCR	Polymerase chain reaction
PEG	Polyethylenglycol
Pho	Rhodanese
PMSF	Phenylmethanesulfonyl fluoride
RPMI	Roswell Park Memorial Institute 1640 Medium
RT	Room temperature
SDS	Sodium dodecyl sulfate
SEC-MALS	Size exclusion chromatography coupled to multi-angle-light-scattering
TCA	Trichloroacetic acid
TCEP	tris(2-carboxyethyl)phosphine
TEM	Transmission electron microscopy
TEMED	Tetramethylethylenediamine
Tris-HCl	Trizma Base
β-Me	β-Mercaptoethanol

Publications

Publication in progress:

Riedl, M., Lim, N., Schmid, P. W., and Buchner, J., (2020). Insight into determinants of substrate binding in the molecular chaperone α B-crystallin. *Manuscript in preparation*.

Publication completed:

Riedl, M., Mymrikov, E. V., Peters, C., Weinkauff, S., Haslbeck, M., and Buchner, J. (2020) Regulation of small heat shock proteins by hetero-oligomer formation. *Journal of Biological Chemistry*, 295 (1), 158-169

Danksagung

An erster Stelle möchte ich mich bei meinem Doktorvater Prof. Dr. Johannes Buchner für die Betreuung meiner Doktorarbeit bedanken. Johannes hat mir durch die hervorragende Infrastruktur am Lehrstuhl, die wissenschaftlichen Diskussionen und auch durch den nötigen kreativen Freiraum alle Möglichkeiten eröffnet meine Doktorarbeit erfolgreich abzuschließen.

Explizit möchte ich mich auch bei meinem Mentor Dr. Martin Haslbeck bedanken, der mir bei Problemen stets zur Seite stand und auch mit seiner fachlichen Kompetenz im Bereich der kleinen Hitzeschock Proteine eine gute Hilfe war. Ein weiterer besonderer Dank gilt Fr. Rubinstein für ihre immerzu freundliche Art und ihre Hilfe in allen bürokratischen Angelegenheiten.

Des Weiteren möchte ich mich bei Evgeny Mymrikov, PhD, Carsten Peters, PhD, und Prof. Dr. Sevil Weinkauf für die gute Zusammenarbeit während des Hetero-Oligomer Projektes und für sämtliche wissenschaftliche Diskussionen zu meinem Promotionsthema bedanken. Nicole Lim, PhD und Dr. Philipp Schmid möchte ich für ihren kompetenten Input zum NTR Projekt danken.

Ein großer Dank gilt außerdem allen Technischen Assistenten des Lehrstuhls insbesondere Anja Osterauer und Bettina Richter für ihre Zuarbeiten sämtlicher Art, ebenso wie Florian Rührnößl und Laura Meier für die Durchführung und Auswertung der MALDI-MS und HDX-MS Experimente. Bedanken möchte ich mich auch bei Katja Bäuml vom AK Sieber für die gute Zusammenarbeit und die Durchführung der CX-MS Messungen. Bei Susanne Mayer und Max Fottner möchte ich mich für die immer unkomplizierte und schnelle Durchführung der Vollängen Massenspektrometrie Messungen bedanken.

Weiterhin möchte ich allen Mitarbeitern des Lehrstuhls danken, die mir während meiner Doktorarbeit mit Rat und Tat zu Seite standen. Dr. Marina Kreuzeder danke ich herzlich für die gute Einführung in die Massenspektrometrie, Dr. Benedikt Weber für seine Hilfe mit der SEC-MALS, Dr. Christina Nickels für ihre aufbauenden Worte, Vinay Dahiya, PhD für ihre äußerst kompetente Hilfe bei den Rückfaltungs-Assays und Stefan Riedl für seine IT-Tätigkeiten.

Ein herzlicher Dank geht an meine liebsten Büro- und Nachbarbüro-Kollegen aus Büro 1 und 2 für sämtliche „fruitful discussions“ mit oder ohne Kaltgetränken und für die entspannte Arbeitsatmosphäre. Besonders möchte ich mich bei Moritz Mühlhofer und Pamina Kazman bedanken – ohne euch wäre es nicht das Gleiche gewesen. Danke für die gemeinsame Zeit!

Mein besonderer Dank gebührt meinem Ehemann Martin, der mit mir während der Doktorarbeit alle Höhen und Tiefen durchleben durfte, aber auch musste. Zu guter Letzt möchte ich meinen Eltern danken, denn ohne euch wäre ich heute nicht hier!

Eidesstattliche Erklärung

Hiermit erkläre ich an Eides statt, dass ich die vorliegende Arbeit selbständig verfasst und keine anderen als die angegebenen Quellen und Hilfsmittel verwendet habe. Die aus fremden Quellen übernommenen Gedanken sind als solche kenntlich gemacht. Die vorliegende Arbeit wurde noch keiner anderen Prüfungsbehörde vorgelegt. Teile dieser Arbeit wurden in einem wissenschaftlichen Journal veröffentlicht.

München, 24.04.2020

Ort, Datum



Mareike Riedl